

# The Time-Domain Response of Coupled-Resonator Filters with Applications to Tuning

Joel Phillip Dunsmore

Submitted in accordance with the requirements for the degree of

Doctor of Philosophy

The University of Leeds

School of Electronics and Electrical Engineering

January 2004

The candidate confirms that the work submitted is his own and the appropriate credit has been given where reference has been made to the work of others.

This copy has been supplied on the understanding that it is copyright material and that no quotation from the thesis may be published without proper acknowledgement.

## Acknowledgements

I acknowledge the sponsorship of Agilent Technologies in the development of the research for this thesis. In particular, I thank the following individual managers for their direct support: Tom Fetter, Manager for Microwave Instrument Division for inspiration of the original concepts in the time-gated tuning method; Roger Stancliff, Lab Manager of Microwave Instruments Division; Andy Botka, Manager for the Component Test Marketing Solutions Unit; John Stratton, Manager for the Component Test Marketing Solutions Unit; Mike Dethlefsen, Section Manager for the Component Test Division; Steve Fossi, Lab Manager for the Component Test Division; and Bob McClung, General Manager for the Component Test Division.

I also thank Prof. Roger Pollard, my thesis adviser, for his help, advice and support in the opportunity to pursue this advanced degree; and Dr. Mohamed Sayed, my industrial adviser for this thesis.

My thanks to David Sharrit, of Agilent Technologies, for his help in understanding many of the aspects of the time-domain transform which he personally implemented in the HP 8510 network analyzer.

The filter tuning software application was substantially developed by a team of 4 members, including the author as principal contributor to the time-gated algorithms. Dara Sariaslani was the principle software implementer of the time-gated algorithms, and contributed to the search algorithms in the time-gated method. Sean Hubert was the developer of the instrument control links and compensation software, and Johan Ericsson was the designer of the graphical display and tuning indicators. In addition, Bobby Bhowmik contributed to the software architecture and Phil Hoard was the project manager. Jim Kerr collaborated on the compensation matrix, and was the first to recognize that the interaction matrix, as a simple system of linear equations, could be solved with standard matrix methods. My thanks also to Mirin Lew for editing the Agilent application notes on time-domain tuning methods.

Finally, I thank my wife, Dana, my son Jaymes, and my daughter Emma for giving up family time to support me in this effort.

## Abstract

This thesis develops a new theory of tuning filters based on the time-domain response of the filter. These methods are shown to work very well for all-pole coupled-resonator filters in particular, and may be applied to automated tuning of filters.

Numerous filter-tuning methods are reviewed, and the attributes and limitations of each are discussed. Key results about transfer functions, filter theory and Laplace transform theory are reviewed as applied to all-pole filters. The Fourier Transform theory is reviewed and a new, detailed analysis of the Vector Network Analyzer (VNA) time-domain transform, including gating and windowing is presented, including new work in area of the compensation for the masking effects of time-domain gating.

A complete description of the time-domain tuning method is presented, which includes experimental and empirical results from simulations and measurements on filters. The theoretical underpinning supporting the novel method of time-domain tuning is developed, along with a rigorous mathematical relationship between VNA time-domain response of a simple filter, and the analytic impulse response. The time-domain results observed in experiments are shown to be directly correlated to the filter transfer functions and the specific effects that differentiate the VNA time-domain transform from the analytically derived impulse response.

This thesis includes previously unpublished work that is the basis for two U.S. patents, as well as the development of a commercial filter tuning software program. An improved method for filter tuning, which uses time-domain gating on the  $S_{11}$  response of the filter is introduced, and shown to be a key improvement for developing automated tuning techniques.

The details of a software application for filter tuning are presented, along with methods for determining and compensating the interactions from other resonators. A case study of applying the FTS method to a complex duplex filter is described.

Areas for extension into other filter types are discussed. General guidelines for the successful application of the new tuning method to various filter types are presented, along with other conclusions of this thesis.

## Table of Contents

<b>Acknowledgements .....</b>	<b>2</b>
<b>Abstract.....</b>	<b>3</b>
<b>List of tables and figures .....</b>	<b>6</b>
<b>List of symbols.....</b>	<b>9</b>
<b>Chapter 1 Introduction.....</b>	<b>13</b>
1.1 Introduction .....	13
1.2 Current tuning methods for coupled resonator filters .....	15
1.3 Tuning methods based on frequency response .....	16
1.4 Model matching and optimization methods .....	18
1.5 Limitations of current tuning methods.....	25
1.6 New contributions to filter tuning .....	25
1.7 Outline of the present work.....	28
<b>Chapter 2 Filter Fundamentals .....</b>	<b>31</b>
2.1 Transfer functions and Laplace transforms.....	31
2.2 Low-pass transfer functions.....	36
2.3 Low-pass to band-pass response .....	38
2.4 Time-domain response of band-pass filters .....	40
2.5 Microwave characterization of filters.....	40
2.6 Microwave filters design considerations .....	42
2.7 Coupled-resonator filters.....	43
2.8 Filters with cross coupling .....	45
<b>Chapter 3 Fourier Transform Study.....</b>	<b>47</b>
3.1 The Fourier analysis of filters .....	47
3.2 The discrete Fourier transform.....	49
3.3 Fourier transform (analytic) vs. VNA time-domain transform.....	53
3.4 Low-pass transforms and band-pass transforms .....	62
3.5 Time-domain gating .....	68
3.6 Examples of time-domain transforms of various networks.....	72
3.7 The effects of masking and gating on measurement accuracy.....	75
3.8 Conclusions: .....	83
<b>Chapter 4 Filter Tuning Using Time-Domain Transforms.....</b>	<b>84</b>
4.1 The invention of the time-domain tuning method .....	84
4.2 Experimental and simulated results on the effects of tuning on the time-domain response of filters.....	88
4.3 Filters with transmission zeros .....	100

4.4	<i>Time-domain resolution with respect to filter tuning</i> .....	105
<b>Chapter 5</b>	<b>Theoretical Analysis of Time-domain Filter Tuning</b> .....	<b>108</b>
5.1	<i>Calculating band-pass time-domain responses from low-pass prototypes</i> .	108
5.2	<i>Analytical calculations based on a single-pole low-pass filter</i> .....	112
5.3	<i>Time-domain response of multi-pole filters</i> .....	119
5.4	<i>Conclusions</i> .....	125
<b>Chapter 6</b>	<b>The Time-Domain Gated Response of Filters</b> .....	<b>126</b>
6.1	<i>Time-domain gated response of filters</i> .....	126
6.2	<i>Understanding interactive effects</i> .....	130
6.3	<i>Time gated tuning with cross-coupled filters</i> .....	133
6.4	<i>Conclusions</i> .....	134
<b>Chapter 7</b>	<b>Filter Tuning Software (FTS)</b> .....	<b>135</b>
7.1	<i>Creating the reference filter</i> .....	135
7.2	<i>Using FTS to adjust an un-tuned DUT filter</i> .....	139
7.3	<i>Compensation for resonator interactions</i> .....	145
7.4	<i>Pre-tuning methods in FTS</i> .....	154
7.5	<i>Changing filter center frequency or bandwidth with FTS</i> .....	157
7.6	<i>Case study: applying FTS techniques to duplexer tuning</i> .....	158
7.7	<i>FTS Conclusions</i> .....	161
<b>Chapter 8</b>	<b>Conclusions and Suggestions for Further Work</b> .....	<b>163</b>
8.1	<i>Conclusions</i> .....	163
8.2	<i>Suggestions for further work</i> .....	164
8.3	<i>Areas for investigation for applying FTS methods to other filters</i> .....	167
<b>Appendix 1</b> .....		<b>170</b>
	<i>Time domain reflection response of 3 pole Butterworth filter</i> .....	170
	<i>Response of a 1 pole network</i> .....	172
<b>References</b> .....		<b>173</b>
<b>Published papers</b> .....		<b>178</b>

## List of tables and figures

Table 1-1 .....	24
Figure 1-1 .....	26
Figure 1-2 .....	27
Figure 2-1 .....	37
Figure 2-2.. .....	40
Figure 2-3 .....	44
Figure 2-4 .....	46
Figure 3-1 .....	51
Figure 3-2 .....	54
Figure 3-3 .....	56
Figure 3-4 .....	59
Figure 3-5 .....	61
Figure 3-6 .....	65
Figure 3-7 .....	71
Figure 3-8 .....	73
Figure 3-9 .....	74
Figure 3-10 .....	77
Figure 3-11 .....	78
Figure 3-12 .....	79
Figure 3-13 .....	80
Figure 4-1 .....	85
Figure 4-2 .....	85
Figure 4-3 .....	86
Figure 4-4 .....	86
Figure 4-5 .....	87
Figure 4-6 .....	88
Figure 4-7 .....	89
Figure 4-8 .....	90
Figure 4-9 .....	91
Figure 4-10 .....	94
Figure 4-11 .....	95
Figure 4-12 .....	96
Figure 4-13 .....	96

Figure 4-14 .....	97
Figure 4-15 .....	98
Table 4-1 .....	99
Figure 4-16 .....	100
Figure 4-17 .....	102
Table 4-2 .....	102
Figure 4-18 .....	103
Figure 4-19 .....	103
Figure 4-20 .....	104
Figure 4-21 .....	104
Figure 5-1 .....	109
Figure 5-2 .....	111
Figure 5-3 .....	111
Figure 5-4 .....	112
Figure 5-5 .....	113
Figure 5-6 .....	113
Figure 5-7 .....	114
Figure 5-8 .....	115
Figure 5-9 .....	116
Figure 5-10 .....	116
Figure 5-11 .....	117
Figure 5-12 .....	117
Figure 5-13 .....	118
Figure 5-14 .....	119
Figure 5-15 .....	120
Figure 5-16 .....	121
Figure 5-17 .....	122
Figure 5-18 .....	123
Figure 5-19 .....	123
Figure 5-20 .....	124
Figure 6-1 .....	126
Figure 6-2 .....	127
Figure 6-3 .....	127
Figure 6-4 .....	128
Figure 6-5 .....	128

Figure 6-6 .....	129
Figure 6-7 .....	130
Figure 6-8 .....	131
Figure 6-9 .....	132
Figure 6-10 .....	132
Figure 6-11 .....	133
Figure 6-12 .....	134
Figure 7-1 .....	136
Figure 7-2 .....	137
Figure 7-3 .....	138
Figure 7-4 .....	139
Figure 7-5 .....	140
Figure 7-6 .....	142
Figure 7-7 .....	143
Figure 7-8 .....	144
Figure 7-9 .....	145
Figure 7-10 .....	146
Figure 7-11 .....	149
Figure 7-12 .....	150
Figure 7-13 .....	151
Figure 7-14 .....	152
Figure 7-15 .....	153
Figure 7-16 .....	155
Figure 7-17 .....	156
Figure 7-18 .....	158
Figure 7-19 .....	159
Figure 7-20 .....	160
Figure 7-21 .....	160
Figure 7-22 .....	161

## List of symbols

The following list of symbols is arranged in their order of appearance.

DSP – Digital signal processor

SAW – Surface acoustic wave

IF – Intermediate frequency

RF – Radio frequency

RX – Receiver

TX – Transmitter

LCX – Lossless network including constant reactance

ANA – Automatic network analyzer

RLC – Resistor-inductor-capacitor

Q – quality factor, relates to loss in a resonator

$S_{11}$  – Input reflection coefficient

$S_{21}$  – Forward transmission coefficient

VNA – Vector network analyzer

CPU – Central processing unit

DFT – Discrete Fourier transform

FFT – Fast Fourier transform

$X(\omega, \theta)$  – Arbitrary input signal as a function of radian frequency and input angle

$\omega$  – Radian frequency

$\theta$  – Input angle

$Y(\omega, \theta)$  – Arbitrary output signal as a function of radian frequency and angle

$H(\bullet)$  – Transfer response (in frequency domain)

$a(t)$  – Arbitrary signal as a function of time

$j$  – Square-root of minus one

$s$  – Complex frequency used with Laplace transforms

$\sigma$  – Real part on complex frequency representing a loss term

$x(t)$  – Arbitrary input signal as a function of time

$y(t)$  – Arbitrary output signal as a function of time

$f(t)$  – Time response of a function

$\mathbf{L}(f(t))$  – Laplace transform of  $f(t)$

$h(t)$  – Transfer function as a function of time

$\delta(t)$  – Unit impulse function

VSWR – Voltage standing wave ratio

$\mathbf{F}(f(t))$  – Fourier transform of  $f(t)$

$F(\omega)$  – Frequency response of a function

$\mathbf{F}^{-1}(H(\omega))$  – Inverse Fourier transform of  $H(\omega)$

LHP – Left half plane (in reference to poles in the complex plane)

RHP – Right half plane (in reference to poles in the complex plane)

$S$  – Low-pass prototype complex frequency

$\gamma$  – Low-pass to band-pass frequency scaling factor

$\omega_0$  – Center (radian) frequency of a band-pass filter

$\omega_1$  – Lower corner frequency of a band-pass filter

$\omega_2$  – Upper corner frequency of a band-pass filter

$L_n$  – The  $n^{\text{th}}$  inductive element in a filter

$C_n$  – The  $n^{\text{th}}$  capacitive element in a filter

$L_{nBP}$  – The  $n^{\text{th}}$  inductive element in a band-pass filter

$C_{nBP}$  – The  $n^{\text{th}}$  capacitive element in a band-pass filter

$Z_{in}$  – Input impedance of a network

$Y_{in}$  – Input admittance of a network

$H_N(\bullet)$  – Normalized transfer function

$Z_0$  – Reference impedance

$\rho$  – Reflection coefficient

$R(\omega)$  – Real part of a  $S_{11}$

$X(\omega)$  – Imaginary part of  $S_{11}$

$S_{12}$  – Reverse transmission coefficient

$S_{22}$  – Output reflection coefficient

$L_R$  – Resonator inductance

$C_R$  – Resonator capacitance

$C_C$  – Coupling capacitance

$R_{in}$  – Source impedance where the impedance is real

$R_{out}$  – Load impedance where the impedance is real

$Z_R$  – Resonator impedance

$L_{XC}$  – Cross-coupling inductance

IFT – Inverse Fourier transform

$E(\omega)$  – An even function

$O(\omega)$  – An odd function

$F^*(\bullet)$  – Complex conjugate of a function

$\Delta\omega$  – A small shift in frequency, or step in frequency

$H_{BP}$  – Band-pass transfer function

$H_{LP}$  – Low-pass transfer function

$h_{BP}$  – Band-pass time response

$h_{LP}$  – Low-pass time response

$f(\tau)$  – Discrete time function

$\tau$  – Discrete time value

$F(\nu)$  – Discrete frequency function

$\nu$  – Discrete frequency in cycles per sample

IFFT – Inverse fast Fourier transform

IDFT – Inverse discrete Fourier transform

CZT – Chirp Z transform

$III(\omega)$  – Frequency sampling function

$F_s(\omega)$  – Frequency response of a sampled function

$f_s(t)$  – Time response of a sampled function

$III(t)$  – Time sampling function

sinc – Sinc function ( $\sin x / x$ )

$W(n)$  – Windowing function,

$I_0(\bullet)$  – Modified Bessel function of the first kind

$\beta$  – Kaiser-Bessel windowing factor

$f_{SW}$  – Time response for a sampled, windowed function

$W_0$  – Window normalization factor

$f_{VNA}(t)$  – The VNA time-domain response

$f_{LP}(t)$  – The low-pass time-domain impulse response

TDR – Time-domain Reflectometer

$U(t)$  – Unit-step response

$f_{Step}(t)$  – The low-pass time-domain step response

$\tau_d(0)$  – Group delay of a filter as frequency approaches DC

$x_r(t)$  – A ramp input signal as a function of time

$\varepsilon(s)$  – Difference between a two signal responses

- $\omega_c$  – Center frequency, typically of a band-pass filter
- $f_{BP}(t)$  – The band-pass time-domain impulse response
- $F_{BP}$  – Band-pass frequency response
- $F_{LP}$  – Low-pass frequency response-
- $f_{Imp}(t)$  – Analytic impulse response of a filter
- $F_g(\omega)$  – Time-gated frequency response
- $\Gamma$  – Reflection coefficient
- $T$  – Transmission coefficient
- $\hat{\Gamma}$  – Apparent reflection coefficient
- $S'_{11}$  – Reflection response relative to the line impedance
- $Z_{eff}$  – Effective impedance after normalizing for change in line impedance
- $Z_{line}$  – Line impedance
- $S_{11(eff)}$  – Effective reflection response after normalizing for change in line impedance
- $V^+$  – Forward voltage wave
- $V^-$  – Reverse voltage wave
- $BW$  – Bandwidth
- $T(j\omega)$  – Transfer response
- $D(s)$  – Denominator of transfer function
- $R$  – Resistance
- $C$  – Capacitance
- DUT – Device-under-test
- FTS – Filter tuning software
- $RN$  – The  $N^{\text{th}}$  resonator in a filter
- $C_{NM}$  – Coefficients of the resonator interaction matrix between resonators  $N$  and  $M$
- $\Delta f_n$  – Difference between the actual and the target frequency of the  $n^{\text{th}}$  resonator
- $\Delta f_n^*$  – Difference between the apparent and the target frequency of the  $n^{\text{th}}$  resonator
- $CN$  – The  $N^{\text{th}}$  coupling element
- GSM – Global System Mobile; European cellular phone standard
- ANT – Antenna
- dB – decibel, 20 times the common log of a voltage ratio (10 times for power ratios)
- $RXN$  – The  $N^{\text{th}}$  RX resonator
- $TXN$  – The  $N^{\text{th}}$  TX resonator
- LNA – Low noise amplifier

# Chapter 1 Introduction

## 1.1 Introduction

Electric wave filters have one of the longest histories of any modern electronic component. Despite this longevity, the importance of their role in modern systems remains undiminished. For many lower frequency applications, the form that these filters take is increasingly turning toward digital techniques. However, in the area of wireless communications, the nature and form of filters used today, especially those used for higher power applications, would be quite familiar to engineers of a half a century ago. One key change is that with increasing usage of the wireless spectrum, the filtering requirements are becoming ever more stringent, with less margin for error, and system and regulatory requirements are pushing filter requirements ever closer to the theoretical performance limits.

### 1.1.1 Analog and digital filters

Today, filters can be broadly divided into two general classes: digital filters and analog filters. With the advent of high speed Digital Signal Processors (DSP), low frequency filtering has been largely replaced with DSP techniques. However, for many wireless, high frequency and high power applications, analog filters remain the only practical implementation. Analog filters can be separated into several classes [1], such as passive filters with lumped components, active filters, and passive filters with distributed components. In large part, filters with lumped component design have been replaced with DSP technology, due to the fact that DSP speeds have increased past the point where elements can be considered lumped. Higher speed amplifiers have also allowed active filter designs to be used at intermediate frequencies, and Surface Acoustic Wave (SAW) filters are increasingly used at intermediate frequency (IF) and even low radio frequency (RF) ranges, when power loss and power handling are not an issue.

### 1.1.2 Applications of coupled-resonator filters

For high power or high frequency applications, passive distributed filters are used almost exclusively. Most of these filters can be sub-classified as coupled-resonator filters. Unlike low frequency filters, these filters are almost always doubly terminated in the system impedance. That is, these filters are designed and tuned to match the system impedance in the pass band. In a coupled-resonator filter, the center frequency of each resonator must be precisely tuned. The center frequency of the filter is set entirely by

the resonator tuning. The filter shape, such as bandwidth and return loss, is set entirely by the coupling. The couplings between resonators must also be precisely set to achieve the proper pass band response, low return loss (reflection), and small pass band ripple.

### **1.1.3 Filters used in wireless transmissions**

A key application of coupled-resonator filters is for receiver (RX) and transmitter (TX) signal separation. The TX filter must have low reflection, to avoid damaging the TX drive stage, and low loss to avoid excessive heating and loss of signal strength. The TX filter must have rejection in the RX portion of the band sufficient to avoid spurious signals from overpowering the desired RX signal. The RX filter must have high rejection of the TX signal to avoid saturation of the RX front-end. Both TX and RX paths must have good amplitude, phase and delay flatness to avoid distortion in modulated signals. This is increasingly important in wide-band digitally modulated signals.

Precise filter shapes can be determined which optimize tradeoffs between filter complexity, cost, and performance [2]. For the coupled resonator filters, much of the difficulty is ensuring that the final filter construction and tuning matches the designed filter attributes. A new approach to solve the problem of tuning and verifying that the filter has been manufactured to the proper design values is a key contribution of this thesis.

### **1.1.4 Filters used in frequency converters and multi-carrier power amplifiers**

For filters used in communications systems, the filter characteristics of importance may go beyond insertion loss and isolation. For example, in frequency converters, where filters are used to remove mixer image products, it may very important to have a flat delay response to avoid dispersion in the channel. Filters of these types typically follow some minimal phase or delay distortion characteristic, such as Bessel or Gaussian type [3], and require more stringent adherence to some pass band shape, with an accompanying increase in the difficulty of tuning.

For multi-carrier power amplifiers, the filter delay and absolute phase may need to be set to a particular value for use in feed forward or delay compensation networks. Current tuning techniques are a key bottleneck to achieving these exacting filter performance criteria while maintaining the high throughput needed in the growing wireless marketplace.

### **1.1.5 Filters using distributed elements**

High frequency designs often use low cost printed circuit board (PCB) elements, including distributed filters such as coupled-line filters. Even though in general the elements cannot be real-time adjusted, the performance of these filters is often limited by mistuning of the resonant elements and coupling values in these filters. Therefore, tuning methods that determine these values may be useful as an analysis technique in modifying the design of PCB filters for improved performance.

### **1.1.6 The need for filter tuning**

Limitations in manufacturing of these filters lead to the requirement that elements of these filters must be tuned or adjusted to create the desired transfer function. This tuning process is often the longest and most expensive step in the manufacture of filters, and typically requires very skilled technicians to accomplish the tuning. This thesis looks at filter characteristics in a new way with respect to aspects of their frequency and time relationship to lay a framework for a novel tuning technique. Several filter-tuning methods are presented and the attributes of each are discussed. This chapter provides a survey of published work in the area of filter tuning, automated filter tuning, and determining filter characteristics derived from measured responses. The methods used in each paper are outlined, and placed into context with other papers, and with the work presented in this thesis.

## **1.2 Current tuning methods for coupled resonator filters**

Coupled resonator filters require tuning due to mechanical tolerances in the manufacturing of the resonators and coupling. Tuning is required to achieve the proper pass band shape and center frequency. For filters with adjustable resonators, and fixed coupling, only the center frequency of the filter may be changed. The optimum, or tuned response of the filter is fixed by the coupling (for example, the pass band ripple). For filters with adjustable coupling, the filter shape and center frequency may be adjusted.

Resonator construction may limit the amount of tuning range available. Additionally, the construction will also determine if the resonators can be shorted, or if the coupling can be shorted. This in turn can affect the tuning method used. For example, some tuning methods require shorting one resonator while tuning another. Some resonator structures cannot be shorted, and do not have sufficient tuning range to allow mistuning the resonator far enough off frequency to consider it shorted. For filters of this type, tuning methods based on short-circuiting a resonator will not be successful. Re-

viewed below are various tuning methods for coupled resonator filters. These are tabulated concisely in table 1-1.

### **1.3 Tuning methods based on frequency response**

#### **1.3.1 Tuning based on amplitude response**

Possibly the first deterministic tuning method, a tuning based on amplitude response, was developed by Dishal [4]. This method requires that all resonators be de-tuned, or shorted, and that tuning be applied in a specific order. This method relies on a detector lightly coupled to the first resonator of a filter, and the realization that odd resonators present a high impedance to the input terminal (thus giving a large signal in the detector) and even resonators present a low impedance to the input (thus giving a small signal to the detector). Also, this method does not account for “pushing” of one resonator by tuning another. The effect of this pushing may be due to resonator coupling, or due to the physical implementation of the tuning mechanism. As part of the development of this thesis, a new methodology for dealing with frequency pushing is introduced in chapter 6. Dishal’s method does not allow for tuning of coupling factors.

#### **1.3.2 Tuning based on phase response**

Williams *et al* present a paper [5] on calculating the inter-cavity coupling by looking at the phase response of the filter. This describes tuning the first resonator for a symmetric response, then using the phase response to determine the inter-cavity coupling. It is based on the short circuit response of the filter. It counts upon tuning the resonators for symmetric response, then looking at the phase response to determine inter-cavity coupling factors. This is an evaluation method for inter-resonator coupling, which does not directly suggest a tuning method if the evaluated parameters are not the desired ones.

##### **1.3.2.1 Short-circuit tuning**

For filters that are singly terminated, Chen [6] proposes a tuning method that relies on the phase of a short-circuited filter reflection response. This work extends that of Williams, and applies it to waveguide filters. A significant contribution is handling the error introduced by the offset of the input aperture from the waveguide input. This method centers the phase of each resonator (tuning in ascending order) at the filter center frequency, and sets the phase angle of bandwidth of the filter by adjusting the cou-

pling between resonators. Thus, for each resonator, the phase increases by 180 degrees. This method can be related to Dishal's method by recognizing that Dishal's method relies on the resonators input impedance changing from high (open) to low (short) and realizing that it must also correspond to the reflection phase going from 0 to 180 degrees, as resonators are tuned in ascending order.

Atia presents a method [7] that extends his earlier work to create a tuning method based on the short circuit phase response of a network. This paper may be the most definitive paper on short circuit phase tuning of filters, and relies on the deriving the singularities of an all-pole function based on the phase response of the filter. This response configuration is based on the short circuit response of a filter, so some modification will be required to apply this to the case of a filter terminated in a matched impedance.

### 1.3.3 Tuning based on delay response

Recently, Ness proposed a new idea in filter tuning [8]. This method makes use of the group delay of the input reflection coefficient to determine the proper tuning of a coupled resonator filter. In this paper, the values for the group delay of the  $S_{11}$  are determined for a low-pass prototype. These values are then used to tune a band-pass filter having the same characteristics as the low-pass filter. The calculations are done for an low-pass prototype, and a band-pass consisting of alternating series and shunt resonators, and an inverter coupled resonator filter. The basis for this appears to be tuning the resonators for symmetric responses across the pass band, and then tuning the coupling for a specific value of group delay to set the coupling factor.

This tuning method appears to be closely related to Chen's method, if one recognizes that the phase bandwidth (the bandwidth or frequency separation between +90 and -90 degree phase points on the input reflection of a filter) is related to the group delay of the filter. That is, the phase difference (180 degrees) divided by the bandwidth is the same calculation as group delay. This method would seem easier than Chen's in that the  $\pm 90$  degree points do not need to be found, but only the group delay at the center frequency. Tuning for group delay essentially tunes the coupling factor. Ness's method for tuning resonators is essentially the same as Dishal's.

This method appears to require tuning resonators in a specific ascending order. Chapter 4 describes a time-domain method for tuning filters, and there may be an interesting correlation between the group delay response presented by Ness and the time-domain response.

### 1.3.4 Tuning resonators singly

Accatino presents a method [9] of tuning a coupled resonator filter by accessing resonators individually, and looking at the short circuit response of each in the context of what he calls an LCX network (lossless network including constant reactance). This method requires a filter structure in which resonators can be put in a “stand-alone” configuration.

The key measurement is extending the work of Williams and Atia [5], [10] which determined the singularities of a short-circuited network based on the phase response. This method is not suitable for a filter without a method for individually accessing resonators. This paper does address the case of a multi-pole filter where individual resonators are not accessible, for example, it does address the issue of multiply coupled filters for the 6 pole case presented. But the tuning is done individually, and may only be applicable in filters such as waveguide filters where they resonators may be reasonably disassembled. At the 4-pole stage of assembly, a “pattern search optimization” is noted as being used to set the de-tunings of each resonator, but no further information is given on the pattern search methods.

## 1.4 Model matching and optimization methods

The methods above rely on knowledge of the input response of a filter, and correlate a measurement (amplitude, phase or delay) to some aspect of the input response (high and low impedance points, for example). Other methods of tuning rely on optimization techniques to provide a fit between a measured response of a filter, and a simulation model of the filter, or even more generally, create an error function, and a mathematical formulation that generates a relationship between tuner settings and an error function. Some of these methods are described below.

### 1.4.1 Optimization based on models

One of the earliest papers on using optimization of models is from Thal [11] which describes using an Automatic Network Analyzer (ANA) to make measurements on filters, transferring the data to a computer program, then fitting the best circuit-model response to the measured parameters. There are no details on the fitting methods, and the model for the circuit responses is a simple resistor-inductor-capacitor (RLC) model with mutual coupling between and across resonators. Examples are given for a 6-pole and 4-pole filter. Information is provided on calculating sensitivity of tuning element changes. This is not a real-time procedure (limited by computing power available and

measurement instrument speed) but does provide an early example of using computer techniques to address the filter tuning process.

Ishizaki, *et al*, presented a paper [12] describing an optimization procedure for tuning resonators of cellular band filters. In this paper, an error function was derived from the difference between  $S_{11}$  and  $S_{21}$  modeled and measured results. The paper appears to assume the resonators have identical  $Q$ , and the coupling between resonators is fixed. There is some discussion of calculating the  $Q$  and coupling based on a single resonator measurement, and determining the correct reference plane for calculating something he refers to as admittance slope. His method appears to make several calculations with different coupling capacitances. For each capacitance, the reference plane is varied (presumably using port extensions in the network analyzer) and a curve is drawn. By overlaying the curves, he finds one position of reference plane where all curves cross. He refers to a paper by Kajfez [13], which provides the extraction of  $Q$  factor and coupling based on the admittance slope.

The tuning is achieved by optimizing a model to minimize the error function, and then reading the resonant frequency of the resonators based on the model. This is compared to the desired resonator frequency, and displayed as a normalized frequency. The filter resonators are then trimmed according this estimated frequency, and the process is repeated. This process does not appear to handle the cases of adjustable coupling, nor does it handle cross-coupled resonators. Also, it relies on a good model of the filter. It is not real-time (as the optimization process is the limiting factor). However, its chief advantages are it does not require any prescribed tuning order, the filter can be properly terminated, and it can start with a filter that is partially tuned. This is not the case with the previous methods discussed.

#### 1.4.2 Other optimization based tuning

Kahrizi, *et al* recently presented a paper [14] that describes using a filter modeling approach, which uses model-based parameter extraction to locate the zeros of  $S_{11}$  and  $S_{21}$ . These values are used in a multi-level modeling approach to generate element values for a model of the filter under test. A mapping of the determined values with the desired valued is obtained.

What is interesting here is in the determination of loop equations of matrix form that relate the offset from center frequency of each resonator, and the coupling between desired resonators, which may be a useful representation for evaluating filter tuning. This paper assumes defects of the filter tuning in the form of noise effects and coupling per-

turbations. Unfortunately, no results were shown for real filters, only mathematical models of filters. The paper did not discuss the real world effects such as multiple undesired coupling, and resonator detuning due to coupling tuning. Neither these effects, nor the their consequences on the tuning method are discussed.

### 1.4.3 Sensitivity based tuning

Marshall and Tissi present an algorithm [15] developed for a sensitivity analysis of the network response with respect to the adjustable elements, and does not require knowledge of the network model. They point out that a fault of model-based algorithms is the limit of being able to derive a network model in which all adjustable elements are accurately represented. This refers to the fact that particular tuning elements may affect several parameters at once. A good example of this is a metallic coupling screw, which is used to short-circuit electric field coupling in a coupled resonator filter, that can also affect the shunt capacitance of the adjacent resonators, thus affecting the resonator tuning. The method presented uses a sensitivity analysis of the measured network to adjustable elements in terms of a defined error function. The key aspect of this method is in casting the problem as an optimization problem, where one portion of the solution is determining the sensitivity responses of individual tuning elements. This method has been demonstrated on several filters, but only in the case where they are partially aligned. Also, one step requires the adjustment of each element over a range of settings to determine a sensitivity function, which would not be practical for many filter implementations, such as ceramic or dielectric resonator filters. This work appears to be very general, and does not require complex test equipment (for example, they use a scalar network analyzer).

Yu *et al* present a paper [16] that describes different optimization algorithms and their effectiveness in obtaining a solution, with the focus on a technique called Simulated Annealing. This paper relied on computer modeling instead of experimental tests, and essentially compared different search algorithms. They cited using an in-circuit element measurement or other parameter identification techniques to determine actual parameter values, but gave no details. It was assumed that filters were constructed of fixed capacitors and tunable inductors. The problem to be solved was tuning the inductors to get a desired response given a spread of 2% in the capacitor values. Thus, in some ways, this was a synthesis problem and not a tuning problem (synthesize a set of inductors which with the given capacitors, provides the desired frequency response). This paper does not address the problem presented by microwave filters of not knowing

the effective values of the elements, but rather, assuming that the element values are knowable, presents an optimization technique to generate proposed tuning values to satisfy a prescribe tuning result. This might be more applicable to a design phase of a microwave filter.

In a recent paper by Harscher and Vahldieck [17], a technique using both optimization and sensitivity analysis of tuning elements versus an model was presented. In this paper a tuning procedure is described which consists of pre-tuning a filter to a basis position, and measuring the filter response. From this response element values are extracted, using optimization to match to a model. Next sensitivity of each element in the model determined for each tuning screw by measuring the response and extracting the values as each tuning screw is singly adjusted. This allows interactions such as coupling screws affecting resonator tuning to be captured. The tuning screw positions are adjusted and values are again extracted to allow an analysis of the tuning screw position to model element correspondence. Finally, the tuning screw positions for proper tuning are calculated and the screws adjusted. If this does not yield a sufficiently good result, the process is repeated. This method has the distinct advantage of accounting for actual interactions between tuning screws and each filter element. However, the experimental results were provided only for a 3-pole coupled resonator filter. While the results showed the filter could be tuned, one might question the extraction and model-matching optimization process efficacy for higher order filters or filters with cross-coupling. Tuning times quoted for a 3-pole filter were 5 minutes, but there is no suggestion of how one might extrapolate tuning times to more complex filters.

In a follow-up paper, Harscher, Vahldieck and Amari [18] provided additional experimental examples for 4 and 6-pole filters with cross coupling, but without the details of tuning time or accuracy when compared to the desired prototype response.

#### 1.4.4 Tuning methods using fuzzy logic

Recently, a new technique for tuning filters employing fuzzy logic has been presented by Miraftab and Mansour [19]. Fuzzy techniques differ from normal optimization techniques in that they do not need to compare circuit model characteristics directly to measured results, but rather, can have an *inference system* that maps input fuzzy sets to output fuzzy sets. The input sets come from a *fuzzifier* that maps the crisp input numbers into fuzzy sets. Combinations of these inputs are passed through the inference system, which produces output results based on logical rules set for combining the fuzzy inputs. The inputs are measured results and the desired output is a coupling

matrix in the form described by Atia [2]. Comparing this to the desired matrix will yield a tuning method that identifies mistuned elements. The results described give approximately (within 5%) correct values for the matrix elements, but from the results presented, it does not appear that this method would be successful for final tuning of filters, as the errors in extracted elements would not enable sufficient accuracy in tuning filters. Also, this paper uses only simulated results, so the errors associated with spurious cross-couplings and system noise are not accounted for. Still, it might be an interesting technique when combined with other techniques, including using the time-domain response as one of the inputs to create the fuzzy sets.

#### **1.4.5 Rational-polynomial-function fitting techniques**

A recent improvement in optimization techniques was presented by Ibbetson [20] where measured data was fitted to rational-polynomial functions. Band-pass filter data is translated to a low-pass prototype response, and matched to rational-polynomial functions that are allowed to have complex coefficients to account for non-hermitian low-pass functions. This technique has advantages of being over-determined in the solutions for the polynomial coefficients, based on the frequency response data taken. Thus, effects of noise are reduced in the process of least-squares-fit calculation of the polynomial coefficients. More recently, Ibbetson presented newer results [21] where the order of the polynomial functions is increased by one for both numerator and denominator, allowing a much closer fit to the measured data. The resulting pole-zero diagrams show one pole-zero pair that are quite close together, and typically far away from the filter center frequency, but allow for a better fitting to occur. This technique appears to be well suited to the problem of cascaded triplet filter configurations used by Ibbetson's company, Filtronic PLC. This technique has some limitations which include the fact that the polynomial function is only an approximation for distributed filters found at microwave frequencies, measurement error and noise can lead to difficulty in extracting coefficients, and limitations of the filter manufacturing can mean that it is not possible for a given filter to match the desired rational-polynomial function due to the inability to tune some elements, such as the input and output coupling elements.

#### **1.4.6 Fully robotic tuning**

The goal of providing a fully automatic robotic tuning application was demonstrated by Wu at a recent conference [22] showing a tuning process for a duplex filter. The techniques used for tuning were not revealed, but stated to include combinations of

coupling matrix extraction, time-domain cloning, and phase cloning. The results showed an average tuning time of about 30 minutes for an 8-pole filter with two cross-couplings. This can be compared with the results of this thesis in the case study of chapter 7. Interesting aspects of this paper include the details on tuning screw selection and locking, as a part of a practical manufacturing tuning system.

#### **1.4.7 Performance criteria for filter tuning**

Since various tuning methods have been described for tuning coupled resonator filters, it is natural to compare the various methods. Jervis presents a paper [23] that compared some optimization techniques, and provides criteria for comparisons. However, this paper was written with respect to low frequency filters, and does not account for a range of difficulties presented with microwave filters, some of which are described below.

The criteria for evaluating filter-tuning methods will depend upon the structure of the tuning element, and how the tuning is accomplished. For manual (human) tuning, the response of any tuning indicators must be updated with sufficient rapidity such that the tuner will not overcompensate while waiting for an update. Experience, and discussions with manufacturing managers of several well known filter companies, indicate that about 0.25 seconds is the maximum acceptable cycle time for human tuning. For machine (automated) tuning, the cycle time is not important, but longer cycle times can limit the speed benefit of machine tuning. A major difficulty to overcome in machine tuning is hysteresis effects in the tuning elements. These tuning elements, typically screws, can have backlash, and the grounding point of the screw can change. This causes discrete discontinuities in the tuning response of these screws, and the nonlinear behavior can cause machine-tuning programs to fail. For example, when turning a screw in, the grounding is on the bottom of the thread, but when turning the screw out, the grounding can be on the top. Thus there can be a discrete change in the resonator tuning with no change in the screw position. Humans can account for this without difficulty, but machines must be programmed to look for such discontinuous responses. A tuning criteria that assumes perfect tuning elements is not a realistic criteria for determining the best algorithms to use on a manufacturing floor.

The table presented below summarizes the various tuning methods described above:

<b>Table 1-1: Summary of Filter Tuning Methods</b>				
<b>Filter Tuning Method</b>	<b>Ref.</b>	<b>Date</b>	<b>Author</b>	<b>Notes</b>
<b>Amplitude Response</b>	4	1955	Dishal	Prescribed tuning order, interactions not accounted for, requires additional probe port.
<b>Phase Response</b>	5	1983	Williams	Good for inter-cavity coupling
<b>Phase Response – Short circuit tuning</b>	6	1977	Chen	Requires short circuit, prescribed tuning order, interactions not accounted for
<b>Phase Response – extracting pole/zeros</b>	7	2000	Atia	Requires short circuit at output, no tuning order needed, cross coupling solution not shown, commented on
<b>Delay Response</b>	8	1998	Ness	Prescribed tuning order, similar to Dishal's, does not account for interaction, cross coupling
<b>Optimization</b>	9	1986	Accatino	Optimizes a model to match a response
<b>Optimization</b>	11	1978	Thal	Optimization to extract model element values
<b>Optimization</b>	12	1990	Ishizaki	Applied to a small number of resonators, no coupling tuning.
<b>Rational Function</b>	14	2000	Karizi	Optimizes a pole/zero model to match a response
<b>Optimization-Sensitivity based</b>	15	1991	Marshall	Optimizes on performance goal, model independent, treats tuners as unknown inputs to the optimizer
<b>Optimization /Synthesis Simulated Annealing</b>	16	1996	Yu	Synthesis technique to account for component difference; new set of L values for given variations on C
<b>Optimization/ Sensitivity</b>	17	2001	Harscher	Using optimization and sensitivity to match models to tuning position
<b>Sensitivity</b>	18	2001	Harscher	Same as above, extended to cross-coupled filters
<b>Fuzzy Logic</b>	19	2002	Miraftab	Uses Fuzzy logic to extract coupling matrix values
<b>Rational Function</b>	20	2000	Ibbetson	Optimize coefficients of rational functions to fit measured data
<b>Rational Function</b>	21	2002	Ibbetson	Extend above by increasing the order of rational functions used
<b>Multiple/ Robotic Tuning</b>	22	2003	Tang	Use multiple methods in a commercial robotic tuner

## **1.5 Limitations of current tuning methods**

Each of the previously described methods suffers from limitations that render them less than optimal for filter tuning applications. Some require a specified order of tuning filter elements, or require extensive computation (in the form of optimization) to determine the status of tuning elements. The interactive nature of coupled-resonator filters makes it difficult to determine which resonator or coupling element needs to be tuned. While most of the tuning methods described above can achieve approximately correct filter responses, final tuning often requires the seemingly random adjustment of each element until the final desired filter shape is obtained.

The solution to these difficulties would be a tuning method that is simple, flexible and deterministic, where the individual adjustment goals for each tuning element would not depend upon the other elements in the filter. The response to each tuning and coupling screw would be immediately seen and accounted for. Ideally, each tuning screw would only need one adjustment. This thesis details a solution approaching that ideal, and provides a theoretical justification for the results demonstrated.

## **1.6 New contributions to filter tuning**

An entirely new tuning technique, using the vector network analyzer (VNA) time-domain response of a filter, is the core topic of this thesis. In 1999 the author presented a novel filter tuning method [24], [25], [26] based on the time-domain response of a filter. References [25] and [26] are included at the end of this thesis as published papers 1 and 2, respectively. The technique, which was empirically developed, describes a method of tuning coupled-resonator filters by looking only at the time-domain response using the built-in time-domain function of a VNA

The first filter for which the time-domain response was documented was a 5-cavity all-pole filter. The filter was being tuned in the frequency domain on one channel of a VNA while the time-domain was active on another channel, for the purpose of evaluating the effect of enhanced CPU speed on overall tuning response. Activating the time-domain function, which requires significant CPU time, posed a good challenge to the new CPU. During this testing, the author noted that turning a tuning screw on the filter caused a change in just one portion of the time-domain trace, and turning a different screw caused a change at a different point. It appeared that the time-domain trace could separate the effects of the tuning screws, whereas the frequency response showed no

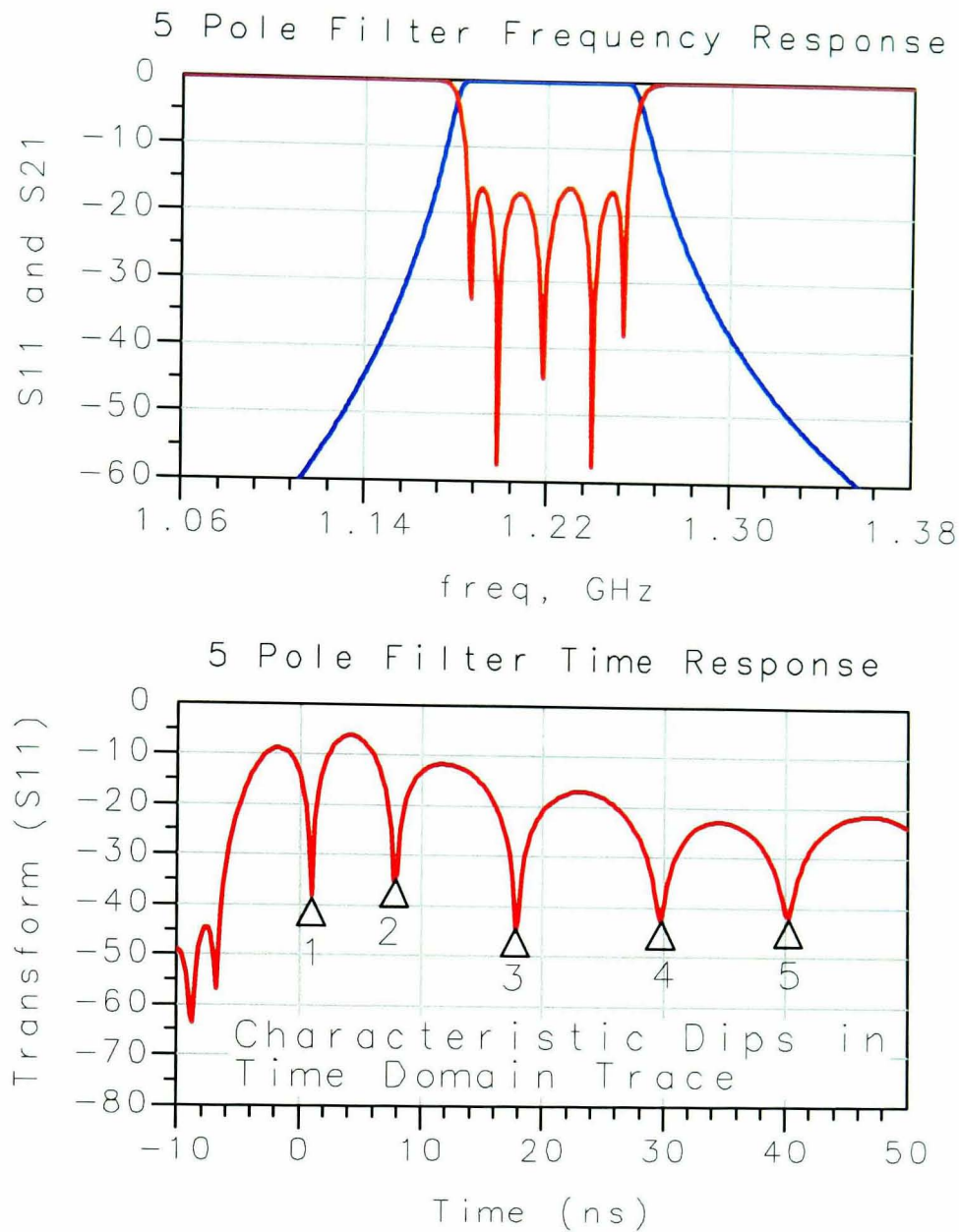


**Figure 1-1: Frequency response (S21 and S11) of a 5 pole filter (upper plot) and time-domain response of S11 (lower plot).**

such direct cause-and-effect relationship. An example is shown in figure 1-1, with the frequency response of  $S_{11}$  and  $S_{21}$  in the upper plot, and the time-domain (band-pass mode) shown in the lower plot. Note the characteristic dips in the time-domain plot, as indicated by the markers.

This effect is illustrated in figure 1-2, where only the tuning screws associated with second and third resonators have been individually adjusted. The upper plot shows the frequency response of the filter with only resonator 2 mistuned (in the blue), and only resonator 3 mistuned (in the green). The original response is shown in light red for reference. The lower plot shows the time-domain response, for the same conditions. Note that in the case of mistuning only the second resonator, leaving all other resonators untouched, the time-domain response is nearly unchanged near marker 1, but the null in the time-domain response near marker 2 is very distinctly changed. The nulls past marker 2 are affected as well, but to a somewhat lesser amount.

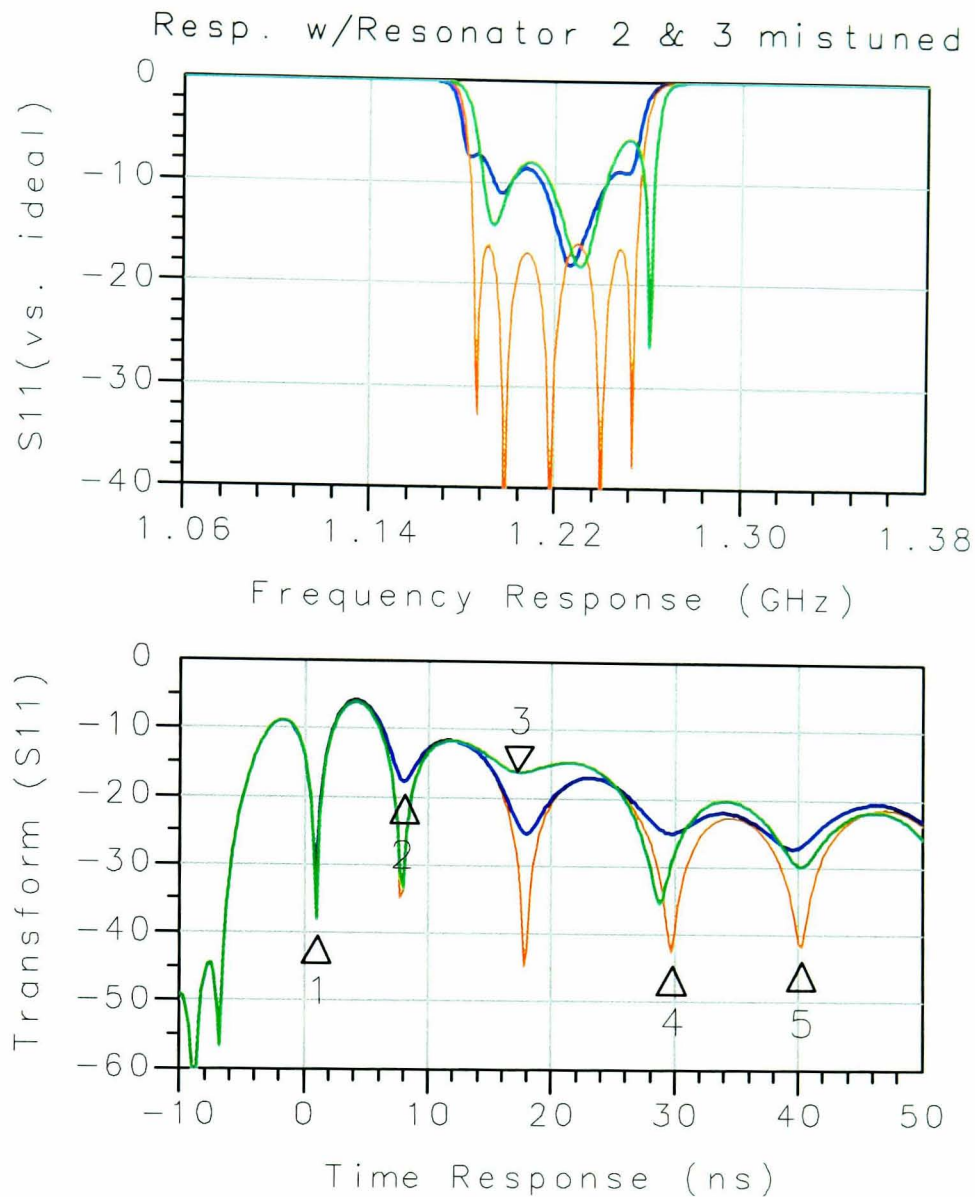


**Figure 1-2: Frequency (upper) and time-domain (lower) response with resonator 2 (blue) and resonator 3 (green) individually mistuned respectively**

For the case of mistuning only resonator 3, note that the time-domain trace is not changed near marker 1 or marker 2. Only the null near marker 3 shows a distinct change. Thus, it appeared that the tuning screw adjustment was in some way linked to the associated nulls in the time-domain. Finally, if the mistuned resonator was adjusted while monitoring the associated null, and tuned until the null was deep, the filter frequency response would show that a properly tuned filter results.

Further investigation demonstrated that coupling screws also had a distinguishable effect on the time-domain response, resulting in a complete tuning method for all-pole filters using the time-domain response. What is remarkable and unexpected about this new technique is that for these filter types, the filters may be optimally and deterministically tuned looking at only the time-domain response.

Much investigation and extensions beyond the previously published work has been undertaken, resulting in even newer techniques that takes advantage of aspects of time-domain gating, and two U.S. patents have been granted for this new tuning method, fi-

nally resulting in a commercial filter tuning software program that has been created based on the techniques developed for this research and presented in this thesis. This thesis documents the investigation into the time-domain response of filters, and the steps taken to build a theoretical basis to explain the reported time-domain effects.

## **1.7 Outline of the present work**

In the discussion of filter tuning and filter response verification, it is helpful to collect the important and appropriate results from the vast amount of work on filter theory and transform theory to support the proposed new ideas. Chapter 2 and chapter 3 contain these results, organized in such a way as to provide a sufficient background for the material in the chapters that follow. The following outlines the flow of this thesis.

Chapter 2 develops the results from transfer functions, filter theory and Laplace transform theory, as applied to all-pole filters. In particular, the frequency response and time response are defined for use later. The results presented represent a small but key fraction of the concepts of filtering, which will be referenced in the chapters that follow. This chapter also provides the reference for applying the filter theory results to the case of microwave filters, and introduces some of the special details that are important in measuring and tuning microwave filters. Those skilled in the art of filter design and network theory will find the material in chapter 2 is substantially review.

Chapter 3 departs from filter theory to introduce Fourier transform theory and the relationships between the DFT, FFT, and data sampling, as well as introducing the Chirp-Z transform. It provides for the first time a detailed analysis of the Vector Network Analyzer (VNA) time-domain low-pass and band-pass transforms, including gating and windowing. A key point to note is that the VNA time-domain transform differs significantly from the analytically derived impulse (time) response of a filter. Importantly, this difference is shown in later chapters to be the key factor which makes time-domain filter tuning work. New work is presented in area of the effects of time-domain gating and masking, and compensation for these effects, as well as uncertainty estimates. Time-domain gating will be cited in chapters 6 as an important enhancement to the time-domain tuning method

Chapter 4 presents a complete description of the time-domain tuning method briefly outlined earlier in this chapter. This description includes experimental and empirical

results from simulations and measurements on filters. The empirically derived techniques are applied to all-pole filters with some extensions to filters with cross-coupled resonators as well. The tuning method described here is done entirely by looking at the time-domain response (with the exception of setting the transmission zeros of cross-coupled filters). The examples shown in this chapter include real filters as well as the response from simulated filters. Practical considerations, including the effects of loss, are included in the discussion. Some of this material was first introduced in a peer-reviewed conference paper [25] written by the author.

Chapter 5 presents the results of work to determine a theoretical underpinning supporting the novel idea of tuning filters in the time-domain. This chapter provides a rigorous mathematical relationship between VNA time-domain response of a simple filter, and the analytic impulse (time) response. A mathematical argument is presented which shows that the time-domain results observed in experiments can be directly correlated to the filter transfer functions and the specific effects that differentiate the VNA time-domain transform from the analytically derived time-impulse response, as outlined in Chapter 3.

Chapter 6 of the thesis includes previously unpublished work that is the basis for two U.S. patents, as well as the key technology used in the development of a commercial filter tuning software program. This chapter uses the new material on time-domain gating and masking developed in Chapter 3, to show that the masking effect is a key source of the apparent interactions that make filter tuning so difficult. A superior method for filter tuning, which using time-domain gating on the  $S_{11}$  response of the filter is introduced, and shown to be a key improvement for developing automated tuning techniques.

Chapter 7 describes the details of a software application for filter tuning utilizing the work of chapters 4, 5 and 6. Many practical aspects of filter tuning and human interface issues are discussed. A new method for determining and compensating the interactions between resonators is presented, and detailed examples showing improvements from resonator compensation are presented. One example demonstrates nearly ideal deterministic tuning of an 8-resonator all-pole filter utilizing this software. The time required to tune this filter, which has adjustable couplings and resonators and which experienced tuners could adjust in 15 minutes, is reduced to less than 3 minutes using

the filter tuning software. Limitations or difficulties in applying the time-gated tuning are discussed, and a method using phase pre-tuning is presented to overcome these difficulties. Important user-interface aspects of the filter-tuning program that affect tuning time are also presented. A case study of applying the filter tuning software method to a complex filter type, a duplex filter with 8-poles and two cross-coupling on each side, is described.

Chapter 8 concludes by describing areas for extension into other filter types (such as filters with strong cross-coupling and closely spaced duplex filters). Limitations of the new tuning method are discussed for several filter types. From this general guidelines for the successful application of the new tuning method to various filter types are presented, along with other conclusions of this thesis.

## Chapter 2 Filter Fundamentals

### 2.1 Transfer functions and Laplace transforms

The new work presented in this thesis relies on previously unknown relationships between the frequency response and time-domain response of filters, under certain conditions. As described in the introduction, a primary purpose of a filter is to pass signals from the input to the output, applying a desired change to the signals. For convenience the response can be described as the collection of changes that occur to any particular single-frequency sinusoidal signal, where the change is different for different frequencies of input signals. This is the well know frequency response of a filter, and can be determined experimentally by applying a sinusoidal signal to the filter input, and measuring the response of the output, comparing the magnitudes and phase of each, and is repeated for as many frequencies as desired.

The most common filtering function is to pass some signals with little or no attenuation over a defined pass band, and to attenuate signals over a defined stop band. A transfer function is the function that describes the relationship between the input and output signals. Plotting the magnitude of the transfer function on a log/log scale yields the familiar Bode Plot. If the input signal is represented by

$$X(\omega, \theta) = |X| \cos(\omega t + \theta) \quad (2.1)$$

and the output signal is represented as

$$Y(\omega, \theta) = |Y| \cos(\omega t + \phi(\theta)) \quad (2.2)$$

then the transfer response of the filter is defined as

$$Y(\omega, \theta) = H(X(\omega, \theta)) \quad (2.3)$$

For linear, causal, time invariant networks (the response of which depends only on the frequency of the applied signal), the output signal is linearly related to the input signal, and time shifting the input signal causes a similar time shift in the output signal [27]. Mathematically, we can write this as:

$$Y(\omega) = H(\omega) \cdot X(\omega) \quad (2.4)$$

and it follows that the frequency response can be defined in terms of the input an output signals as

$$H(\omega) = \frac{Y(\omega)}{X(\omega)} \quad (2.5)$$

Note that the input and output signals may be defined to be voltages, currents, powers or other signal attributes that are desired. This definition of a transfer function is particularly useful in that the frequency response of a network may be determined by measurements of output response signal and the input stimulus signal, and many measurement instruments, such as Vector Network Analyzers (VNAs) provide such signals and measurements. The definition of the particular signal attribute determines the particular transfer function. For example, input impedance is the transfer function of the current measured at the input in response to the voltage applied at the input. An alternative transfer function, the reflection coefficient, is related to the power reflected from the filter as a function of the power incident to the filter. For filters such as waveguide filters, this transfer function is more useful than the input impedance, where voltage and current may be ambiguously defined.

The above provides a quantitative result in describing a filter response based on measurements of the responses of sinusoidal signals. We will see below that the theoretical analysis of filters is made more convenient using sinusoidal analysis as well, and the frequency response function described by measurements above is exactly analogous to the transfer function derived by mathematically analyzing the network, as described below.

### 2.1.1 Frequency response of a network expressed as a transfer function

The use of sinusoids to define a measurement of a filter can be traced to the wide range of analyses that have been applied to the field of electric circuits and networks. Introductory circuit theory [28] provides the basic nomenclature and symbols for representing signals and transfer functions. Sinusoids are represented by complex notation as follows:

$$a(t) = |A| \cos(\omega t + \theta) = \text{Re}[Ae^{j\omega t}], \quad (2.6)$$

where  $A = |A|e^{j\theta}$ , and  $j\omega$  is sinusoidal frequency

For convenient computation, signals are represented by  $Ae^{j\omega t}$ , and it is understood that only the real parts of this signal are to be considered.

A transfer response function defined as equation (2.5), and with input and output signals of the form in equation (2.6), will have the form [29]

$$H(j\omega) = |H(j\omega)| e^{j\phi(\omega)} \quad (2.7)$$

with an amplitude response that depends upon frequency, and a phase response that also depends upon frequency. Together these comprise the frequency response of the network.

In filter analysis, the frequency response is often represented by the more general transfer response,  $H(s)$  with  $s$  representing the complex frequency  $s = \sigma + j\omega$ , and where the special case of  $s = j\omega$  ( $\sigma = 0$ ) represents the frequency response, as described by the Laplace transform below.

The Laplace transform provides a useful representation of the transfer function. If the input signal is of the form  $x(t)$ , and the output signal is  $y(t)$ , then the input signal can be represented by  $X(s)$  in the complex frequency domain, and the output signal by  $Y(s)$ , where  $X(s)$  and  $Y(s)$  are the Laplace transforms of  $x(t)$  and  $y(t)$ , respectively. The Laplace transform [30] is defined as

$$\mathbf{L}(f(t)) = \int_{-\infty}^{\infty} f(t) e^{-st} dt \quad (2.8)$$

and is the two-sided Laplace transform. For functions which are causal, the one sided Laplace transform is used, where the lower limit of integration is replaced by a 0. Looking at the previous definition of the transfer function, rewritten now as  $Y(s) = H(s) \cdot X(s)$ , we can see that if  $X(s)$  is identically 1, then  $Y(s)$  is identical to the transfer function  $H(s)$ .  $X(s) = 1$  is equivalent to applying all frequencies to the input of the filter, with uniform amplitude and zero phase. The resulting output signal determines the transfer function. This is in fact what a vector network analyzer attempts to do in characterizing RF filters.

The Laplace transform is valid for a large variety of signals, both sinusoidal and transient. Additionally, the Laplace transform provides a convenient method for solving problems involving transient input signals  $x(t)$ . If  $H(s)$  is known, then the output signal for any input signal can be computed by simply taking the Laplace transform of  $x(t)$ , multiplying by  $H(s)$ , and taking the inverse Laplace transform of the resulting  $Y(s)$ .

An alternative definition of the transfer function to that represented by the frequency domain in equation (2.7) can be derived. If  $h(t)$  is defined as the inverse Laplace transform of  $H(s)$ , then it follows that [31]

$$y(t) = \int_0^t h(\tau) \cdot x(t - \tau) d\tau \quad (2.9)$$

or

$$y(t) = h(t) \cdot \text{conv} \cdot x(t) \quad (2.10)$$

For the case of a stimulus  $X(s) = 1$ ,  $x(t)$  is the unit impulse function  $\delta(t)$  [32]. The response  $y(t)$  can be determined from the definition of convolution, with the result  $y(t) = h(t)$ ; thus  $h(t)$  is called the impulse response or time-domain response of the network.

For RF filters there are two important transfer functions: input response, and transmission response. The input response may be viewed as the input impedance, reflection coefficient, VSWR, etc. depending upon the definition of the input and output signals. Likewise, the transmission response may be the voltage transfer function, the current transfer function, power transfer function, etc. These functions may be derived mathematically, if the network construction is known, from the network equations that describe the response of the network to sinusoidal responses. This is the analytically calculated transfer response or frequency response.

### 2.1.2 Relationship between Fourier transform and Laplace transform

The Fourier transform, defined as [33]

$$\mathbf{F}(f(t)) = F(\omega) = \int_{-\infty}^{\infty} f(t) e^{-j\omega t} dt \quad (2.11)$$

is a special case of the Laplace transform, with  $s = j\omega$ , provided that the  $j\omega$  axis is in the region of convergence of the Laplace transform [34]. There are some limits on the functions that are Fourier transformable, but in general these are functions for which

$$\int_{-\infty}^{\infty} |f(t)| dt < \infty \quad (2.12)$$

Even functions for which this integral does not exist may be transformable in the limit, with some very useful functions among these, such as a sine, cosine and  $U(t)$  [35]. This limitation is in general not applied to the Laplace transform, which has the extra

exponential portion  $e^{-\sigma t}$ , and which makes Laplace transformable those functions which are of exponential order [36]. The inverse Fourier transform can be defined (see equation (3.2)) , and represents the time-domain response of that signal. If  $H(j\omega)$  is the frequency response of filter, then  $h(t) = \mathbf{F}^{-1}(H(\omega))$ . The time-domain impulse response calculated from the inverse Fourier transform is identical to the impulse response described above for the inverse Laplace transform of  $H(s)$ .

Thus, to describe a filter function, it is sufficient to describe the frequency response  $H(j\omega)$ . However, it is often more convenient to use the transfer function  $H(s)$ . While either the transfer function or the frequency response of a network can be calculated directly from the network equations, synthesis techniques that are used to create a network with a specified frequency response are more readily adapted to the transfer response  $H(s)$  [37]. The relationship between the Fourier transform of a network, and the VNA time-domain transform will be discussed at length in Chapter 3.

### 2.1.3 Transfer functions viewed as pole-zero responses

Transfer functions  $H(s)$  for a network may be represented in the form

$$H(s) = \frac{c(s-s_1)(s-s_3)(s-s_5)\cdots}{(s-s_2)(s-s_4)(s-s_6)\cdots} \quad (2.13)$$

where  $c$  is a real constant and  $s$  is the complex frequency variable  $s = \sigma + j\omega$ . Circuits constructed of lumped elements will have a finite number of poles and zeros. Circuits constructed of distributed elements require an infinite product of poles or zeros to represent the associated transcendental functions [38]. This thesis will be limited to the case of lumped or quasi-lumped element analysis. As such, all derived transfer functions will be of the form in equation (2.13).

The magnitude of the frequency response  $|H(j\omega)|$  may be obtained from the transfer response by

$$|H(j\omega)|^2 = H(s) \cdot H(-s) \Big|_{s=j\omega} \quad (2.14)$$

Alternatively, the transfer function may be obtained from the frequency response by replacing  $\omega^2$  with  $-s^2$ , factoring the numerator and denominator, and identifying the left half plane (LHP) poles with  $H(s)$  [39].

### 2.1.4 Hurwitz Functions

Finding  $H(s)$  from  $|H(j\omega)|$  does give some degree of freedom in choosing  $H(s)$ . Choosing zeros in the LHP ensures a minimum-phase function [40]. For a filter to be realizable, the transmission response poles must be in the LHP or lie on the  $j\omega$  axis.

Additionally, if  $H(s)$  is a rational function in the form of equation (2.13), it is possible to use partial fraction expansion to put  $H(s)$  in the form of

$$H(s) = \frac{A}{(s-s_2)} + \frac{B}{(s-s_4)} + \dots \quad (2.15)$$

which is more easily transformed into the time-domain through the inverse Laplace transform. A special class of filters, called all-pole filters, are described by functions in the form of (2.13) where the numerator contains only a constant, that is, where the function has no zeros except as  $s \rightarrow \infty$ . While the transfer function can be of arbitrary complexity, many very important filtering functions can be achieved while limiting the transfer function to all-pole functions.

## 2.2 Low-pass transfer functions

### 2.2.1 All pole networks

All-pole networks can be synthesized using lumped elements through the transfer function by using standard techniques [41]. These networks will lead to Low-pass transfer functions. For all-pole responses, it is sufficient to study low-pass functions, as additional transformations can be applied to the networks to generate band-pass functions [42]. Additionally, though these low-pass networks are normalized, they may be scaled to any frequency and input impedance.

An interesting point [43] is that more than one set of element values can realize the same transfer function, based on the fact that reflection coefficient zeros are not unique. All pole networks result from having one reactive element in each arm of a ladder network. Low-pass all-pole networks have inductive series elements and capacitive shunt elements. The all-pole design can place reflection zeroes in either the LHP or RHP, yielding different filter elements that realize the same transfer function. Choice of the element configuration (series first element or shunt first element) determines the configuration. The low-pass filter in figure 2-1 has a shunt first element, and as such will have an impedance with tends to 0 as  $\omega \rightarrow \infty$ . A filter with a series (inductive) first element creates an input impedance that tends to  $+\infty$  as  $\omega \rightarrow \infty$ . Both filters will have

the same  $V_{out}/V_{in}$  transfer function. However, when these low-pass prototypes are transformed into a specific configuration of band-pass filter, such as the coupled-resonator filter using capacitive coupling, this degree of freedom will be constrained.

The filter transfer function is controlled by the element values. For a given filter bandwidth, many filter factors may be traded off. Among these are filter flatness (in some sense), cut-off, return loss, phase response and group delay response. Some common filter functions with the attributes that are optimized are listed below.

### 2.2.1.1 Butterworth

Butterworth, also known as maximally flat response, optimizes the filter response in the sense that  $n^{\text{th}}$  order derivatives at  $\omega = 0$  are zero, where  $n$  is the number of elements in the filter. The values can be found by using a Taylor approximation of transfer response and making  $n^{\text{th}}$  order terms of the Taylor error function expanded about  $\omega = 0$  go to zero [44].

### 2.2.1.2 Chebyshev

The Chebyshev response is also known as the equal ripple response. This response minimizes the deviation of a function over some interval. The Chebyshev polynomials possess the equal ripple property, and coefficients for these may be found using a recursive formula [45]. The Chebyshev filters trade off maximum flatness for steeper stop-band slope. Many filters designed for RF work are based on an equal ripple response.

### 2.2.1.3 Bessel

The Bessel response generates maximally flat group delay response. This is flat in the sense that the first  $2n - 1$  derivatives of the filter delay are zero at  $\omega = 0$  [46]. This

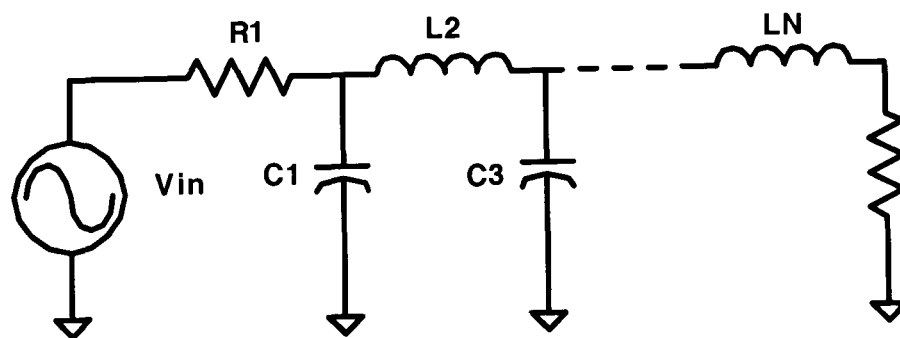


Figure 2-1: Low-pass Filter with a series first element

filter is commonly used in the design of RF amplifiers where feed-forward or other techniques are used to create better non-linear response. In these cases, it is important that the delay of the filter be constant over some specified bandwidth.

### **2.2.2 Networks with poles and zeros**

Though the focus of this thesis is on all-pole networks, equation (2.13) indicates that the transfer response can have zeros as well as poles. Properly placing these zeros in the stop band of the filter can result in steep filter skirts without much compromising the pass band results, or zeros can be used for delay compensation [47]. Examples of these filter types are the elliptic or Cauer filters, that have equal ripple pass band responses and equal ripple stop band responses. For low-pass filters, this means that resonant structures are needed in either the series or shunt arms of a ladder network. The synthesis of the zeros to achieve desired pass band or stop band responses has particular application to microwave filters, and their structures as described in section 2.5.

### **2.2.3 Determining filter structure from Transfer Function**

The transfer function of a ladder network is determined using nodal or mesh analysis, and the result can be equated with the set of coefficients for a particular desired transfer function. Other techniques can be used to more directly determine the element values, in particular, looking at the input impedance as a continued fraction, and determining the values of the elements from inspection of the expansion [41].

### **2.2.4 Input impedance of an all pole network**

For a simple ladder network, the input impedance may be derived as continued fraction starting at the output  $Z$ . This will generate the input impedance transfer function, which can be used to calculate the input reflection coefficient. Transfer functions related to the input impedance are used extensively in many filter tuning methods, as described in Chapter 1, and is used in the new tuning method described in Chapter 4.

## **2.3 Low-pass to band-pass response**

All the tuning methods described in this thesis relate to band-pass filters. All-pole band-pass filter designs are usually based on low-pass prototype filters. Thus, one may say that a band-pass filter is optimally tuned when its band-pass characteristics are identical to those of the low-pass prototype. Band-pass filters can be derived from low-pass filters using well know transformations:

$$S = \frac{1}{\gamma} \cdot \left( \frac{s}{\omega_0} + \frac{\omega_0}{s} \right) \quad (2.16)$$

where  $S$  is the low-pass prototype complex frequency,  $s$  is the band-pass complex frequency and

$$\gamma = \frac{(\omega_2 - \omega_1)}{\omega_0} \text{ where } \omega_0 \text{ is the filter center frequency} \quad (2.17)$$

and  $\omega_2$ ,  $\omega_1$  are the upper and lower cut-off frequencies, respectively. This transformation allows easy manipulation of the low-pass network to create a band-pass network. In general, the transfer response is not a perfect translation and scaling of the low-pass response, but results in distortion of the frequency skirts, and pass band response. The distortion is inversely proportional to the bandwidth, and is quite good for narrow band filters.

This transformation is demonstrated in figure 2-2. Each series inductive element is replaced with a series resonant circuit. Each capacitive shunt element is replaced with a parallel resonant circuit. If a low-pass network has elements  $L_n$  and  $C_n$ , the transformations on the network elements are as follows: replace the  $S$  in  $SL_n$  with equation (2.16) to find that the normalized inductor is replaced with a series resonant circuit

$$Z_{in} = s \cdot \left( \frac{L_n}{\gamma \omega_0} \right) + \frac{1}{s \cdot \left( \frac{\gamma}{L_n \omega_0} \right)} \quad (2.18)$$

with series inductance and capacitance given by the bracketed quantities in equation (2.18). Replace the  $S$  in  $1/SC_n$  by equation (2.16) to yield a parallel resonance circuit

$$Y_{in} = s \cdot \left( \frac{C_n}{\gamma \omega_0} \right) + \frac{1}{s \cdot \left( \frac{\gamma}{C_n \omega_0} \right)} \quad (2.19)$$

with shunt capacitance and shunt inductance given by the bracketed quantities in equation (2.19). Figure 2-2 shows the result of transformations of (2.18) and (2.19) on the network from figure 2-1. These transforms in general give unrealizable element values; therefore the network must be transformed again to a network that is more conducive to RF realization [48].

For RF filters, the band-pass response may be achieved by using coupled resonators. One example for transformation from low-pass to band-pass, which also results in the coupled resonator configuration, for all pole networks is presented in [49] for example.

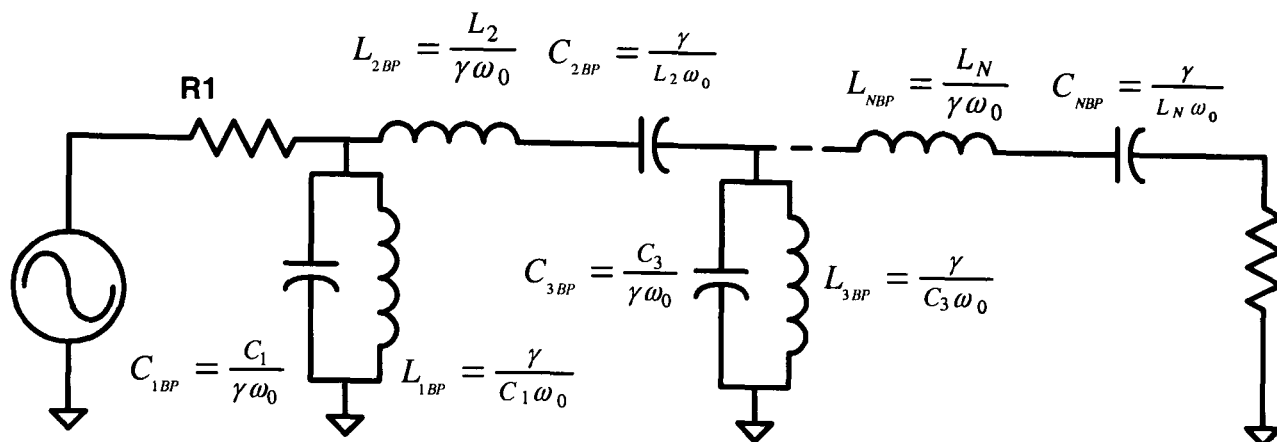


**Figure 2-2: Band-pass filter derived from a low-pass prototypes using transformation**

## 2.4 Time-domain response of band-pass filters

The time response of band-pass filters can be found by solving the network equations using differential equations in time, but this becomes difficult for any complex networks. To simplify calculations, the impulse response may be calculated by applying an inverse transform to the band-pass transfer-function or frequency response after it is derived from the low-pass prototype. However, the band-pass transfer functions will be of  $2n$  order for an  $n$  order low-pass prototype, again yielding a more difficult computational problem. An alternative method for generating a band-pass impulse (time) response can be achieved by recognizing that the band-pass frequency response can be viewed as translation and scaling of the low-pass frequency response; the effect of these operations can be applied to the time-domain response of the low-pass network to yield the band-pass time response, as described in section 3.1.3.

## 2.5 Microwave characterization of filters

A common set of transfer functions and filter configurations have been developed to apply basic filter theory for filters used in RF and microwave applications. The traditional voltage and impedance transfer functions are not typically used due to the difficulty of comparing design objectives to measured results. New measurements are introduced, which take into account the difficulties of operating at high frequencies, as discussed below.

### 2.5.1 S-parameters

The characterization of RF filters is almost always done in terms of the S-parameter response. This response was developed from a wave-based analysis of a network, but

is easily applied to lumped element analysis [50]. This resulting S-parameter matrix is defined in terms of power delivered to a matched load vs. power available to a matched load, where the matched load is defined by a reference impedance  $Z_0$ . These parameters can be related to the more common voltage transfer function and input impedance. One result of this formulation is that for a loss-less network, it can be shown that

$$|S_{21}|^2 + |S_{11}|^2 = 1 \quad (2.20)$$

which follows from power conservation, where power must either be transmitted to the load or reflected back to the source [51].

### 2.5.2 Transmission Response and Reflection Response

The transmission response may be related to  $S_{21}$  by  $S_{21}(j\omega) = 2 \cdot H(j\omega)$  where  $H(j\omega)$  is defined for an impedance matched, doubly terminated network.  $H(j\omega)$  is sometimes taken as normalized to the DC loss,

$$H_N(j\omega) = \frac{H(j\omega)}{H(0)} \quad (2.21)$$

which makes  $H_N(j\omega) = S_{21}(j\omega)$ .

The reflection response,  $S_{11}$ , may be related to the input impedance through the well-known formula

$$S_{11} = \frac{Z_{in} - Z_0}{Z_{in} + Z_0} \quad (2.22)$$

where  $Z_{in}$  is the input impedance and  $Z_0$  is the reference impedance, provided that the network is terminated in the reference impedance [51]. This is the same as the reflection coefficient,  $\rho(s)$  or  $\rho(j\omega)$ .

### 2.5.3 Phase Response

The phase response of the S-parameters of a filter can be readily determined from its response polynomial. The phase response can be applied to any of the S-parameters of a filter. The phase of the  $S_{11}$  of a filter is

$$\text{Phase}(S_{11}(\omega)) = \tan^{-1} \left( \frac{X(\omega)}{R(\omega)} \right) \quad (2.23)$$

where  $\text{Re}(S_{11}(\omega)) = R(\omega)$  and  $\text{Im}(S_{11}(\omega)) = X(\omega)$

For input impedance in the form of equation (2.13), the poles and zeros of the input impedance produce  $S_{11}$  phase values of 0 degrees and 180 degrees respectively [10].

## 2.5.4 Delay Response

The group delay response of a network is defined as  $-d\phi/d\omega$ , and can be calculated from the transfer response by taking the derivative of the phase response. This can be applied to any of the S-parameters. The delay response of  $S_{21}$  of a filter is a common figure of merit in measuring and tuning filters. Typically, the absolute group delay is not as important as its deviation over the pass band. For some applications, such as feed forward networks, the absolute delay response is important. The delay response of  $S_{11}$  of a filter is used by Ness in his development of a tuning method (see section 1.3.3).

## 2.6 Microwave filters design considerations

The design of filters for RF and microwave applications must deal with the high frequency effects of distributed elements and parasitic effects. While low frequency band-pass filters can utilize a variety of network configurations, for the most part RF and microwave band-pass filters follow two main configurations: coupled resonator design and distributed transmission line design. For narrow band filters, coupled resonator designs are most commonly used.

### 2.6.1 Loss vs. Match and Isolation

For filters described by polynomial transfer functions, larger isolation (stop band attenuation) is achieved by increasing the number of poles. The filter return-loss is determined by the given bandwidth, and number of poles of a filter, and shape of the stop band skirts. There exists a relationship between the filter ripple and return loss, for loss-less filters, and can be expressed in S-parameters by equation (2.20). Descriptively, any power reflected which appears as non-zero  $S_{11}$ , is removed from transmission and decreases  $S_{21}$ . The ripple of a filter is directly related to the minimum and maximum  $S_{11}$ . Assuming the filter is sufficiently matched to give zero reflection at some frequency in the pass band, the maximum  $S_{11}$  sets the ripple in  $S_{21}$ .

For an all-pole filter response, the cutoff or isolation of the filter is similarly linked to the return loss of the filter. For example, in the Chebyshev transfer function there is trade off between filter ripple and the cutoff steepness. Since this filter ripple is directly related to return loss, there is a similar relationship between cutoff and filter return loss.

Loss in filters can be represented as a resistive element in the resonator, or equivalently, as a non-infinite  $Q$  in the resonator where  $Q$  is defined as [13]

$$Q = \frac{R_0}{\omega_0 L_0} \quad (2.24)$$

In a loss-less filter, equation (2.20) holds true, but with loss in the resonators, the equation becomes an inequality. It is still true that  $S_{21}=S_{12}$ , but  $|S_{11}|$  may no longer equal  $|S_{22}|$ , due to loss effects.

## 2.6.2 Power Handling

Filters used for the transmit path in communications systems must handle high power, up to 200 watts typically for cellular applications. The loss in these filters must be quite small, typically less than 0.8 dB. The “re-entrant” cavity configuration provides for very low loss when high  $Q$  elements are used [52,53]. In general, the larger the volume of the resonator, the higher the  $Q$  and smaller the loss. Often, the tuning mechanism, such as a screw coming close to a post, is the limiting factor on power handling, as it provides a high field area where breakdown can occur. For this reason, these filters are designed to be very near the desired frequency and tuning is made quite small, allowing the gap in tuning elements to be larger.

For receive filters, low loss is necessary as the loss directly affects the noise figure of the communications receiver. The same attributes that give good power handling also give low loss. In many cases, the isolation requirements of receive filters are much higher than for transmit filters, in order to reject the transmit signal during duplex operation.

## 2.7 Coupled-resonator filters

For most low-loss, narrow-band applications, coupled-resonator designs are used. Occasionally the resonators may be stripline or microstrip structures, but they are more commonly structures such as coaxial cavities or dielectric resonators in the case of RF filters, and waveguide cavities in the case of microwave filters. Planar transmission line structures are typically much more lossy than cavity type structures, and exhibit large spurious pass bands at multiples of the desired pass band.

### 2.7.1 Coupled resonator filter design

A design process for an all-pole coupled-resonator filter proceeds by choosing a low-pass prototype with the desired attributes, then transforming it to the band-pass

form as shown in figure 2-2. From this form, there are two main transformation forms that yield coupled resonator structures [54, 55]. The transformation method consists of recognizing that a series-resonant circuit can be transformed to a shunt-resonant circuit by adding admittance inverters at the input and the output, and shunt-resonant circuits can be transformed to series-resonant circuits using impedance inverters. Thus, either the series or the shunt resonators in figure 2-2 can be replaced with its dual. Impedance or admittance inverters can be implemented in a variety of ways [56]. A common representation to use in narrow-band cases is the three capacitor version of an admittance inverter to replace the series-resonant structures in figure 2-2 with shunt-resonant structures, and absorb the negative capacitance into the capacitor portion of the shunt resonator, as shown in figure 2-3. For capacitively coupled filters, the frequency distortion tends to make the lower skirt steeper than the upper skirt, as the coupling zero occurs at  $\omega = 0$  on the lower side, and as  $\omega \rightarrow \infty$  on the upper side.

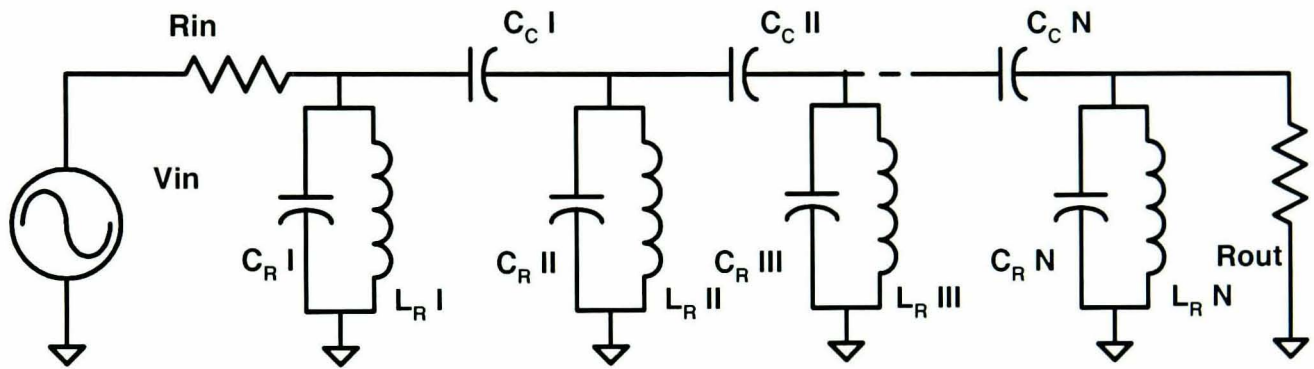


**Figure 2-3: A representation of a coupled-resonator filter in the form of capacitively-coupled shunt resonators.**

If the input is directly coupled to the resonator, the resonator impedance, defined as

$$Z_R = \sqrt{L/C} \quad (2.25)$$

is set to the desired system impedance. In other cases, where the resonator has an impedance other than the system impedance, the input and output connections are commonly modeled with transformers magnetically coupled to the input and output resonators, with the transformer ratio providing the impedance match to the resonator. It is also possible to add a series capacitive input coupling which can be chosen to provide the desired impedance at the input from any resonator impedance [54].

As a result of these re-configurations, the value of the capacitance in each resonator is reduced by the value of the coupling capacitors connected to the same node. Since each coupling capacitance may be different, this configuration gives the appearance that the resonators are tuned to different frequencies. This is a consequence of absorb-

ing the negative capacitance of the admittance inverter. As far as the design process is concerned, each resonator is designed to be exactly on the desired center frequency of the filter.

### **2.7.2 Cavity filter realizations**

For applications where low loss is required, the resonators are often re-entrant coaxial cavities. These consist of short lengths of transmission line created by forming an outer conductor from a shield, and an inner conductor by a post. The center frequency of this type of filter is set by the equivalent effective impedance of the transmission line (typically inductive) in parallel with a shunting capacitance from the top shield of the filter structure. This shunting capacitance is often created by a screw in the top shield, and can be adjusted by bringing the screw closer to the center post. For even more adjustment range, the center post is made hollow, and the tuning screw is allowed to go down inside the center post, creating a capacitance proportional to the length of the screw in the center post.

These filters have coupling between elements by creating a gap in the wall between adjacent elements. The coupling is both magnetic and electric, with the magnetic coupling being predominant. The electric coupling is out of phase with the magnetic, and is easily adjusted by “shorting out” the coupling gap from the ungrounded side of the center post, through the use of a “coupling” adjustment screw. As the screw is lowered into the gap, the electric field coupling is reduced, increasing the effect of the magnetic field coupling. In general, the magnetic field coupling is increased if the center posts are closer, or if the gap in the shield between posts is wider. One difficulty with tuning these types of structures is for strongly coupled filters, which are required for wider bandwidths, the shunt capacitance from the coupling screws can add significantly to the resonator center post, causing a change in center frequency as the coupling is changed. Thus, the coupling tuning interacts with the resonator tuning.

## **2.8 Filters with cross coupling**

Coupled resonator filters with coupling only between adjacent resonators produce all-pole frequency responses. If, however, coupling occurs between non-adjacent resonators, then transmission zeros will occur in the transfer response [57]. An example schematic is shown in figure 2-4.

While the tuning method described in this thesis focuses on all-pole filters, the effect of transmission zeros on the response will be illustrated as well, and modifications to the tuning methods to account for these effects will be described.

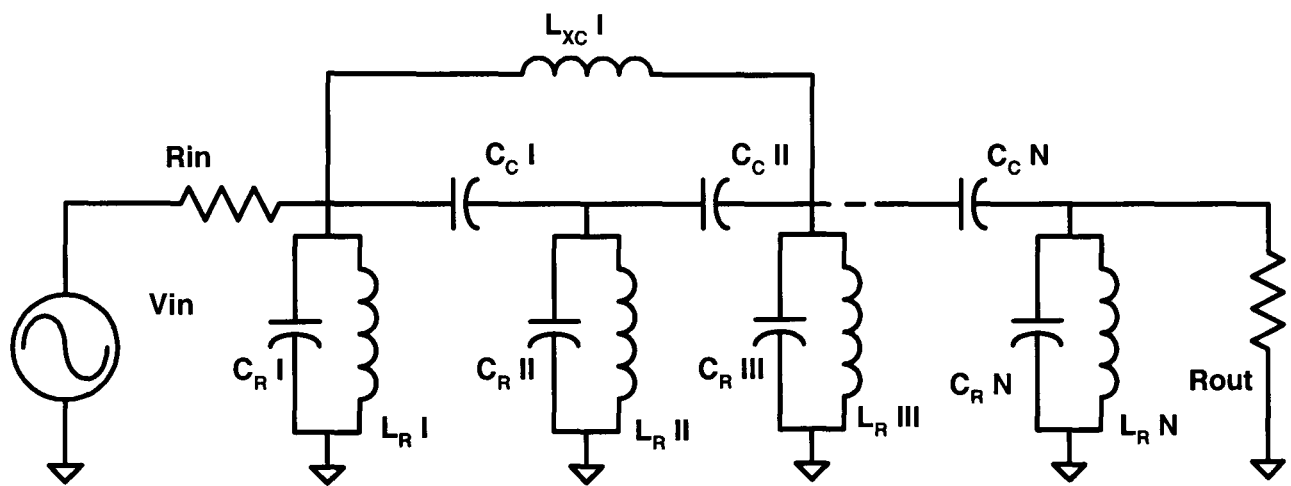


**Figure 2-4: An example of a schematic of a filter with cross coupling ( $L_{xc1}$ ), in this case from resonator 1 to 3.**

## Chapter 3 Fourier Transform Study

### 3.1 The Fourier analysis of filters

While a filter network is mathematically characterized by its transfer function, the frequency response of a network provides the physically measurable response of a network, utilizing sinusoidal signals as the stimulus, and measuring the response as magnitude and phase changes in the stimulus signals. Fourier analysis is ideally suited to represent the physical response, and can provide for useful analysis of a filter network. However, measurement systems are limited to measuring finite frequency points over specified bandwidths, so any interpretation of the measurements must include these limitations. A somewhat unexpected result of these limitations is described in chapter 4 of this thesis, which provides very useful information on the nature of the filter being measured. This chapter provides some important details of Fourier analysis as applied to filter measurements using vector network analyzers (VNAs). Since the data is measured in the frequency domain, the transformation we are most interested in is the Inverse Fourier Transform (IFT), generating the time-domain response from the frequency domain data. Most statements about the IFT have corollaries in the forward transform.

#### 3.1.1 The continuous Fourier transform

As cited in chapter 2, the Fourier transform can be interpreted as a Laplace transform with the special case of  $s = j\omega$ . Many of the significant theorems of the Fourier transform are quite similar to their Laplace counterparts, and those that are particularly useful in the study filter networks are presented here. When data is measured in the frequency domain, an inverse Fourier transform is used to determine the time-domain response of the filter. If the data represents the frequency response of the filter, then the inverse transform represents the impulse response of the filter. Since the Fourier Transform plays such a key role in the VNA time-domain transform, it is appropriate to review some of its details, as well as standardize the nomenclature. The Fourier transform pair (forward and inverse) are defined as

$$\mathbf{F}(f(t)) = F(\omega) = \int_{-\infty}^{\infty} f(t) e^{-j\omega t} dt \quad (3.1)$$

$$\mathbf{F}^{-1}(F(\omega)) = f(t) = \frac{1}{2\pi} \cdot \int_{-\infty}^{\infty} F(\omega) e^{j\omega t} d\omega \quad (3.2)$$

applied to analytic functions  $f(t)$  and  $F(\omega)$  over all time and all frequency, respectively [58], [59]. The careful reader will note that nomenclature used in the forward transform by electrical engineers differs slightly from the commonly defined transform [59], where here (3.1) and (3.2) use  $\omega = 2\pi s$ .

### 3.1.2 Even and odd functions and the Fourier transform

Functions are even if  $F(\omega) = F(-\omega)$ , and are odd if  $F(\omega) = -F(-\omega)$ . All functions can be represented as a sum of an even function and an odd function. Evenness, oddness, and other types of symmetry can simplify calculating transforms, and is often assumed for cases of some transforms. A function  $f(t) = e(t) + o(t)$  has the Fourier transform

$$F(\omega) = 2 \int_{-0}^{\infty} e(t) \cdot \cos(\omega t) dt - 2j \int_{-0}^{\infty} o(t) \cdot \sin(\omega t) dt \quad (3.3).$$

From this result many Fourier transform relationships can be deduced. For modeling physical functions, a key relationship is that for a pure-real time function, then

$$\mathbf{F}[f(t)] = E(\omega) + jO(\omega) \quad (3.4)$$

that is, the Fourier transform of a pure real time function has an even real part and an odd imaginary part [59].

#### 3.1.2.1 Hermitian functions

Functions such as those described in equation (3.4), which have a transform with an even real part, and an odd imaginary part are called hermitian. This can also be written as  $F(\omega) = F^*(-\omega)$ . Time functions which are real and symmetric (even) have pure real transforms. Time functions that are real and non-symmetric have hermitian transforms. Note that all physically realizable networks have non-symmetric real impulse responses, due to causality, and thus must have hermitian Fourier transforms.

### 3.1.3 Modulation (shift) theorem

Many filter derivations are based on low-pass to band-pass transformations. This represents a shift in frequency. The shift or modulation theorem can be derived from the definition of Fourier transform:

$$\text{if } \mathbf{F}^{-1}(F(\omega))=f(t), \text{ then } \mathbf{F}^{-1}(F(\omega + \Delta\omega))=f(t)e^{-j\Delta\omega t} \quad (3.5)$$

Note that this is in general a complex function, so pure shift in frequency is not physically realizable. To transform a low-pass prototype to a realizable band-pass filter, one must replicate a positive shifted response and a negative shifted response. Thus, if  $H_{LP}(\omega)$  is a low-pass filter's frequency response, then

$$H_{BP}(\omega) = H_{LP}(\omega + \omega_0) + H_{LP}(\omega - \omega_0) \quad (3.6)$$

is the band-pass filter frequency response and the inverse transform of this is

$$h_{BP}(t) = h_{LP}(t)e^{-j\omega_0 t} + h_{LP}(t)e^{+j\omega_0 t} \quad (3.7)$$

expanding the complex exponential we find that

$$h_{BP}(t) = h_{LP}(t)\cos(\omega_0 t) - j \cancel{h_{LP}(t)\sin(\omega_0 t)} + h_{LP}(t)\cos(\omega_0 t) + j \cancel{h_{LP}(t)\sin(\omega_0 t)} \quad (3.8)$$

with the result

$$h_{BP}(t) = 2 \cdot h_{LP}(t)\cos(\omega_0 t) \quad (3.9)$$

The sum of these two shifts results in the imaginary terms canceling. The real portions add and the result is that if  $h_{LP}(t)$  is the low-pass prototype time (or impulse) response, the impulse response of the band-pass filter will be a cosine wave at the center frequency of the band-pass, with an envelope of two times the low-pass prototype's impulse response. This band-pass time response is not the same as the response obtained from the band-pass mode of a network analyzer time-domain transform. The differences are key to applying transforms to the time-domain tuning of filters.

## 3.2 The discrete Fourier transform

Since measured frequency response of networks consists of discrete data, it is appropriate to discuss the discrete version of the inverse Fourier transform to determine the associated time response. The inverse discrete Fourier transform, which is defined only at discrete time points, for a discrete frequency data set, is

$$f(\tau) = \sum_{n=0}^{N-1} F(\nu) e^{j2\pi(\nu/N)\tau} \quad (3.10)$$

where  $(\nu/N)$  is analogous to frequency in samples per cycle,  $\tau$  is the discrete time increment, and  $F(\nu)$  is the discrete frequency data set [60]. The inverse Fast Fourier transform (IFFT) is a very efficient way to compute  $f(\tau)$  over the entire discrete time set. It might appear that the conversion of VNA frequency domain data to the time-domain can be simply accomplished with an IFFT for computational efficiency. However, the IFFT limitations on the flexibility of the data (time) output can hide important effects that occur between calculated time samples, as described below. Further, much more conditioning is done in the VNA transform to enhance its applicability to practical problems.

### 3.2.1 FFT (Fast Fourier Transform) and IFFT (Inverse Fast Fourier Transform)

The FFT and IFFT are well-known algorithms for calculating the Fourier transform pair of a discrete data set as described in (3.10). If the discrete data set is generated from a sampled data set of a frequency response, and the data is sufficiently sampled as describe below, then the IFFT generates the time response of the network associated with the sampled data. FFTs and IFFTs have the attribute of greatly reducing the numbers of computations needed to compute a Fourier transform, but are limited in the data that is used and presented. One common limitation on FFT/IFFT transforms is that the number of points in the transformed domain must be equal to the number of data sample points. Some transforms also require that the number be points be in the form of  $2^n$ .

#### 3.2.1.1 Fine structure response

If an IFFT is applied to a frequency response, the resulting time response must have the same number of points, and the time intervals must evenly span the time period. A consequence of this is that fine grain time response is not necessarily evident in the IFFT data. The IFFT is equivalent to the analytic inverse Fourier transform (IFT) sampled evenly over a time period with the number of sample points equaling the number of frequency response points. Thus, any time-domain response information that is present between these points is not evident in the IFFT data. This is also true of the FFT of a time-sampled signal.

It is illustrative to use a familiar example to demonstrate this fact. Take a time function consisting of a cosine signal of known frequency (8.5 Hz), as shown in figure 3-1 (left). If several cycles of the time signal are sampled at higher than the twice the highest frequency, it is sufficiently sampled to avoid aliasing. One might naively assume

that the FFT of this time signal should return the original frequency of the time waveform. However, if the frequency of the signal is not synchronous with the sampling, the FFT does not have an output at the frequency of the cosine, and the FFT appears to have two main output signals as the spectrum of the sampled time waveform shows in figure 3-1 (middle), neither of which is the correct amplitude of 0.5 based on the time function. Thus the fine grain nature of the signal is not revealed by the FFT. A Fourier transform can be performed at discrete frequencies over the range of the two largest FFT outputs, using the same time data set, from which the correct magnitude of the original frequency of the signal is revealed, figure 3-1 (right). In fact, since the time data is a finite set of discrete sampled points, the frequency response must be a periodic and continuous function with an infinite response to represent the transitions at the start and end of the data set. The FFT is exactly a sampled version of this continuous frequency function. The non-zero values of the FFT for all the other frequencies is a consequence of the taking the time data over a finite time. Reducing this effect is a key attribute of the VNA time-domain transform.

In order to get faster computation speeds, FFTs are often used instead of direct calculations of the DFT. However many commercially available signal analysis tools take further short cuts in calculating the FFT. One common short cut is to assume that the time response is real. From this the frequency response must be hermitian, and therefore only half the FFT need be calculated to obtain the full frequency response. With an IFFT, it is common to assume a hermitian frequency response input, and only calculate the real portion of the output time signal. Thus, the IFFT is simply 2 times the

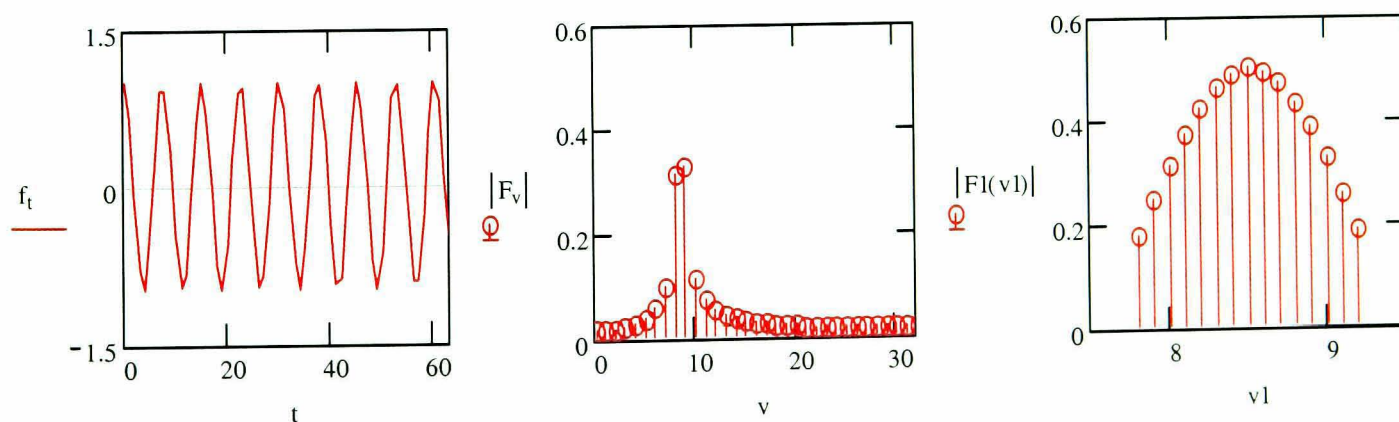


**Figure 3-1 (left) Cosine of frequency 8.5 Hz, (middle) FFT of the waveform in the left plot, (right) Fourier transform of the waveform around the frequency 8.5 Hz**

IFFT of the positive half of the real part of the input frequency response, plus the DC term. However, chapter 5 shows several cases where it is useful to consider frequency responses that are not hermitian, and in these cases, care must be used in considering the shortcuts that are permissible when calculating IFFTs.

## 3.2.2 Calculating the DFT

### 3.2.2.1 Direct calculation

The fine structure of a time response can be determined if an inverse discrete Fourier transform (IDFT) is used, in which the time axis can be arbitrarily small. If this same time spacing were used for the FFT, an extremely large number of frequency points would have to be used as the input, greatly slowing measurement time to generate the frequency response terms. However, the DFT takes considerably longer to calculate than the FFT, and therefore is also not satisfactory where real time transformation is needed. Fortunately, if the transform is needed over a relatively small portion of the time response, the Chirp-Z transform is an attractive alternative for high speed, and high-resolution transformation [61].

### 3.2.3 Chirp Z transform

The Chirp-Z transform (CZT) makes use of the relationship between convolution and transformation to create a transform that is nearly the speed of an IFFT, but has the arbitrarily small resolution of an IDFT. If the IDFT is performed over a time span with a uniform time spacing, the IDFT can be re-written as a convolution of two equal length inputs, with the inputs and outputs multiplied by scaling factors. Convolution can be accomplished by transforming the inputs, multiplying them together, then transforming the output. Since each input is equal length, FFTs may be used for the transformation, and an IFFT used for the transformation back. Thus an N-point IDFT can be computed with 3 N-point FFTs, with a dramatic reduction in computation time.

#### 3.2.3.1 Fixed point transforms

The standard CZT or ICZT uses a fixed size input array and a fixed size output array. The input is complex and the output is complex as well. In configuring the ICZT, the input array consists of the frequency response to be inverse transformed, plus the start time and stop time of the inverse array. The time spacing will be the time span divided by the number of points minus one. However, there are no restrictions on the start or stop times. If the start and stop times are chosen to be  $t_{start} = 0$  and  $t_{stop} = 1 / \Delta\omega$ , then the ICZT will return the same values as the IFFT.

### 3.2.3.2 Flexible transforms

Inspection of the derivation of the CZT shows that the restriction of similar size inputs and outputs is not absolute. It is possible to configure the CZT or its inverse to create an output array of a size either larger or smaller than the input array. One might want a larger output if finer resolution is desired over the same time span. However, repeating the CZT over two time spans may yield similar computation times [61].

### 3.3 Fourier transform (analytic) vs. VNA time-domain transform

The limitations of the IFFT as applied to microwave measurements required other techniques for analyzing these networks. The time-domain transform of vector network analyzer measurements was first introduced in 1974 [62] and has been widely used since its real-time commercial introduction with the HP 8510A (1984), which allowed increased accuracy and real-time gating [63,64]. This VNA provided the capability to calculate the time-domain response of the frequency domain data, using a form of the inverse Fourier transform. However, there were several modifications that are important to note, which causes the time-domain response of the VNA to be different than the actual inverse Fourier transform of the frequency response of a network, that is, different from the impulse response of the network being measured. These differences come from the mode of the VNA transform (Low-pass Step, Low-pass Impulse or Band-pass Impulse), data windowing and truncation, window re-normalization, and data gating. For much of this time, the principal use was in low-pass-impulse mode for fault location, and much has been written about the interpretation of the low-pass step-mode time-domain response [64]. Recently, the time-domain response has been applied to solving the problem of filter tuning, using the band-pass mode [25,65].

A rigorous analysis comparing this time-domain mode to the analytically derived impulse response may be obtained by applying appropriate functions to the analytical frequency response until the inverse Fourier transform of this modified response exactly matches the VNA time-domain response. Each of these functions applied to the frequency response can be evaluated in the time-domain, and their associated time-domain effects can be individually determined. This approach differs from [62] in that Hines and Stinehelfer develop the time-domain response from assuming a periodic time function, the Fourier transform of which reproduces the measured frequency response. Here, a continuous analytic frequency response is assumed, and modifications are applied to account for discrete frequency sampling and windowing to directly obtain the

VNA time-domain transform in terms of the original frequency response and these modifications.

### 3.3.1 Defining the Fourier Transform

The IFT in equation (3.2) of a function provides directly the impulse response of that network and is the same result, in time, as driving the network with an impulse,  $\delta(t)$ , and determining the time response. Figure 3-2 shows the analytically derived transform of a 3-pole Butterworth filter (meaning the reflection frequency response is calculated using standard network theory, and the inverse Fourier transform from (3.2) is calculated to get the time response), along with a VNA time-domain transform of the same function. Clearly they are not the same. The differences will be reconciled in the following sections by describing the way in which each aspect of the VNA measurement must be accounted for with the appropriate mathematical transformation to achieve the same result as the IFT.

### 3.3.2 Effects of discrete sampling

The Fourier transform operates on continuous functions, while the VNA time-domain transform must operate on measured (discrete) data. One approach is to assume the measured data is a sampled version of a continuous analytic frequency response. Since the data applied to the time-domain transform is discrete, the time-domain trans-

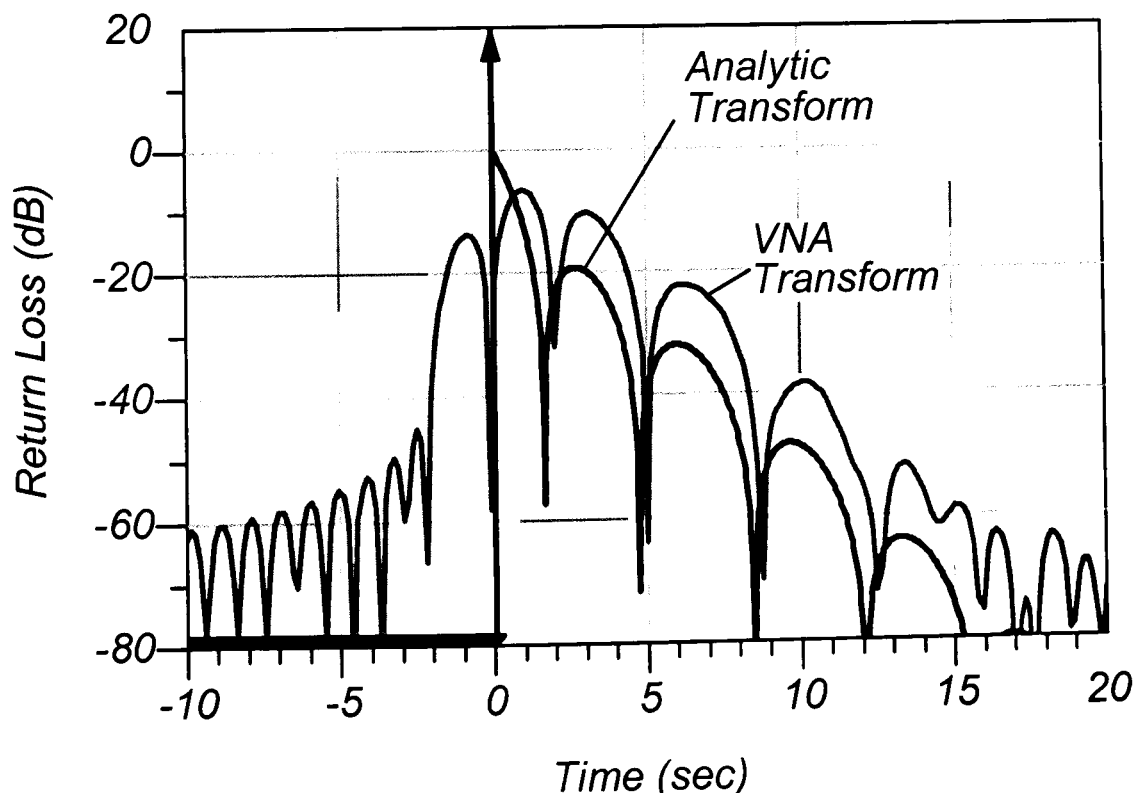


**Figure 3-2 Analytically derived impulse reflection response vs. VNA time-domain response for a 3 pole Butterworth filter**

form must differ from the analytically calculated IFT of the network, but an equivalent discrete representation of an analytic function can be obtained by a mathematical representation of the sampling process. Note that such a time function would be identical to one determined in [62] but this approach is more readily applicable to the problem of comparing the VNA time-domain transform to the analytic impulse response of a network.

A frequency sampling function can be represented as  $III(\omega)$ , which is defined as [66],

$$III(\omega) = \Delta\omega \cdot \sum_{n=-\infty}^{\infty} \delta(\omega - n\Delta\omega) \quad (3.11)$$

and can be visualized as a collection of delta functions with  $\Delta\omega$  spacing. The effect of discrete data in the measured frequency response can be analyzed by forming a sampled function composed of the analytic frequency response multiplied by the sampling function, such that its value is zero between measured points, and the scaling factor of the delta function at each frequency is the measured value of the frequency response. The IFT of the sampled function,  $f_s(t)$ , can now be represented analytically by multiplying the original frequency response function by a sampling function:

$$f_s(t) = \mathbf{F}^{-1}(F_s(\omega)) = \frac{1}{2\pi} \cdot \int_{-\infty}^{\infty} F(\omega) \cdot \Delta\omega \cdot \sum_{n=-\infty}^{\infty} \delta(\omega - n\Delta\omega) \cdot e^{j\omega t} d\omega \quad (3.12)$$

or, through the operation of the integral on the delta function:

$$f_s(t) = \mathbf{F}^{-1}(F_s(\omega)) = \frac{1}{2\pi} \cdot \sum_{n=-\infty}^{\infty} F(n\Delta\omega) \cdot \Delta\omega \cdot e^{jn\Delta\omega t} \quad (3.13)$$

This operation can also be understood by noting that multiplication of two functions in the frequency domain is the same as convolving the inverse transforms of functions in the time-domain. Convolution of a function by a delta function returns the original function, at the origin of the delta function. Thus, the inverse transform of the sampling function returns another sampling function,

$$III(t) = \frac{1}{\Delta\omega} \cdot \sum_{n=-\infty}^{\infty} \delta\left(t - n \frac{1}{\Delta\omega}\right) \quad (3.14)$$

Sampling in the frequency domain is the same as convolving the original time-domain response by the sampling function  $III(1/\Delta\omega)$ . Therefore the transform of an analytic function can be related to the transform of the discrete sampled version by con-

volving the inverse impulse response of the original function with the sampling function of (3.14). The effect of discrete data sampling can be seen to create images of the original function (sometimes called aliases) spaced at the inverse of the sampling spacing. The time range of  $\pm 1/2\Delta\omega$  is referred to as the alias-free range of the inverse transform for sampled data. Many commercial products display a maximum range of  $\pm 1/\Delta\omega$ . If the impulse response of the original function does not tend to zero by  $\pm 1/2\Delta\omega$ , then the appearance of the inverse of the sampled function in the alias-free range will be distorted by effects from previous and subsequent images. Figure 3-3 up-

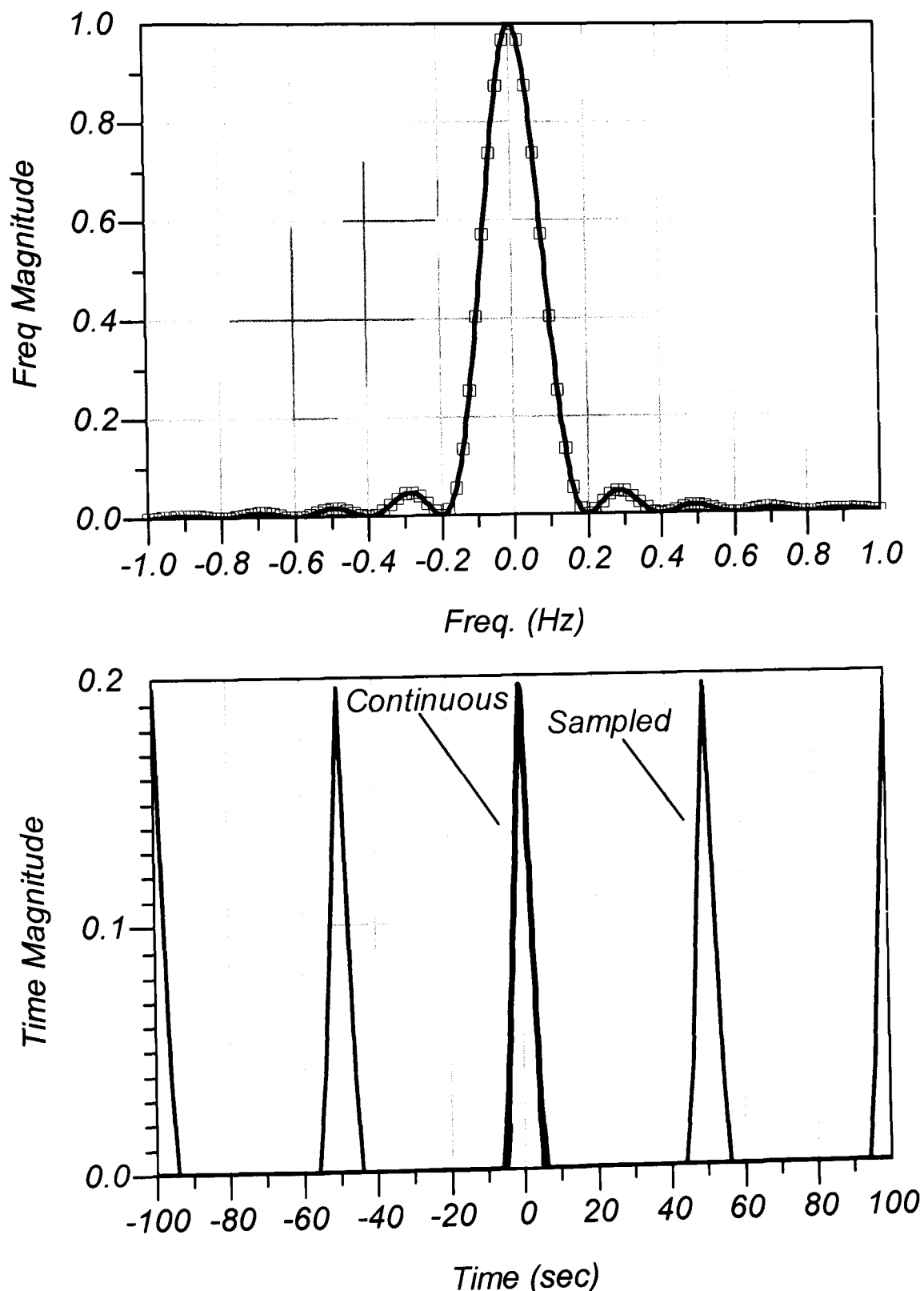


**Figure 3-3: Sinc squared frequency response continuous and sampled (upper), time-domain response continuous and sampled (lower)**

per shows a frequency plot of the  $\text{sinc}^2$  function, along with the sampled data points. The lower plot shows the IFT of the continuous function, and also the IFT of the sampled function.

The inverse transform of a sampled frequency response must have an infinitely repetitive (periodic) time response. Even if the frequency response is discrete, the time response may still be continuous. Only if the frequency response is discrete and periodic will the time response be discrete. Since any real sampled frequency response must be sampled over a finite frequency span, the time response associated with any measured frequency response will be continuous and periodic [67].

### 3.3.3 Effects of truncated frequency

Another consequence of taking a transform of measured data is that the frequency response must be truncated, rather than extend to plus and minus infinity. For transmission responses, this does not present much of a problem, as the response of most filters gets arbitrarily small at high frequencies, and its contribution to the inverse Fourier integral is negligible. However, for reflection responses, the value of the response remains large at high frequencies. In fact, these responses are not strictly Fourier transformable, as they do not satisfy equation (2.12). However, most reflection functions can be represented with the help of the generalized function,  $\delta(t)$ . But, if the response is truncated, and the response data is finite, then the Fourier transform of the data strictly exists.

Truncation of the frequency response data of a network is mathematically equivalent to multiplying the data by a rectangular window. In the time-domain, this can be represented as convolving the impulse response of the network with the inverse transform of the rectangular window, which is a  $\sin x/x$  function. In this way, the inverse transform of truncated data will always have a response with “side-lobes” if the original data does not go to and remain zero sometime before truncation occurs. These side-lobes can be so large as to obscure the impulse response, and much work has been done to reduce this effect. For the most part, side-lobes, or ringing as it is sometimes called, can be controlled through the appropriate use of windowing. In chapter 5, truncation will be shown to be of primary importance when explaining the time-domain response of band-pass filters. Taking the IFT of the product of the original function and a rectangular window can represent the effect of truncated data in the VNA time-domain transform. Referring to equation (3.12), this truncation is equivalent to redefining the limits of the integral to be the endpoints of the measured data. Figure 3-4 shows an ex-

ample of a 1-pole filter response with the analytic function  $F(s)=1/(s+1)$ , or  $F(\omega)=1/(1+j\omega)$  where  $s=j\omega$ , figure 3-4 (upper, grey trace) along with its truncated frequency response, figure 3-4 (upper, black trace). Figure 3-4 (middle) shows the time domain response of the truncation function, which is IFT of a rectangular window, which is a  $\sin x/x$  function. The filter response has an analytic time response of  $f(t)=e^{-t} \cdot U(t)$  (where  $U(t)$  is the unit step function) as shown in Figure 3-4 (lower, grey trace). The truncation effect on the analytic time response can be obtained by convolving the IFT of the original function with the  $\sin x/x$  function, and is shown in figure 3-4 (lower, black trace). For a sampled data set, over the range of  $\omega = -N\Delta\omega$  to  $+N\Delta\omega$ , the IFT becomes

$$f_s(t) = \frac{\Delta\omega}{2\pi} \cdot \sum_{n=-N}^N F(n\Delta\omega) \cdot e^{jn\Delta\omega t} \quad (3.15)$$

Equation (3.15) might be called the sampled inverse Fourier transform. Note the similarity to the inverse discrete Fourier transform of equation (3.10). The sampled inverse Fourier Transform of equation (3.15) can calculate the inverse transform for any time, but for a given series of time values, the computation of  $f(t)$  is quite inefficient using equation (3.15) directly. However, for a given set of equally spaced time samples with arbitrary start, stop and time spacing, equation (3.15) can be very efficiently computed using the Chirp-Z transform [68].

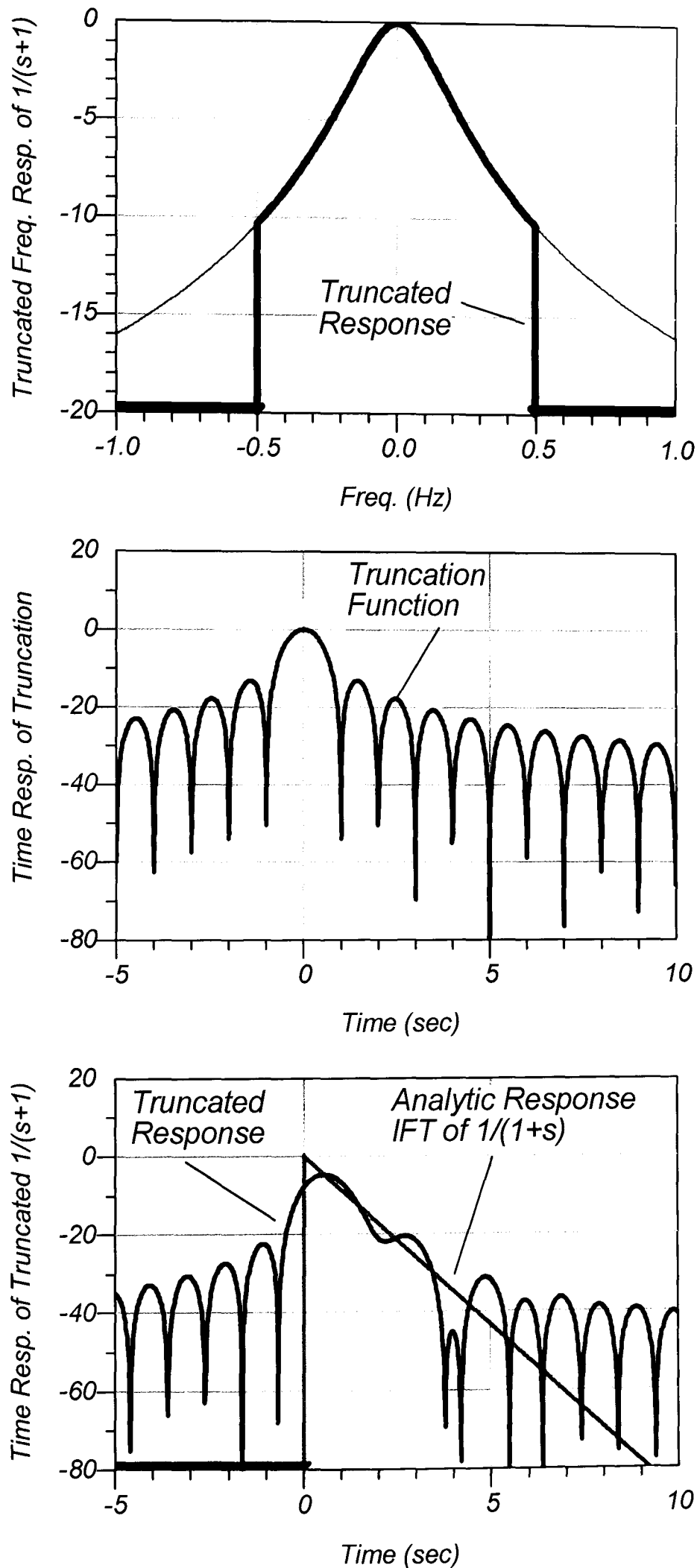


**Figure 3-4 (upper) 1-pole filter frequency response with and without truncation, (middle) Analytic time response of the truncation function. (lower) Analytic response of the 1-pole filter compared with the truncated response**

### 3.3.4 Windowing to reduce effects of truncation

Data truncation is shown above to have the effect of convolving the original transform with a  $\sin x/x$  function. The side-lobes of this function are quite high, and continue for a substantial extent, often obscuring the desired response of the original function. The effects of truncation are minimized if the original function tends to zero at the frequency endpoints. A windowing function may be applied that gradually reduces the frequency response, thus controlling the side-lobes created during the truncation process.

However, the windowing process tends to reduce the sharpness of the original response, spreading pulses and stretching out slopes, thereby reducing the resolution of the transform, and distorting the transitions of the original function. This makes it difficult to assess the true nature of the transformed function. Thus, there is a trade off between side-lobe height and resolution when determining the windowing function. Window functions have been extensively described [69]; a window function used commonly in commercial products is the Kaiser-Bessel function, defined as

$$W(n) = \frac{I_0\left(\beta \cdot \sqrt{1 - \left(\frac{n}{N}\right)^2}\right)}{I_0(\beta)} \quad (3.16)$$

where  $I_0(\bullet)$  is the modified Bessel function of the first kind,  $\beta$  is a constant that controls the amount of roll-off of the window function [70], and the window is centered on the data at  $n=0$ , taken from  $n=-N$  to  $N$ . Higher values of  $\beta$  will increase the endpoint roll-off of the original function, thereby reducing the height of the side-lobes. Figure 3-5 (upper) shows various window factors, figure 3-5 (middle) shows these applied to a 1-pole filter response. Figure 3-5 (lower) shows the time response of windowed functions for  $\beta = 0$  and 6, along with the analytic impulse response.

In order reconcile the analytic impulse response with the VNA time-domain transform, the effects of finite frequency, sampling and windowing on the analytic IFT can be mathematically represented below as  $f_{sw}$  (for sampled, windowed)

$$f_{sw}(t) = \frac{\Delta\omega}{2\pi} \cdot \sum_{n=-N}^N F(n\Delta\omega) \cdot W(n\Delta\omega) \cdot e^{jn\Delta\omega t} \quad (3.17)$$

where  $W(\omega)$  is the windowing function, and the function is sampled over  $\omega = -N\Delta\omega$  to  $+N\Delta\omega$ . This response includes the all the obvious changes to the ana-

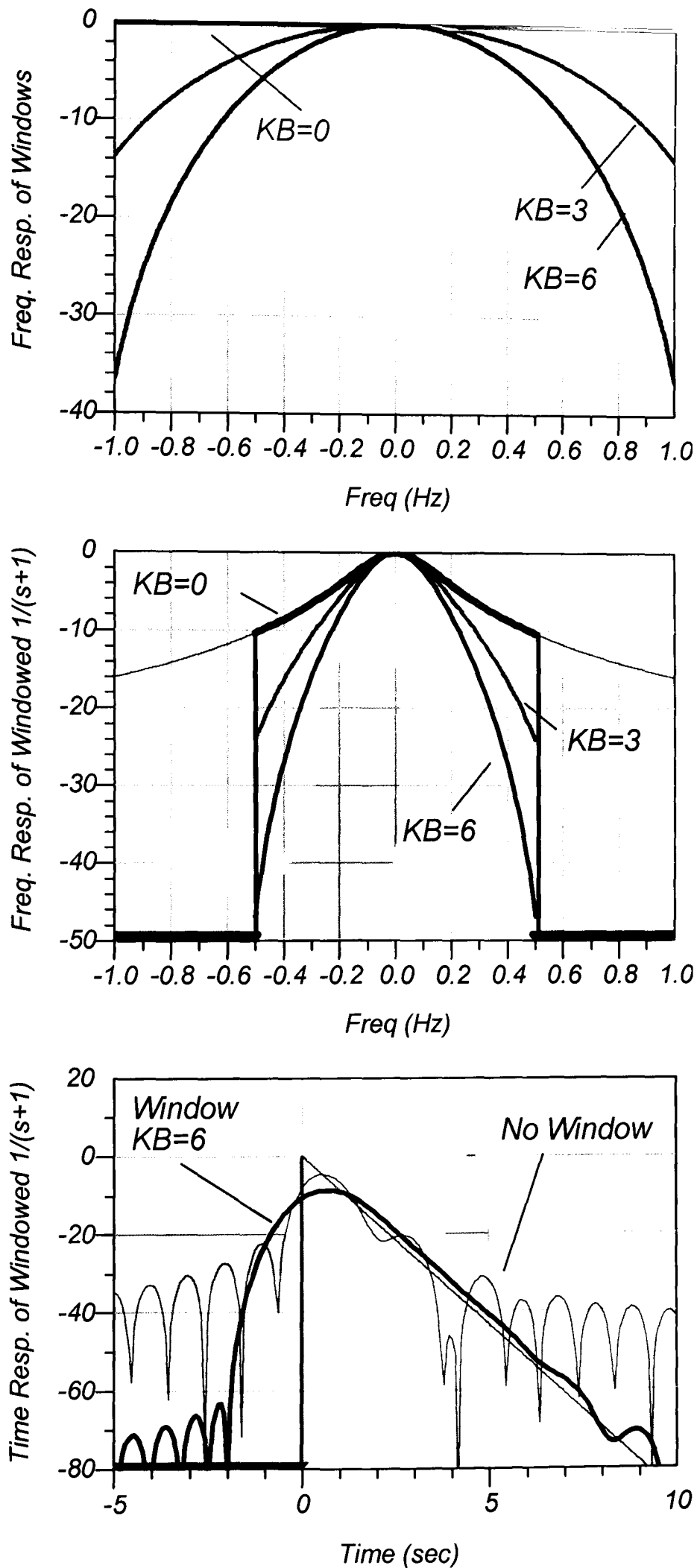


**Figure 3-5 (upper) Kaiser-Bessel Windows for Beta factors 0, 3 and 6; (middle) Windows applied to a 1 pole filter; (lower) Time response of windowed trace.**

lytic function but there is one final modification that must be included such to completely match the VNA time-domain transform, as described below.

### 3.3.5 Scaling and re-normalization

The value of the time-domain transform has to be re-normalized such that it retains its physical meaning. For example, the frequency response of the  $S_{11}$  of an ideal open circuit, with no delay, has a value of 1 for all frequency; its inverse transform is a delta function. However, when the data is sampled and windowed, the time-domain transform of the response of an open circuit will be spread by the windowing function and does not return an impulse of unity height. It would be preferable if the time-domain response of the open circuit had a value of unity at time  $t=0$ . Taking the sum of the windowing factors provides the correct scaling factor for subsequent transforms:

$$W_0 = \frac{\Delta\omega}{2\pi} \cdot \sum_{n=-N}^N W(n\Delta\omega) \quad (3.18)$$

and the re-normalized transform becomes

$$f_{VNA}(t) = \frac{1}{W_0} \cdot \frac{\Delta\omega}{2\pi} \cdot \sum_{n=-N}^N F(n\Delta\omega) \cdot W(n\Delta\omega) \cdot e^{jn\Delta\omega t} \quad (3.19)$$

Note that this scales the transform to always return 0 dB for a unit frequency input, regardless of windowing factor. If the data that is being transformed already tends to zero at the band edges, the windowed response will appear higher after this normalization, when compared to an analytic time response. Since the window scaling always maintains a unity peak amplitude, regardless of how wide the window has made the response, it is in effect amplifying the DC and low frequency responses. For some data, such as a low-pass filter response, this can result in a windowed response that is higher in amplitude than the corresponding analytic impulse response.

## 3.4 Low-pass transforms and band-pass transforms

Since measured data has a finite frequency sampling, some assumptions are made about the behavior of the sampled function. Vector network analyzers offer alternative assumptions, which yield two different modes of transformation: low-pass mode and band-pass mode.

### 3.4.1 Low-pass impulse mode

The assumption for low-pass-impulse mode is that the underlying frequency response is that of a real network. As such, the frequency response is hermitian [59] and the time-domain response is pure real. Also, it is assumed that the network response becomes asymptotic at low frequencies and that the frequency response beyond the measured frequency range contains no important information about the network. In other words, everything of interest occurs over the frequency of measurement. The data points must be linearly spaced over the range of  $\omega = n\Delta\omega$  from  $n=1$  to  $N$ . Thus, the frequencies must be harmonically related. For this transform, the windowing function is centered at  $\omega = 0$ , and extends to the max frequency  $\omega = N \cdot \Delta\omega$ . From this, it follows that the complex sum in (3.19) becomes [59]

$$f_{LP}(t) = \frac{\Delta\omega}{2\pi} F(0) \frac{W(0)}{W_0} + \frac{1}{W_0} \frac{\Delta\omega}{2\pi} 2 \cdot \text{Re} \left[ \sum_{n=1}^N F(n\Delta\omega) \cdot W(n\Delta\omega) \cdot e^{jn\Delta\omega t} \right] \quad (3.20)$$

Given a hermitian function, the imaginary parts of the negative and positive transform cancel, and the real parts double. Further, it is clear that a value must be determined for  $F(0)$ , which is done with DC extrapolation. From equation (3.20), it can be seen that the time-domain transform consists of sums of sines and cosines, and that the highest frequency measurement point determines the highest frequency element. Thus, the rise time is determined by the maximum slope of the highest frequency measured. The transform will repeat itself at intervals determined by the frequency step value, which is the same as the lowest frequency point.

### 3.4.2 DC extrapolation

In addition to being limited in upper frequency response, measurement equipment is limited to its minimum frequency response. However, the Fourier transform includes effects of the DC value on the frequency response. Since VNAs do not commonly measure the DC response, DC extrapolation is used. DC extrapolation requires the assumption that the network response approaches DC asymptotically. If the function has linear phase, and the phase shift is small, the DC extrapolation can be simply the real value of the first measured point. As the phase shift between points gets large, choosing a good algorithm is not trivial. The DC response can be extrapolated by assuming the first two frequency points lie on a circle with a center on the real axis, that cuts the real axis at DC. The original algorithm in the HP8510A, used this method, but gave unexpected results for negative delay, or for very long delay. This would result in

traces with a ramp in the DC base line, or a jumping trace from sweep to sweep. Negative delays can occur with errors in calibration, or un-calibrated measurements, or when the delay exceeds the alias free range as described above. Newer algorithms generate better values for DC terms given large, or even negative delay in the device being measured, by using the phase shift between the first two pairs of points to determine the sign of the delay. Problems may still exist if the first three data points lie exactly 120 degrees apart, but in that case a positive delay is assumed. Alternatively, the reference plane can be extended to ensure a positive delay.

### 3.4.3 Low-pass Step Mode:

The step response of a network can be useful in directly determining the network characteristics, particularly in the case of concatenated transmission lines, and evokes the normal mode of operation of a Time-Domain Reflectometer (TDR). The step response  $U(t)$  is defined as

$$U(t) = \begin{cases} 0 & \text{for } t < 0 \\ \frac{1}{2} & \text{for } t = 0 \\ 1 & \text{for } t > 0 \end{cases} \quad (3.21)$$

and from this its Fourier transform may be determined [71] as

$$\mathbf{F}[U(t)] = \pi \delta(\omega) - j \frac{1}{\omega} \quad (3.22)$$

The time step-response may be found by multiplying the Fourier transform of the step response by the frequency response,  $F(\omega)$ , of a network and taking the inverse transform:

$$f_{Step}(t) = \frac{1}{2\pi} \int_{-\infty}^{\infty} F(\omega) \cdot \left( \pi \delta(\omega) - j \frac{1}{\omega} \right) e^{j\omega t} d\omega = \frac{F(0)}{2} - \frac{j}{2\pi} \int_{-\infty}^{\infty} \frac{F(\omega)}{\omega} e^{j\omega t} d\omega \quad (3.23)$$

Taking the derivative of the step response in (3.23) yields the desired impulse response of the network.

The low-pass mode of the VNA time-domain transform has two forms: low-pass impulse, which is defined by equation (3.20), and the low-pass step, which is essentially the integral of the low-pass impulse response, with respect to time and with some particular choice for the constant of integration. The step response of the VNA should retain the property that its derivative is the VNA time-domain impulse response, and since the sampling function creates a periodic time-domain, with a period of  $1/\Delta\omega$ , the step response should retain this aspect of the periodicity.

Figure 3-6 shows the step-response stimulus (labeled “VNA Unit Step Response”) that meets the properties of having a periodic impulse response for its derivative. This response differs from the square-wave response described by Hines and Stinehelfer, and from the plot, it is obvious that this function cannot have a Fourier transform. However, it may be written as the sum of two functions, the first one being periodic (labeled “Periodic Portion” in figure 3-6) and the second being a ramp function (labeled “Ramp Portion in figure 3-6).

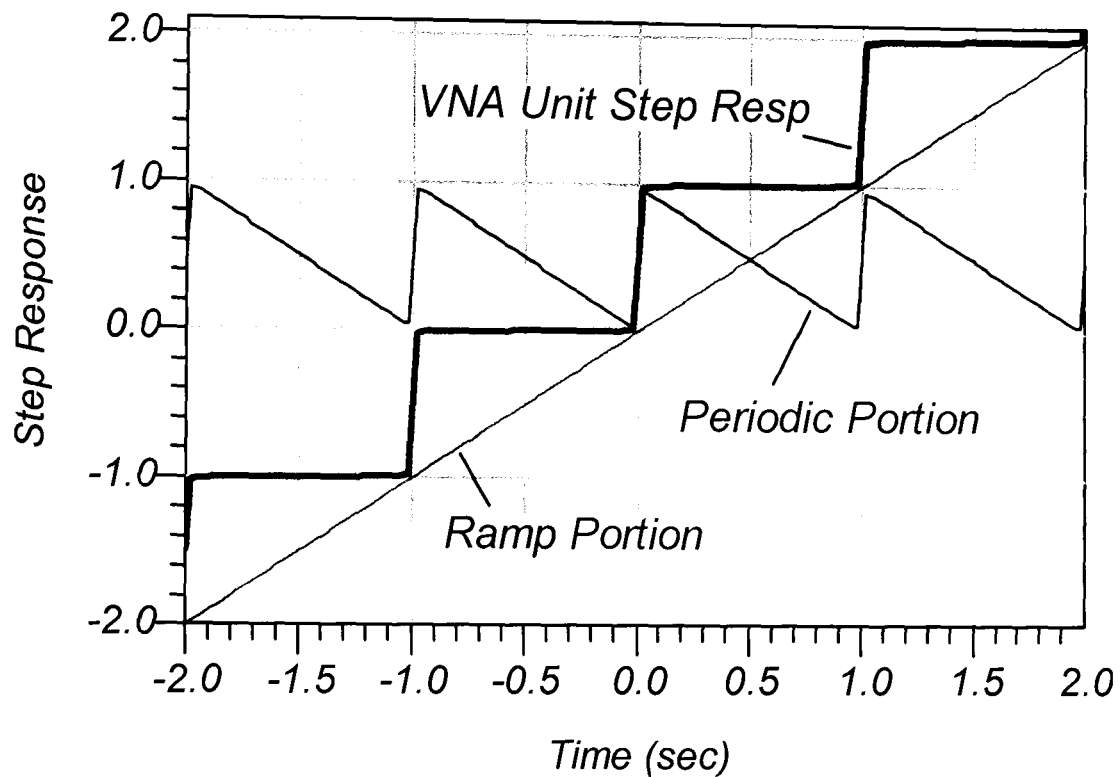


**Figure 3-6: VNA Unit Step response comprised of a periodic portion (which is Fourier transformable) and a ramp portion**

The time step-response can be determined from the network function and the unit step stimulus by applying the appropriate Fourier transform to the periodic portion, and some appropriate Laplace transform to the ramp portion. From equations (3.20) and (3.23) the step response for a sampled, truncated, windowed function can be proposed to be

$$f_{Step}(t) = \left\{ \frac{F(0)}{2} + \frac{\Delta\omega}{2\pi} \cdot 2 \cdot \text{Re} \left[ \sum_{n=1}^N \frac{F(n\Delta\omega) \cdot W(n\Delta\omega)}{jn\Delta\omega} \cdot e^{jn\Delta\omega t} \right] \right\} + F(0) \cdot \frac{\Delta\omega}{2\pi} \cdot t + C \quad (3.24)$$

Differentiation of equation (3.24) clearly results in equation (3.20), except for the window normalization factor of  $W_0$ , which is not used in the step response. For the case of  $F(\omega) = 1$ ,  $W(\omega) = 1$ ,  $C = 0$ , the equation (3.24) produces the unit-step stimulus.

The portion in the braces pertains to the periodic portion, while what remains is the response to the ramp function, with  $C$  being a constant associated with the ramp function response, and is determined from the DC group delay,  $\tau_d(0)$ , of the network as

$$C = -F(0) \cdot \frac{\Delta\omega}{2\pi} \cdot \tau_d(0) \quad (3.25)$$

An argument for this choice of constant is can be developed from an argument on the response of the network to a ramp input signal of the form  $x_r(t) = k \cdot t$ , as shown in figure 3-6. The Laplace transform of the output signal obtained by applying a ramp to a network with a response of  $H(s)$  is in the form of

$$Y(s) = \frac{H(s)}{s^2} \quad (3.26)$$

The output time signal is assumed to be in the form of  $y(t) = k \cdot H(0) \cdot t + C$ ; the difference between the transform of this assumption and equation (3.26) can be stated as

$$\varepsilon(s) = \frac{k \cdot H(0)}{s^2} + \frac{C}{s} - \frac{k \cdot H(s)}{s^2} \quad (3.27)$$

and the final, steady-state value of the difference can be found by applying the final value theory [72] to equation (3.27) as

$$\lim_{s \rightarrow 0} s \cdot \varepsilon(s) = \lim_{s \rightarrow 0} \left( \frac{k \cdot H(0) - k \cdot H(s)}{s} \right) + C \quad (3.28)$$

which, after applying L'Hospital's rule, becomes

$$\lim_{s \rightarrow 0} s \cdot \varepsilon(s) = \lim_{s \rightarrow 0} (-k \cdot H'(s)) + C \quad (3.29)$$

and making this final value difference zero finds

$$C = k \cdot H'(0) \quad (3.30)$$

To evaluate  $H'(0)$  it is assumed that the amplitude response of  $H(s)$  is nearly constant near DC, such that

$$H(s)|_{near DC} = |H(0)| e^{j\phi(s)}, \text{ so } H'(s)|_0 = H(0) \cdot j \cdot \phi'(s) \quad (3.31)$$

Recognizing that  $j \cdot \phi'(s)|_0 = d\phi/d\omega|_0 = -\tau_d(0)$ , where  $\tau_d(0)$  is the group delay near DC, we find

$$C = -k \cdot H(0) \cdot \tau_d(0), \text{ where } k = \frac{\Delta\omega}{2\pi} \quad (3.32)$$

from ramp driving function in equation (3.24).

Thus the step response can be obtained by taking the inverse Fourier transform of the frequency response divided by  $j$  times the step frequency, and adding to this a linear time ramp. The time-domain step response is only available in the low-pass mode.

### 3.4.4 Band-pass mode

The band-pass mode provides an alternative method of time-domain transform that may be used when the low-pass mode assumption of harmonically related frequencies cannot be met. This might occur, for example, in the measurement of a network that is band-pass or high-pass filtered. The output of a VNA measurement is typically an odd-numbered set of points, linearly spaced in the form of  $\omega = \omega_c + n\Delta\omega$  from  $n = -N/2$  to  $N/2$ , and  $\omega_c$  is the center frequency of the data. The inverse Fourier transform is calculated only on the data points measured, rather than taking the negative frequency response to be the conjugate of the measured data. Windowing is applied, where the center for the windowing function is the center frequency of the data set. (In contrast, the center of the windowing function in low-pass mode is centered on the DC term, or the first point of the data set). The inverse band-pass transform is defined by

$$f_{BP}(t) = \frac{1}{W_0} \frac{\Delta\omega}{2\pi} \cdot \sum_{n=-N/2}^{N/2} F_{BP}(\omega_c + n\Delta\omega) \cdot W(n\Delta\omega) \cdot e^{j(\omega_c + n\Delta\omega)t} \quad (3.33)$$

This is an important difference between the VNA band-pass mode and that described by Hines and Stinehelfer [62] which results in a pure real time-domain response. In contrast, the VNA band-pass response is complex, and this choice of transform is key to the results described in chapter 5, and in earlier papers [25,65]. To illustrate the band-pass transform mode, consider the frequency function of a band-pass filter. The frequency response tends to zero away from the center frequency, so the windowing function will have little effect on the transform. If the frequency response  $F_{BP}$  represents a band-pass version of a low-pass prototype response [73], such that  $F_{BP}(\omega) = F_{LP}(\omega - \omega_c)$  and thus  $F_{BP}(\omega_c) = F_{LP}(0)$ , the relationship between the time-domain band-pass transform of band-pass filter and the low-pass prototype's frequency response can be established as

$$f_{BP}(t) = \frac{e^{j(\omega_c)t}}{W_0} \frac{\Delta\omega}{2\pi} \cdot \sum_{n=-N/2}^{N/2} F_{LP}(n\Delta\omega) \cdot W(n\Delta\omega) \cdot e^{j(n\Delta\omega)t} \quad (3.34)$$

or in terms of the low-pass time-domain response

$$f_{BP}(t) = e^{j\omega_c t} \cdot f_{LP}(t) \quad (3.35)$$

From this it follows that the band-pass time-domain mode always returns a complex time-domain response. This effect is due removing the assumption that the frequency response is hermitian. The magnitude response of the band-pass transform is the same as the low-pass prototype

$$|f_{BP}(t)| = |f_{LP}(t)| \quad (3.36)$$

Thus, the band-pass mode response of the time-domain transform is quite different from the analytic impulse response of the network. Consider a network, such as a filter, that has a low-pass response  $f_{LP}(t)$ . If this filter is used as a prototype for a band-pass filter, and is shifted to create a band-pass response [74], the band-pass filter will have an analytic impulse response of

$$f_{Imp}(t) = 2f_{LP}(t) \cdot \cos(\omega_C \cdot t) \quad (3.37)$$

which is pure real as would be expected of an analytic transform of a real network. So, the band-pass mode transform has, in addition to the windowing, sampling and frequency truncation effects, an effect due to the data being taken as though the network has a single-sided (positive frequency only) response. Also, since the windowing function is centered on the center-frequency of the transform, it forces the function to zero at the lowest as well as highest frequency; there is no point in extrapolating the DC term.

One consequence of the band-pass transform is that the resolution is half that of the low-pass transform. This can be seen from equation (3.33), which shows the maximum frequency in the complex exponential is one-half of the frequency span (since the data ranges from  $n = -N/2$  to  $N/2$ ). The alias-free range for this transform remains the same as the range of the low-pass transform.

With this introduction to the time-domain transformations used in VNAs, the concept of time-gated measurements can be better understood.

### 3.5 Time-domain gating

Time-domain gating refers to the process of selecting a region of interest in a portion of the time-domain, removing unwanted responses, and displaying the result in the frequency domain. Gating can be thought of as multiplying the time-domain response by a mathematical function with a value of one over the region of interest, and zero outside this region. The gated time-domain function can then be forward transformed to

display the frequency response without the effect of the other responses in time. The gating effects, however, are somewhat subtle in their response and there are consequences of the gating function that are not readily apparent.

In practice, the gating is not a “brick-wall” function. This is because a sharp transition in the gate function causes a similar sharp transition in the gated time function. As such, the frequency response will have ringing associated with the sharp transition (as the frequency response is limited to the measured data region). Because of this, the gating function is windowed in the frequency domain before being transformed to the time-domain. For a rectangular time gating function centered at  $t = 0$ , the Fourier transform can be calculated analytically, with the result that the gate frequency response will have a  $\sin(\omega)/\omega$  or  $\text{sinc}(\omega)$  function. The width of the sinc main-lobe is inversely proportional to the width of the time gate. If the center of the gate time is not at  $t = 0$ , the resulting Fourier transform produces a response that corresponds to the sinc function multiplied by a complex exponential factor, namely  $\text{sinc}(\omega) \cdot e^{j\omega t_c}$ . This is windowed in the frequency domain by a Kaiser-Bessel window that sets the maximum gate transition slope in the time-domain. The gate function is then transformed to the time-domain and multiplied by the time-domain response, before being transformed back to the frequency domain. Alternatively, the time-gated frequency response may be determined by convolving the gate frequency response by the measured frequency response, and this view of the gating allows a more intuitive understanding of one of the subtle gating effects, described below.

A curious effect of the gating function occurs at the endpoints of the time-gated frequency-domain response: these endpoint regions are lower by 6 dB. The 6 dB offset can be understood by comparing the center point and last point of a gated frequency response of a unit function  $F(\omega) = 1$ . The time-domain response will approach a delta function,  $f(t) = \delta(t)$ . In the convolution of the gate frequency response  $G(\omega)$  with the original frequency response  $F(\omega)$ , the gated value at any frequency  $\omega_1$  can be determined by multiplying the original frequency response by the reverse of the gating frequency function centered at that frequency, and summing the result (this being the definition of convolution):

$$F_g(\omega_1) = \sum_{n=-N}^N F(n \cdot \Delta\omega) \cdot G(\omega_1 - n \cdot \Delta\omega) \quad (3.38)$$

For the center point (zero frequency, or DC) of a gated frequency response where the time gate is centered at  $t=0$ , the response is the sum of a multiplication of the sinc function (which is the gate frequency response as described above) with the original measured frequency response. For the case of the last frequency point (highest), the sinc function is centered on the last data point, and half the gate function is multiplied by zero (for frequencies above  $\omega = N \cdot \Delta\omega$ ), and does not add to the sum. Thus, the last data point will be one-half the value of the DC point, or 6 dB lower. This creates the unfortunate result that any gating will distort the last points (and first points in band-pass mode) of the gated frequency response.

The VNA time-domain compensates for this roll-off through a post-gate renormalization. The post-gate renormalization is determined by creating a frequency response that is unit magnitude. A pre-gate window is applied to this unit-response that is the same as the pre-transform window applied to the normal frequency response data. This unity-magnitude frequency response is convolved with the gate frequency response, to generate the final normalizing frequency response. The time-gated frequency response is divided by this function to remove the roll-off effects of the time gating. This normalizing function works perfectly for a unit time response at the center of the gate. If the gate is not symmetric around the time function, there will be show errors in the gated response when compared to the original frequency response.

It is instructional to view the actual gate shape in the time-domain, which can be done using a function not normally available in commercial VNAs. The gate shape may be generated by creating a delta-like frequency response ( $F(0) = 1$ ;  $F(\omega) = 0$  for  $\omega \neq 0$ ), applying gating, and transforming the result to the time-domain to see the actual gate shape. This is useful in understanding how the gate shape affects the gated response.

Figure 3-7 (upper) shows the gating function for various gate center times. Figure 3-7 (middle) shows a unit frequency response ( $F(\omega) = 1$ ) in the time-domain, with gates applied at various gate times. Note that the peak of the time-domain response is nearly unchanged as the time-gate fully encompasses the impulse at all three center times, but there is some difference in the side lobes for the shifted gates. Figure 3-7 (lower) shows the frequency response after gating. Here there is a substantial difference in the response at high frequency for the different gate center times. It is clear that normalization is optimal when the gate is centered on the response being gated.

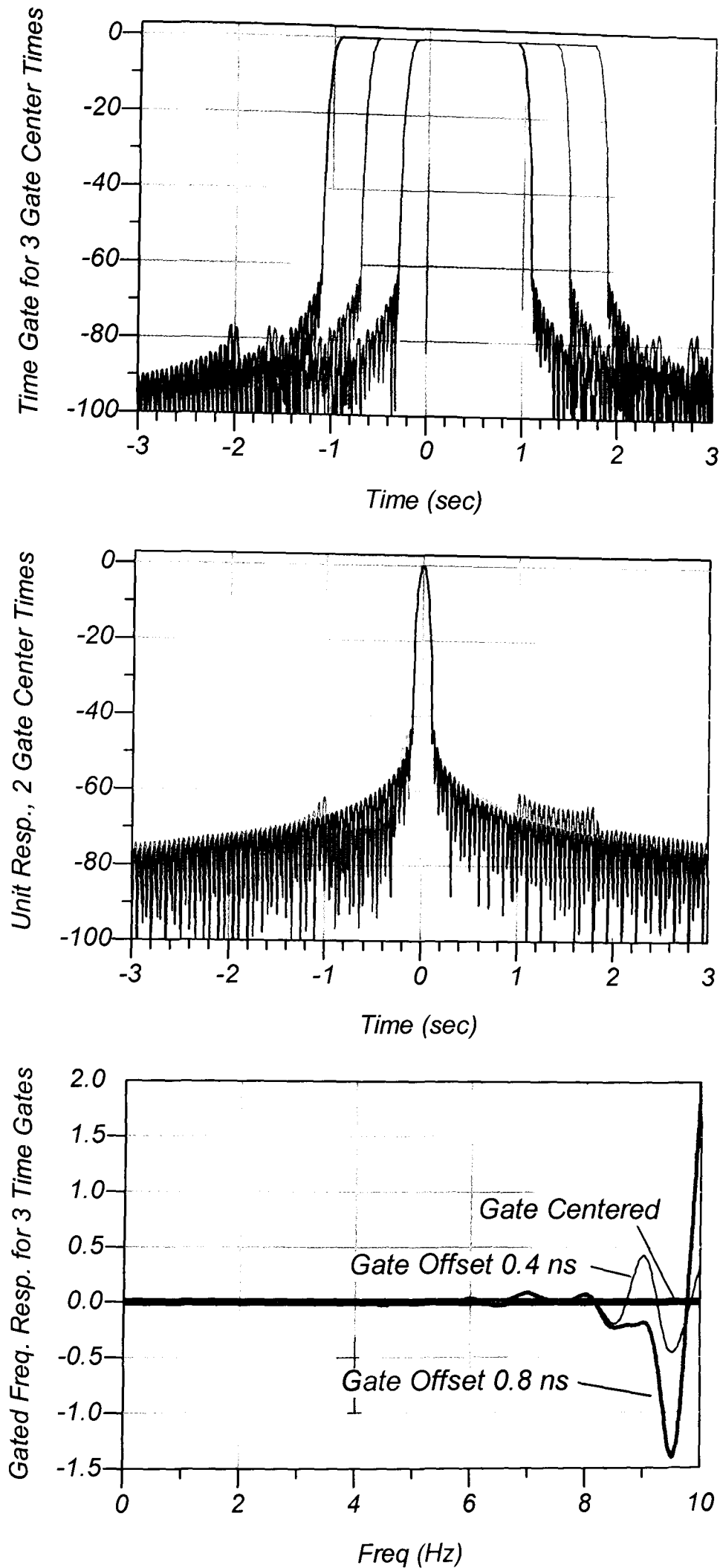


**Figure 3-7 (upper) Time gates at 3 center times; (middle) time response of Gated Unit Response, with the first and last gate center; (lower) gated frequency response of 3 gate centers, showing normalization error at the band edge (only positive frequency shown).**

The gated time-response may be viewed in time-domain by taking the IFT and displaying the result. In fact, it is almost always required first view the time-domain response to assign proper gating start and stop values: the transform function is turned on, and the resultant time-domain response is displayed, and the gate start and stop are set. Next gating is turned on. Finally, the transform is turned off, and the time gated frequency response is shown in the frequency display.

A study of the time-domain response of several examples of composite responses of several component elements will show how time gating can be used to separate the responses in time and display the individual frequency responses of the component elements, but with some distortion due to masking effects [75]. From this a method is developed that compensates for these effects.

### 3.6 Examples of time-domain transforms of various networks

#### 3.6.1 Time-domain response of changes in line impedance

For ladder networks, that is, networks that consist of series connected elements, the time-domain transform provides very good insight into the nature of the discontinuities by which the frequency response is generated. As a first example, consider a network in figure 3-8 (upper) of a short  $Z_0$  line followed by a  $Z_0/2$  impedance line segment terminated in a  $Z_0$  line. Note that there will also be re-reflections if the time scale is extended. There are two main reflections from the impedance steps at the beginning and end of the  $Z_0/2$  line segment. The impedance value of a discontinuity caused by a step in impedance of a transmission line can be directly related to the time-domain step response, which shows reflections as a function of time. The reflections are relative reflection coefficient, so for a 50 ohm reference impedance, a 1% reflection relates to approximately 1 ohm change in impedance, as

$$\Gamma = \frac{Z - Z_0}{Z + Z_0}, \text{ and for } Z \cong 50, \Gamma(\%) \cong \Delta Z, \text{ where } \Delta Z = Z - Z_0 \quad (3.39)$$

Care must be used in this interpretation, as other factors such as loss in the transmission line, changes in line impedance, and previous reflections can affect the apparent reflection being investigated. For the lines in figure 3-8, the step in impedance is quite large, and the reflection coefficient of each step is the same,  $|\Gamma| = 0.33$ . However, the apparent reflection coefficient of the second transition,  $\Gamma_2$ , is only 0.30, as shown in

figure 3-8 (lower). Also, the impulse response shows a similar “masking” effect in the second reflection response.

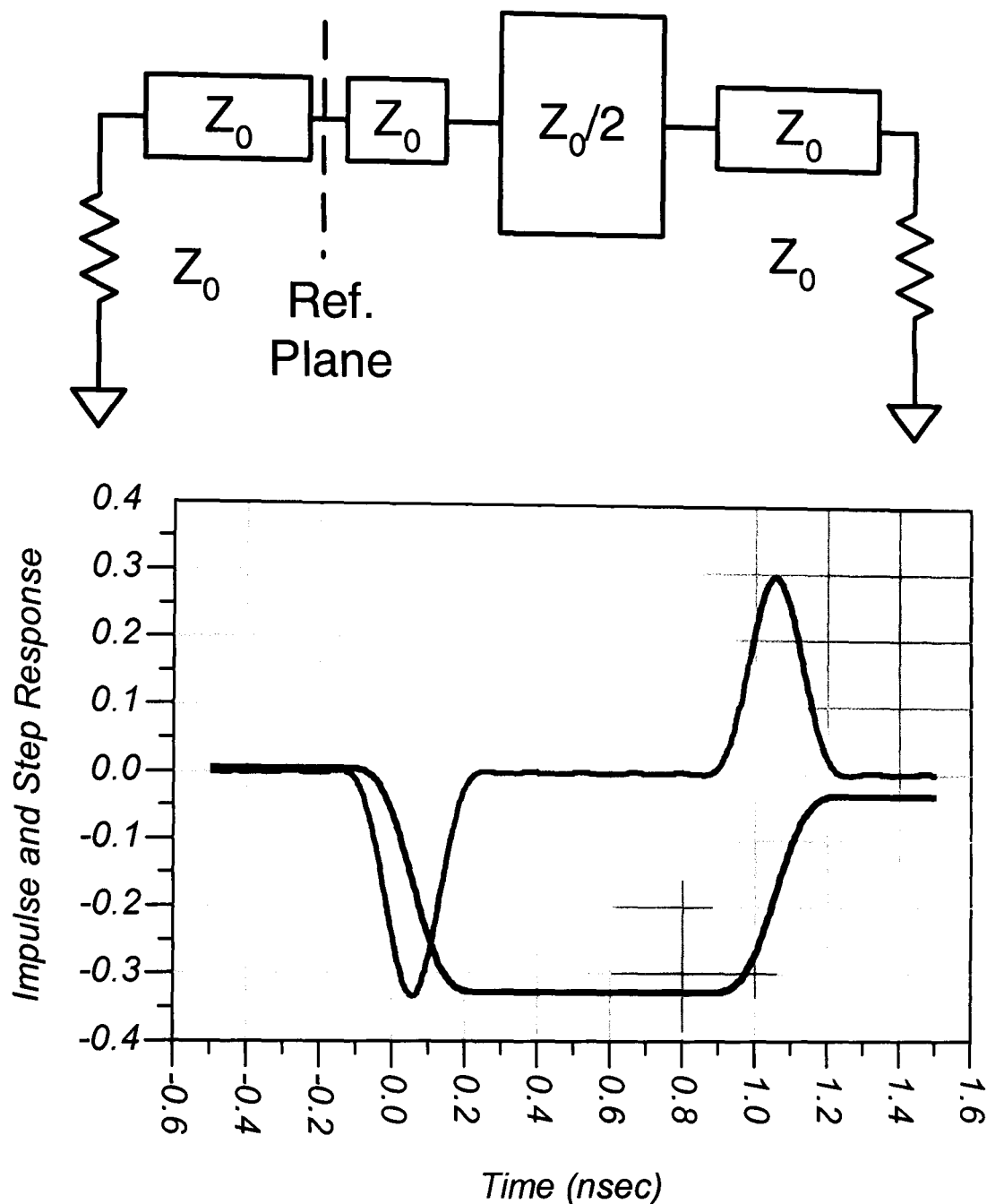


**Figure 3-8 (upper) Model of concatenated lines of different impedances, (lower) Step (black) and Impulse (gray) response of the lines in time.**

### 3.6.2 Time-domain response of Discrete Discontinuities

As a second example, concatenated transmission lines with discrete discontinuities between sections are evaluated with a time-domain transform of the frequency response, and the values of the various discontinuities are individually determined. Figure 3-9 (upper) shows a schematic of a  $Z_0$  reference, followed by a first capacitive discontinuity, and followed by a  $Z_0$  line then a second identical capacitive discontinuity terminated in a  $Z_0$  load.

The time-domain response of this network is shown in figure 3-9 (lower). This is the low-pass step response, which shows capacitive discontinuities as negative dips in the time-domain. The reflections of the discontinuities repeat at the spacing of the discontinuities, and these repetitive reflections should ideally continue on, at diminishing levels, for infinite time (though actually they get added to all the aliased responses). Also, note that even though the responses are caused by identical discontinuities, the response of the second discontinuity appears smaller than the first. The second response is somewhat masked by the first, though by a different amount than in the example of figure 3-8, indicating a different masking mechanism.

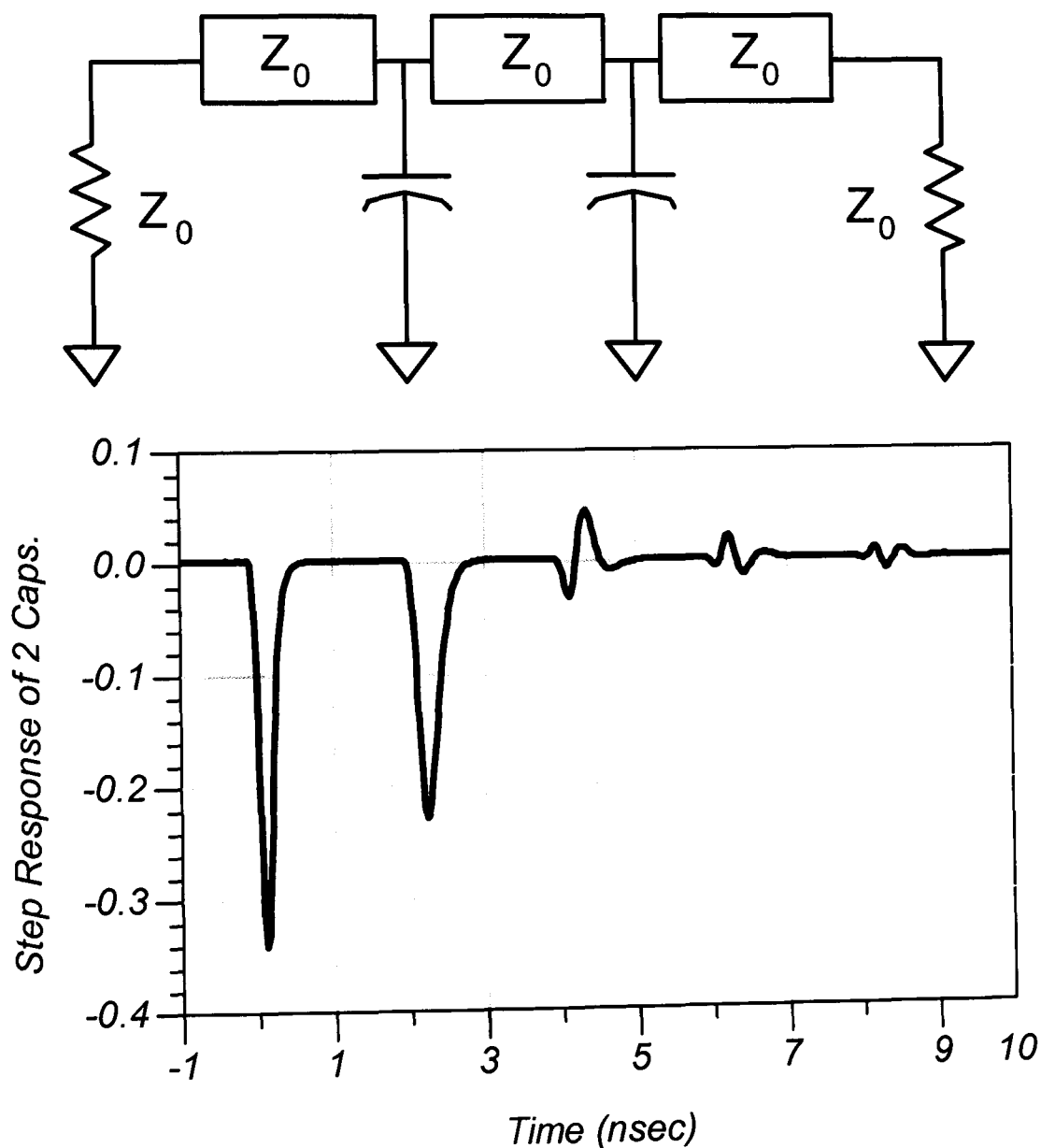


**Figure 3-9 (upper) Model of 2 capacitive discontinuities, (lower) Step response of the S11 of two discontinuities**

### 3.7 The effects of masking and gating on measurement accuracy

The concept of time gating above refers to mathematically removing a portion of the time-domain response, and viewing the result in the frequency domain. The intent is to remove the effects of unwanted reflections, say from connectors and transitions, leaving the desired response of the device being measured. This should improve the quality of the response, that is, the gated response should more closely resemble the device response as if it were measured with no other reflections. However, the effects of previous reflections can have an effect on the time-gated measurement. Previous work has reported on the compensating for the effect of loss [76] but ignored the effect of previous reflections. Others have proposed an error associated with previous reflections [75] but have not provided for compensation methods, or for errors associated with change in impedance. These effects are mathematically described below, along with new compensation methods, and with an uncertainty analysis on the time-gated frequency response, applied to several particular examples.

#### 3.7.1 Compensation for changes in line impedance

For the lines in figure 3-8, the apparent reflection coefficient of the second transition,  $\Gamma_2$ , is only about 90% of the actual value. To understand this, consider that at the interface of the first reflection, the reflection coefficient is calculated as defined in (3.39). However, the signal that continues down the transmission line structure is changed by the transmission coefficient defined as [77]

$$T_1 = \frac{2 \cdot Z_1}{Z_1 + Z_0} \quad (3.40)$$

where  $Z_0$  is the input line, and  $Z_1$  is the second section of line. The reflection apparent at the input due to the second step in impedance,  $\Gamma_2$ , is further changed by a second (reverse) transmission coefficient,  $T_2$  as defined by

$$T_2 = \frac{2 \cdot Z_0}{Z_1 + Z_0} \quad (3.41)$$

The total apparent reflection,  $\hat{\Gamma}_2$ , due to the second step is now computed as

$$\hat{\Gamma}_2 = \Gamma_2 \cdot T_1 \cdot T_2 = \frac{(Z_0 - Z_1) \cdot (4Z_1Z_0)}{(Z_1 + Z_0)^3}; \text{ where } \Gamma_2 = \frac{(Z_0 - Z_1)}{(Z_1 + Z_0)} \quad (3.42)$$

recognizing the reference impedance for  $\Gamma_2$ , is the  $Z_1$  line. For the example of Figure 2,  $\hat{\Gamma}_2 = +0.30$ . This precisely matches the measured value in figure 3-8.

Further, for the case of a response following a change in line impedance, where the first line impedance is not the reference impedance, two compensations are required. First the reflection response must be compensated by dividing the apparent response by the transmission coefficient term product,  $T_1 \cdot T_2$  to produce a reflection response relative to the line,  $S'_{11} = S_{11} / T_1 \cdot T_2$ , (derived from  $\hat{\Gamma}_2$  as shown above). The second compensation is re-normalizing the response by the impedance of the line just before the desired response. The frequency response assumes a reference impedance of the system impedance, typically 50 ohms. The re-normalization consists of converting the reflection response to an effective impedance  $Z_{eff}$ , using the line impedance  $Z_{line}$  just before the desired response ( $S'_{11}$ ), as the reference impedance. This is then re-converted from the resulting effective impedance back to effective reflection response ( $S_{11(eff)}$ ) using the system impedance:

$$Z_{eff} = Z_{line} \cdot \frac{1 + S'_{11}}{1 - S'_{11}}, \quad S_{11(eff)} = \frac{Z_{eff} - Z_0}{Z_{eff} + Z_0} \quad (3.43)$$

### 3.7.2 Compensation for discrete discontinuities

Figure 3-9 shows the time-domain response of two capacitive discontinuities. The second discontinuity, which is caused by an identical element in the circuit, has a different time-domain response from the first element. The most noticeable aspect is the magnitude of the response is smaller, which is consistent with the first example. However, in this case, there is no change in reference impedance to account for the difference. Instead, the first reflection removes some of the energy from the forward (incident) wave, such that there is less energy available at the second discontinuity. A similar effect occurred in the first example, and was accounted for by the transmission coefficients. For a localized discontinuity, with the same impedance on each side, the effect on the transmitted wave must be determined in a different manner.

From power conservation, the magnitude of the voltage wave incident on the second reflection,  $|V_2^+|$ , (assuming the first reflection is loss-less) is

$$|V_2^+| = |V_1^+| \cdot \sqrt{1 - |\Gamma_1|^2} \quad (3.44)$$

where  $V_1^+$  is the incident voltage wave and  $\Gamma_1$  is the first reflection. The magnitude of the reflected voltage,  $|V_2^-|$ , from the second reflection is

$$|V_2^-| = |V_2^+| \cdot \Gamma_2 = |V_1^+| \cdot (\sqrt{1 - |\Gamma_1|^2}) \cdot \Gamma_2 \quad (3.45)$$

The signal  $V_2^-$  reflects again off  $\Gamma_1$  with a portion transmitted,  $V_3^-$  (the portion of the signal from  $\Gamma_2$  that is actually measured at the input port), which is reduced in the same manner as equation (3.44) to yield the effective value of the second reflection as

$$|\hat{\Gamma}_2| = \frac{|V_3^-|}{|V_1^+|} = (1 - |\Gamma_1|^2) \cdot \Gamma_2 \quad (3.46)$$

This result only applies to the magnitude of the reflection as the power conservation argument does not apply the phase of the transmitted signal, and while consistent with the result described by Lu [75], goes further to provide a means to remove the effects of the first discontinuity.

### 3.7.3 Gating the first of two discontinuities

The effectiveness of gating can be evaluated using the circuit from figure 3-9. Figure 3-10 shows the original frequency response in light gray, with the characteristic ripple pattern found from two discontinuities separated by a length of line. The thin black trace is the result of computing the ideal  $S_{11}$  of just a single capacitive discontinu-

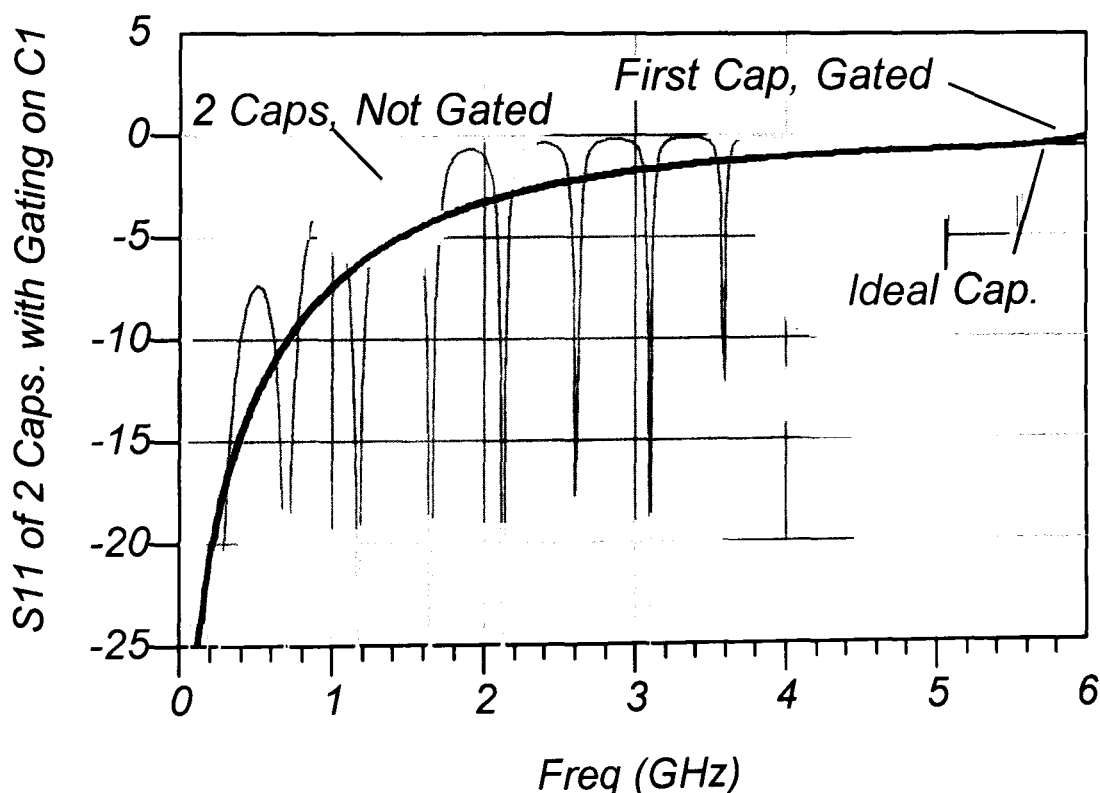


**Figure 3-10:  $S_{11}$  response of 2 capacitive discontinuities (light gray) and gating around the first cap (dark grey). Also shown is the  $S_{11}$  of just the first cap (black)**

ity, terminated in  $Z_0$ . Gating around the first capacitive discontinuity yields a response (Fig. 10-3, dark grey) nearly identical to the frequency response calculated for only the first discontinuity. The difference is seen only at the high frequency of the response, most likely due to the errors in the re-normalization, as described in figure 3-7 (lower). Clearly, gating about a first discontinuity terminated in  $Z_0$  is very effective in removing effects of other elements. However, if the gate is applied to the second discontinuity, the response is not similar.

### 3.7.4 Gating the second of two discontinuities

The time-gated response of the second discontinuity is quite different from the underlying response as shown in figure 3-11, (thin dark trace, labeled “2nd Cap, Gated, No Comp.”). The frequency response of the gated measurement of the second discontinuity may be compensated by taking the gated response of the first discontinuity, and applying equation (3.46) as compensation. This compensation has been applied in figure 3-11, with the result showing remarkably good compensation over most of the frequency range (thick black trace, labeled “2nd Cap, Gated & Comp.”). However, the band edge response deviates because of the normalization does not completely compensate the error due to the gate, as described in the figure 3-7.

Also shown in figure 3-11 is the un-gated  $S_{11}$  measurement of both discontinuities

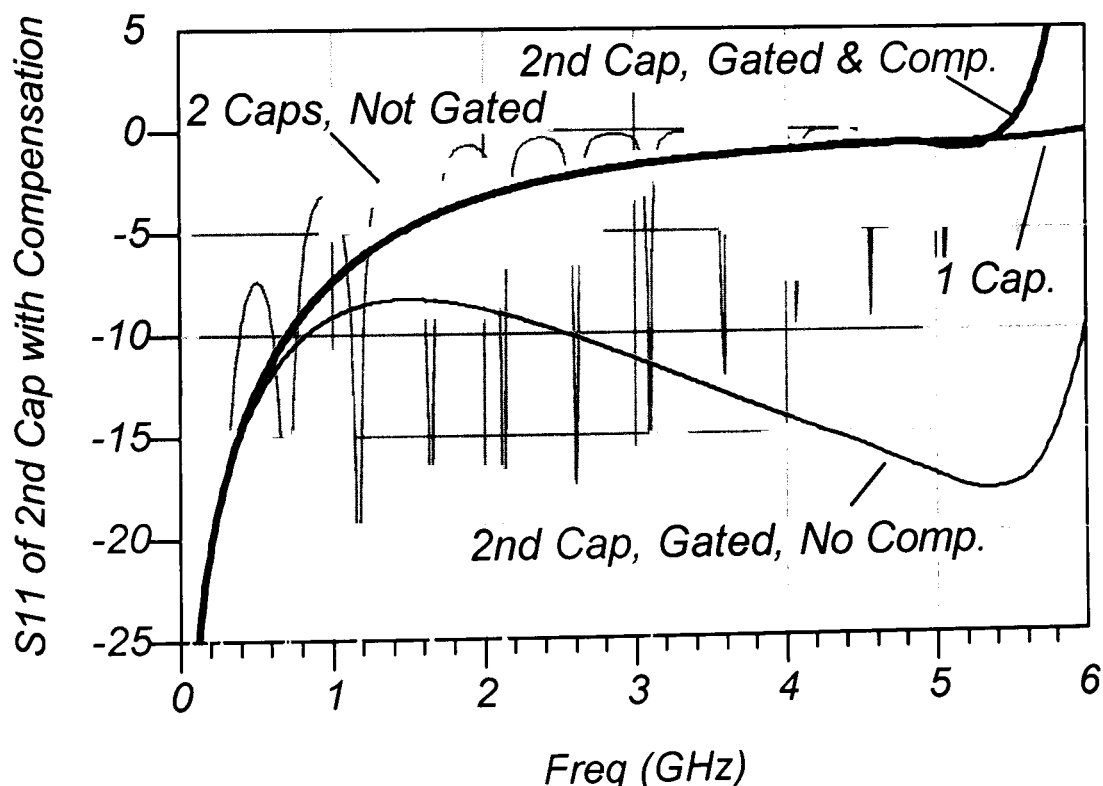


**Figure 3-11:  $S_{11}$  of 2 capacitive discontinuities (light gray) not gated,  $S_{11}$  response of 1 capacitive discontinuity (dark gray),  $S_{11}$  of 2nd discontinuity gated (thin black) with no compensation, and  $S_{11}$  of 2nd discontinuity, gated and compensated (thick black).**

(light gray), and, for reference, the  $S_{11}$  of just a single discontinuity (dark gray, labeled “Ideal Cap.”). This shows the effectiveness of the compensation method, where there is substantial deviation from ideal of the un-compensated gated response of the second capacitive discontinuity. Also note that this is a very large discontinuity, having a frequency response return loss value of nearly 0 dB over much of the frequency range.

### 3.7.5 Compensation for a combination of discontinuities and line impedance changes.

Many practical applications of time-gated measurements include effects of both discrete discontinuities and impedance steps. For example, the measurement of a connector at the far end of a cable is affected by the cable’s near end connector, and the impedance of the cable. Figure 3-12 (upper) shows a circuit diagram and (lower) time-domain response of a 55-ohm cable with a 20 dB return loss (at 1 GHz) input and output mismatch due to capacitive loading, terminated in 50 ohms. The cable itself has a

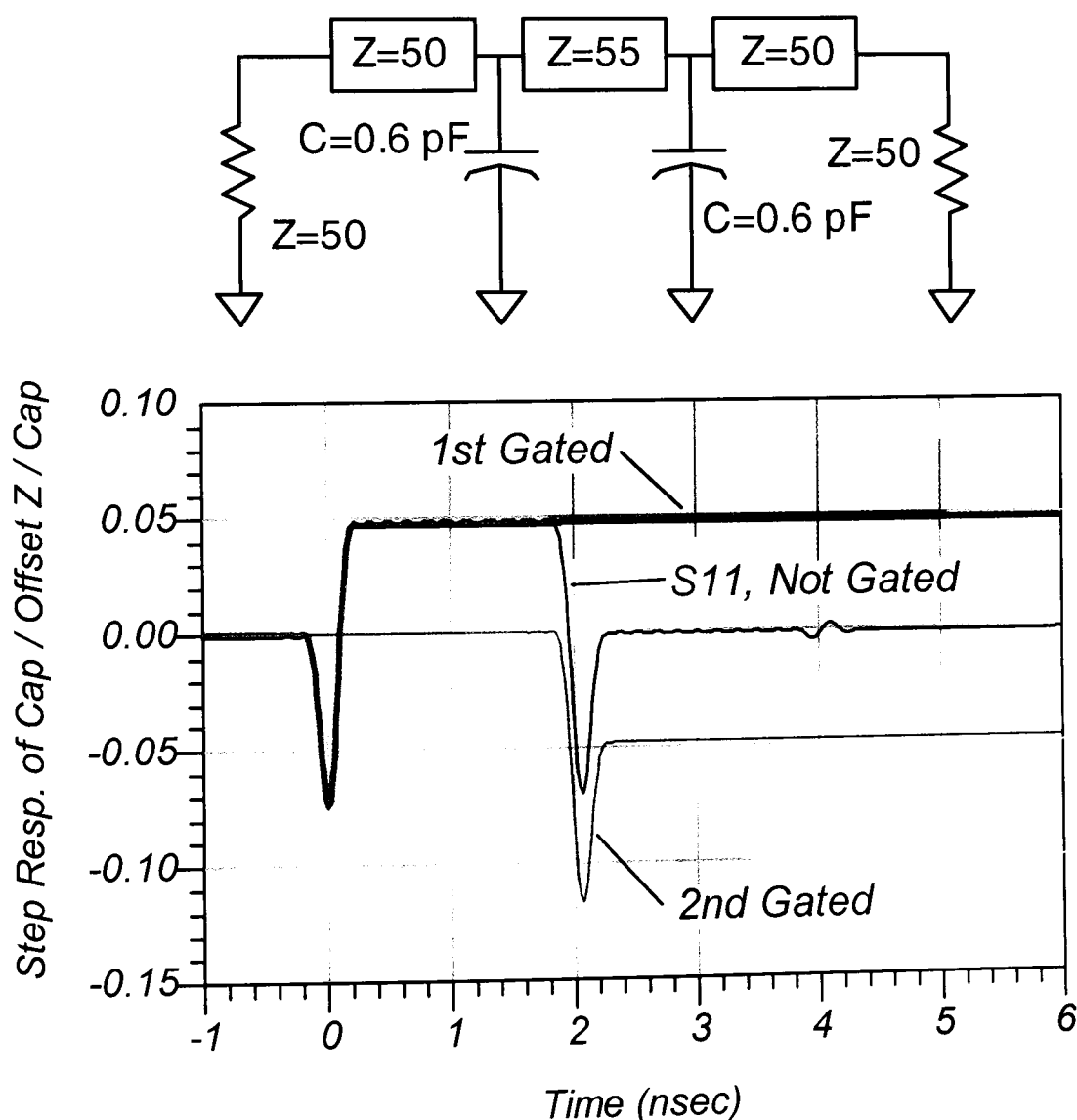


**Figure 3-12 (upper) Circuit with 2 capacitive discontinuities, and an offset impedance line; (lower) Time-domain response of the circuit (black) with gating around the first cap (wide gray) and second cap (thin gray)**

5% reflection, and each discontinuity is approximately 10% at 1 GHz.

Figure 3-13 (upper) and (lower) shows the time-gated frequency response of the first and second discontinuity as a result of gating about each respectively. In the case of gating the first discontinuity, there is only an impedance step to be accounted for.

A normalization of the first case can be performed by recognizing in the step re-

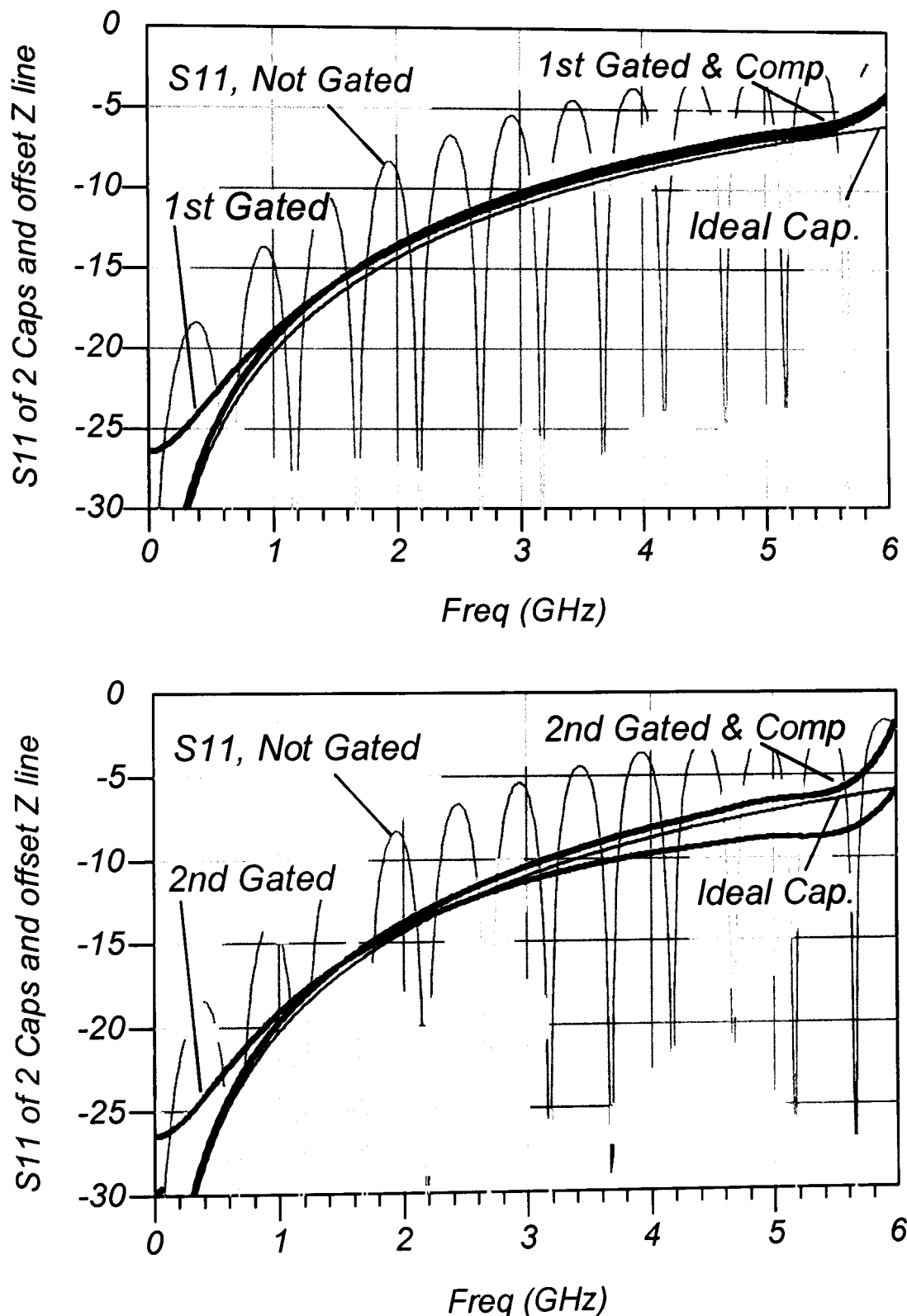


Figure 3-13 (upper) Time gated response of the first discontinuity (thick gray, “1st Gated”), and with compensation (thick black, “1st Gated & Comp”), along with original S11 (light gray) and ideal single capacitive discontinuity (thin black); (lower) similar to the upper trace but with gating and compensation applied to the second discontinuity

sponse that the value of the step after the gate represents an offset impedance in the termination. The effective reflection results in

$$\hat{\Gamma}_1 = \Gamma_1 + \frac{\Gamma_2}{(1 - \Gamma_1 \cdot \Gamma_2)} \quad (3.47)$$

which, using

$$\frac{1}{1-x} = 1 + x + x^2 + \dots \text{ for } x < 1 \quad (3.48)$$

can be reduced to find the value for  $\Gamma_1$ , for small reflections, as

$$\Gamma_1 \approx \hat{\Gamma}_1 - \Gamma_2 - \frac{\Gamma_1(\Gamma_2)^2}{(1 - \Gamma_1 \cdot \Gamma_2)} \approx \hat{\Gamma}_1 - \Gamma_2 \quad (3.49)$$

Here  $\Gamma_2$  is the reflection coefficient of the 55-ohm cable that forms the termination after gating, and there is assumed no delay before  $\Gamma_1$ . Figure 3-13 (upper) shows the first discontinuity, after gating and gating plus compensation. If there is delay before the first discontinuity, the phase of  $\Gamma_2$  must be shifted to account for the delay.

The masking of the second discontinuity is more difficult to account for. There are three effects: first masking due to signal loss in the first discontinuity as described by equation (3.46), and second, by the change in reference impedance as described by (3.42), and finally, by the change in terminating impedance, relative to the modified reference impedance, as described by equation (3.49). Thus three compensations are required. First, the effective reflection after the first discontinuity is found by applying the first compensating equation, then the effect of the impedance transformation is compensated by applying the equation (3.42) to the result of the first equation, which in this case is a small effect, and finally, compensating for the step in impedance from the at the termination. Also, as this compensation includes an additive element associated with the terminating impedance, phase becomes important. Both  $\Gamma_2$  and  $\Gamma_3$  are phase shifted by the delay of line  $Z_1$ , which may be determined directly from the time-domain response. Thus, the effective impedance  $\hat{\Gamma}_2$  is

$$\hat{\Gamma}_2 = \frac{\Gamma_2 \cdot (4Z_1Z_0)}{(Z_1 + Z_0)^2} \cdot (1 - |\Gamma_1|^2) \cdot e^{j\omega \cdot 2\tau_d(Z_1)} + \Gamma_3 \cdot e^{j\omega \cdot 2\tau_d(Z_1)} \quad (3.50)$$

where  $\hat{\Gamma}_2$  is the gated response of the second discontinuity,  $\Gamma_2$  is the reflection of only the second discontinuity,  $\Gamma_1$  is the (gated) first discontinuity,  $Z_1$  is the 55 ohm line,  $\Gamma_3$  is the reflection from  $Z_1$  to the terminating impedance,  $Z_0$ , and  $\tau_d(Z_1)$  is the delay

corresponding to the length of the line  $Z_1$ . The compensation is determined by solving equation (3.50) for  $\Gamma_2$ :

$$\Gamma_2 = \left( \hat{\Gamma}_2 \cdot e^{-j\omega \cdot 2\tau_d(Z_1)} - \Gamma_3 \right) \frac{(Z_1 + Z_0)^2}{(1 - |\Gamma_1|^2) \cdot (4Z_1 Z_0)} \quad (3.51)$$

Figure 3-13 (lower) shows the results of gating the second discontinuity, and applying the compensations as described in (3.51). Also shown is the frequency response of a single (ideal) discontinuity associated with the first capacitance as though it were on a matched line, and the original response of the 2 discontinuities with the offset impedance line in between. In figure 3-13, for both the (upper) and (lower) plots, there is remarkable improvement in the gated measurement, especially at low frequencies, when evaluated against the ideal response. In this example, the compensated result is quite sensitive to the delay selected for the 55-ohm line. This delay was determined by choosing the delay displayed at the peak of the second discontinuity. These compensations are appropriate for single discontinuities that are loss-less and non-distributed.

### 3.7.6 Estimating an uncertainty due to masking.

The proposed compensations described above may generate some error, in part due to lack of consideration of loss in the network, and due to inability to totally separate responses. In some cases it may not be necessary to actually compensate the network for gated response, but rather to establish an estimate of uncertainty associated with the response that is gated out. This uncertainty can be derived from equation (3.46), for a second gated response on matched line. Additional uncertainty will come from non-matched lines leading up to the reflection of interest, and following the reflection of interest. The magnitude of the uncertainties can be determined in a manner similar to (3.42) and (3.50) with the resultant total uncertainty after gating determined as

$$\Delta\Gamma_2 = \frac{\Gamma_{2G}}{1 - |\Gamma_1|^2} \left( |\Gamma_{Z_1 Z_0}|^2 + |\Gamma_1|^2 \left| \frac{(4Z_1 Z_0)}{(Z_1 + Z_0)^2} \right| \right) + \Gamma_{Z_2 Z_1} \quad (3.52)$$

where  $\Gamma_1$  is the first (gated out) discontinuity and  $Z_1$  and  $Z_2$  are the lines before and after the desired reflection  $\Gamma_2$ , respectively, and  $Z_0$  is the system impedance, and  $\Gamma_{Z_1 Z_0}$  and  $\Gamma_{Z_2 Z_1}$  are the reflection between lines  $Z_1$  &  $Z_0$  and  $Z_2$  &  $Z_1$  respectively, and  $\Gamma_{2G}$  is the value of the gated response.

### **3.8 Conclusions:**

The exact relationship of time-domain transform used in vector network analyzers to the analytic impulse response of measured networks has been described for the first time with mathematical rigor, and details of the time gating function have been presented. From this background, the effects of time gating on measured results have been explored, and a method is given for compensating for undesired masking effects, yielding superior time-gated measurement results. Additionally, the uncertainty of time-gated measurements has been quantified, and qualitative errors due to the subtle effects of gate properties and renormalizations have been presented. The results of this masking investigation will be useful in understanding the resonator interactive effects of tuning filters in time domain.

## Chapter 4 Filter Tuning Using Time-Domain Transforms

In 1999 this author presented a novel filter tuning method [24-26] based on the time-domain response of a filter. References [25] and [26] are included as published papers 1 and 2, respectively, where the first contains an outline of the method, and second reports details on applying the tuning method. The technique, which was empirically developed, describes a method of tuning coupled resonator filters by looking only at the time-domain response using the built-in time-domain function of a VNA. The following sections document the experimental investigation into the time-domain response of filters.

### 4.1 The invention of the time-domain tuning method

The first filter for which the time-domain response was documented was a 5-resonator all-pole filter. As noted earlier, the discovery of the relationship between the VNA time-domain response and the proper tuning of a filter was serendipitous, but provides good motivation for a broad basic training for all electrical engineers, as well as good observational skill, and provides some insight into why this relationship between a filter's tuning and its time-domain response had not been previously noted.

The author was tasked with evaluating improvements in network analyzer measurements resulting from an enhancement of the CPU speed. Until this time, full two-port calibration [78] required significant post processing time that slowed the real-time sweeping of components, such as filters, and filter tuning was often done without full calibration. Since filter tuning was a key application for the network analyzer, a 5-pole band-pass filter was chosen as a test device. Turning on time-domain was done solely to add an additional computation burden to the CPU. Figure 4-1 shows the  $S_{21}$  and  $S_{11}$  frequency response of the filter in the upper plot, and the  $S_{11}$  time-domain response in the lower plot. While tuning the filter, and evaluating the real-time "feel" of the trace response, the author noted that turning a tuning screw on the filter caused a change in the time-domain trace over one region of the trace, and turning a different screw caused a change at in different region. Thus, the time-domain appeared to separate the effects of tuning screws, with the tuning screws closest to the test port affecting the earlier portions of the time-domain trace, and tuning screws farther from the test port affecting latter portions of the time-domain trace. This in itself was surprising, as conventional wisdom held that the time-domain function was not useful when looking at band-pass filters. The reasoning was that the time resolution of the time-domain function is in-

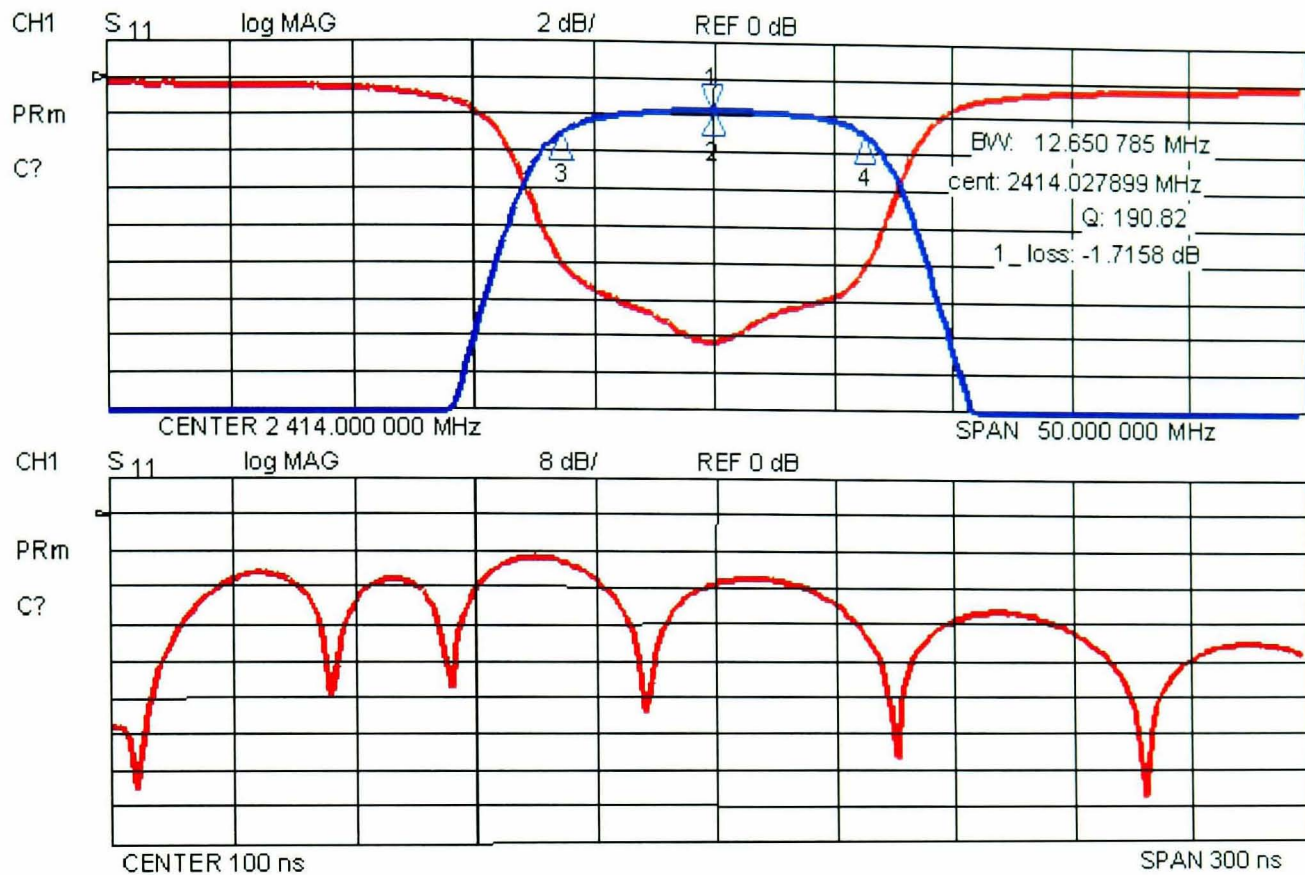


**Figure 4-1: Frequency response ( $S_{11}$  and  $S_{21}$ , upper plot) and time-domain response (lower plot) of a 5-pole band-pass filter**

versely proportional to the frequency span. With a wide frequency span (to get narrow resolution) almost all the energy is reflected from the filter, so the time-domain response shows essentially the response of a short- or open-circuit, depending upon the first element of the filter.

Consider the circuit of a 3-pole Butterworth filter shown in figure 4-2. This is a 50 MHz wide filter, centered at 1 GHz, and is one of the filters used throughout the rest of the thesis to illustrate several aspects of time-domain tuning. Figure 4-3 shows the frequency response for  $S_{21}$  and  $S_{11}$  of this filter. From this frequency response one can see that the filter is not ideally symmetric due to the fact that capacitors are used as coupling elements. One might note the unusual frequency settings for the measurement. These were chosen to be consistent with the requirements for the low-pass mode

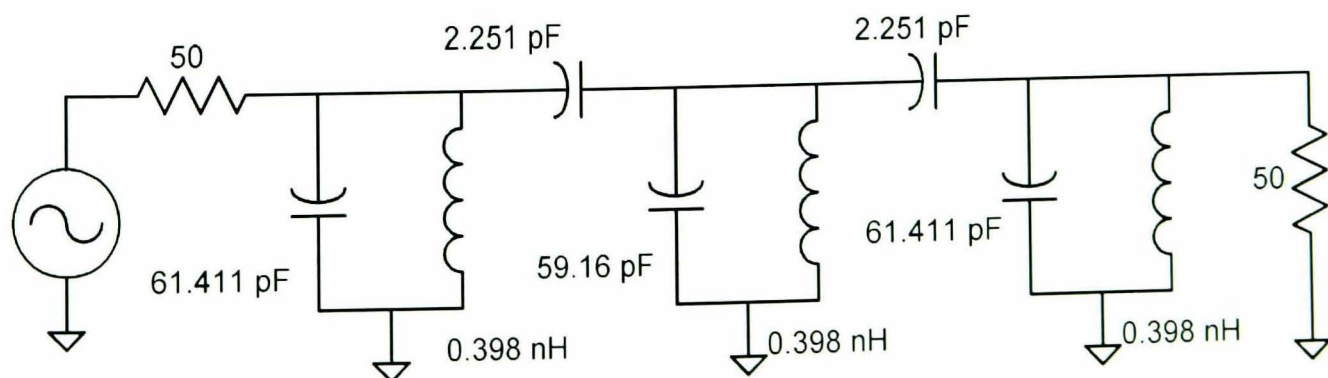


**Figure 4-2: Schematic of a 50 MHz wide, 1 GHz center frequency band-pass filter used to illustrate time-domain tuning effects**

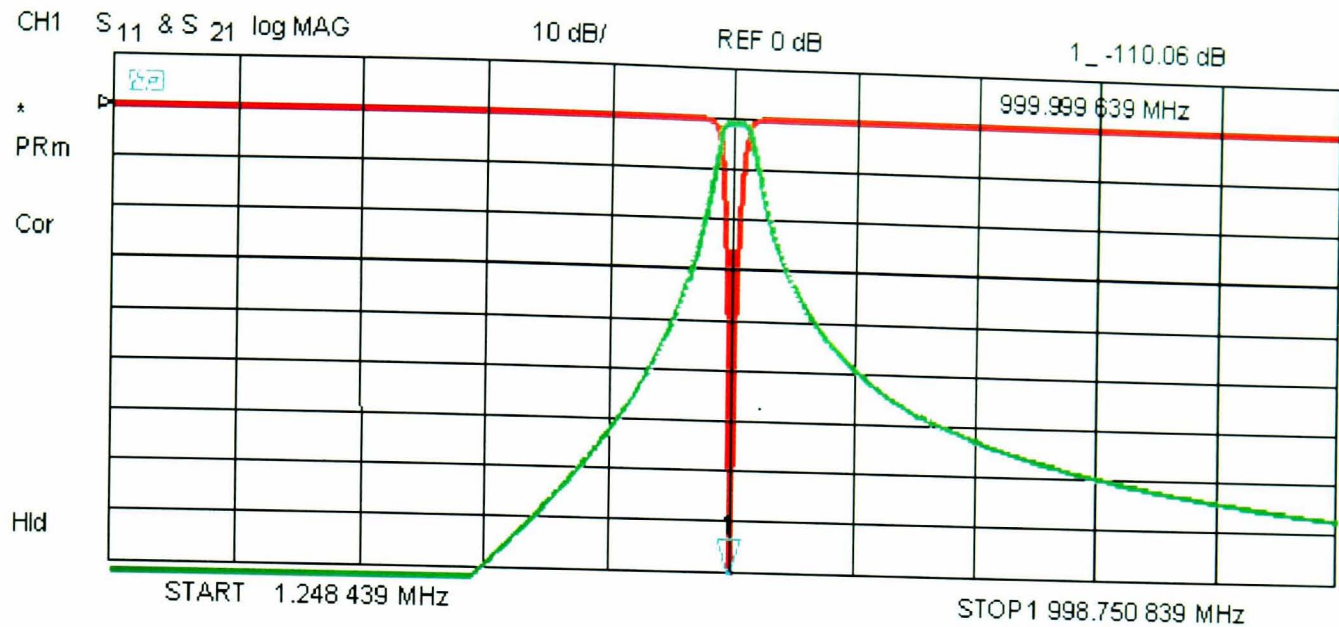


**Figure 4-3: S11 and S21 frequency response of a 3-pole band-pass filter**

time-domain transform as described in section 3.4.

From the frequency settings shown, one can calculate a time-domain resolution of about 500 psec, or about 75 mm in air. The time-domain transform for this filter is shown in figure 4-4. It is clear that there is a nearly unity response at time zero, with what looks like a substantial ringing response that follows. Since almost all the energy reflected is in the first peak, at time  $t=0$ , there does not appear to be any useful information in the time-domain response with respect to filter tuning. The band-pass mode, which may be used over a narrow range, was considered unsuitable as the frequency span used to view the filter, perhaps 2 or 3 times the filter bandwidth, would yield a time resolution of about 7 nsec, or roughly 2 meters in air, which is many times longer than the physical length of the filter.

However, the fact that the tuning screws appeared to have some relationship to the

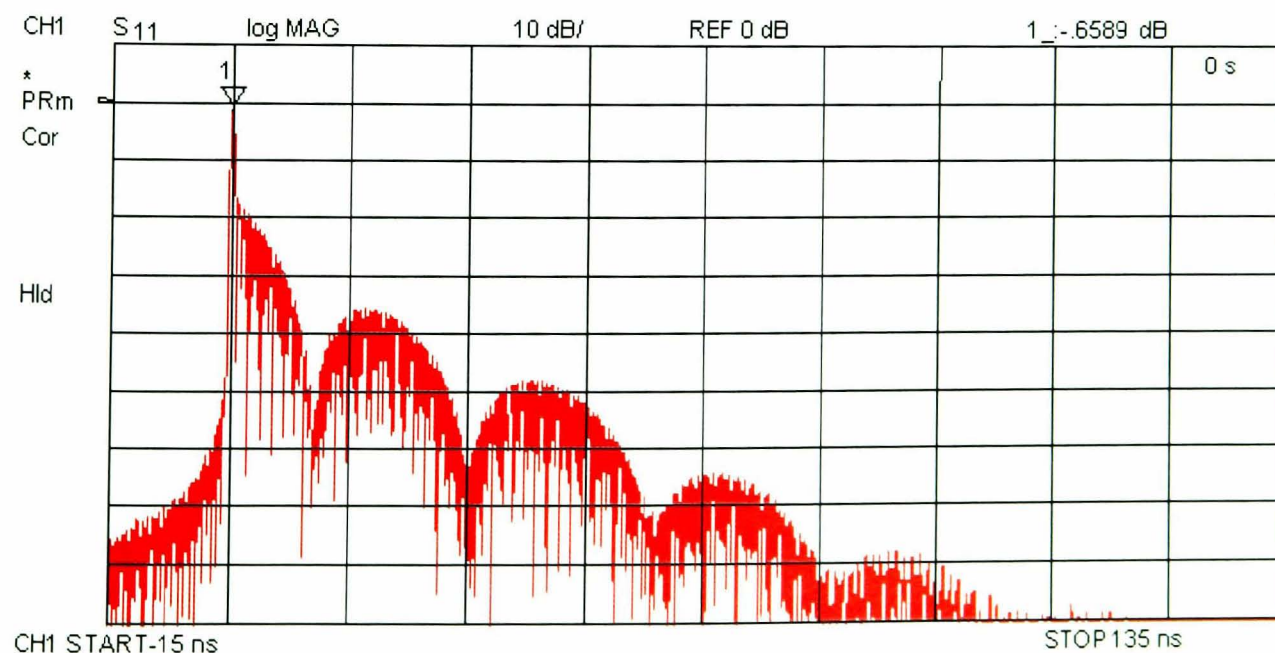


**Figure 4-4: Low-pass mode time-domain response of a 3-pole filter**

time-domain response was not the only or even the key observation from which the development of the time-domain tuning method was set in motion. Another feature of modern network analyzers is the ability to change frequency, and interpolate the error-correction arrays that are used in the 2-port calibration. On older models, the interpolation takes about 10 seconds, but on the faster CPU, the interpolation takes less than 1 second. To test interpolation, with the time-domain on, the display was changed to time-domain only, and the center frequency of the network analyzer was changed by about half the filter bandwidth.

Figure 4-5 shows the resulting time-domain response of the original 5-pole filter of figure 4-1, after shifting the network analyzer center frequency (dark green), as well as the time-domain response before shifting the center frequency (light blue) as a reference. It was noted that the nulls in the time-domain were no longer deep. Adjusting the tuning screws affected each null in turn, and starting with the first null, the tuning screws were adjusted until the time-domain trace looked about the same as the reference. While there was some interaction, each null was substantially affected only by its associated tuning screw. After the time-domain response was lined up, the transform was turned off to see what, if any, affect there had been in the frequency domain. The author was surprised to note that the frequency response was identical to the original frequency response in shape, but was now tuned exactly to the new center frequency! It was this observation that convinced the author that there was a substantial opportunity for investigating new filter tuning techniques using time-domain transforms.

From this beginning, extensive testing was performed, both on real filters and in simulations, to understand the time-domain tuning process, and to try to explain why it



**Figure 4-5: Dark green: time-domain response after shifting the VNA center frequency; light blue: before shifting center frequency**

should work. The results of these experiments are reported below.

## 4.2 Experimental and simulated results on the effects of tuning on the time-domain response of filters

The tuning relationship between resonator tuning and the time-domain response can be illustrated with the following example of tuning the original 5-pole filter, starting from an un-tuned state (all the resonator screws turned out – all resonators high in frequency). This filter had fixed coupling, so only the resonators were adjustable.

### 4.2.1 The relationship between time-domain dips and resonator tuning

The 5-pole filter was tuned by adjusting the first resonator, and looking for a deep null. This was repeated for the second, third, fourth and fifth resonators. Figure 4-6 shows as overlaid traces the five responses in frequency domain in the upper plot, time-domain for tuning the first two resonators in the middle plot, and time-domain for tun-

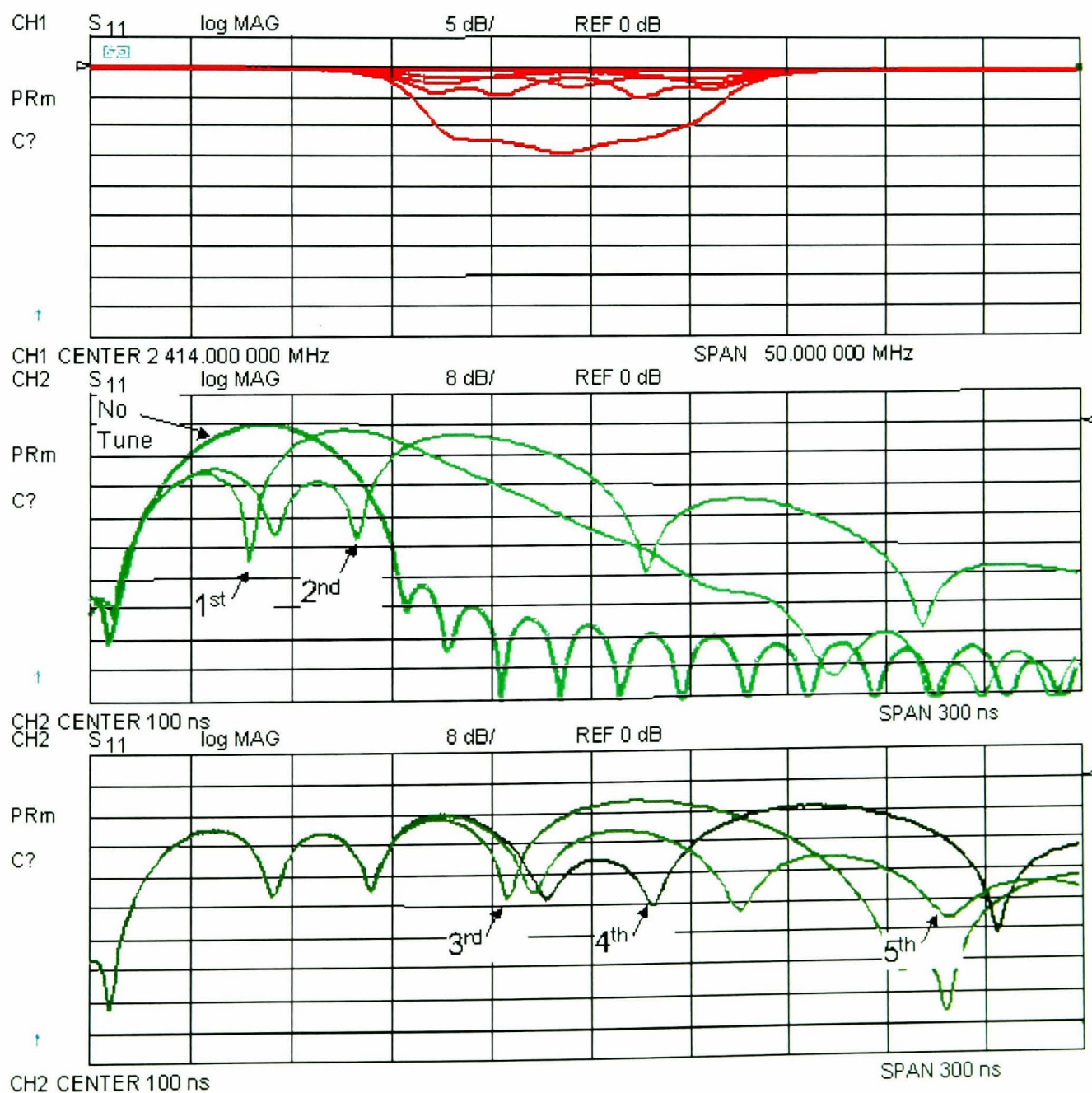


**Figure 4-6: Tuning of a 5-pole filter, one resonator at a time**

ing resonators 3 through 5 in the lower plot. Each labeled trace corresponds to each tuning screw adjustment. It was noted that there was some difficulty in tuning the fourth and fifth resonators for deep nulls, as they seemed quite interactive, that is, tuning the fourth resonator for a deep null, then tuning the fifth, resulted in the null disappearing somewhat for the fourth. Re-tuning the fourth for a null caused the null associated with the fifth to be affected as well. Iterating between the two allowed deep nulls to be achieved for both tuning screws. The final result of tuning the fifth resonator is seen in the upper plot as a symmetrical return loss, of about 15 dB, centered nearly perfectly on the center frequency of the network analyzer. Further tuning allowed the nulls to be deepened, and after tuning, the filter was very nearly perfectly symmetric about the center frequency of the analyzer sweep.

Whether the nulls associated with the tuning screws in the time-domain transform are inherent in a properly tuned band-pass filter is a key question to answer. In an attempt to discern this, the 3-pole filter of figure 4-2 was evaluated by simulation over a narrower range, corresponding to approximately five times the bandwidth. The frequency response of  $S_{21}$  and the band-pass mode time-domain response of  $S_{11}$  of the narrow sweep is shown in figure 4-7. From this simulation it is clear that there are nulls in the time-domain response. A further simulation was performed on the low-pass prototype filter used for the design of this band-pass filter, and the low-pass time-domain

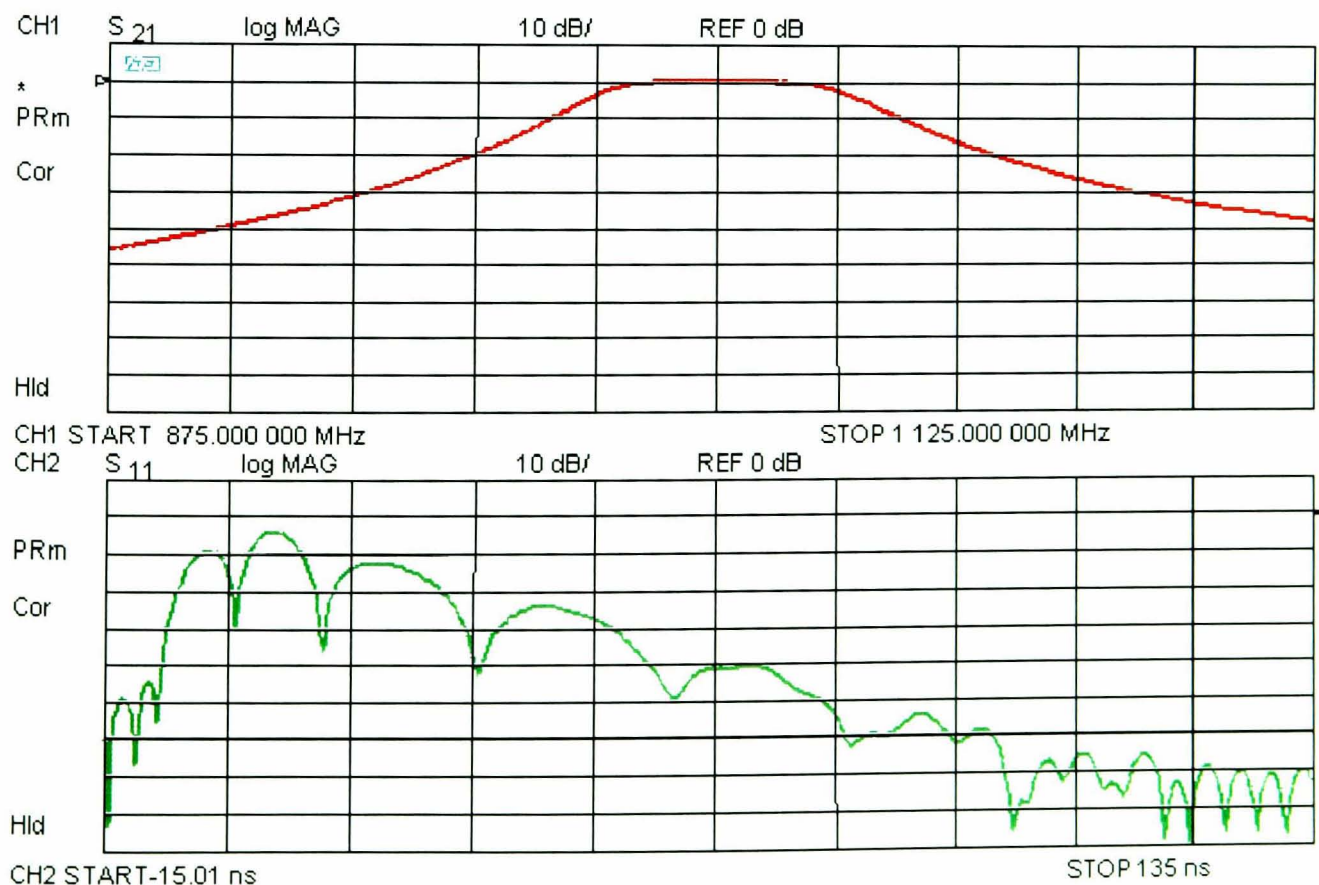


**Figure 4-7: The narrow band frequency response and band-pass mode time-domain response of a simulated 3-pole filter**

response was taken and compared with the band-pass time-domain response of figure 4-7. This is shown in figure 4-8. Note that the band-pass version and the low-pass prototype response are nearly identical. The time-domain responses were generated by downloading the simulated frequency response of the filter into the VNA, and using the VNA band-pass impulse transform function to perform the IFT. The built in time series function of Agilent's Microwave Design System (MDS) simulator was used at first, but this function generated a transform assuming that the frequency response represented a real time-periodic function, and interpreted the frequencies similarly to the low-pass mode of the VNA, thus, did not give the same representation as the VNA time-domain band-pass mode.

From the result of equation (3.36), it is expected that the magnitude of the VNA band-pass transform and low-pass transform are the same. Since the nulls also appear in the low-pass prototype, they are likely due to some fundamental aspect of the filter structure.

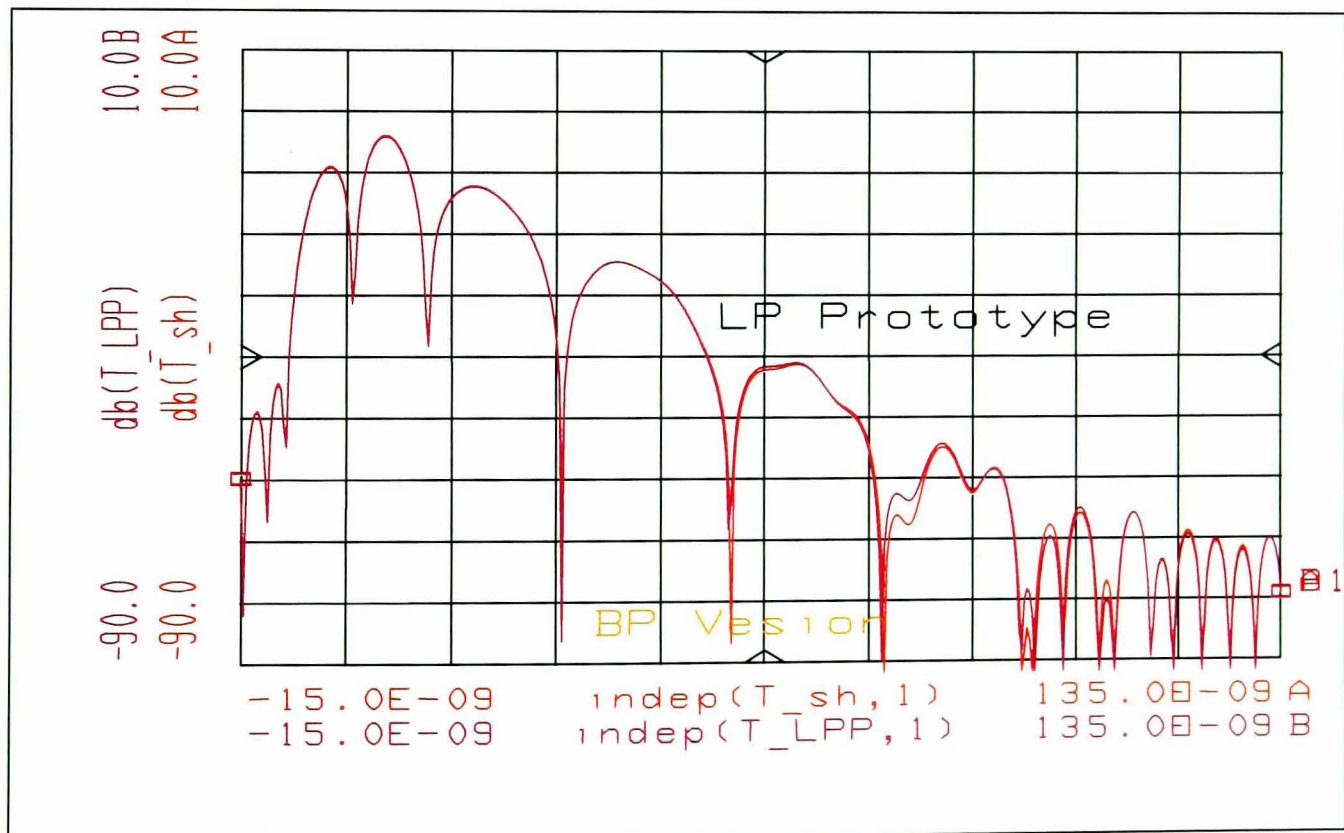


**Figure 4-8: Comparison of the time-domain response of a band-pass filter and its low-pass prototype, for the simulated 3-pole filter**

## 4.2.2 Verifying the time-domain effects of tuning resonators

To verify that the tuning effect was not some artifact of the particular filter, simulations of the model of a 3-pole, capacitive coupled filter were conducted using Agilent's Advanced Design System (ADS, a replacement for MDS) simulation software. In the simulation, the filter was analyzed by tuning only the capacitor in the last (third) resonator by  $\pm 2\%$ , and viewing the results in (figure 4-9 top) for several values, with the time-domain (right) and frequency (left). Note that the third null shows substantial change, with the null being deepest only when the resonator is tuned to the center frequency, but the first two nulls show very little change. Also note the effect of variation on the frequency response, where the deepest response is with the resonator tuned.

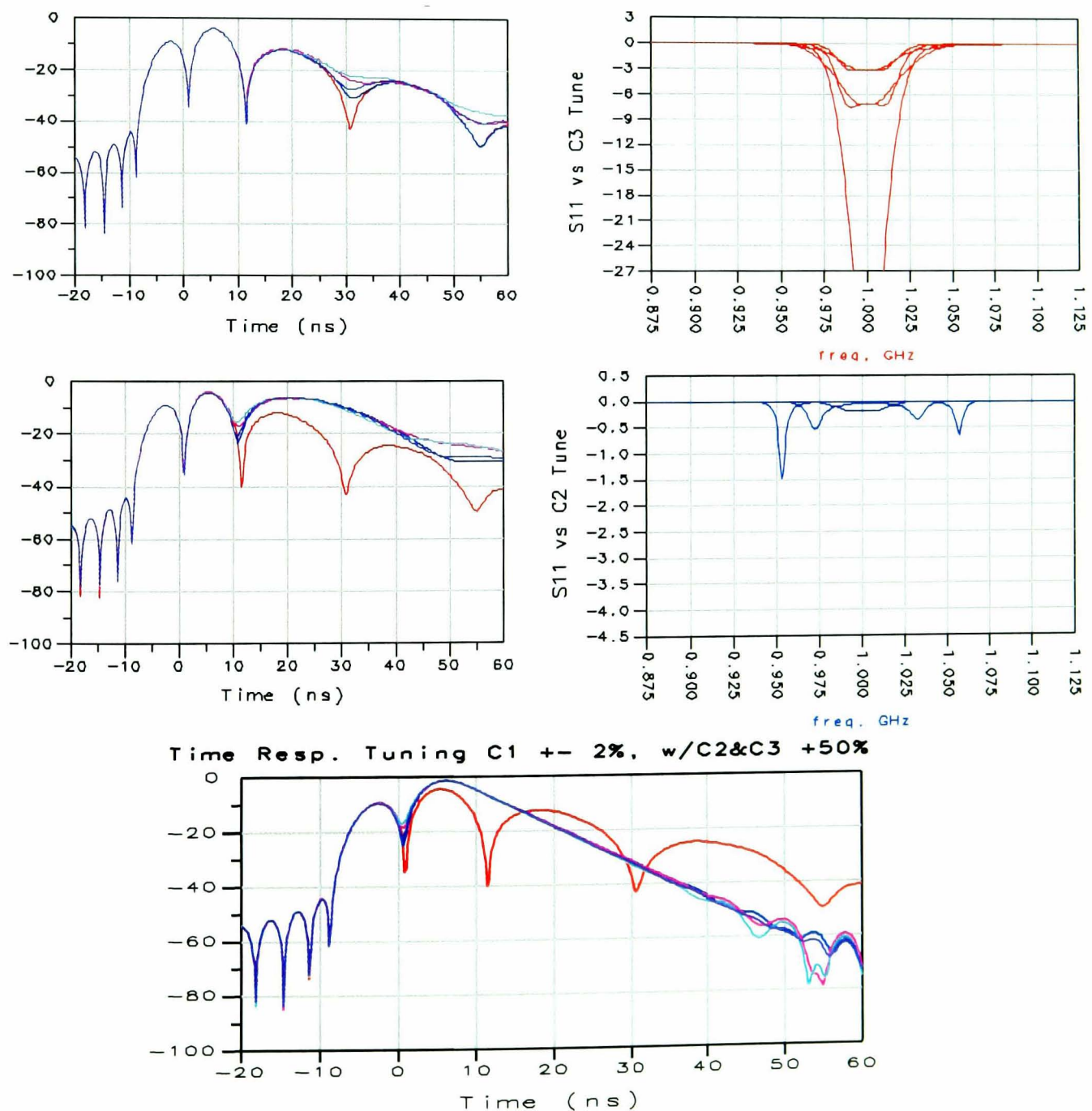


**Figure 4-9: Time-domain response tuning C3 (top), C2 (middle) and C1 (bottom). In all these curves, it is clear that tuning the each resonator (through the tuning of its associated capacitor) affects the associated null.**

Next, the third capacitor was mistuned 50% low, and the capacitor of second resonator was tuned over  $\pm 2\%$  (this is the reverse of a normal tuning process, in that the resonators are sequentially un-tuned). The result is shown in figure 4-9 middle. Again, the second null is only deep with the resonator tuned. Finally, both the second and third capacitors are tuned  $+50\%$ , and the capacitor of the first resonator is tuned  $\pm 2\%$ , shown in figure 4-9 bottom. Here, only the time-domain plot is shown, as the frequency response shows an essentially flat response at 0 dB, due to the nearly total reflection from the second and third resonator. Once again, the null is deepest with the first resonator tuned.

From these results one can conclude that tuning the resonators does appear to have a direct effect on the depth of the nulls, and suggest a tuning process, namely reverse the process shown in figure 4-9 to achieve a properly tuned filter. This simulation essentially verifies the experimental results shown earlier, and confirms that the results were not merely due to some peculiarity of the particular 5-pole filter used.

### 4.2.3 Changes of the time-domain center frequency of a tuned filter

One of the first experiments with the original filter was to change the center frequency of the VNA. It was noted that all the nulls disappeared. The result of this experiment is shown in figure 4-5, above. In this case, the center frequency was changed by about half the bandwidth of the filter. Many coupled-resonator filters are designed with very wide ranges of coupling and resonator tuning. This allows a single mechanical structure to be mass-produced for low cost, and custom tailored to a variety of applications at the time it is tuned. Occasionally, one filter is retuned to a different center frequency, while trying to maintain the same filter shape. This can be easily accomplished by setting the VNA at the current center frequency of the filter, and storing a trace into the analyzer's display memory. With both data and memory displayed, the VNA center frequency is changed to the new desired frequency, in incremental amounts. If this is a large change, it may not be possible to see any dips in the time-domain, so the size of the frequency change is chosen to maintain a time-domain response with recognizable nulls. The filter is tuned to the new, incremental center frequency, and the process is repeated until the desired frequency is reached. A more direct tuning method is demonstrated below that removes the need for the incremental changes.

If the procedure for changing the center frequency as described above is followed, it may be noted that the bandwidth of the filter (and the time-positions of the resonator

nulls) will not match those of the originally tuned filter. This is readily understood by realizing that the coupling factors of the filter, from which the filter bandwidth is determined, are always determined from a ratio of the bandwidth to the center frequency. If the center frequency is changed, without changing the coupling values, the resultant filter bandwidth will change as well.

Thus, several simulated and real experimental examples all support the conjecture that by observing the nulls associated with each resonator, and tuning for deep nulls, a properly tuned filter will result, for the all-pole type filters tested. A theoretical basis to underpin this conjecture is presented in chapter 5.

#### **4.2.4 Compensating for resonator interactions**

When starting with a completely un-tuned filter, and sequentially tuning the resonators, there is an interactive effect of one resonator on another. This can be noted by observing, for example, the first null of the band-pass filter in the middle plot of figure 4-6. When the second resonator is tuned, the first null becomes less deep. This is also observed in the third null of the lower plot of figure 4-6. The depth of the null is changed when tuning the fourth and fifth resonators. The interactions follow certain behavioral patterns. For example, if all the resonators are tuned too high, and the first resonator is tuned down, to create a deep null in the time-domain, and then the second resonator is tuned also for a null, the first null will no longer be deep. It is necessary to return to the first resonator and tune it further (in the same direction) to get a deep null again. This has some small effect on the second resonator, which must be re-tuned as well. The effect diminishes as the tuning becomes closer but the interactions do result in more iterations. Experimentally, it appears that if the preceding resonator is tuned high in frequency, it has the effect of making the resonator which follows appear somewhat lower in frequency, so that the following resonator is not tuned down low enough while it is being tuned.

#### **4.2.5 The relationship between time-domain peaks and coupling tuning**

Since the response of a band-pass filter is set almost entirely by the coupling factors, assuming the resonators are properly tuned, it is often necessary to tune couplings to achieve the desired pass band shape. The coupling principally affects the bandwidth, ripple, and skirt steepness in all-pole filters. In an effort to understand if the time-domain response would show the effects of changes in coupling, several simulations and experiments were performed.

In one simulation of a 5-pole filter, the values of individual coupling elements were changed, and the results recorded. An example is shown in figure 4-10. Here, the coupling between resonators 1 and 2 is increased by 10%, in the blue trace. Notice the second peak in the time-domain trace has been reduced, and every peak after the second peak has increased. Also note that the first peak is essentially unchanged. This is consistent with the intuitive idea that increasing the coupling between resonators 1 and 2 will cause more signal to couple into resonator 2, thus less is reflected, causing the peak to be reduced. Since more energy is coupled into resonator 2, more is available to reflect off the other coupling elements, thus the peaks of all the rest of the couplings are increased. Also note that the second peak occurs at a slightly earlier time value. This is consistent with the results of Ness [8], which utilizes the group delay of the reflection response to tune the coupling values of a filter. In this case, the peak value of the coupling appears to give a better resolution than using the delay value, but both values might reasonably be used in tuning method. Unlike the method proposed by Ness, it is possible to determine which coupling element is mistuned even on a nearly tuned filter.

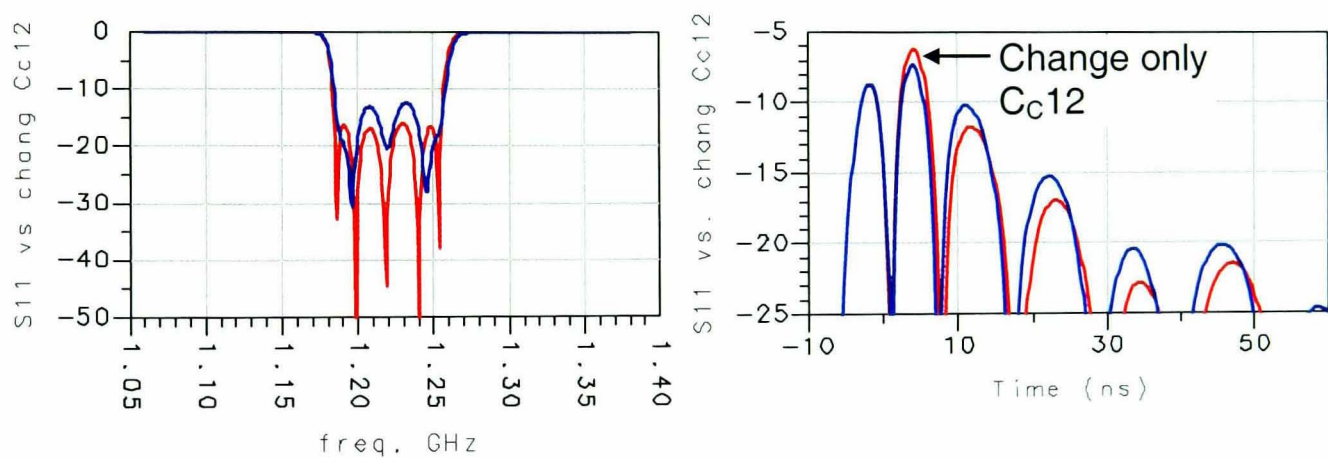


**Figure 4-10: Response of a 5-pole filter after changing the first coupling ( $C_{c12}$ ) by +10% (blue) vs the original (red)**

Figure 4-11 shows a similar experiment, where the coupling between resonators 2 and 3 has been decreased by 10%. Following the insight of the previous result, decreasing the coupling results in an increase in the reflected signal associated with that coupling (the peak between nulls 2 and 3), and a decreasing of all the peaks to follow, as there is less energy entering resonator 3, to be available to reflect off the remaining coupling elements. Note also that the time associated with the peak is slightly longer after decreasing the coupling, again consistent with the results of Ness that the delay response contains coupling information. From these simulations one might imagine a coupling tuning process where the peaks between nulls represent the coupling between the resonators associated with the nulls. Changing one coupling value results in a

change with the associated peak in the time-domain. If a target filter shape is captured by the VNA in memory (from a “golden” filter or from a simulation), another filter may be tuned to the same response by tuning the coupling to match the peaks, and tuning the resonators for nulls.

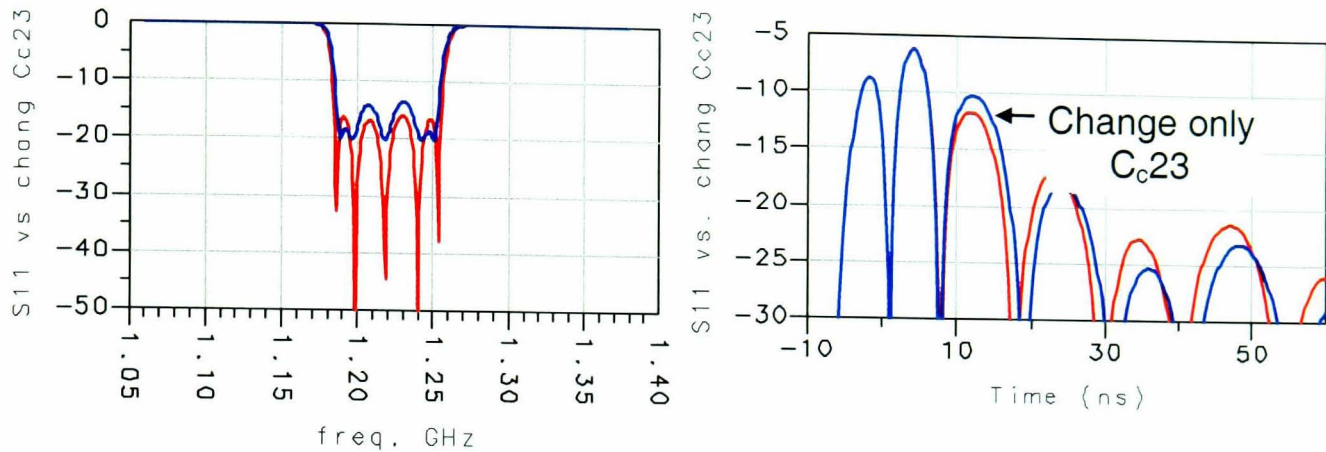


**Figure 4-11: Response of a 5-pole filter after changing the second coupling capacitor ( $C_{c23}$ ) by -10% (blue) vs. the original (red)**

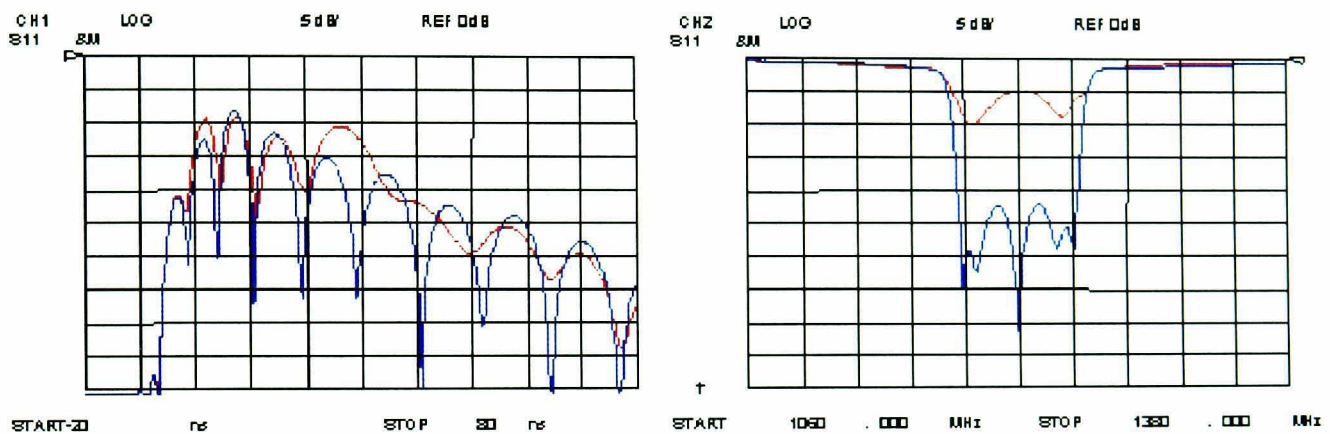
#### 4.2.6 Interactive effects on coupling peaks from tuning other couplings

The tuning of any coupling has interactive effects on the couplings that follow. This is illustrated very clearly in figures 4-10 and 4-11. This interactive effect must be considered when using time-domain to tune filters. Experimental tests indicate that it is necessary to properly adjust the outer couplings before attempting to adjust the couplings for inner resonators. Misalignment of the outer couplings will cause increasing misalignment of the center couplings. Note how well the time-domain separates one coupling from another, in that changes in  $C_{c23}$  (the coupling between resonators 2 and 3) has almost no effect at all on the peaks that come before it (figure 4-11, right). Also note from figure 4-10 and 4-11 that the frequency response appears almost the same; it would be very difficult to know what has changed between the two frequency responses.

However the time-domain makes the difference very clear. For some filters, the input and output coupling is fixed, so that the associated first and last time-domain peak does not align with that of the target filter shape; thus proper tuning of the remaining couplings becomes in doubt. An area for further study is the interactive effect, which may allow for compensation techniques that remove the restriction of tuning the couplings in order from the outer resonators to the center resonators, and provide guidance as to how to compensate for misaligned but fixed input coupling.

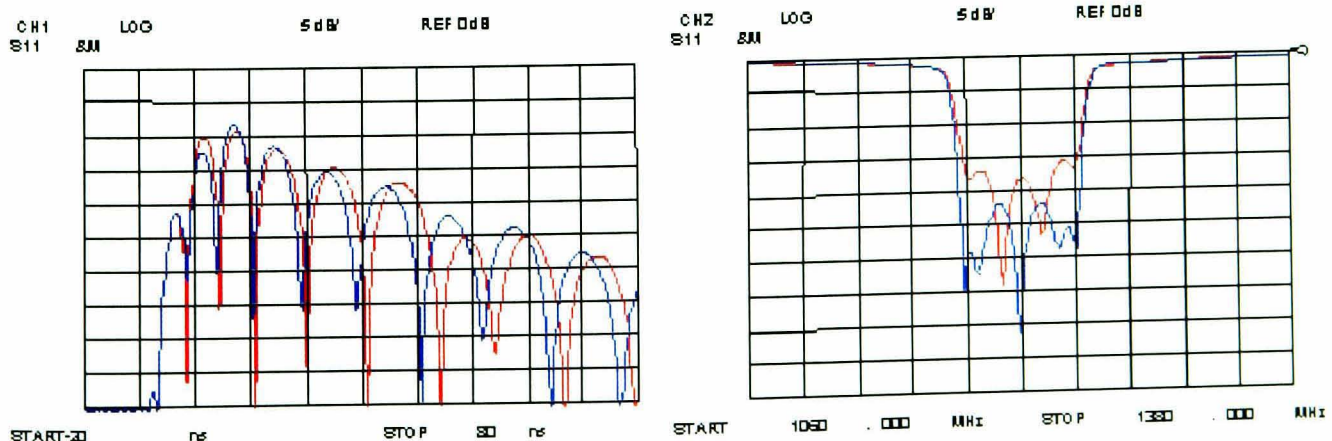
### 4.2.7 Examples of tuning filters with adjustable coupling

An example of the coupling tuning process is shown in figure 4-12 below, starting with an un-tuned (red) and tuned (blue) 8-pole filter shown in the time-domain (left) and frequency domain (right). From this figure we can see that the filter is not properly tuned in frequency (notice the nulls are not deep in the red trace as compared to the blue trace), due to resonator mistuning. The resonators are first tuned by making the nulls associated with each as deep as possible. For this filter, the first four resonators were tuned looking at  $S_{11}$ , and the last four resonators were tuned looking at  $S_{22}$ . (Only  $S_{11}$  is shown in the figure,  $S_{22}$  plots are similar).



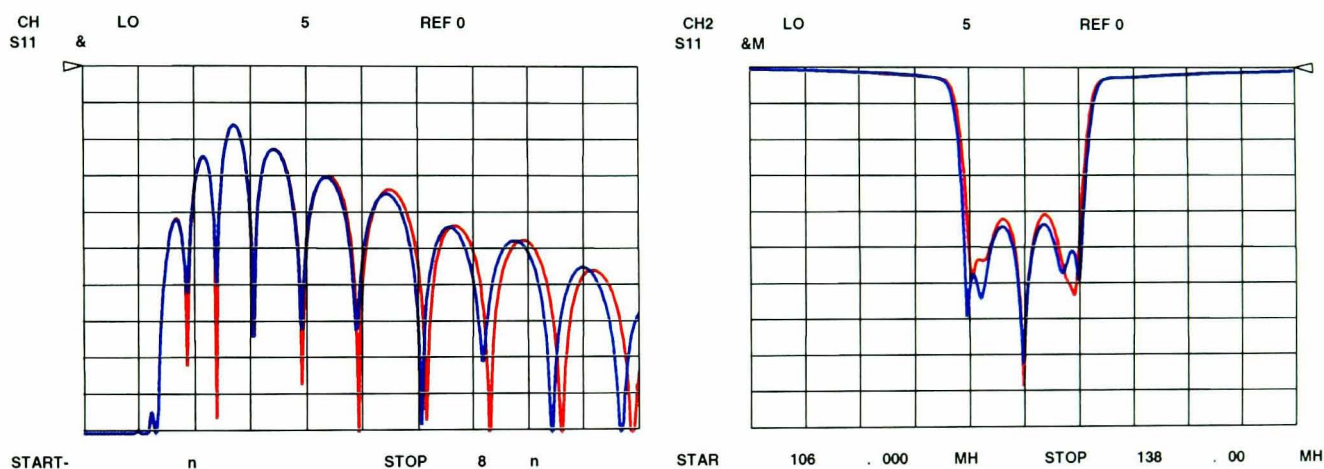
**Figure 4-12: Time-domain (left) and frequency response (right) of a "golden" or reference filter (blue) and an un-tuned filter (red)**

Figure 4-13 shows the results after tuning all the resonators. The filter response is well centered, but the return loss does not match the target return loss. Notice in figure 4-13 (left), that the coupling must be mistuned, as the peaks do not align. The next step is to tune the coupling elements, so that the peaks associated with the couplings line up with the peaks of the target or reference filter. During the process of tuning the coupling, it is necessary to start by tuning the outside elements first, and proceeding to the center elements. For this tuning, the couplings 1-4 are tuned from  $S_{11}$ , and couplings 5-8 are tuned from the  $S_{22}$  side. In this filter, tuning the coupling changes the resonator



**Figure 4-13: Same filter as in fig. 4-12, but with resonators tuned for nulls. Note the frequency response is not the same, and the peaks in the time-domain trace do not line up.**

tuning, so that each resonator must be re-tuned such that its associated null is maintained. This process is continued until all the peaks in the time-domain trace are lined up, as shown in Figure 4-14. Note that the 5<sup>th</sup> peak, (which represents the coupling between resonator 4 and 5) is slightly off, as are the peaks that follow. This is because it was adjusted to be a compromise between its response as seen from  $S_{11}$  and  $S_{22}$ . The peaks that follow the fifth peak are more than halfway through the filter. It was not possible to exactly match the peaks on both sides, as the input coupling (first peak in the time-domain trace) is not adjustable, and it's not perfectly aligned. Thus, it will affect all the other peaks and cause the overall response to be slightly different. However, after the real filter's couplings were adjusted to align the peaks in the time-domain response to the best extent possible, the resulting frequency domain bandwidth and return loss levels were nearly identical.



**Figure 4-14: An 8-pole filter tuned after aligning the coupling peaks, and tuning for deep nulls in the resonators. Note that this filter does not line up perfectly with the target filter, probably due to differences in the loss between the fixed input couplings**

#### 4.2.8 Tuning to a simulated target response

The filter above was tuned to a target filter response created by measuring a previously tuned filter. The application note [26] included at the end of this thesis as paper 2 shows an example where a simulation was used to create a target response for a filter with a 60% wider bandwidth than the filter above. This target response was used to reset the filter couplings, and allowed the filter to be tuned to match the desired specifications over a wider bandwidth. The application note includes other examples of filter tuning which are not repeated here.

### 4.2.9 The effects of loss on the time-domain response

One effect of non-ideal resonators is that of loss in the resonators, which results in non-infinite  $Q$  in the filter. The effect of loss may become important when attempting to create a target time-domain response from a simulated ideal filter. Figure 4-15 shows that loss causes each subsequent coupling peak to become progressively smaller. This makes intuitive sense if one considers the couplings as reflecting some energy, and passing some along. If energy is lost in each resonator, then one might expect the effect of the loss to be greater farther into the filter. Figure 4-15 shows just such behavior. If an ideal filter simulation is used as a template for tuning a real, lossy filter, then the coupling tuning process described above will result in the couplings towards the center of the filter being too small (because the peak associated with the coupling would be higher than intended, to accommodate the loss in the real filter), thus yielding a filter with a bandwidth that is narrower than intended.

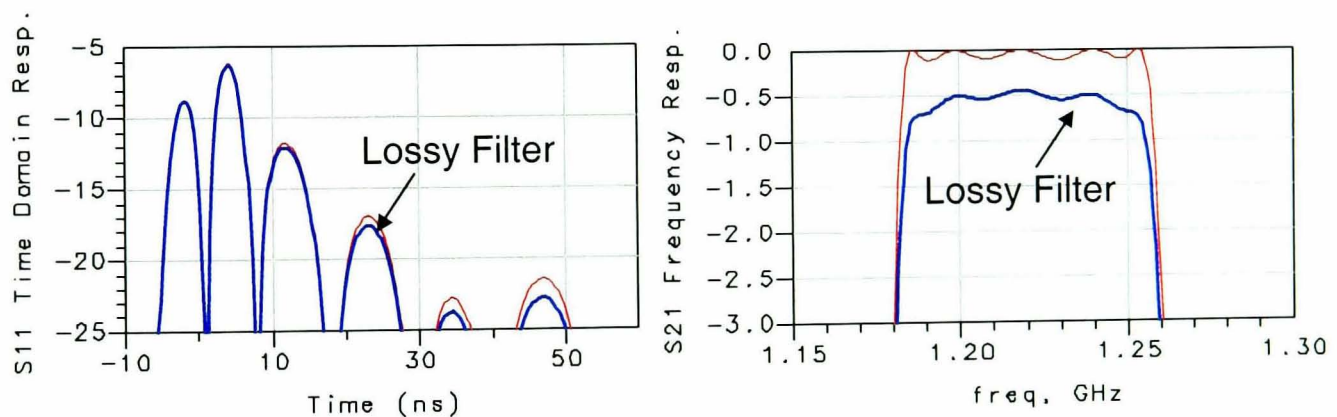


**Figure 4-15: The time-domain response (left) and frequency response (right) of a lossy filter (blue) compared with a lossless filter (red)**

#### 4.2.10 Synopsis of time-domain tuning method for all-pole filters

The time-domain tuning process is outlined in table 2 below.

Table 4-1: Synopsis of Time-domain Filter Tuning for All-Pole Filters

1. Set the center frequency of the network analyzer equal to the desired center frequency for the filter.
2. Set the frequency span to be 2 to 5 times the bandwidth of the filter.
3. Use 201 points in the sweep for a good compromise between sweep speed and resolution.
4. Measure  $S_{11}$  on one channel and  $S_{22}$  on the other channel. If desired, a 4-parameter display can be used to view both the frequency and time-domain responses at once. Viewing both domains while tuning may provide better insight for optimizing the filter's response.
5. Select the band-pass mode time-domain transform.
6. In the time-domain, choose the start limit to be about one resonator delay on the minus side; approximately  $t = -(2/\pi BW)$ . Choose a stop limit of about 2 to 3 times the full filter delay; approximately  $t = (2N+1)/(\pi BW)$ , where  $N$  is the number of filter sections (resonators) and  $BW$  is the filter 3 dB bandwidth in Hz.
7. Use log magnitude format (dB), and set the reference position to 10 (top of the graticule) and the reference value to 0 dB.
8. If the filter has tunable coupling, set the coupling screws approximately correct; for example, by adjusting them to the same physical height as those on a "golden" filter.
9. Tune the resonators first, adjusting for deepest dips in the time-domain trace. Start with the resonators at the input and output sides and work towards the middle.
10. Tuning one resonator may cause the previous resonator to become slightly un-tuned. In this case, go back and retune the previous resonator, then optimize the current resonator again.
11. Tune the coupling apertures from the input and output sides first and work towards the middle. After adjusting each coupling screw, readjust the resonators on each side to make the dips as low as possible.
12. Repeat the tuning process at least once to fine-tune, or as needed to achieve desired response.

### 4.3 Filters with transmission zeros

For many communication applications, it is necessary to make a filter skirt response steeper than normally obtained by all-pole type filters. Discrete transmission zeros (where the  $S_{21}$  goes to zero) can be obtained in the filter stop band by adding cross-coupling (coupling between resonators other than nearest neighbors). Filters are often designed with transmission zeros to sharpen the stop band rejection. The transmission zeros can be generated by a variety of means. Common among these are using cross coupling between non-adjacent resonators to create a transmission zero [57,79], or using additional resonators to create a notch in the stop band [80]. Typically, the number of resonators over which the coupling crosses will determine the characteristics of the transmission zeros. Crossing over an odd number of resonators, as seen in Fig. 2-4, results in an asymmetric frequency response, with a zero on only one side of the pass band. Crossing over two resonators results in transmission zeros on both sides of the pass band. Filters with cross coupling present additional difficulties compared to tuning all-pole filters, especially if the value of the cross coupling is also adjustable.

#### 4.3.1 Time-domain response of filters with cross-coupling

The time-domain response of filters with cross coupling to create transmission zeros may be useful in tuning these filters [65,81] (included as published papers 3 and 4 at the end of this thesis). The time-domain response of these filters differs from all-pole filters, in that tuning the characteristic nulls to be as deep as possible does not result in the filter being properly tuned. Fig. 4-16 shows the frequency and time response of the 4-pole filter with asymmetric cross coupling from resonators 2 to 4. The filter, in this case, had coupling adjustments for only the input, output and cross coupling. The cou-

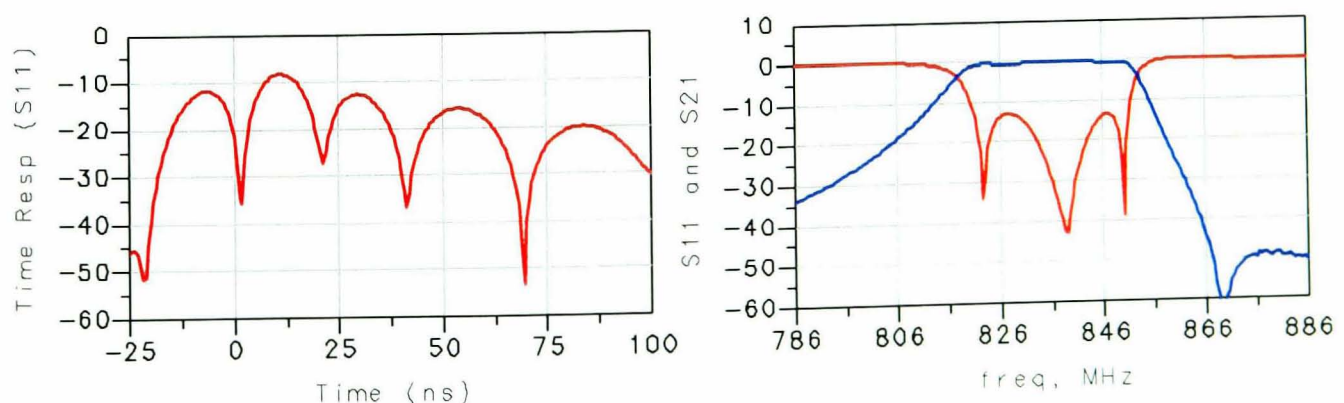


**Figure 4-16: Time-domain response (left) and frequency response (right) of a 4-pole filter with cross-coupling between resonators 2 and 4. Notice the null associated with the second resonator is not at all deep.**

pling between resonators was fixed. The filter was optimized for return loss in the pass band and rejection in the upper stop band. Note that the level of the two peaks in the return loss over the pass band are the same, even though the shape of the two are different, showing that the filter is properly tuned.

Interestingly, the time responses of the nulls are not deep for many of the resonators, especially resonator 2. To understand why this is, and how to tune these filters, one must first look back at the design methods for the simple, all-pole filters.

With cross coupling added to the filter, the time-domain response no longer has the simple relationship to filter tuning. Further, especially in filters with asymmetric transmission zeros, the tuning of the filter is not optimum when each node frequency is centered at the filter center frequency. (The node frequency is here defined to be the resonant frequency of the node with all connected couplings -- including cross coupling -- grounded). The resonators are often “pulled” to compensate for the effect on the pass-band of the transmission zeros in the stop-band, thus achieving the desired pass-band return loss specification. This results in an asymmetric shape to the return loss, as demonstrated in Fig. 4-16. Tuning for deep nulls results in a filter that does not meet the return loss specifications. However, the tuning of these filters may be addressed using time-domain techniques as described below.

Assume that argument still holds that the time response of any particular node of a filter displays a deep null when the node frequency is exactly centered on the network analyzer center frequency. The difficulty with these complex filters is that the node frequencies are no longer easy to determine. But one can use the network analyzer itself, on a properly tuned or “golden” filter, or on a simulated filter, to discover the individual node frequencies. This is done setting up the vector network analyzer in dual channel mode, with one channel on frequency domain and one on time-domain. The center frequency of the VNA is adjusted while looking at the null associated with a particular resonator. When the null is maximized, that frequency is recorded as the node frequency for that resonator. Fig. 4-17 illustrates the time response of the filter tuned at the filter center frequency, and then tuned to a frequency that maximizes the null associated with resonator 2 (one of the resonators with cross coupling).

This process is repeated for each of the filter’s resonators, adjusting the VNA center frequency until each null is maximized. For best sensitivity, the VNA frequency span is reduced to just two times the bandwidth. Table 4-2 below gives the node frequencies determined for each resonator for the filter from Fig. 4-16. Armed with this informa-

tion, and using the measurement from Fig. 4-17 as the tuning template, a filter tuning process for complex filters can now be defined.

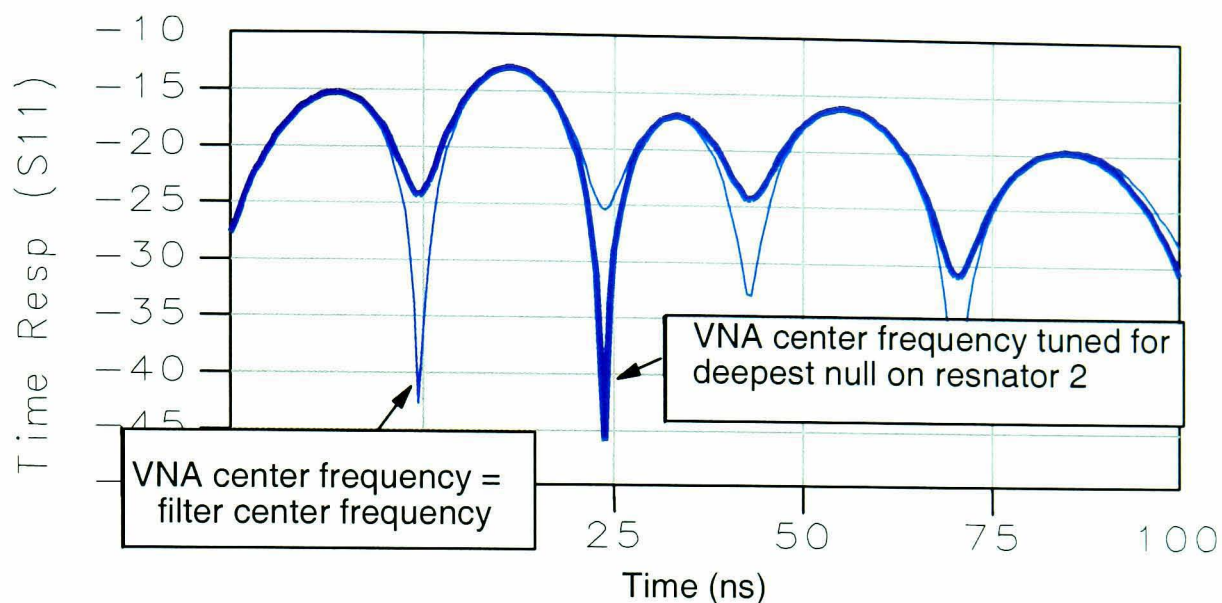


**Figure 4-17: The time-domain response of a cross-coupled filter, with the center frequency of the VNA changed to give the maximum null for resonator 2**

Resonator No.	Node Frequency
1	836.25 MHz
2	833.85 MHz
3	834.55 MHz
4	836.45 MHz

### 4.3.2 Tuning method for filters with cross-coupling

The experimental results on all-pole filters demonstrate that nulls in the time-domain have a correlation to an associated resonator, and when the resonators are tuned such that the nulls are deep, the filter is properly tuned in the time-domain. However, if the same simple tuning method is used on filters with cross coupling which result in transmission zeros, the filter is not properly tuned.

The experimental results on tuning filters with cross coupling are described below. The key result is that cross coupling causes the nulls to be not deep, when the filter is properly tuned, perhaps because the cross coupling alters the effective resonant frequency of any particular resonator so that it is not exactly on the center of the filter pass band, as shown in figure 4-16. The effective values of the resonators are found by shifting the center frequency of the VNA while monitoring the time-domain response of the

input and output match, as shown in figure 4-17. When the null associated with any particular resonator of a properly tuned filter is deepest, the value of the VNA center frequency is recorded, and assigned to the associated resonator, see table 4-2.

A tuning method was developed using these values as a template for an un-tuned filter. An example of using the time-domain method for tuning cross-coupled filters is shown below, for the 4-pole filter depicted by the responses of figure 4-16. Figure 4-18 (left) shows (in red) the time-domain response of the un-tuned filter as well as the target or “golden” filter response (black). The filter is initially tuned for deep nulls associated with the resonators (blue). Also shown (right) is the frequency response of  $S_{11}$  and  $S_{21}$  of the un-tuned filter (red) and the filter tuned for deep nulls (blue) and the target response (black).

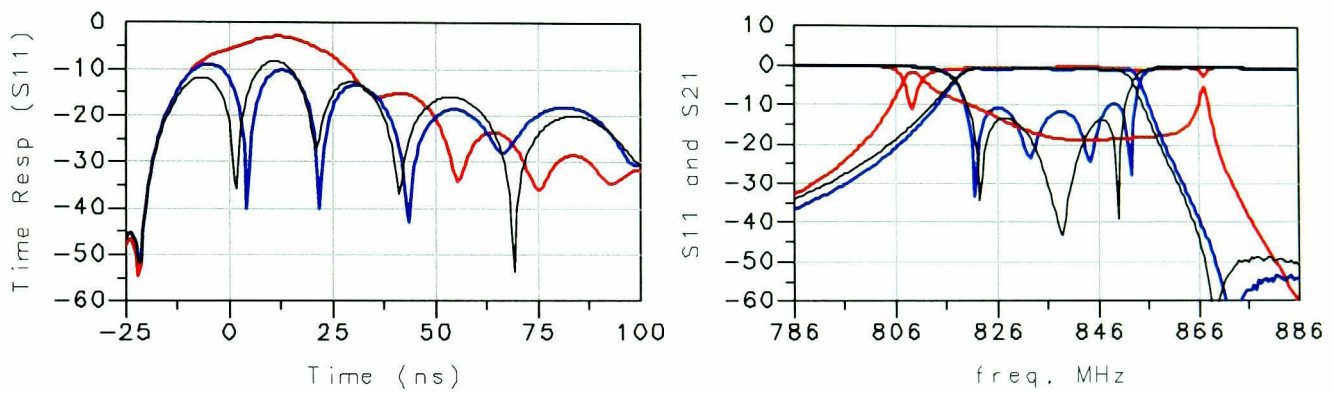


**Figure 4-18: Time-domain response (left) and frequency response (right) of an un-tuned -pole filter (red), a filter tuned for deep nulls (blue) and the target or "golden" filter (black)**

Next, the main couplings are adjusted to match the values of the peaks of the target filter, just as in the simplified tuning method, as shown in figure 4-19. During this process, the resonators are re-tuned to maintain deep nulls.

The cross coupling value is tuned to set the transmission zero to the proper frequency in the stop band, by observing  $S_{21}$  in the frequency domain, as shown in figure

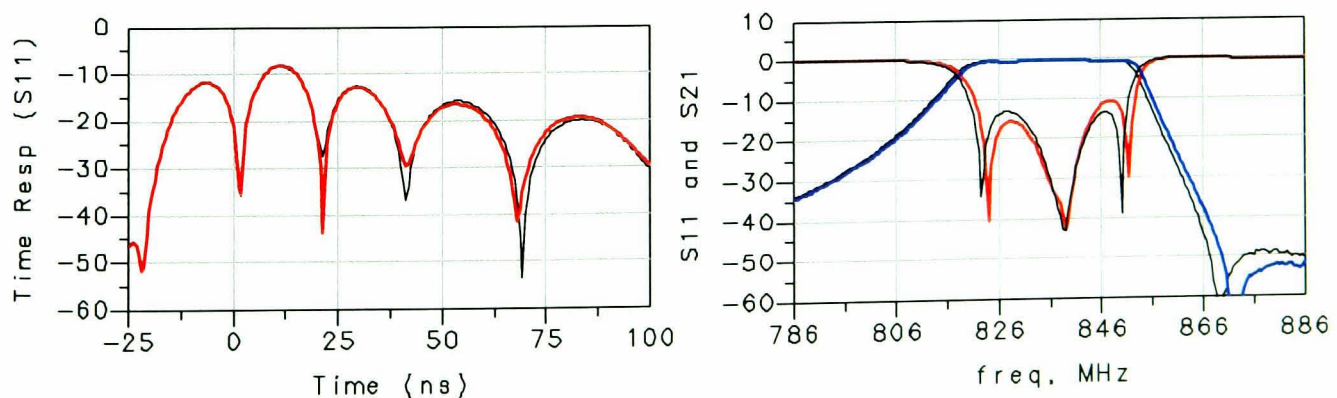


**Figure 4-19: Time-domain response (left) and frequency response (right) of the filter after tuning the coupling (red), to match the peaks of the target or "golden" filter (black).  $S_{21}$  of the filter to be tuned is shown in blue**

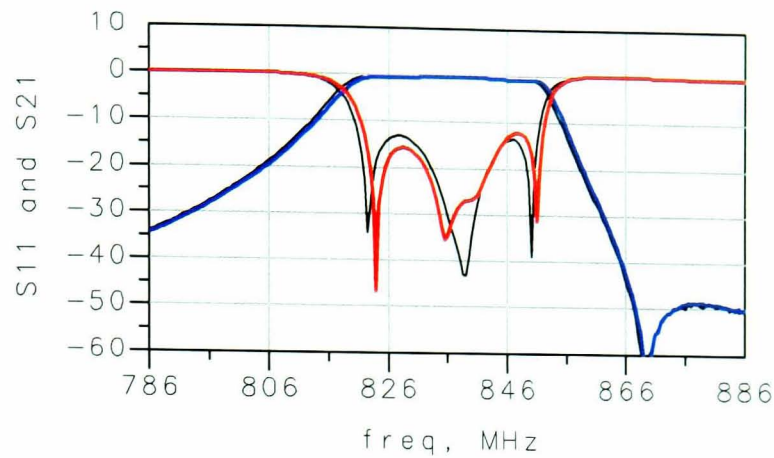


**Figure 4-20: The cross-coupling value is adjusted until the filter S21 (blue) trace matches the target filter trace (black), in the frequency domain. Also shown is the S11 response (red) of the filter to be tuned**

4-20.

Finally, the center frequency of the VNA is reset for each resonator, in turn, to the value in table 4-2, and the associated resonator tuned for a deep null. Each resonator is tuned for a deep null at its respective frequency, starting from the outside in. Because of interactions between resonators, this is an iterative process, repeated until the null for each resonator is maximized at its respective target frequency as listed in table 4-2. Figure 4-21 shows the final result of this tuning: the filter is tuned almost perfectly to match the target response.

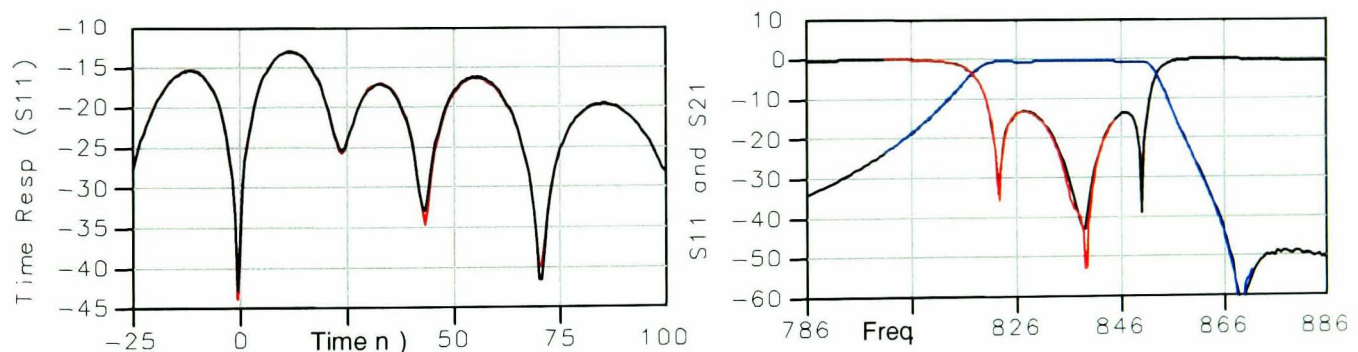


**Figure 4-21: Time-domain response (left) and frequency response (right) of the filter after final tuning of each resonator (red), to create a maximum null at its respective target frequency. Target filter is in black and S21 of the tuned filter is shown in blue**

Many questions remain with respect to filters with transmission zeros, such as how to predict the value of the resonator frequency based on the filter structure, and alternative methods for tuning the cross coupling. This cross coupling may be used to flatten the group delay responses of filters [47], but the effect of this cross coupling on the time-domain response has not been investigated.

### 4.3.3 Filters with zeros from adjacent coupled resonators

As an alternative to cross coupling, it is also possible to create a transmission zero by adding a notch filter resonator, typically coupled to the input or output of the filter. The effect on the time-domain response of a filter of adding a notch resonator has not been investigated, but may be closely related to tuning duplex filters.

### 4.3.4 Filters with arbitrary resonator tuning

The experiments described above demonstrate a key hypothesis with respect to the time peaks and resonator nulls. For all-pole filters, each resonator is tuned to the center frequency of the filter. For filters with transmission zeros, the apparent resonator frequency may be different than the filter center frequency. This can even be extended to filters that are not designed to mimic exactly some low-pass prototype filter. For example, some filters used in communication systems must have a specific phase requirement at the center frequency, but not have tight control on the return loss. In tuning these filters, the return loss is tuned to achieve a good response, then one or more of the resonators are adjusted to create the correct phase value (often this is the outside resonator). In this case, an all-pole filter tuned to meet the phase specification will not have all resonators set at the filter center frequency. However, using the techniques from section 4.3.2, the resonator values can be characterized using time-domain techniques and subsequent filters can be deterministically and successfully tuned to match the response of the initial filter.

## 4.4 Time-domain resolution with respect to filter tuning

Section 4.1 noted that the time-domain transform of filters had not previously been considered useful with respect to band-pass filters, as the narrow frequency span used to measure band-pass filters would result in a distance resolution many times the filter's length. However, the experiments described above clearly show that there is sufficient resolution to resolve individual filter tuning elements. These apparently conflicting views can be brought together by realizing that filters exhibit what is known as "slow-wave" behavior [82]. That is, the electrical delay through a filter is many times more than expected from its physical length. The delay is approximately given by [82]

$$delay = \frac{n}{BW} \quad (4.1)$$

where  $n$  is the number of resonators in the filter and  $BW$  is the bandwidth of the filter (in Hertz). Thus, any single resonator has an approximate delay of  $1/BW$ , with the re-

flection delay being twice as much, as signals travel forth and back. The time-domain resolution also goes as approximately  $1/BW$ , so if the frequency span is significantly more than the bandwidth of the filter (say, 2 to 5 times more) then the resolution of the time-domain transform should be sufficient to resolve resonators for a filter with any arbitrarily small bandwidth.

There are further questions as to the maximum number of resonators that a filter may have and still have the time-domain tuning method apply, and why there are such interactive effects seen on the last resonators in the filter when tuning from only one end. As to the first question, the time-domain tuning method has been effectively used on up to 17-pole filters, where both  $S_{11}$  and  $S_{22}$  were used to tune the resonators at the inputs and outputs. The practical limit may be due to losses in the filter. As to the second question, experimentally it appears that one can effectively tune a filter to  $N/2+1$  resonators in from one side of the filter, or, halfway through the filter plus one resonator. This makes sense due to the nature of most filter coupling coefficients as described below.

Most filters used are of the equal-ripple, Chebyshev or Butterworth form. All of these filters have the attribute that the coupling factors are largest on the outer elements and smallest on the inner elements. One way to view coupling elements is as coupling bandwidths between resonator sections [5]. Thus, one may consider these filters as a series of one-pole filters, getting progressively narrower as one proceeds from the outer filter elements to the center elements. For a time-domain response from the outermost element (with the largest bandwidth) there should be sufficient resolution to resolve the first resonator as long as the frequency sweep is on the order of 2-5 times the filter bandwidth. Considering the waveform that passes through the first filter and impinges on the second resonator, one may note that the filtering of the first section narrows the effective frequency span of this waveform. Thus, the frequency content might not have sufficient resolution for resolving the second resonator, but as the bandwidth of second coupling is narrower than the first, thereby having longer delay, less frequency span is needed to resolve the second resonator. This argument holds up until the center resonator is reached. At the center resonator, all the coupling bandwidths that follow are progressively wider (i.e., have shorter delay) such that it becomes increasingly more difficult to resolve resonators from one-another as one passes beyond the center resonators. From this one can propose that filters should be tuned from both sides, tuning each side up to the center resonator. Practical experience has shown that trying to use time-domain tuning from only one-side results in substantial interactions between tuning

resonators beyond the center resonator. This is apparent in the tuning of resonators 4 and 5 from figure 4-6 in section 4.2.1.

## Chapter 5 Theoretical Analysis of Time-domain Filter Tuning

Time-domain tuning has been empirically shown to be effective in tuning many common filter types, particularly all-pole filters. The experimental results described in chapter 4 provide compelling evidence that a relationship exists between the time-domain response nulls and resonator tuning, and between the time-domain response peaks and coupling value. However, there has not been any mathematical study that shows why this should be so. In an attempt to justify and quantify this relationship, several avenues of theoretical work were pursued. An analysis of the VNA time-domain response of the input and output reflection of filters, as compared with the filter impulse time-response, is presented which provides a theoretical basis for explaining the success of the time-domain tuning technique. Below, a three-pole band-pass filter is first analyzed analytically, with the result that the analytic impulse response is found to be quite different from the VNA time-domain result, though this example did not provide any intuitive understanding of the cause of the difference or for the behavior of nulls in the time-domain tuning method. A simpler case, that of a one-pole filter, is completely examined in terms of its analytic impulse response and VNA time-domain response, from which a complete understanding of the source of the nulls in the time-domain response, and their behavior with tuning is ascertained. This simple model is then extended to the multi-pole case through an analysis of simulated results on a multi-pole filter.

### 5.1 Calculating band-pass time-domain responses from low-pass prototypes

The first effort in providing a theoretical basis for time-domain tuning was to demonstrate that a properly tuned all-pole band-pass filter must have deep nulls in the time-domain response. Chapter 3 of this thesis illustrated that the band-pass response of a filter can be related to the low-pass prototype filter, using the shift theory. The time-domain response of band-pass filter calculated analytically would always be a sinusoidal waveform with an envelope that follows the low-pass prototype. This sinusoid would make determining nulls in the time-domain very difficult. Figure 5-1 illustrates the transmission responses of a 3-pole low-pass filter (left) and similar band-pass filter (right) in linear (upper) and log magnitude (lower) formats. (The peaks of the low-pass and band-pass responses are made to be the same in this figure). From the dB plot, it is clear that while low-pass plot has a few distinct nulls, the band-pass has many nulls as-

sociated with the carrier term. However, a VNA takes only one-sided frequency data, and thus its time-domain response has both real and imaginary parts. The magnitude of the time-domain response is identical to that of the low-pass prototype as shown in equations (3.35) and (3.36), and figure 5-1 (left, lower). If one can show that the low-

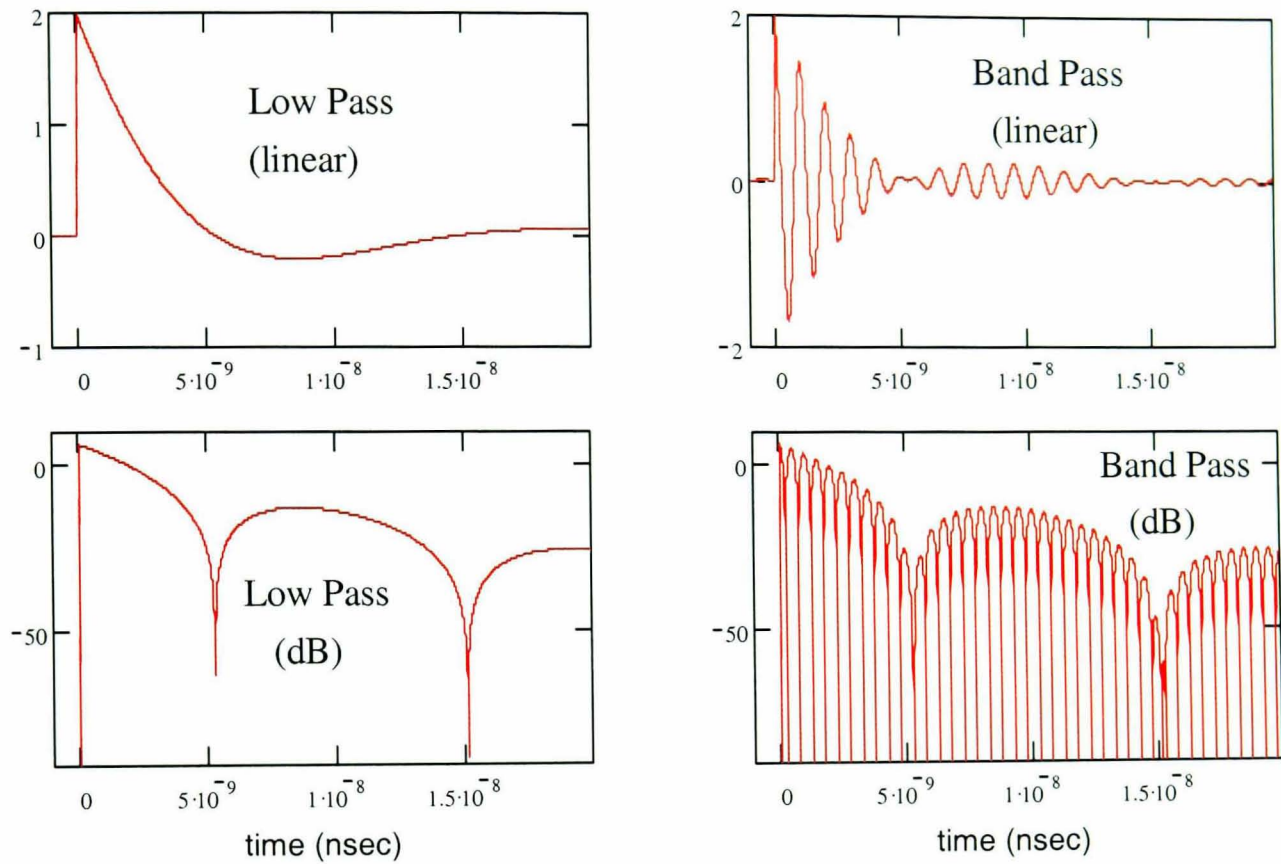


**Figure 5-1 (left) Low-pass impulse response of a 3-pole filter in linear (upper) and log magnitude (lower); (right) band-pass impulse response of 3-pole band-pass filter in linear (upper) and log magnitude (lower) formats**

pass prototype must have deep nulls in the time-domain response, it would follow that a band-pass filter based on this prototype would also have deep nulls. The next sections provide calculations on low-pass filters to show that such nulls must exist, and the depth of the null depends on the tuning of the filter resonators.

### 5.1.1 Time-domain reflection response of 3 pole Butterworth filter

A 3-pole Butterworth low-pass filter was chosen for the first calculations, due to its relatively simple transfer function. Once the time-domain response of the low-pass filter is known, the envelope for a 3-pole Butterworth band-pass filter is determined.

The transfer response of a normalized 3-pole Butterworth filter is [83]

$$|T(j\omega)| = \frac{1}{\sqrt{1 + \omega^6}} \quad (5.1)$$

From this S-parameters can be determined from

$$|S_{21}(j\omega)|^2 = \frac{1}{1+\omega^6} \quad (5.2)$$

From direct calculation, or [83],

$$H(s) = \frac{\frac{1}{2}}{s^3 + 2s^2 + 2s + 1} \text{ and so,} \quad (5.3)$$

$$D(s) = s^3 + 2s^2 + 2s + 1$$

The input impedance for an all-pole Butterworth filter can be written directly as [84]

$$Z_{11}(s) = \frac{D(s) - s^n}{D(s) + s^n} \quad (5.4)$$

and from equations (2.22), (5.3) and (5.4)

$$S_{11}(s) = \frac{-s^n}{D(s)} \quad (5.5)$$

and from equation (5.5),  $S_{11}$  can be computed as

$$S_{11}(s) = \frac{-s^3}{s^3 + 2s^2 + 2s + 1} \quad (5.6)$$

Replacing  $s$  with  $j\omega$  results in,

$$S_{11}(j\omega) = \frac{-\omega^6 + 2\omega^4 - j(2\omega^5 - \omega^3)}{1 + \omega^6} \quad (5.7)$$

and

$$|S_{11}(j\omega)|^2 = \frac{\omega^6}{1 + \omega^6} \quad (5.8)$$

To verify this result, power conservation is used to compute  $|S_{11}|^2$  from

$$|S_{11}|^2 = 1 - |S_{21}|^2 = 1 - \frac{1}{1 + \omega^6} = \frac{\omega^6}{1 + \omega^6} \quad (5.9)$$

The frequency response of  $S_{11}(\omega)$  of the 3-pole Butterworth is shown in figure 5-2.

The time-domain response can be found from the inverse Laplace transform of  $S_{11}(s)$  in equation (5.6) (see appendix 1 for the detailed calculation):

$$S_{11}(t) = -\delta(t) + \left\{ e^{-t} + e^{-t/2} \left( \cos\left(\frac{\sqrt{3}}{2}t\right) - \frac{\sqrt{3}}{3} \sin\left(\frac{\sqrt{3}}{2}t\right) \right) \right\} \cdot U(t) \quad (5.10)$$

The magnitude of the  $S_{11}$  impulse response is shown in figure 5-3 (left), for comparison with the VNA time-domain transform of the frequency response  $S_{11}(\omega)$ , figure 5-3 (right). This is also shown in the linear magnitude format, as it is a complex result. Clearly, the  $S_{11}$  impulse response that was calculated analytically does not match the time-domain transform of the frequency response, such that one must conclude there is some special attribute of the VNA transform that causes the differences in responses shown in figure 5-3. In particular, there is a null near  $t = 0$  in the VNA transform that is not in the impulse response. Unfortunately, this does not give good insight as to why the nulls in the VNA time-domain transform become less deep when the resonators are not properly tuned. Further analytical analysis of the three-pole filter is mathematically difficult, therefore an even simpler circuit will be used to further explore this aspect of the VNA time-domain transform.

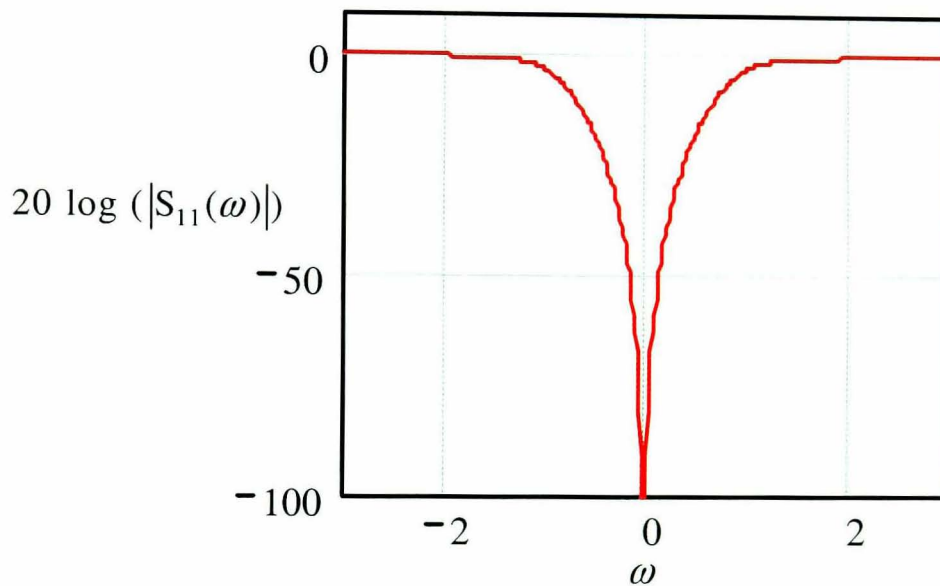


**Figure 5-2: Frequency response of a 3-pole Butterworth low-pass filter, in dB**

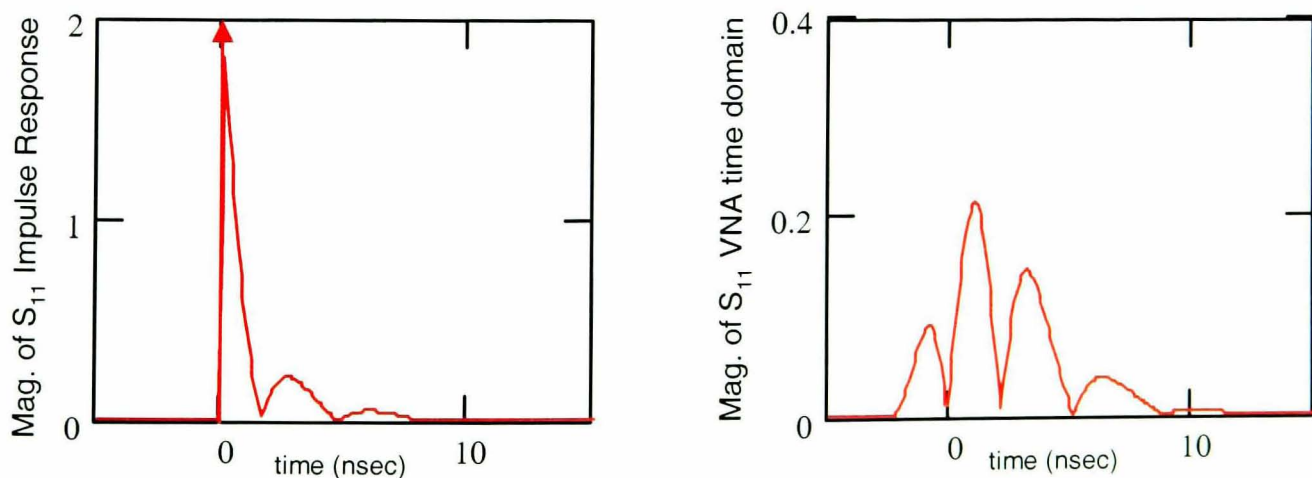


**Figure 5-3 Analytically calculated impulse response (left) and VNA time-domain response (right), of a 3 pole Butterworth filter. Note the change in y-axis scale.**

## 5.2 Analytical calculations based on a single-pole low-pass filter

A single pole low-pass filter will be used to examine the relationship between the VNA time-domain transform and its impulse response, which may then be extended to band-pass filters. A single pole low-pass filter consisting of a series inductor (or shunt capacitor) can represent the single pole band-pass case. Band-pass filters, though, can be mistuned from their desired center frequency, resulting in a non-symmetric response about that center frequency. Low-pass filters consisting of physically realizable parts (e.g., inductors and capacitors) must always have symmetric responses about the origin. However, if the use of non-realizable elements is allowed, then it is possible to “tune” a low-pass filter to have a non-symmetric response about the origin. Adding a fixed reactance, of value  $\omega_0$ , will provide the non-symmetric low-pass response that can be used to investigate the band-pass response of a mistuned single-pole band-pass filter.

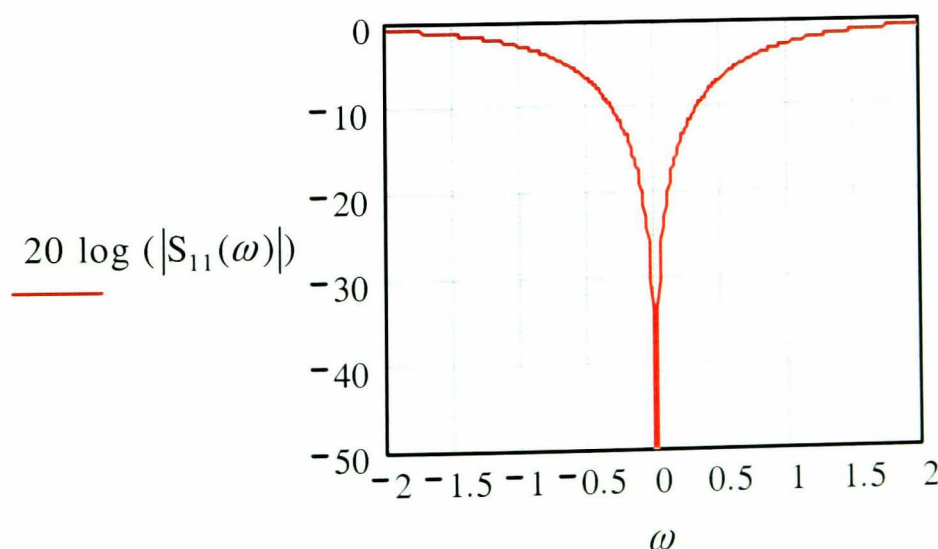
### 5.2.1 Modeling a low-pass response centered about frequencies other than zero Hertz.

Figure 5-4 shows the frequency response with  $\omega_0=0$  for a filter with a cutoff of  $\omega=1$ . For a 1 pole RC filter, the analytical calculation of the frequency response yields

$$S_{11}(\omega) = -1 + \frac{2^2}{2^2 + (\omega RC)^2} - j \frac{2\omega RC}{2^2 + (\omega RC)^2} \quad (5.11)$$

For a corner frequency of  $\omega=1$  and  $R=1$ , then  $C=2$ . The frequency response of the network is shown, with the frequency span equal to 2 times the bandwidth. (Note, this is equivalent to a band-pass filter with a bandwidth of 2).

The impulse response of the network can be calculated analytically (see appendix 1)



**Figure 5-4** Frequency response of a 1-pole low-pass filter, where “ $\omega$ ” represents the radian frequency.

to obtain the result

$$S_{11}(t) = \left[ e^{-t} \cdot U(t) - \delta(t) \right] \quad (5.12)$$

where  $U(t)$  is the Heavyside (or unit) step function. This result is plotted in figure 5-5 (left). Since the frequency response is hermitian, the resulting time response is pure real. Equation (5.12) is also plotted in log magnitude (dB) format in figure 5-5 (right), however the delta function is not shown on this plot. Note that the response forms a straight diagonal line when displayed in log magnitude.

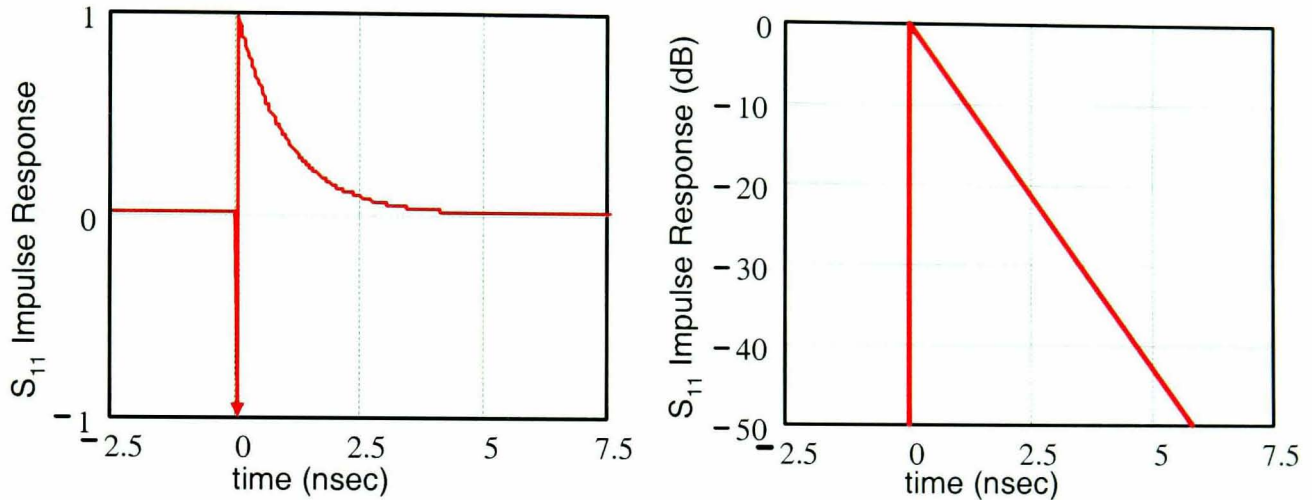


**Figure 5-5 Impulse response of a 1-pole low-pass filter in (left) linear, and (right) log magnitude (dB) formats. Note the negative delta function at time  $t=0$ .**

If the VNA time-domain transform is performed on the frequency response data, the time-domain response can be plotted. Figure 5-6 shows the time-domain response plotted (red) in dB, as is the custom with VNA displays, since the data is often complex and ranges over large values. The analytically calculated result from figure 5-5 (right) of the impulse response is plotted on the same plot for comparison (blue, dashed). Clearly, there is a substantial difference. This difference becomes more interesting when the center frequency of the response is changed.

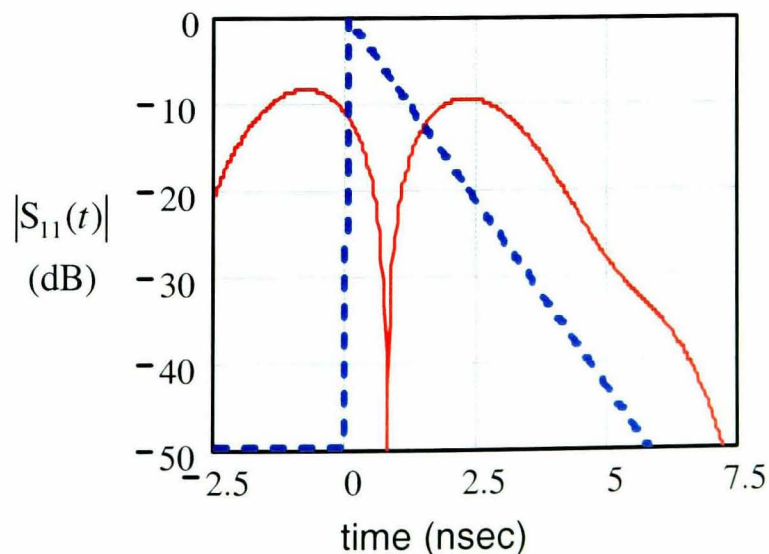


**Figure 5-6 VNA time-domain response of a 1-pole filter (red) and impulse response (blue) both in log magnitude (dB).**

The time response for a frequency-shifted network can be determined analytically from the Fourier transform shift theory to be:

$$S_{11}(t) = \left[ e^{-t} \cdot U(t) - \delta(t) \right] \cdot e^{-j\omega_0 t} \quad (5.13)$$

Figure 5-7 (right) shows the frequency response with  $\omega_0 = -0.2$ . A VNA time-domain transform is performed on the shifted frequency response data and the resulting trace is plotted in figure 5-7 (right, red trace), along with the magnitude impulse response from equation (5.13) (blue trace), (the negative delta function is not shown in the blue trace). There is a change in the magnitude of the time-domain transformed signal, but no change in display of the analytically calculated impulse response. The latter result is evident from equation (5.13) as the complex exponential factor has no effect on the magnitude of this function. This discrepancy leads to questioning the validity of the VNA time-domain transform, and is further investigated in the next section.

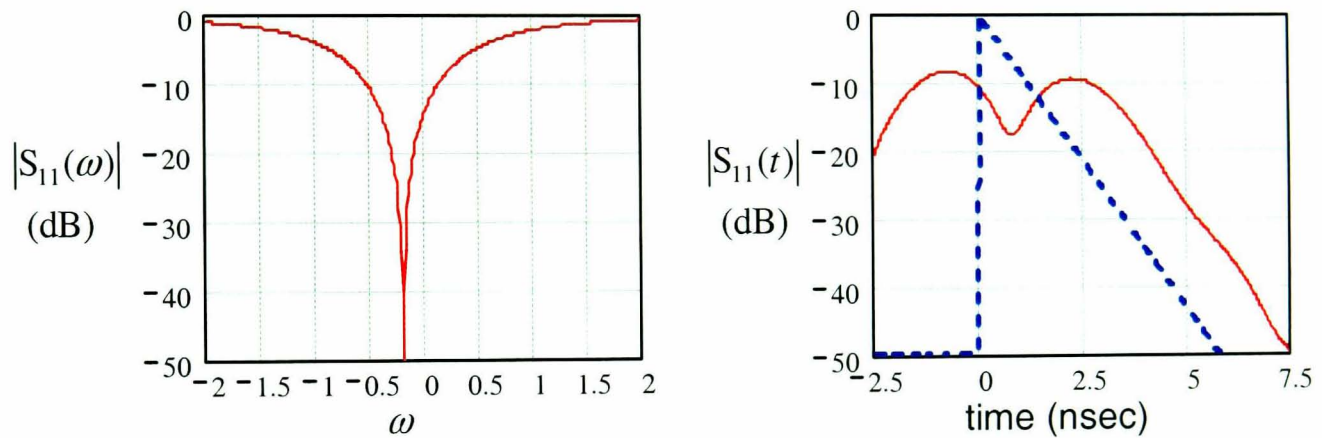


**Figure 5-7 (left) Frequency response of a 1-pole filter offset tuned; (right) time – domain (red) and analytic impulse response (blue) of a 1 pole filter tuned offset. (Negative delta function at  $t=0$  not shown on the impulse response)**

### 5.2.2 Comparison of impulse response & VNA time-domain transforms as applied to a 1-pole low-pass filter

As outlined in section 3.3, the truncation of frequency response data can distort the time-domain transform, effectively adding a rectangular window to the analytically calculated impulse response. The effects of truncation can be applied to the parts of equation (5.12). This effect is the convolution of

$$\frac{\sin at}{at} \quad (5.14)$$

with each of the individual parts of equation (5.12). The convolution of the first (exponential) part is difficult to calculate analytically, but can be numerically computed to illustrate its effect, or the discrete inverse Fourier transform can be performed on

$$S_{11}(\omega)+1 = \frac{2^2}{2^2 + (\omega RC)^2} - j \frac{2\omega RC}{2^2 + (\omega RC)^2} \quad (5.15)$$

which is the frequency response associated with the exponential part. The second part (delta function) convolution is easy to calculate analytically, as convolution of a delta with any function returns that function. For this part of the investigation, the frequency span is increased to 10 times the bandwidth, and the linear magnitude is displayed. The frequency responses of the individual parts of equation (5.11) are shown in figure 5-8 (left); note the flat frequency response (blue trace along the top graticule) associated with the delta function in the time response of equation (5.12). The log magnitude of the impulse responses of the two parts are shown individually in figure 5-8 (right), with the portion attributable to the delta function in blue, and the portion attributable to the frequency dependent function in red. This time response is calculated as though the magnitude of the frequency response is zero outside the plotted region, thus truncating equation (5.11) for  $|\omega| > 10$ . Here one can see that the time responses become confusing due to the side lobes caused by the truncation function.

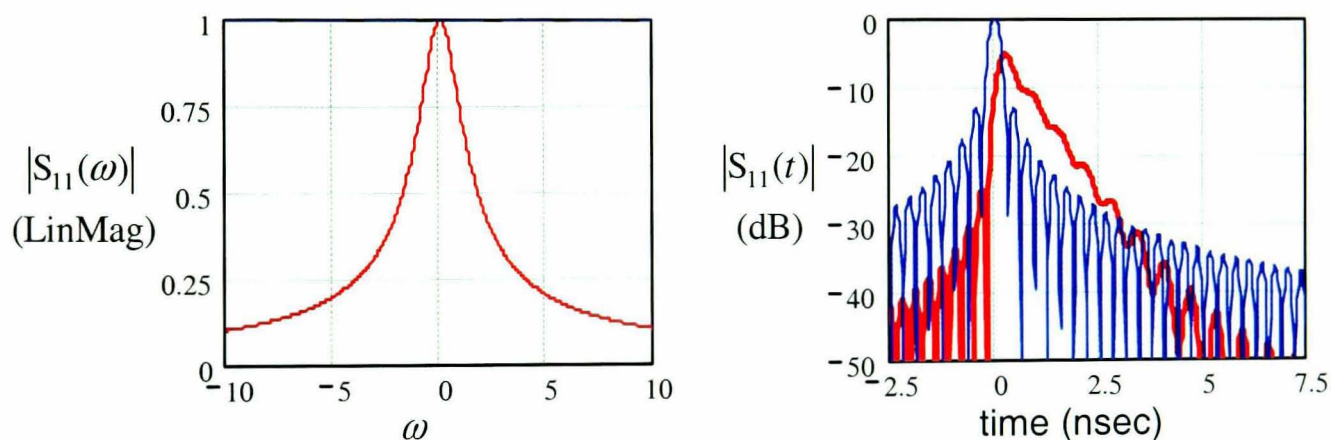


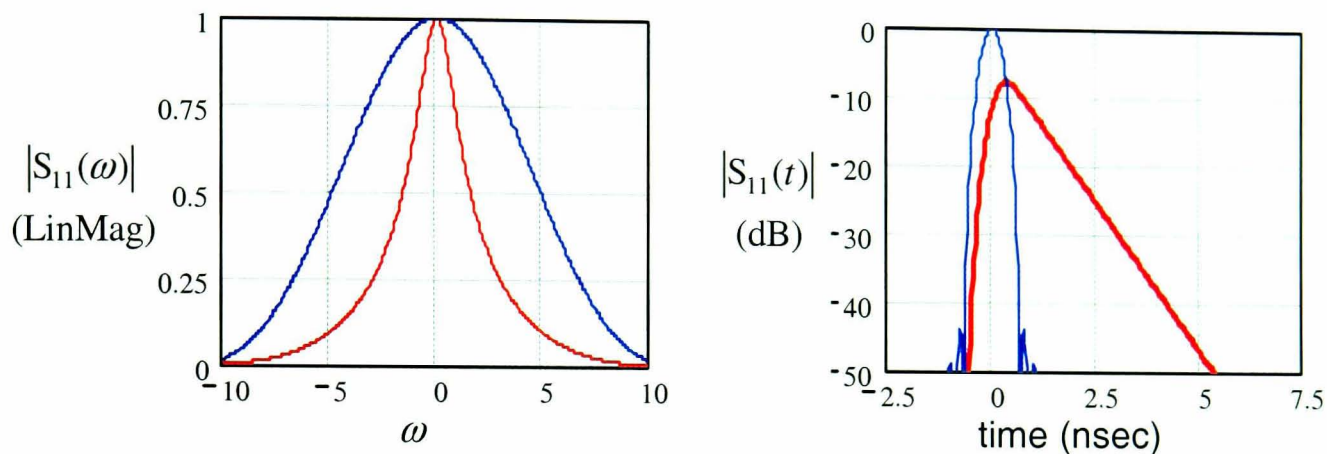
**Figure 5-8 (left) Frequency response associated with the impulse (blue) and the exponential (red) portions of eq. (5.11), (right) the time response of the truncated impulse (blue) and exponential (red) portions of eq. (5.12).**

In the VNA time-domain transform, the side lobes are controlled by a window function that makes a smooth transition to zero at the edges of the frequency response. The window function used in the VNA is a Kaiser-Bessel window, typically of factor 6. The effect of the window function is shown in chapter 3, figure 3-5.

The windowed frequency response of the two parts of equation (5.11) is shown in figure 5-9 (left). The impulse response of these functions is shown in figure 5-9 (right). The data is re-normalized such that the amplitude of the transform of a unit input frequency response is unity at  $t=0$  (that is, normalizing the time response to the sum of the window coefficients, as described in section 3.3.5). Compared with figure 5-8, this

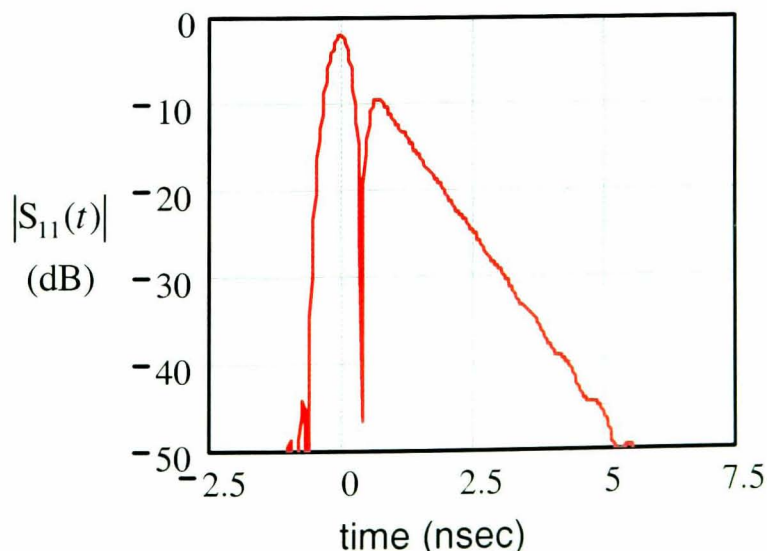
display is visually clearer, with less of the detail obscured by the side-lobes. The penalty for this is a widening of the impulse responses, which if windowed too much would lead to a lack of resolution in the display.

Figure 5-10 shows the result of taking the individual displays of figure 5-9 (right), and combining them into one display that represents the overall impulse response of the windowed  $S_{11}$  function. By adding the effects of windowing and truncation to the im-



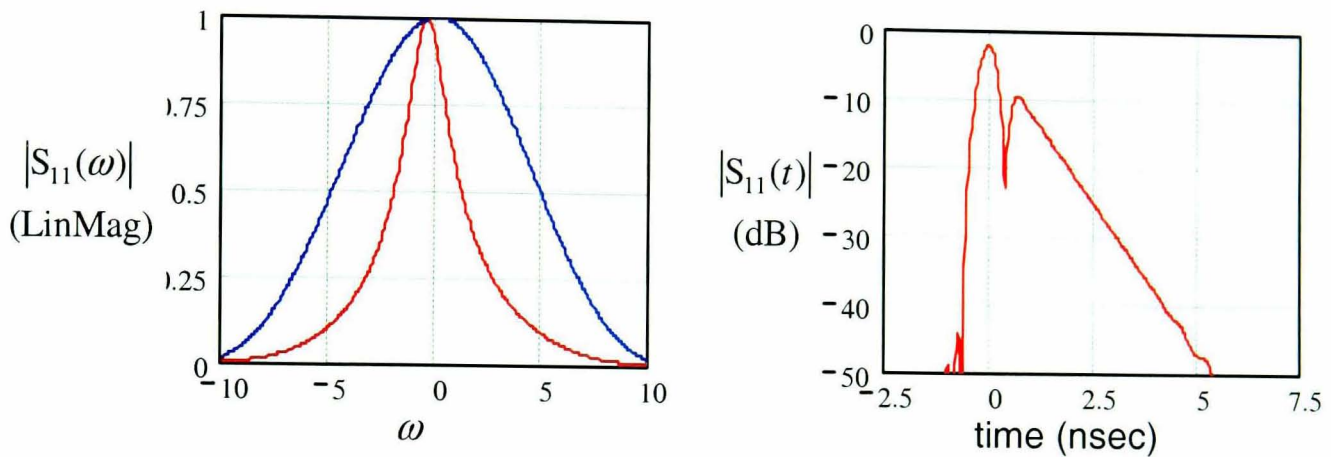
**Figure 5-9 (left) The two parts of equation (5.11) windowed in the frequency domain with the delta portion in blue, and the other portion in red; (right) the time response of the respective parts with windowing applied.**

pulse response of equation (5.12), it becomes the same as the VNA time-domain transform. This has a deep null near  $t=0$ . Inspection of these parts show that the null is caused by the windowed delta portion of equation (5.13) exactly canceling the windowed exponential portion. Thus the deep null is a function of the truncation and windowing of the frequency response widening the delta portion of  $S_{11}(t)$  such that it exactly cancels part of the exponential portion.



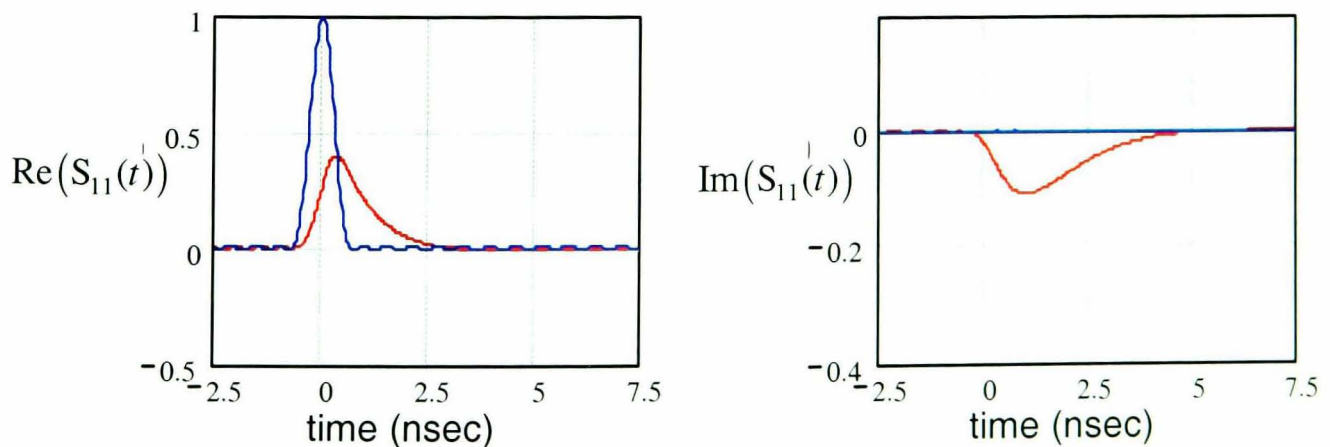
**Figure 5-10 Impulse response of a 1-pole network with truncation & windowing**

Figure 5-11 (left) shows the  $S_{11}$  frequency response of each portion of a filter shifted by  $\omega_0 = -0.5$ . It is clear that the delta function portion has not changed at all (the delta function in time-domain is a constant in frequency domain), but the frequency dependent portion has changed. Inspection of equation (5.13) shows that since  $\delta(t)$  is zero at  $t \neq 0$ , and  $e^{j\omega_0 t} = 1$  at  $t=0$ , the delta function portion of  $S_{11}(t)$  is not affected by the frequency shift. Figure 5-11 (right) shows the impulse response of the shifted filter after windowing. This shows no deep null, thus confirming that offset tuning a filter will affect the null in the time domain.



**Figure 5-12 (left) frequency response of the individual portions of  $S_{11}$  of a windowed and frequency shifted 1-pole network; (right) combined impulse response of the frequency shifted 1-pole network.**

The depth of the null becomes even more clear if one looks at the real and imaginary time responses of the individual parts of windowed version of equation (5.13) as shown in figure 5-12 (left) and 5-12 (right), respectively. Equation (5.13) describes the impulse response when the “center frequency” is changed (that is, a constant reactance added so that the  $S_{11}$  frequency response is no longer centered at zero). Note that for a zero shift, it is the same as equation (5.12). The behavior of the individual parts of equation (5.13) can be observed to better under the effect of frequency shift.



**Figure 5-11 (left) Real part of exponential (red) and delta portion (blue); (right) imaginary part of exponential (red) and delta portion (blue) of equation (5.13).**

The imaginary portion related to the delta function is always zero regardless of the shift. The imaginary portion of the rest of the time response portion of equation (5.13) however grows as the sine of the shift grows, and the real portion is reduced as the cosine of the shift is reduced (both are functions of the complex exponential element). For small shifts, the size of the imaginary portion is very small, but it is noticeable on a log magnitude plot. Since the  $S_{11}(t)$  function is pure real only if there is no shift, the deep null is possible only if each portion, both real and imaginary, of equation (5.13) cancel, but the delta portion is always pure real. Thus, the depth of the null is directly proportional to the remaining imaginary part of the exponential portion of  $S_{11}(t)$ .

This becomes quite clear if the total result of  $S_{11}(t)$  is plotted against the imaginary part of the exponential portion, as shown in figure 5-13. The depth of the null cannot go below the magnitude of the imaginary part. From this it is clear that for a one-pole resonator, a deep null will exist if the resonant frequency is exactly on the center of the data used for the transform. If the resonator is not on the center, the depth of the null will be proportional to the sine of the shift of center frequency.

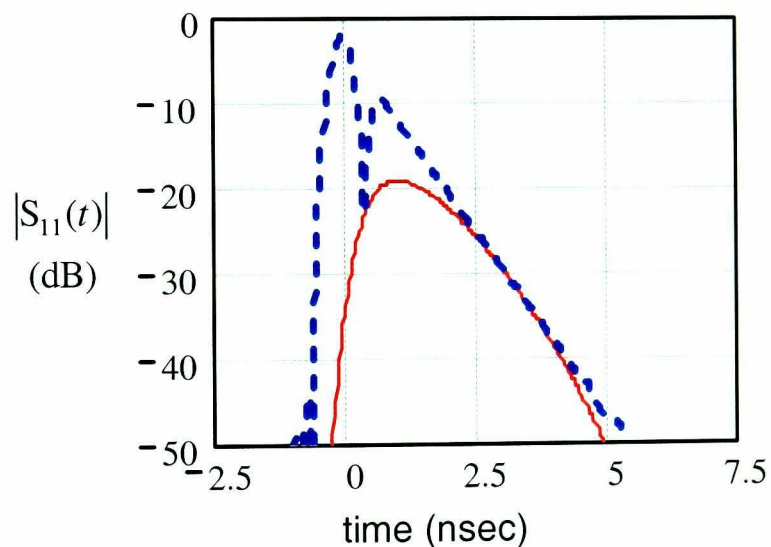


**Figure 5-13** Log magnitude of the overall impulse response of a shifted 1-pole network (blue, dashed), along with only the imaginary part (red).

From the examples above, it is clear that the impulse response of a 1-pole filter differs from the VNA time-domain response only because of the windowing and truncation effects. These effects cause a spreading of the individual portions of the impulse response, and this spreading creates a null in the VNA time response near time  $t=0$ . Further, if the response is shifted from being centered on the transform, the resulting time-domain response will no longer have a deep null, with the depth of the null being proportional to the imaginary portion of the response, which in turn is proportional to the frequency shift. This one-pole response can be extended to multi-pole filters, by



resonator 4 is not shown. Simulations were performed on this filter to investigate the effects of each resonator, and demonstrate the reasons for the interactive effects of tuning in the time-domain.

Figure 5-15 shows the filter's transmission and reflection response (thin red and blue lines, respectively) and the response from the resonator 2 incident signal probe (thick red line). This is the signal that is applied to resonator 2, and shows the bandwidth reduction effects of the first resonator. That is, the thick red line shows that the incident signal to resonator 2 does not have a flat frequency response, but is reduced outside the bands of the filter. (The ringing on the signal is likely due to the way in which the source impedance of the coupling network reacts with the coupling element used as a

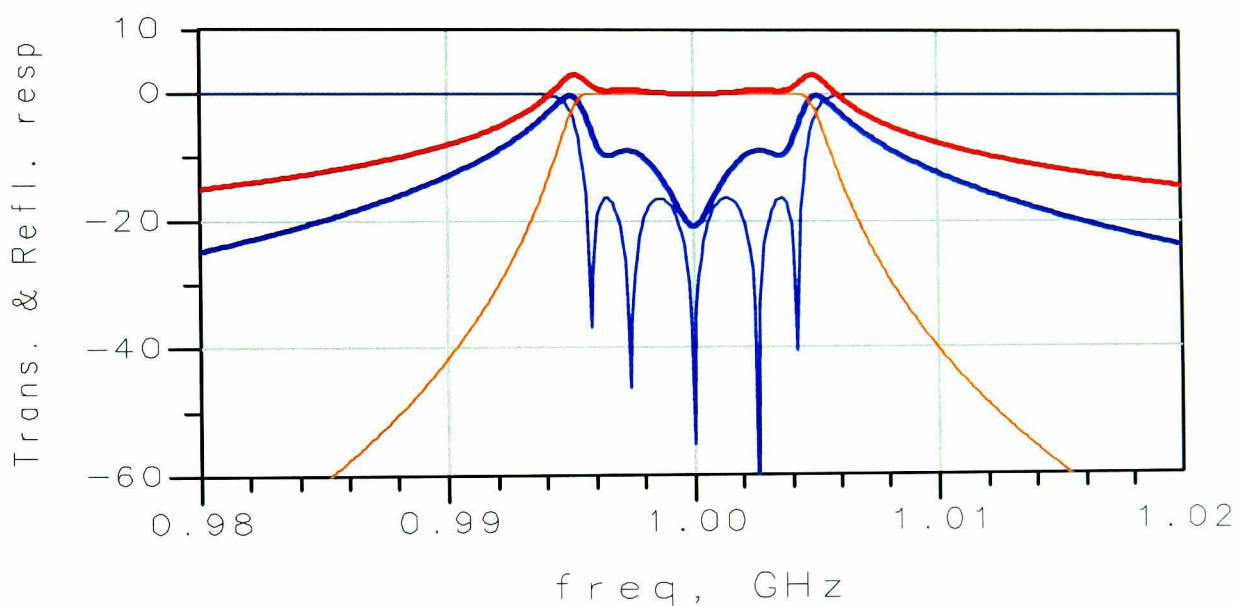


**Figure 5-15: Transmission response (red) and reflection response (blue) from the overall filter (thin lines), along with reflection from just before resonator 2 (thick blue) and incident signal to resonator 2 (thick red)**

probe in the circuit). Also shown in figure 5-15 is the reflection signal from the input to resonator 2 (thick blue line) including the effects of passing back through the copy of the first coupling and resonator elements.

The reflection probe couples the signal off with -40 dB coupling to avoid affecting the overall frequency response. This signal is then amplified to account for the coupling loss, and finally, is passed through a network that is identical to the first interstage coupling and first resonator. Thus, this signal represents the contribution of resonators 2 to 5 of this filter on the overall  $S_{11}$  reflection, but does not include the contribution from the first resonator. Adding in the extra circuitry provides for the same band limiting and delay as that which occurs on the same reflection signal as measured at  $S_{11}$ . This can be most easily understood by viewing this trace in the time-domain. Figure 5-16 shows the time-domain transform of the  $S_{11}$  trace (blue) and the condi-

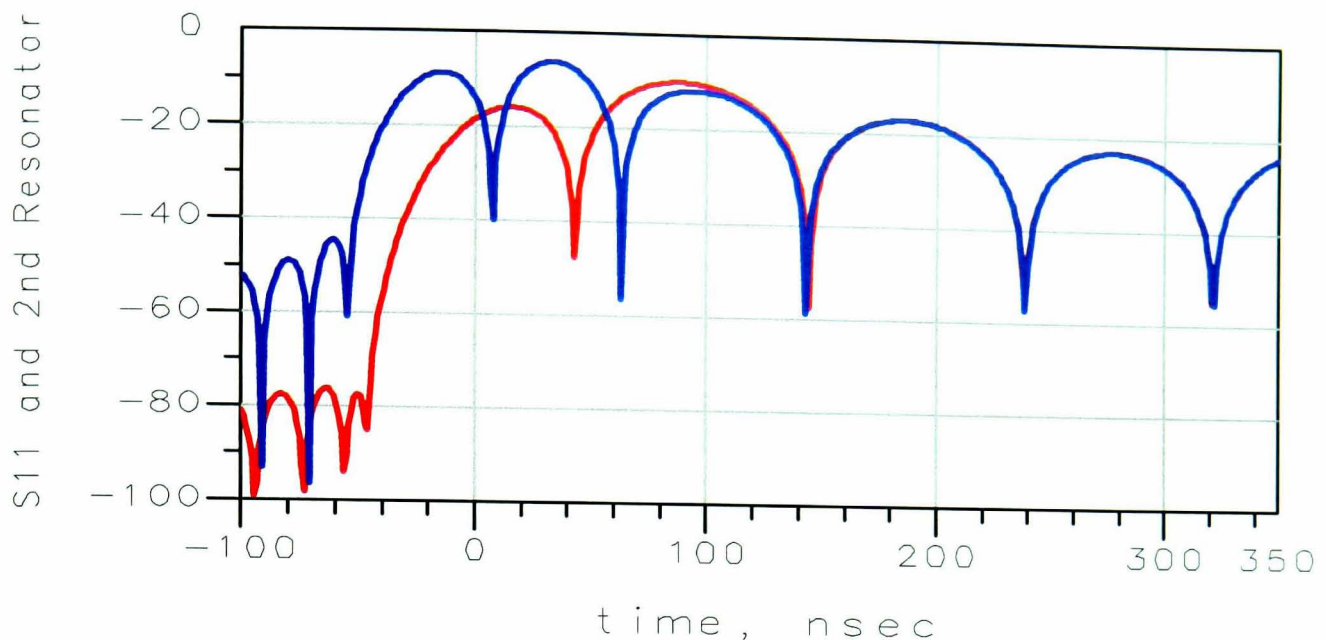


**Figure 5-16: Time-domain response of the  $S_{11}$  of the 5-pole filter (blue) and of the reflection from just before resonator 2 (red)**

tioned reflection from resonator 2 (red). The time of the null for the second resonator is offset by exactly the delay of the first resonator, as can be determined by calculating the delay of only the filtering elements associated with the first resonator in the output of the probe circuit.

Also, it is remarkable that past the second null in the blue trace in figure 5-16 (that is, past the first null in the red trace), the two time-domain plots are identical. This confirms that the red trace represents the reflection from the rest of the filter beyond the first resonator, and that the circuitry added to the reflection probe properly conditions the signal to represent the contribution of resonators 2 through 5 on the  $S_{11}$  response. From this plot, the contribution of the resonators 2 through 5 (red trace) can be subtracted from the overall  $S_{11}$  response to give the contribution of only the first resonator to the overall  $S_{11}$  response. Figure 5-17 shows the overall  $S_{11}$  response (blue) and the response created from subtracting the resonator 2 input response from the overall  $S_{11}$  response to give the response from only the first resonator (red), after shifting the second resonator to account for 270 degrees of phase shift from the first resonator and coupling.

Note that the red trace is nearly identical to that found in the previous section, figure 5-6, for a 1-pole resonator, and which has been shown to have a null that is proportional to the tuning of the resonator center frequency (of course the delay is different as it is scaled by the frequency span of the filter). This remarkable result indicates that the time-domain response can truly separate individual resonator responses, for multi-pole filters.

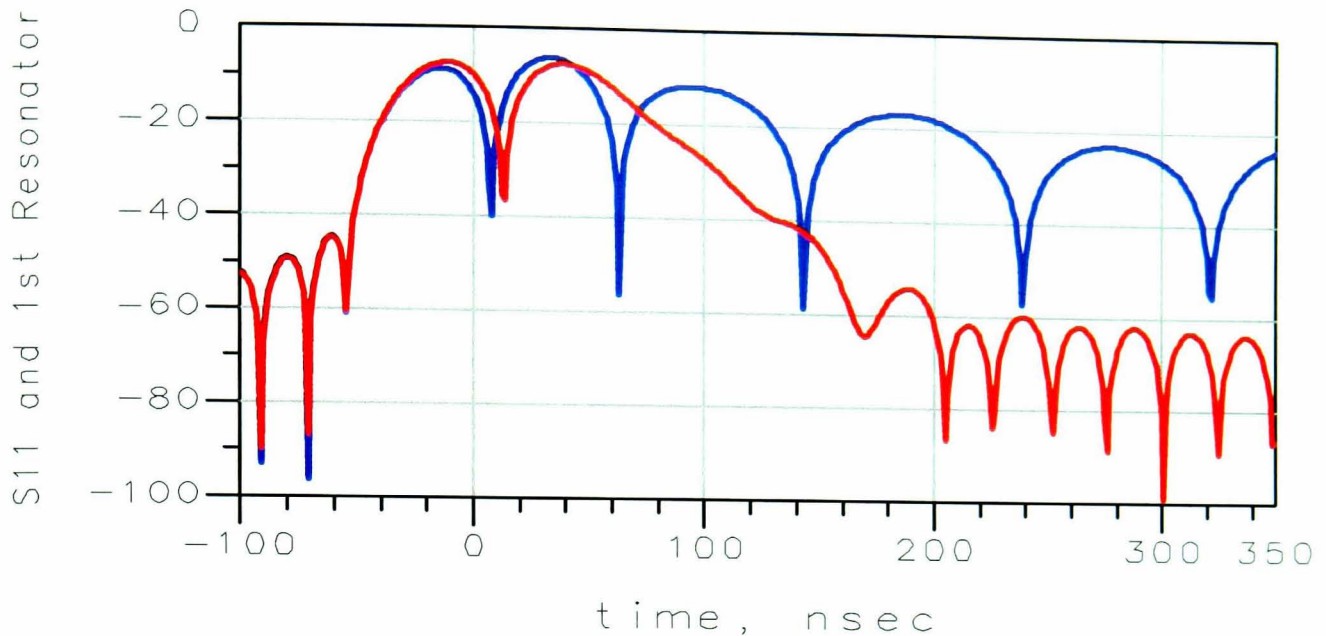


**Figure 5-17: Time-domain transform of overall  $S_{11}$  (blue) and from only the first resonator (red) found by subtraction of the two traces in figure 5-16.**

The technique to display this individual resonator response can be repeated for each additional resonator in the filter to demonstrate the individual response of each. Some observations on these plots are appropriate. Notice that the first resonator null does not land exactly at the same time point as the overall  $S_{11}$  response. This is easily understood by recognizing that the overall response also contains some portion of a real signal from the reflection of resonators 2 to 5 occurring at the same time as the null associated with the overall response of  $S_{11}$ . This causes an apparent shift in the null of the overall response from that of the single resonator response. This also may account for why the resonator null associated with the first resonator sometimes appears just before the  $t=0$  axis.

Also note that these nulls will not be deep if the resonator associated with the null is not properly tuned, as that will yield an imaginary portion which cannot be cancelled out by the real response that occurs from the windowed delta function as shown in figure 5-13 of the previous section.

This also demonstrates why there appears some interactive effect of one resonator tuning on another. The interactive effect can arise from insufficient bandwidth on the frequency response measurement, which will result in a spreading of the time-domain transform, causing the imaginary part of one resonator to land in the region of a null associated with a different resonator. An additional cause of interaction is due to the shift in the center frequency of the signal applied to the second and subsequent resonators. To illustrate this interactive effect, the capacitor on the first resonator of the filter

from figure 5-14 was adjusted up by 1%. The resulting frequency is shown in figures 5-18, and time-domain in figure 5-19.

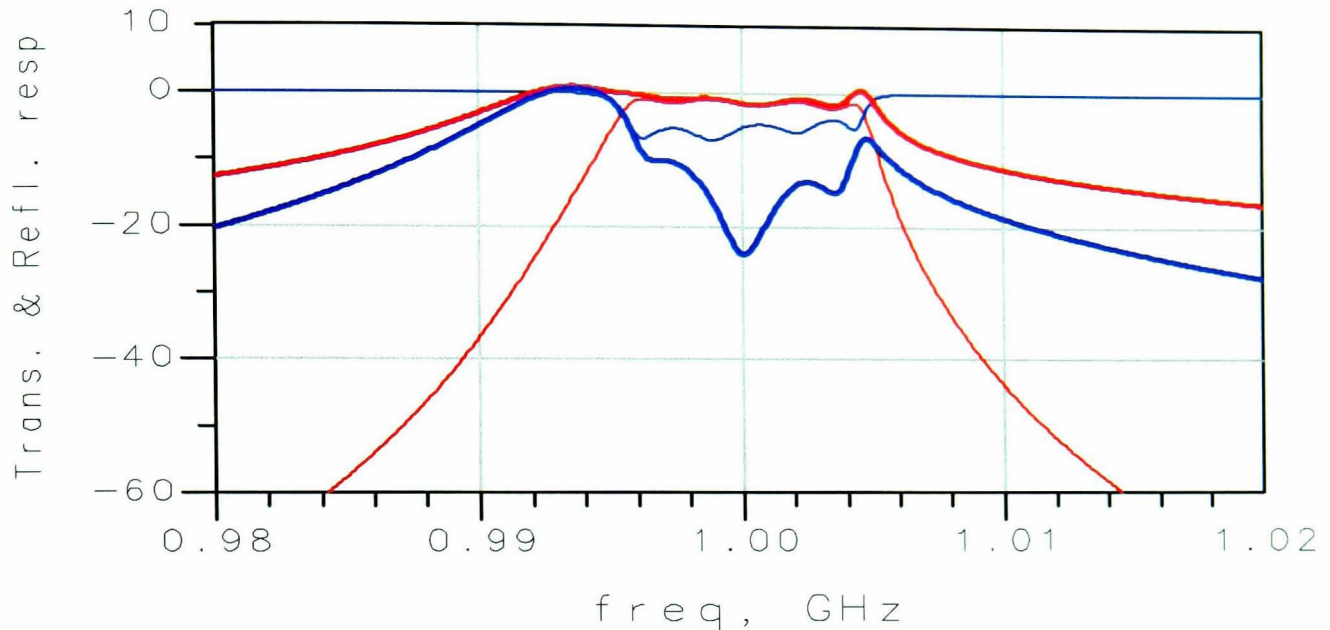


**Figure 5-18: Frequency response of a 5 pole filter with the first capacitor mistuned 1%,  $S_{21}$  (thin red),  $S_{11}$  (thin blue), and the input to resonator 2 (thick red) and the reflection from resonators 2-5 (thick blue).**

Note from figure 5-18 that while the frequency response of the input reflection,  $S_{11}$ , (thin blue line) is dramatically degraded (to only about -5 dB), the response of the reflection to the second resonator (thick blue line) is substantially unchanged in the pass band when compared to figure 5-15. The input to the second resonator (the thick red line) is tuned lower in frequency, resulting in more signal below the pass band center incident on the second resonator, causing a higher reflection in the stop band below the center frequency than in the tuned case. Presumably, this may result in the center fre-

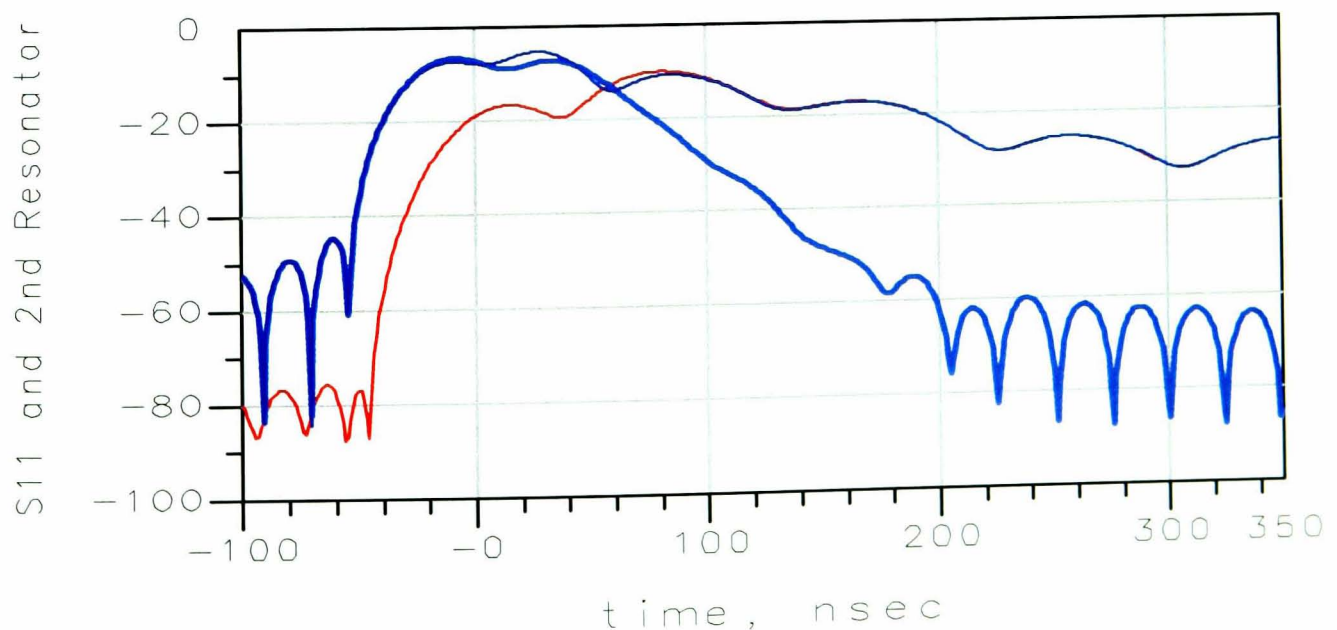


**Figure 5-19: Time-domain response of  $S_{11}$  (thin blue line), reflection from resonators 2-5 (red), and calculated first resonator response (thick, light blue).**

quency of the second resonator appearing higher than it really is. This effect will be explored further in the next chapter.

The time-domain response of the mistuned filter shows all the nulls have nearly disappeared (thin blue trace, figure 5-19). The response from input to the second resonator (thin red line) also shows the nulls associated with the second resonator have been apparently reduced. Subtracting this reflection response from the overall  $S_{11}$  response yields the response expected from only the first resonator, mistuned, as though it were terminated in the reference impedance (thick blue line). This is very similar to the plot of the mistuned single resonator response as described by figure 5-7 (right). In another simulation experiment, the filter was terminated after the first resonator, and the time-domain response obtained was found to be identical to the calculated time-domain response of figure 5-19 (thick blue line), confirming that this simulation technique does properly render the response of individual resonators even when they are not properly tuned.

A similar experiment was performed on the input to resonator 3, using simulation and inter-stage probes to characterize the input reflection response at resonator 3. This response was subtracted from the overall  $S_{11}$  input to produce a signal that corresponds to only the reflection of the first two resonators. Further, the response from the first resonator, as calculated above was also subtracted to produce a response that corresponds to the reflection from only the second resonator, as shown in figure 5-20 below. The response of the second resonator has two nulls: the first is due to the frequency of just the second resonator, and the second null is likely due to the reflection and re-reflection of the signal off of the first resonator. Note that the second resonator time

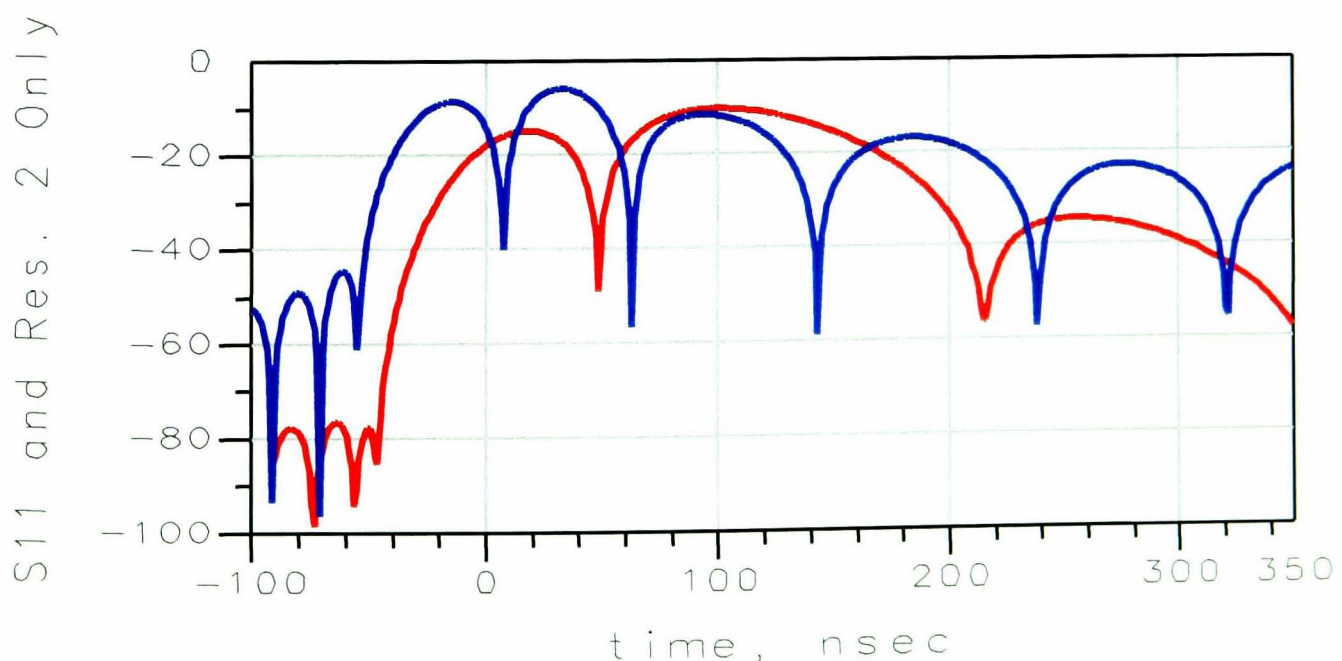


**Figure 5-20:** The calculated time-domain return loss of only the second resonator (red) and the overall  $S_{11}$  (blue)

response is considerably spread out due to the filtering of the first stage, and the narrower bandwidth of the associated coupling, when compared to the  $S_{11}$  trace, but is quite similar to the null associated with the second resonator found in figure 5-16 (red trace).

## 5.4 Conclusions

A closed form analysis has been presented for a 1-pole filter, and has shown for the first time that a deep null must appear in the VNA time-domain transform when the filter is tuned to the center frequency of the VNA, and that the null disappears in proportion to the amount of mistuning of the resonator. Further, it has been demonstrated that the case of a multi-pole filter can be reduced to cascaded 1-pole filters, such that the time-domain response of the multi-pole filter is a sum of responses of 1-pole filters, and as such, the nulls in the time-domain response of a multi-pole filter should be associated with each resonator in turn, and that the nulls are separated in time by a delay that is essentially the delay of each individual 1-pole response.

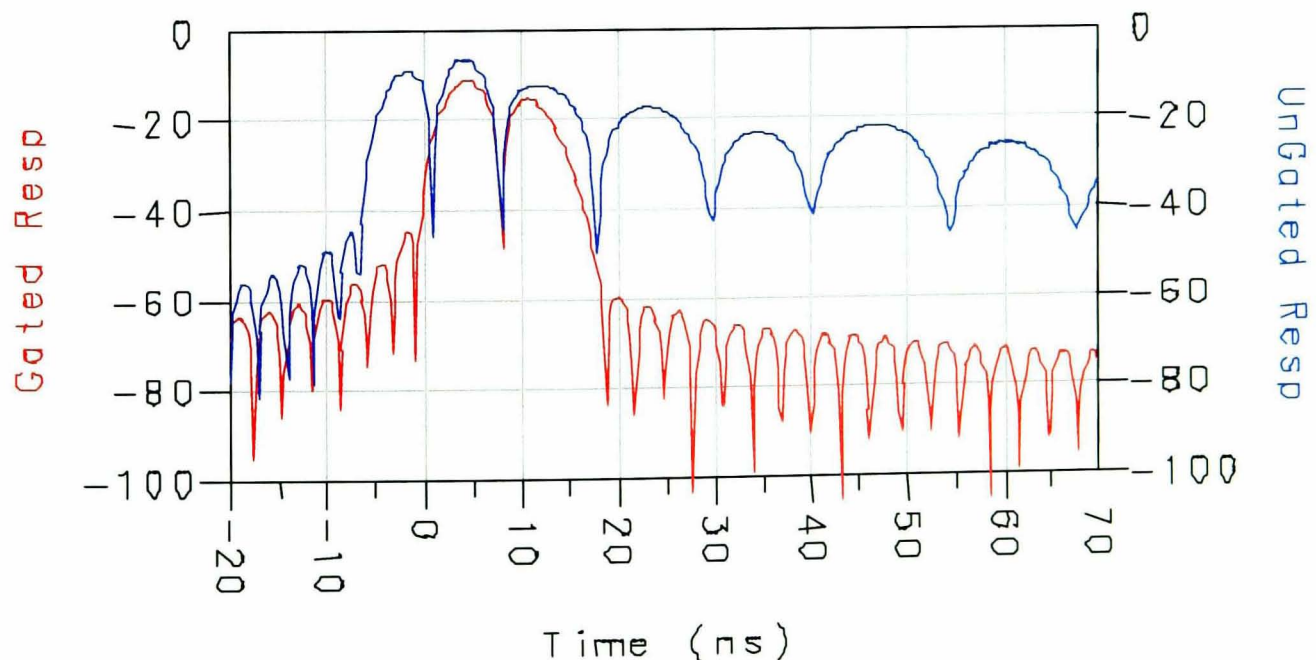
From these simulations and analysis it is clear that the nulls in the time-domain are directly related to the tuning of the associated resonators. The experiments in chapter 4 indicate a tuning method that depends upon tuning each resonator for a deep null. There is no way to determine from the tuning method whether a resonator is tuned too high in frequency or too low in frequency. However, the results of figure 5-19 suggest a new idea for determining the frequency of individual resonators. In this figure, constructed by sampling the signal after resonator 1 and subtracting it from the overall  $S_{11}$ , the time response of only resonator 1 is displayed. From this, taking the forward transform of this response should yield the single resonator frequency response of resonator 1. Of course, it is not practical to sample the internal signals or real-world filters, but considering the discussion in chapter 3 on time-domain gating, a new technique for isolating the individual resonators is suggested, and is developed fully in the next chapter.

## Chapter 6 The Time-Domain Gated Response of Filters.

While the time-domain response has clear application in the tuning of filters, the practical application of interpreting the response has limits. For example, while the tuning of an individual resonator can be identified, it is not clear from the time-domain response alone whether the resonator is too high or too low in frequency. For filters such as filters with cross coupling, where the apparent frequency of resonators may not all be at the same frequency, resetting of the VNA center frequency for each resonator is required to apply the methods developed. The investigation described below develops a new method that overcomes these limitations.

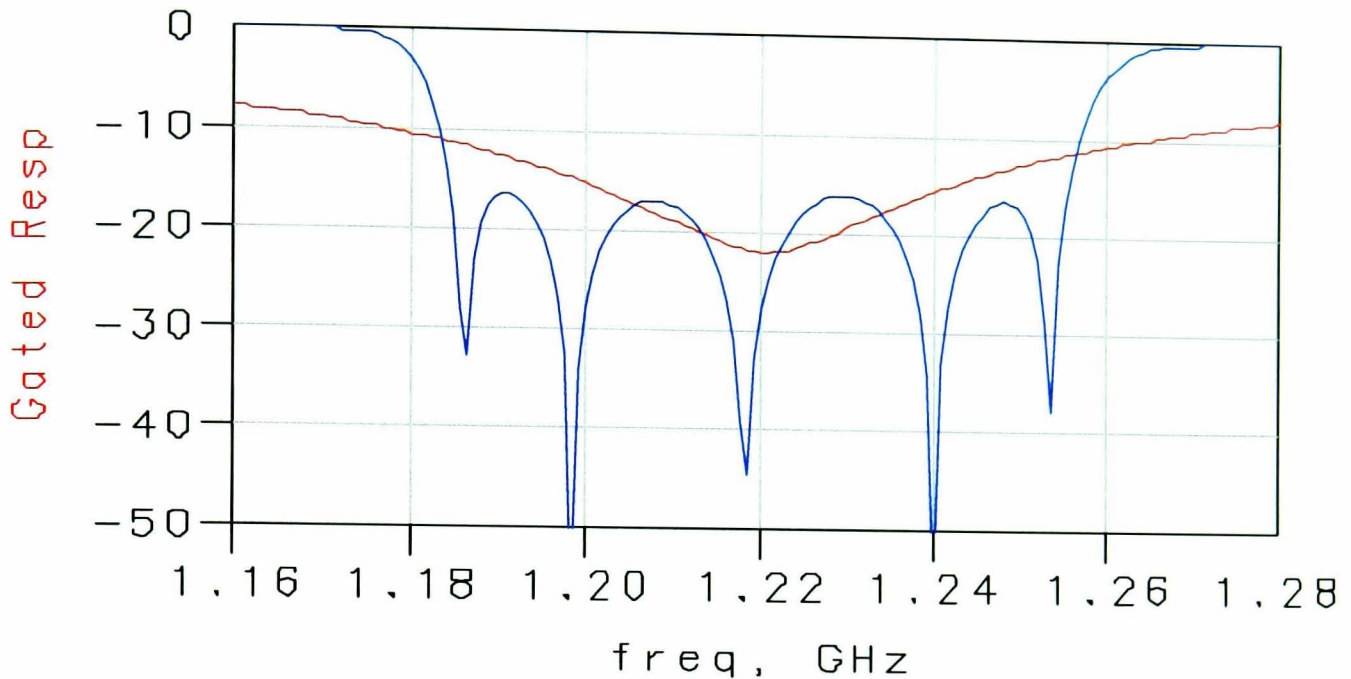
### 6.1 Time-domain gated response of filters

Since individual resonators appear to be associated with specific nulls in the time-domain, it may be possible to isolate the individual responses of these resonators. To investigate this, concepts of time-domain gating from chapter 3 are combined the relationship between a time null and frequency shift described in section 5.2 in an experiment on a 5-pole band-pass filter. The time-domain response of this filter is shown in figure 6-1 (blue) along with a gated time-domain response (red), where the start and stop gates are set to the peak just before and just after the null associated with the second resonator. The time-gated response of figure 6-1 is similar to the impulse response for a 1-pole filter, as shown in figure 5-6.



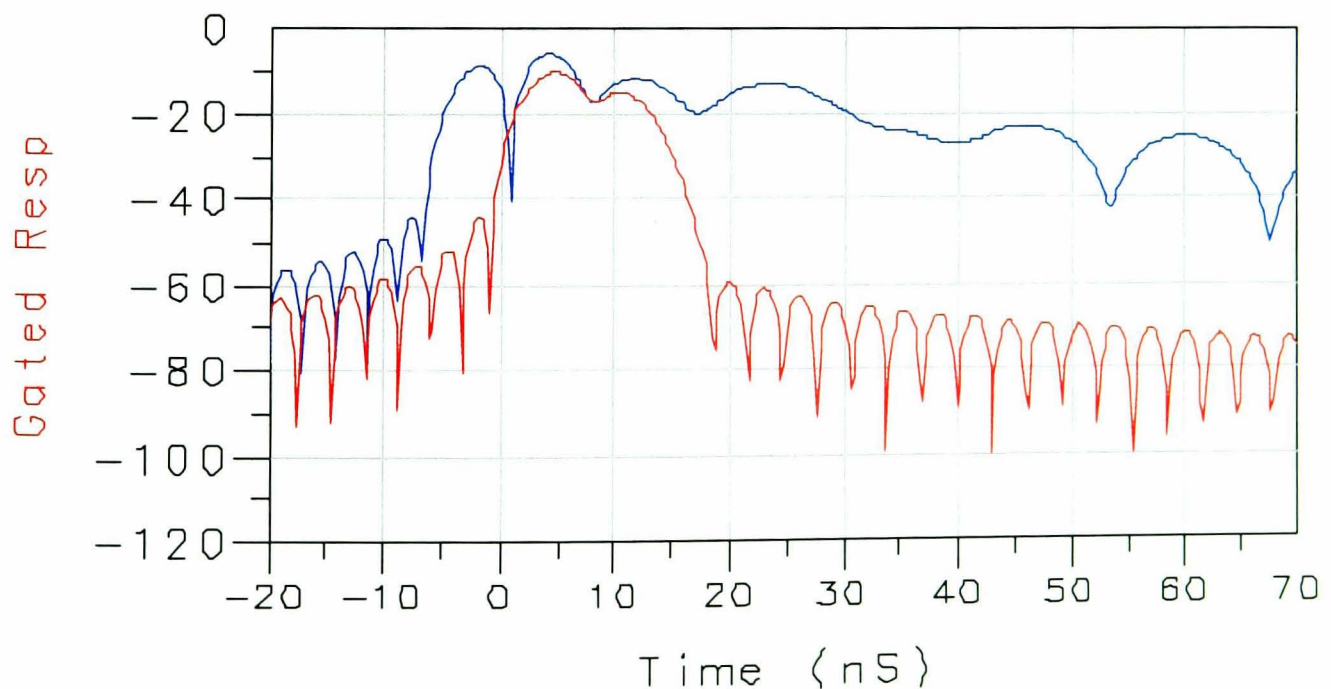
**Figure 6-1** Time-domain response of a 5-pole filter without gating (blue); and with gating (red)

Figure 6-2 shows the frequency response of the filter, with time gating off (blue) and gating on (red). The time-gated response shows a single null exactly centered at the filter center frequency. Again, this is similar to the frequency response one would expect from a 1-pole network.



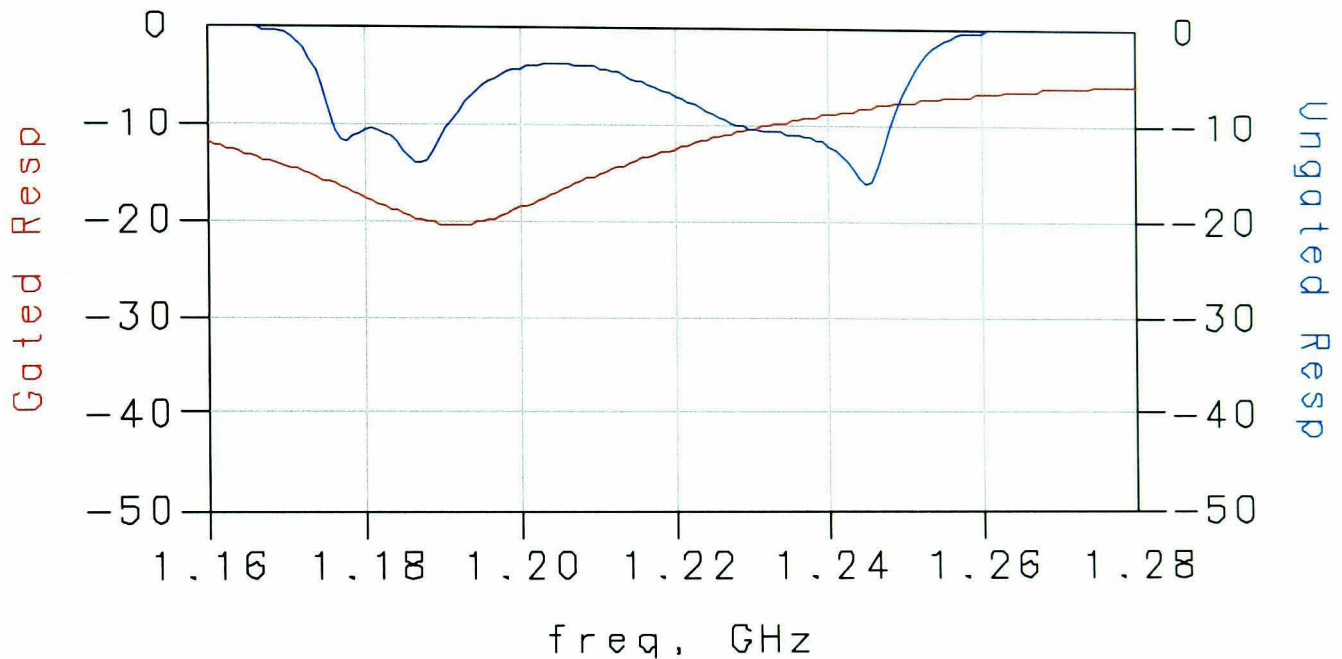
**Figure 6-2** Frequency response of a 5-pole filter (blue), and with gating of resonator 2 (red)

Next, resonators 2 and 4 of the filter were mistuned lower, and the time-domain response was observed as shown in Figure 6-3 with the time gate still applied to resonator 2. The response shows the null associated with the second resonator is not deep, which is evidence in the time-domain that the second resonator is mistuned. Note that the gated response resembles the response of a shifted 1-pole filter (figure 5-7, right).



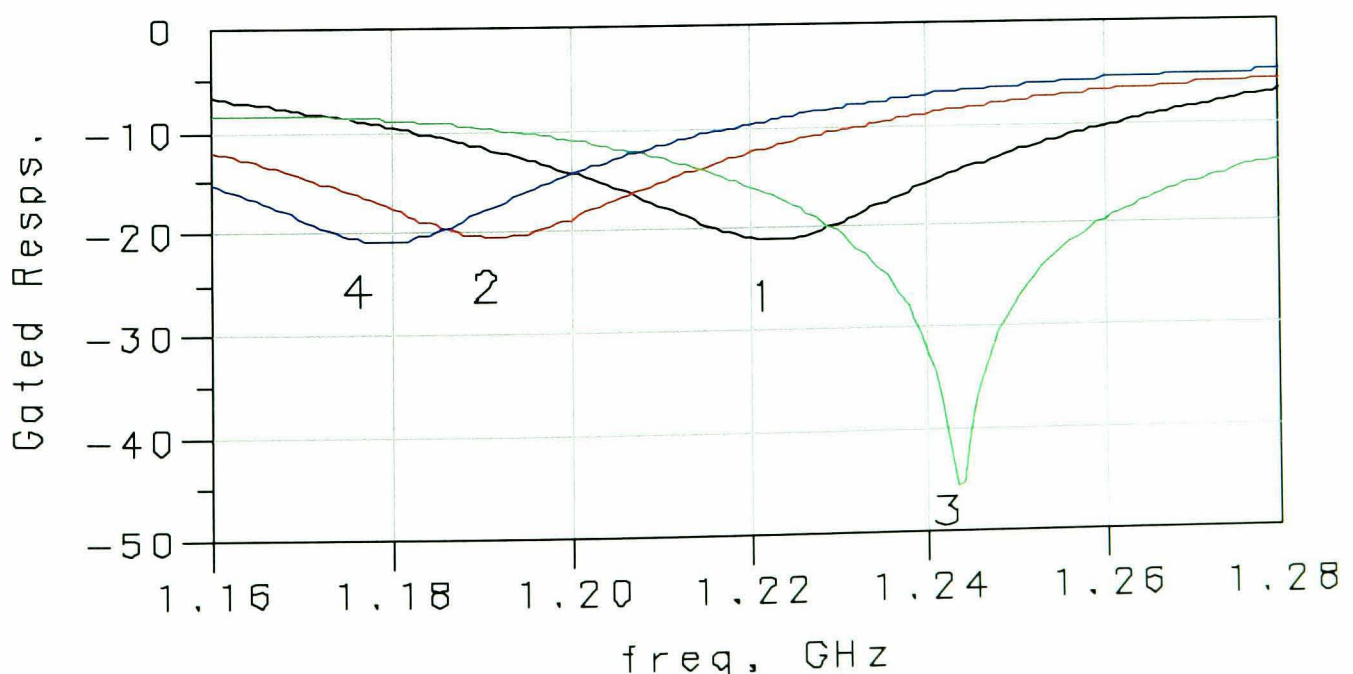
**Figure 6-3** Time-domain response of a mistuned 5-pole filter (blue) and with gating of resonator 2 (red)

Figure 6-4 shows the frequency response of the mistuned filter with gating (red) and without gating (blue) applied. The gated response associated with the second resonator shows the resonator tuned low in frequency. Unlike the time-domain response, it is clear from the gated frequency response that the resonator is low in frequency, and by what amount.



**Figure 6-4 Frequency response of a mistuned 5-pole filter (blue) and with gating of resonator 2 (red)**

The gated time-response is similar to the response seen in section 5-2, where a direct relationship between the frequency shift of a 1-pole response and the depth of the null in the time-domain is demonstrated. Figure 6-5 shows the result of applying the gate function individually to the time nulls associated with each resonator, and overlaying the resulting gated frequency responses on a single plot. It is clear that one can discern



**Figure 6-5 Gated frequency response of 4 resonators, overlaid.**

an equivalent resonator frequency for each resonator. Note that even though only resonators 2 and 4 were mistuned (both tuned low in frequency), resonator 3, and to a lesser extent, resonator 1, both appear to be shifted up in frequency. This interactive effect will be quantified below.

The effectiveness of tuning a filter utilizing the time-gated response is demonstrated by sequentially tuning each resonator to move its gated frequency response to the center of the VNA display. Figure 6-6 shows the response after tuning resonator 2 to be centered on the VNA display. From this display it is the apparent that effect of a mistuning resonator 2 on the shift of resonator 3 is diminished, and the shift of resonator 1 is eliminated entirely. That is, as resonator 2 is tuned to bring the frequency response associated with resonator 2 in the figure 6-6 closer to the center frequency, the response associated with resonator 3 also moves closer to the center frequency.

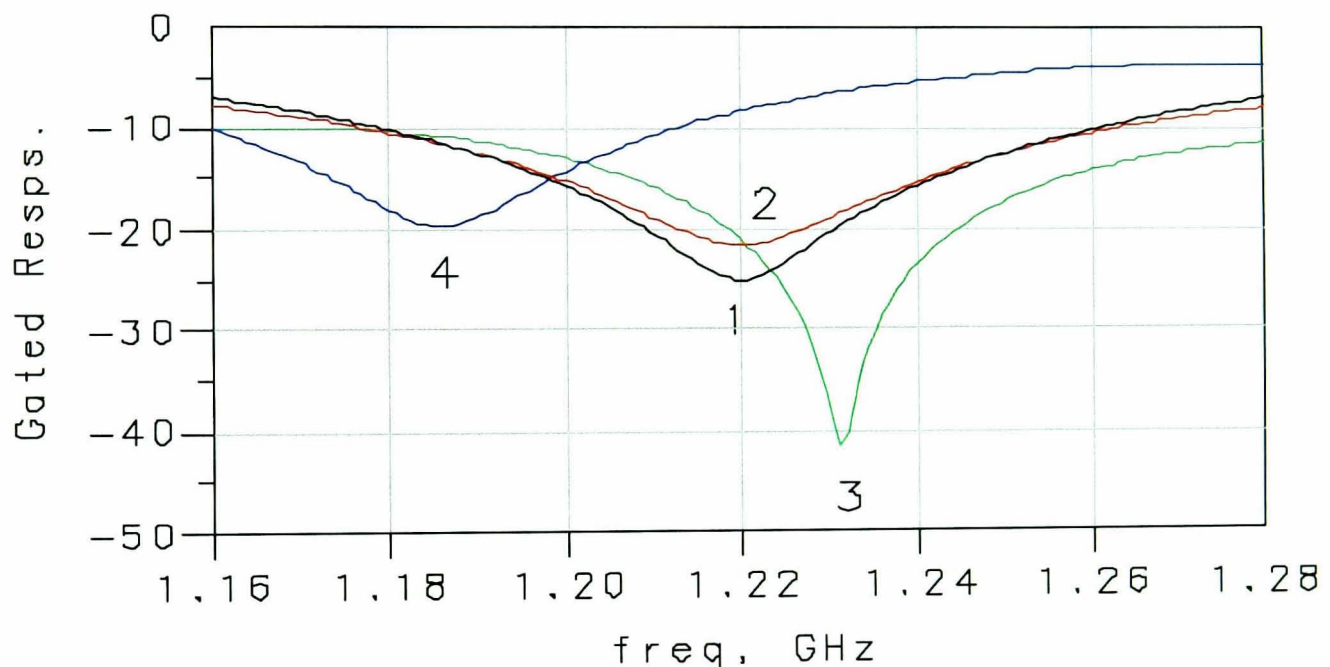


**Figure 6-6 Gated frequency response, after tuning resonator 2**

These interactive effects are observed in resonator 3, and to a lesser extent, resonator 1. Resonator 3 appears to be mistuned high in frequency, even though it is known a priori that only resonators 2 and 4 have been mistuned. These interactive effects caused by the mistuning adjacent sections, are anticipated by the results of section 5.3, and are further examined in the next section.

Finally, resonator 4 is tuned to be centered on the VNA center, figure 6-7, and after this tuning, the apparent frequency of resonator 3 is also on the VNA center frequency. The frequency response of the filter thus tuned is identical to that of figure 6-2, demonstrating that tuning the gated response of individual filter resonators is an effective way to tune filters. This method has not been previously published in any journal, though

patents have been applied for and granted based on this idea of time-domain gating tuning methods [85,86].

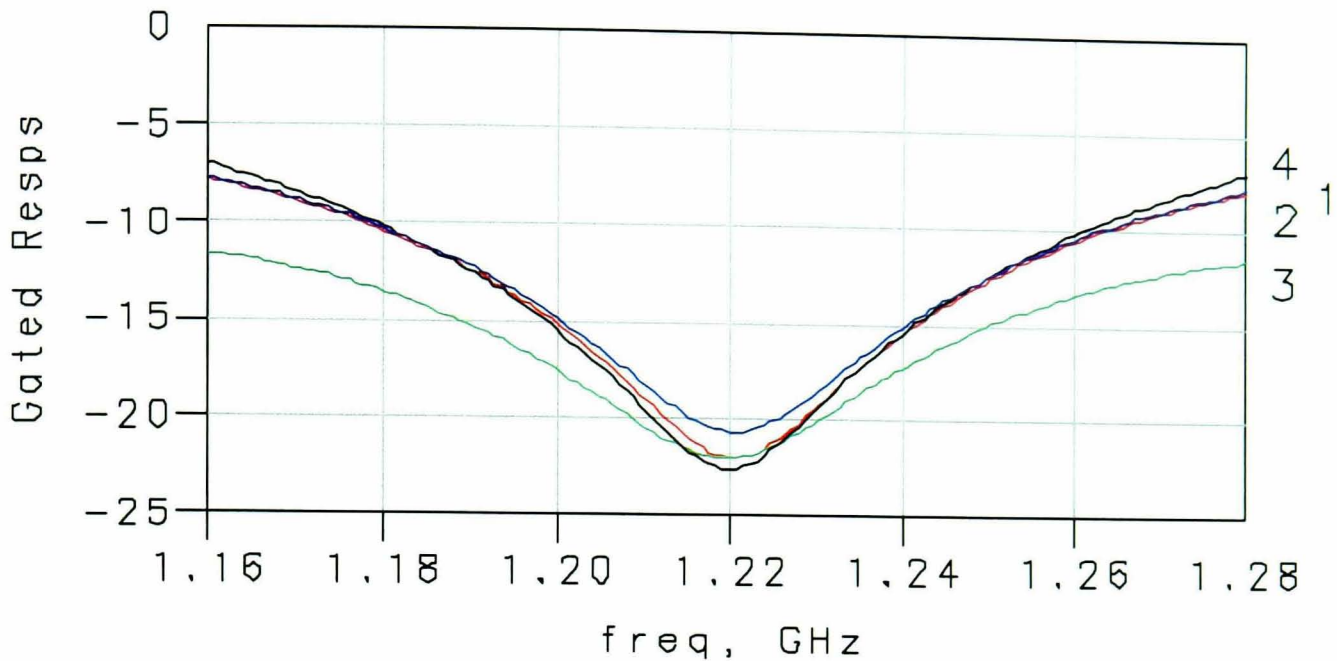


**Figure 6-7 Gated frequency response with all resonators tuned.**

## 6.2 Understanding interactive effects

The development of this time-gated tuning method establishes a very simple way to evaluate the frequency of individual resonators in a coupled resonator filter. This method is found to be quite useful in tuning all-pole filters of high order, but as with the time domain tuning method of chapter 4, the tuning effectiveness suffers by the interactive effects that one resonator's tuning has on other resonators. These interaction effects may be investigated using the techniques of chapter 5.3 combined with the time-gating techniques presented above and the time-domain gate masking effects described in chapter 3, to come to a new explanation of the interactive effects. Reducing the interaction effects promises to reduce the number of tuning passes required to align filters.

### 6.2.1 Using probing and simulation to evaluate interaction compensation

The interactive effects of tuning one resonator on the apparent frequency of an adjacent resonator can be better understood by evaluating the responses seen in figures 5-18, 5-19 and 5-20, and comparing them to the gated responses as described in the section above. Figure 6-8 shows the frequency response of the reflection off the second resonator of the filter from figure 5-14, with the C1 mistuned high, thus mistuning resonator 1. The response of the input reflection to resonator 2 (thick red) is overlaid along with a “normalizing” function (thin blue), and a response where the mistuned re-

response is normalized (thick blue). The normalizing function is created by taking the square of ratio of the transmitted signal incident to resonator 2 (see figure 5-15, thick-red) in the tuned case and the signal incident to resonator 2 in the mistuned case (see figure 5-18, thick red). The ratio must be squared to account for the fact that the response is shifted due to the incident signal changing from the mistuned filter case as it passes through the first resonator, as well as the reflected signal which passes back through the first resonator as it is reflected off resonator two.

This normalizing function is anticipated from the discussion of gating compensation, particularly equation (3.46) and recognizing that  $1 - |\Gamma|^2$  represents the square of the transmitted signal, from equation (2.20). Note that the normalized resonator 2 reflection response in figure 6-8 (thick blue) is a very close fit to the response seen in figure 5-15, indicating that the normalization is almost perfect. Of course, in practice it is not possible to sense the signals used in the probing experiment, but the time-gate masking compensation provides an alternative to probing the transmitted signals.

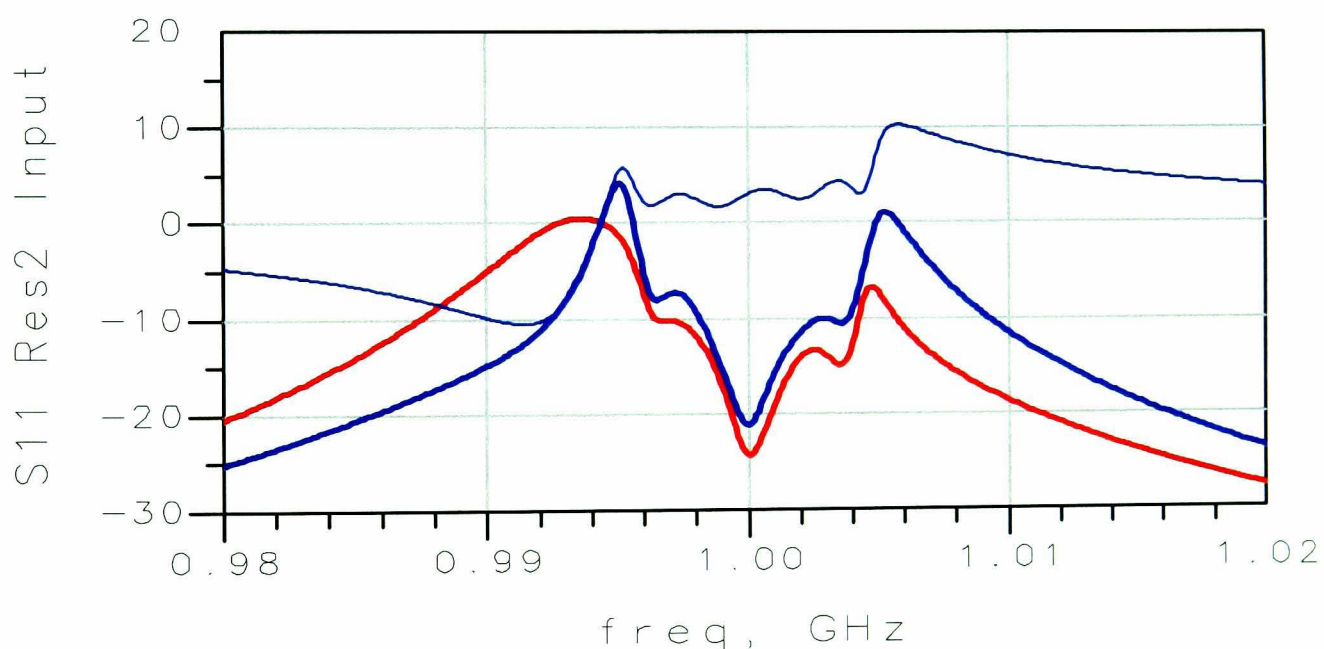


**Figure 6-8:  $S_{11}$  at the input to resonator 2 for the mistuned filter (thick red), and after normalizing the trace (thick blue) The normalizing function (thin blue) is created from the incident signals to resonator 2 for tuned and mistuned cases.**

### 6.2.2 Applying time gating to verify resonator interaction effects

Time gating may be used with the frequency responses of figure 6-8 to show the effects of normalization on the time gated frequency response of resonator 2, as shown in figure 6-9 below. These traces are the reflection response of resonators 2 through 5, obtained by coupling off a portion of the reflection signal at resonator 2. The blue trace on the left of figure 6-9 shows the response as it would appear if gating is applied to the

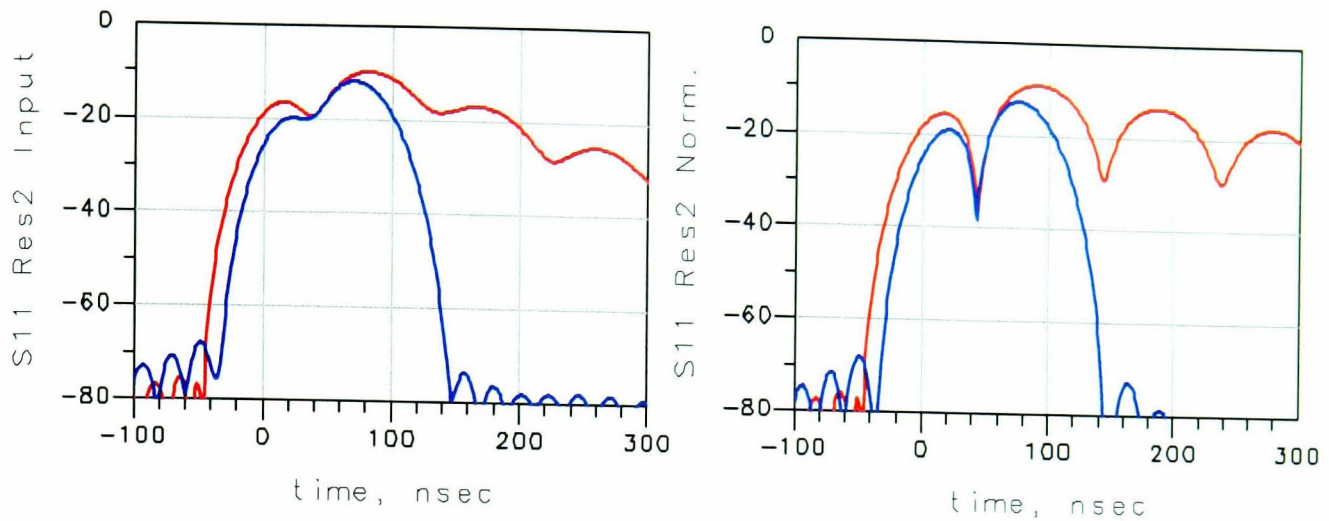


**Figure 6-9: Time-domain response of the mistuned filter resonator 2 reflection (left, red) and normalized reflection (right, red) along with gated response (blue)**

reflection response associated with resonator 2, while the red trace is the un-gated response. The plot on the right shows the response after normalizing to account for the differential signal loss caused by mistuning the first resonator. These plots show a response much more similar to the time-domain response of the tuned filter, with resonator 2 showing a deep null.

Finally, the time-gated frequency response of the two-gated signals is calculated, in figure 6-10, below. In this figure, the gated frequency response of the input reflection of resonator 2 is shown in the red trace, and the gated frequency response of the normalized trace is shown in the blue trace. Clearly, the normalization results in a proper reading of the frequency of resonator 2, when compared to the un-normalized response.

These experiments demonstrate that the apparent frequency of the time-gated resonator response is affected by masking of the signal occurring from previous resonators.

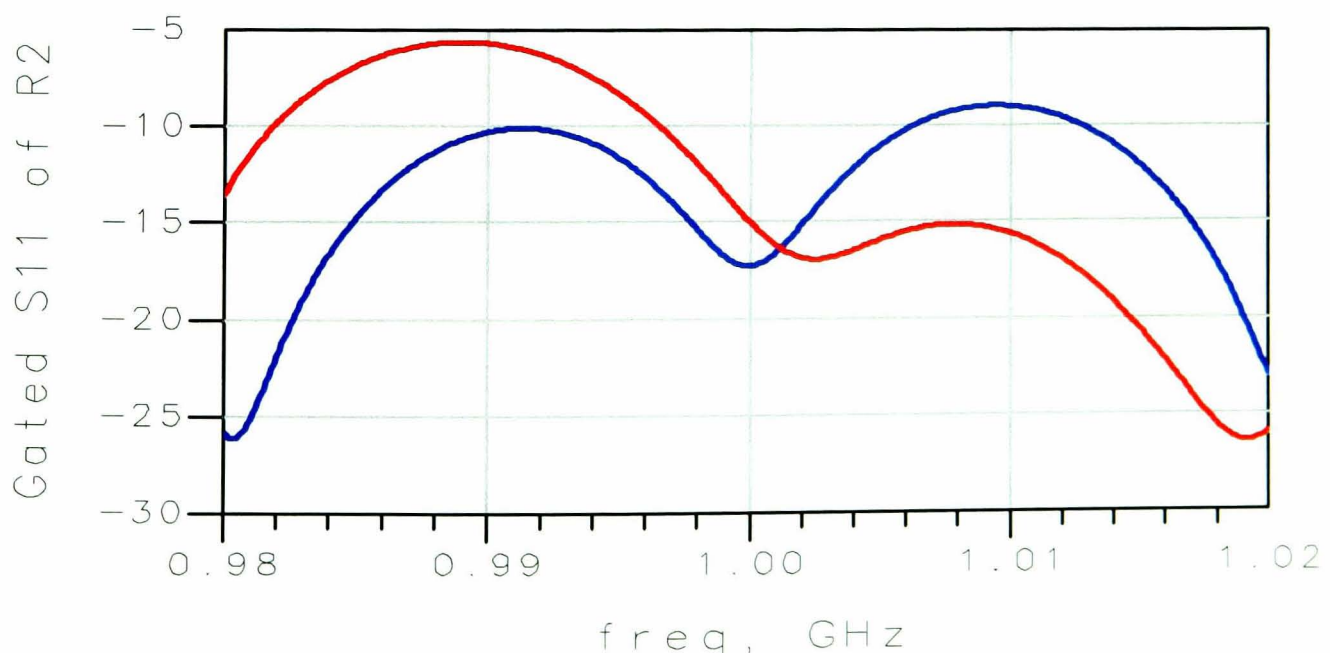


**Figure 6-10: Gated frequency response, for a filter with resonator 1 mistuned, of the input reflection from resonator 2 (red) and the normalized response from resonator 2 (blue).**

An interesting area for future work might be applying more fully the de-masking techniques of chapter 3 to the time-gated tuning method presented in this chapter. An alternative method of accounting for these interactions is described in chapter 7.

### 6.3 Time gated tuning with cross-coupled filters.

This method of inferring the resonator frequency from the time gated frequency response can be combined with the methods of tuning filters with transmission zeros (or other arbitrary frequency responses), as described in section 4.3. As an example, the time gating technique is applied to the filter shown in figure 4- . The individual gated resonator responses are shown in the time-domain in figure 6-11. In this figure, the thin black trace is the normal time-domain response of  $S_{11}$ ;  $S_{22}$  looks similar. Even though the filter is properly tuned, it is clear that the second null, associated with the second resonator, is not deep, indicating that the second resonator is not tuned exactly to the center frequency of the VNA sweep. Gating can be applied to each null to determine the resonator frequency. The thick red and thin blue traces represent the time-

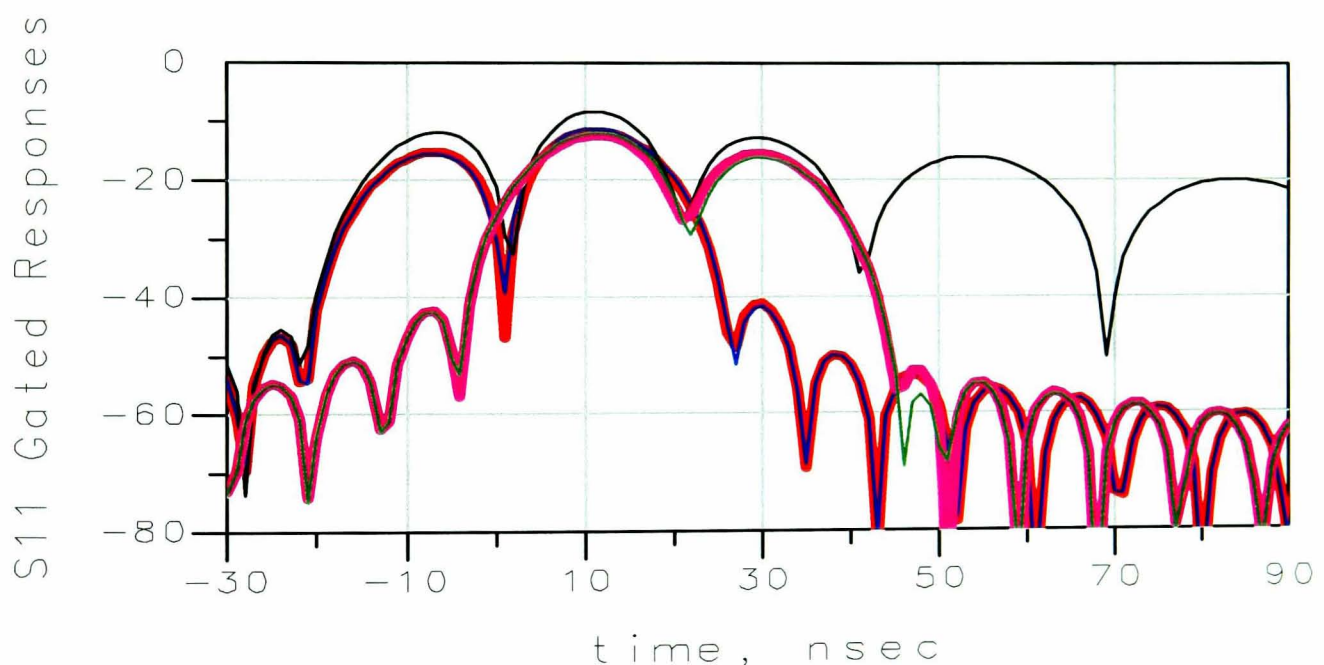


**Figure 6-11: The time-domain response of a cross-coupled filter, with gating applied to individual nulls associated with each resonator**

gated response of  $S_{11}$  for the first resonator, and  $S_{22}$  for the last resonator, respectively. The thick mauve and thin green traces represent the time-gated responses of  $S_{11}$  of the second resonator, and  $S_{22}$  of the third resonator, respectively. This plot shows one un-gated trace, and four gated time-domain responses associated with each resonator.

With time-gating remaining on for each trace, the time-domain transform can be turned off to show the gated frequency response of each of the four resonators, as shown in figure 6-12. Note that the minimums of each trace closely approximate the

resonator values determined in table 4-2. From this time-gated example, it is clear that the need for changing VNA center frequencies for tuning the individual resonators is eliminated. All that is required is to tune the individual resonators to the target values as determined by applying time gating to a properly tuned reference filter.

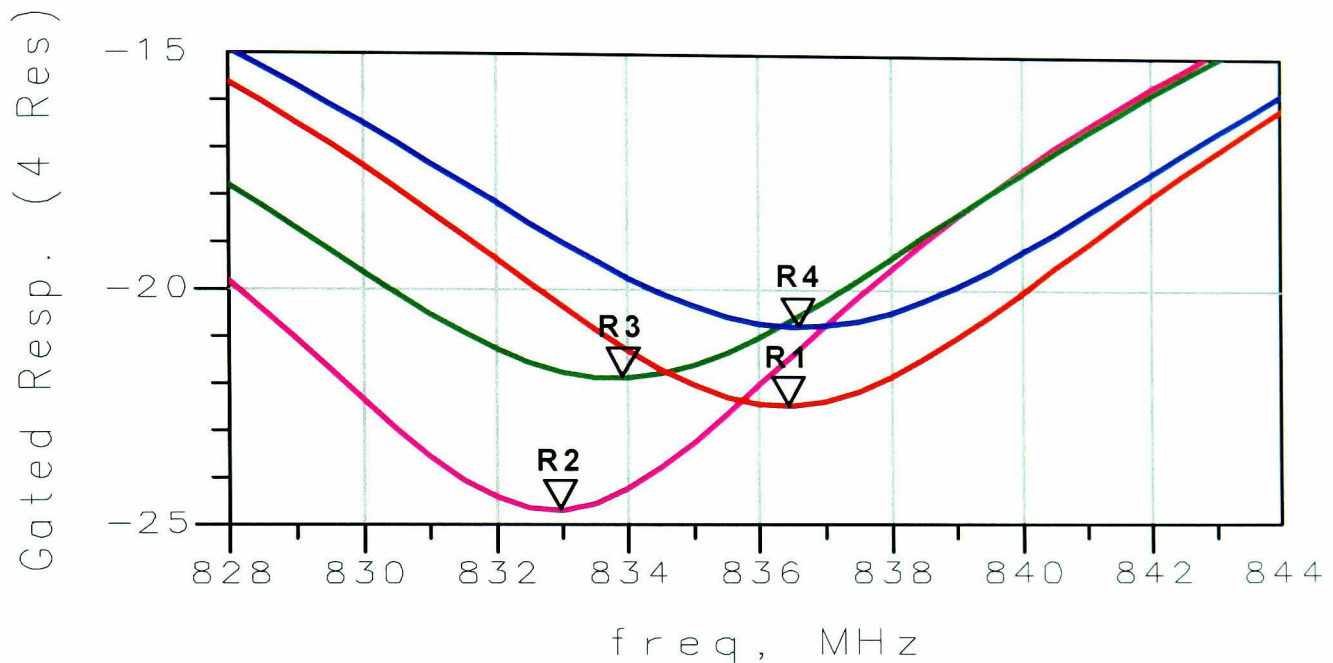


**Figure 6-12: Time-gated frequency response of individual resonators for a four-pole cross-coupled filter. The resonator values match closely to the values determined in table 4-2.**

## 6.4 Conclusions

With the conclusion of this chapter, the theoretical basis of the time-domain tuning of filters has been established. Chapter 5 provided the theoretical basis for the reason nulls are found in the time-domain response when a filter is properly tuned, and why they disappear when it is not properly tuned. This chapter extends that result to establish the cause of interactions between resonators as they are tuned, and introduced a remarkable new technique utilizing the time gating feature of VNAs applied to tuning filters in a novel way. The technique of using the time-gated response as a solution for determining filter characteristics, and thus providing a method for tuning resonators to achieve a desired frequency response, is significant in its simplicity and its feasibility. This provides the technological backbone for developing a software application for semi-automated filter tuning. The details of extending the ideas presented in this chapter into a practical software application are the topic of the next chapter.

## Chapter 7 Filter Tuning Software (FTS)

The ideas of chapters 4 through 6 suggest that filter tuning might be easily and deterministically accomplished using time-domain techniques. The problems of tuning filters in a manufacturing environment include many difficulties not normally considered by a theoretical analysis of the problem of filter tuning, such as filters with interactions between tuning elements, filters for which tuning elements cannot be made to match the desired values, filters with non-ideal filter elements that exhibit loss and dispersion, and finally, filter tuning personnel that lack experience or education to fully understand filter tuning processes. Despite these limitations, thousands of filters are manufactured and tuned everyday, and there has been an ongoing effort to automate the filter tuning process, as indicated by recent workshops on Computer Aided Filter Tuning [87]. This chapter presents the result of an effort to develop a commercial filter tuning software application [88], first introduced in 2001 [89] (included as published paper 5 at the end of this thesis), based substantially on the work of chapters 4, 5 and 6.

Throughout this chapter the tuning display of the filter tuning software application (FTS), is shown as a way to capture the nature and current tuning state of the filter to be tuned, referred to as the device-under-test (DUT). This display consists of a frequency domain portion (typically in the upper third of the display), a time-domain portion (typically in the middle) and a resonator indicator portion (typically in the lower portion of the display). In the frequency and time displays, the target filter responses are shown as dotted lines, and the current DUT responses are shown as solid lines. The time domain displays also show the coupling markers, which are indicative of the time gates for each resonator null, and the peak value used in determining coupling.

### 7.1 Creating the reference filter

The FTS application relies on two key principles from the chapters above: The peaks of the time-domain response can be used to determine the coupling values of the filter, and the time-gated frequency response, found by time-gating around each null, can be used to determine the associated resonator frequency. From these two aspects of the time-domain response of filters, a filter tuning method was developed.

The first step in the filter tuning method is to start with a properly tuned “golden” or “reference” filter, the response of which is the target to which other filters are to be tuned. From this reference filter, key points are taken to ensure proper characterization in the time-domain.

Figure 7-1 shows the set-up screen to start capturing the data for the reference filter. The values in this screen are used to automatically set up the VNA for creating the time-domain transform, and for picking the peak values for characterizing the nulls and the peaks of the reference filter. If adjustable coupling is selected, the values of the peaks are recorded. The center frequency is used to set the center of the VNA frequency sweep, and frequency span is set to 5 times the bandwidth. The number of resonators is used to determine the proper search for peaks, with the  $N/2$  ( $[N+1]/2$  for  $N$  odd) peaks looked for on the  $S_{11}$  side of the filter, and  $N/2-1$  ( $[N-1]/2$  for  $N$  odd) peaks looked for on the  $S_{22}$  side of the filter. The number of points is used to set the VNA to provide a good compromise between measurement speed and frequency resolution. Finally, the electrical delay setting is used to “normalize” the phase response when phase measurements are made, providing a convenient display for characterizing deviation from linear phase.

Once these values are set the software sweeps the VNA over the frequency span and creates two time-domain plots, showing the peaks and nulls, and pre-setting the marker values on the selected peaks, as shown in figure 7-2. Some practical considerations are important to note here. The value of the Kaiser-Bessel  $\beta$  factor, see equation (3.16), controls the height of the side-lobes before the first peak. Marker 1 searches for the

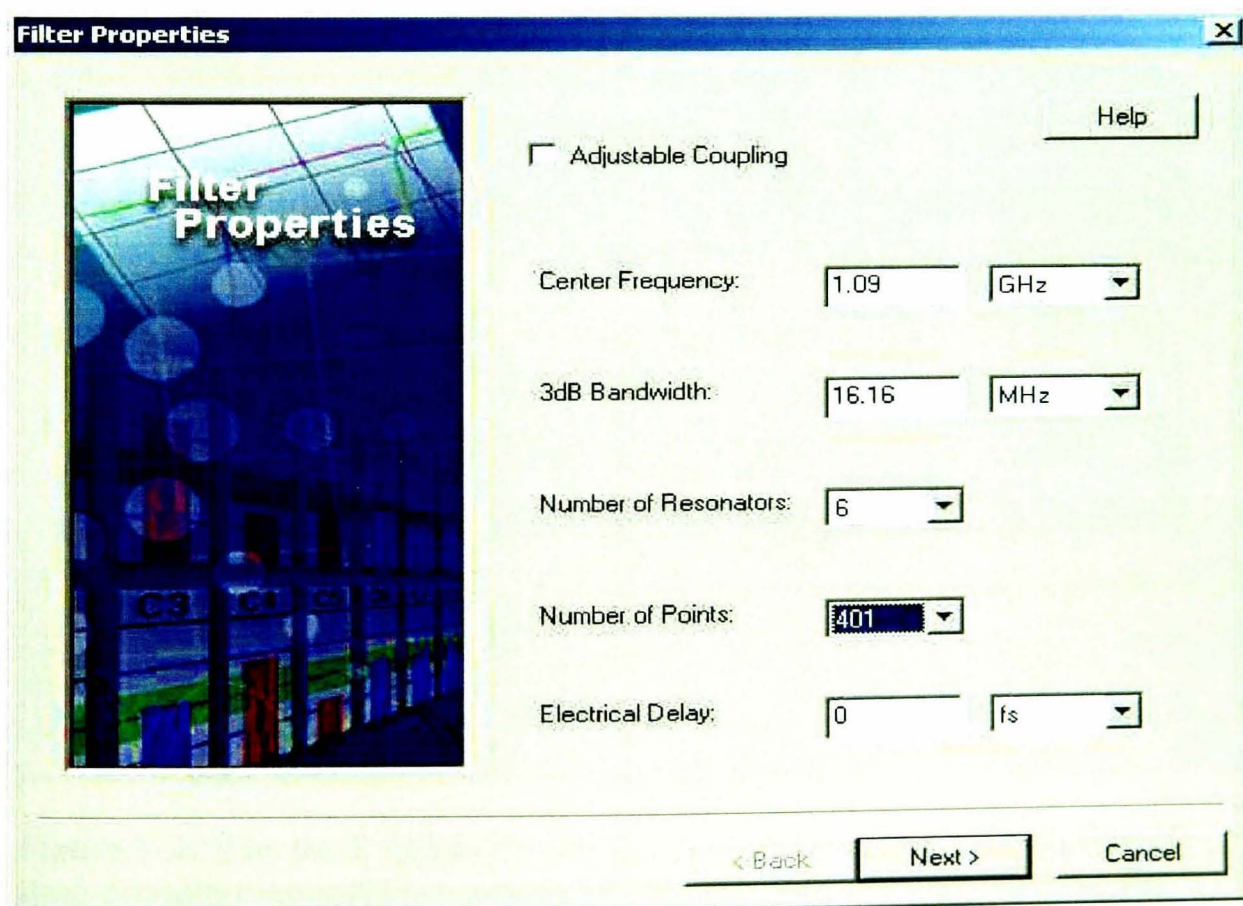


**Figure 7-1: The reference filter setup dialog for the filter tuning software (FTS)**

first -40 dB point in the time-domain trace, then starts the peak searches from there. The peak search algorithms assume some minimum excursion to assign a valid peak, thus reducing the effect of noise on finding false peaks. The dB values of the peaks are recorded, and used as the target values for setting any adjustable couplings in the filter. The time values of the peaks are used to set the time-domain gate start and gate stop for applying the time gate to frequency response at each particular resonator. The gated frequency response is calculated for each of the resonators, and recorded. One issue addressed in the software, for commercial reasons, is concealing the use of time-domain gating to determine the resonator frequencies, thus protecting the key intellectual property described in chapter 6.

While this process is essentially automated, allowances are made for manually setting the coupling peaks for both forward and reverse responses, in case there is some unusual filter response that does not match the expected response of the peak search algorithms.

Next, the values of the resonator frequencies are determined and displayed as shown in figure 7-3, upper, and the coupling peak values are displayed as shown in figure 7-3

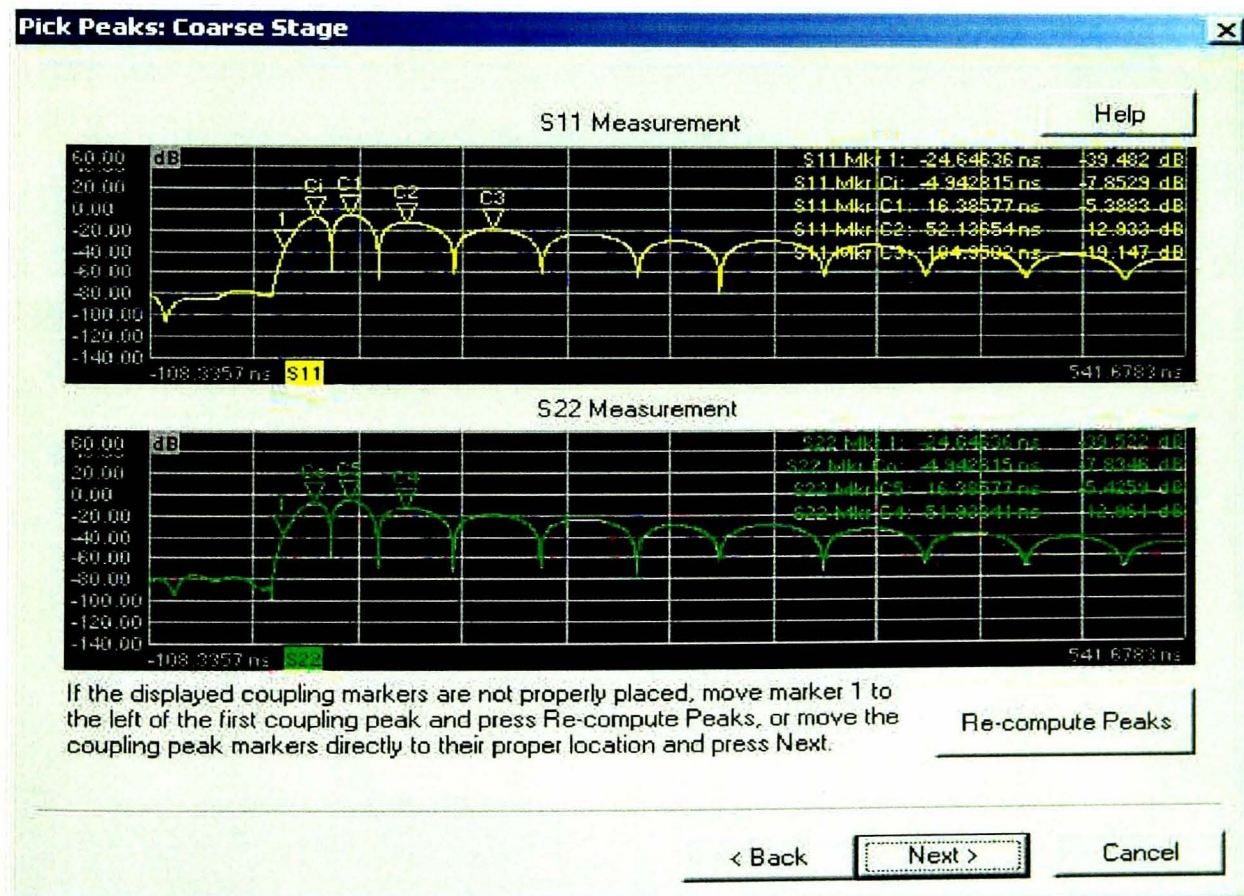


**Figure 7-2:** The peak values for the forward (upper) and reverse (lower) time-domain responses are automatically selected, and recorded for the reference filter.

lower. Here one can see the tuning indicators. After much experimentation, these tuning indicators were developed to have useful human interface attributes [90].

Primarily there is a tuning target represented by the centerline, and a tuning acceptance region, represented by the green zone. The tuning indicator is the blue bar, which moves higher and lower as the resonator frequency is tuned higher and lower. If the bar goes outside the acceptance region, the tuning bar turns red. There are also two blue lines outside the green pass region that represent the linear portion of the tuning indicator. In this region, the tuning indicator moves linearly with the resonator fre-

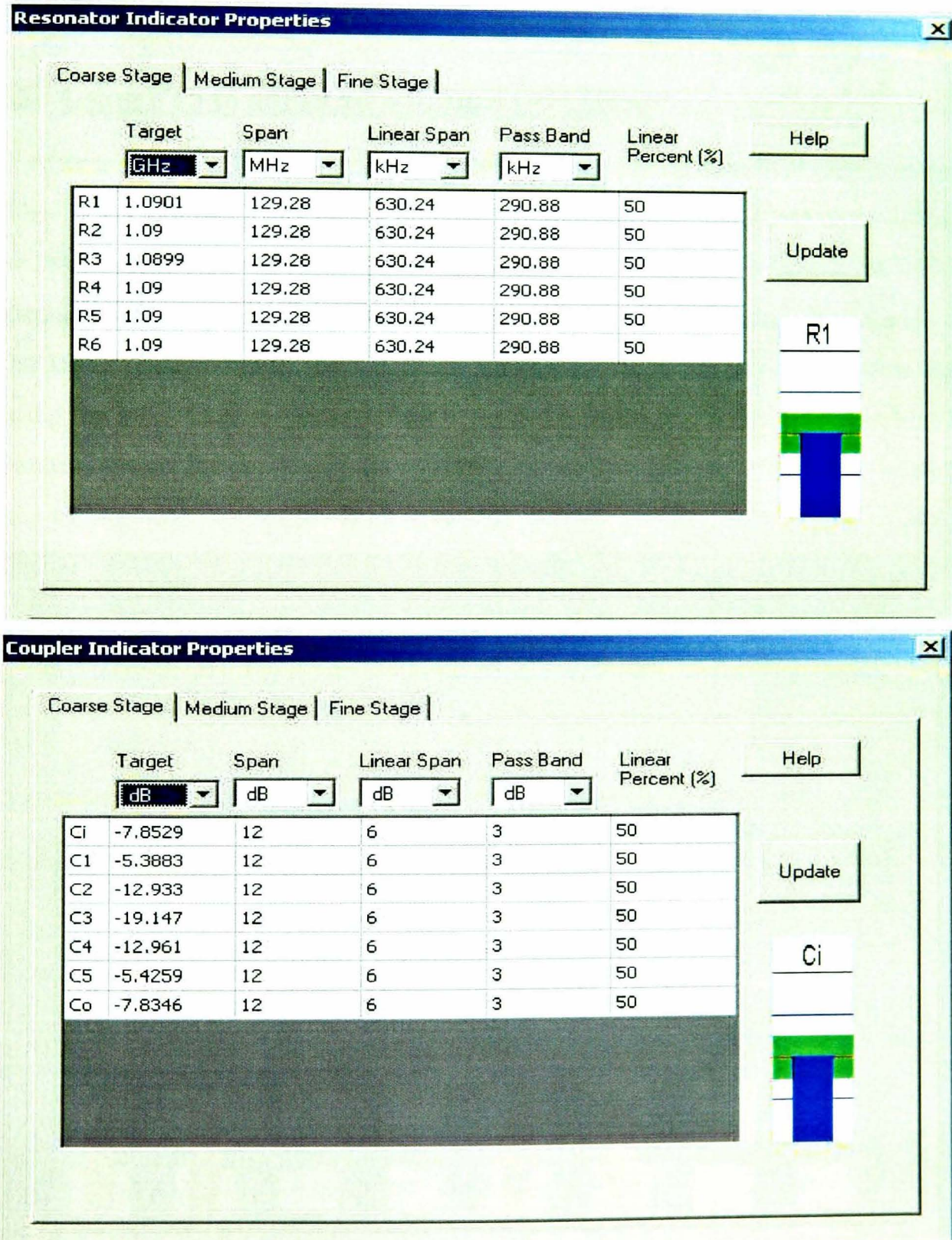


**Figure 7-3: Resonator target values (upper) and coupling peak values (lower) in the dialog boxes used to set the tuning indicator attributes**

quency or coupling peak. Outside this region, the tuning indicator follows a log type movement, where the sensitivity becomes much less at the outside edges. This makes a great deal of sense for a human operator, providing a real-time indication of the current resonator frequency as it is being tuned. Often, the resonators must be tuned within a small percentage of the overall measurement bandwidth. In such a case, it is sufficient to know if the resonator is far above or far below the desired target. However, as the resonator becomes tuned more closely to the target, it is advantages to increase the sensitivity of the indicator. Finally, when the resonator is quite close, it is best to follow a linear tuning function to avoid a hypersensitive region right near the target.

## 7.2 Using FTS to adjust an un-tuned DUT filter

After a reference filter is measured and the values for the resonator targets (and couplings, if adjustable) are captured, an un-tuned DUT filter is connected to the VNA, and the filter tuning process is started with the software. Figure 7-4 shows the frequency response (upper) and time-domain response of  $S_{11}$  and  $S_{22}$  (middle) of an 8 pole DUT. The lower portion shows the values of the resonators as determined by time-domain gating the DUT filter response for each resonator, according to the peaks and nulls determined during the capture of the reference filter. The complete first pass tuning process, tuning one resonator at a time, is shown on the next page, figure 7-5.

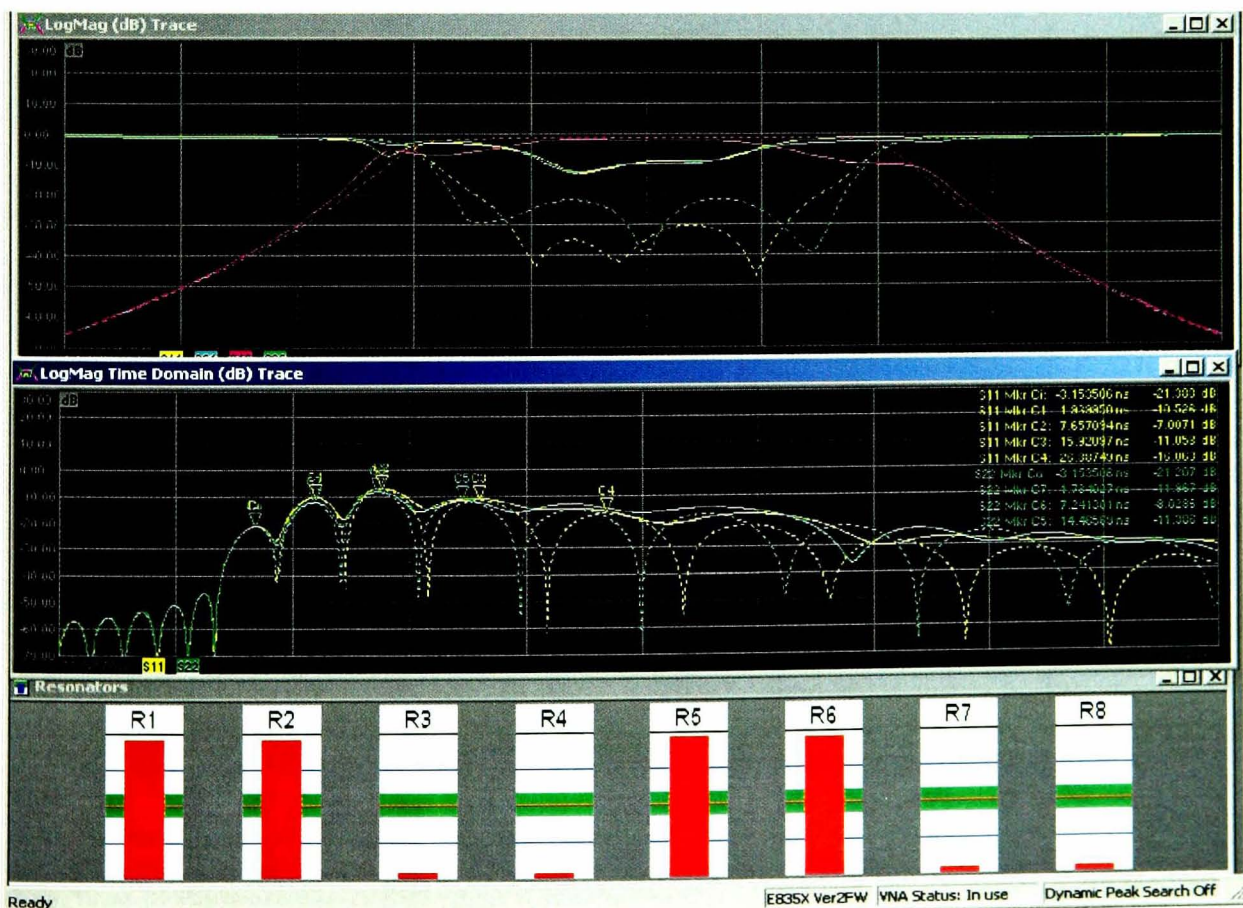


**Figure 7-4: An un-tuned filter, showing the frequency response (upper), and  $S_{11}$  and  $S_{22}$  time-domain response (middle). The lower portion shows the value of the resonators as extracted by the time gating technique.**

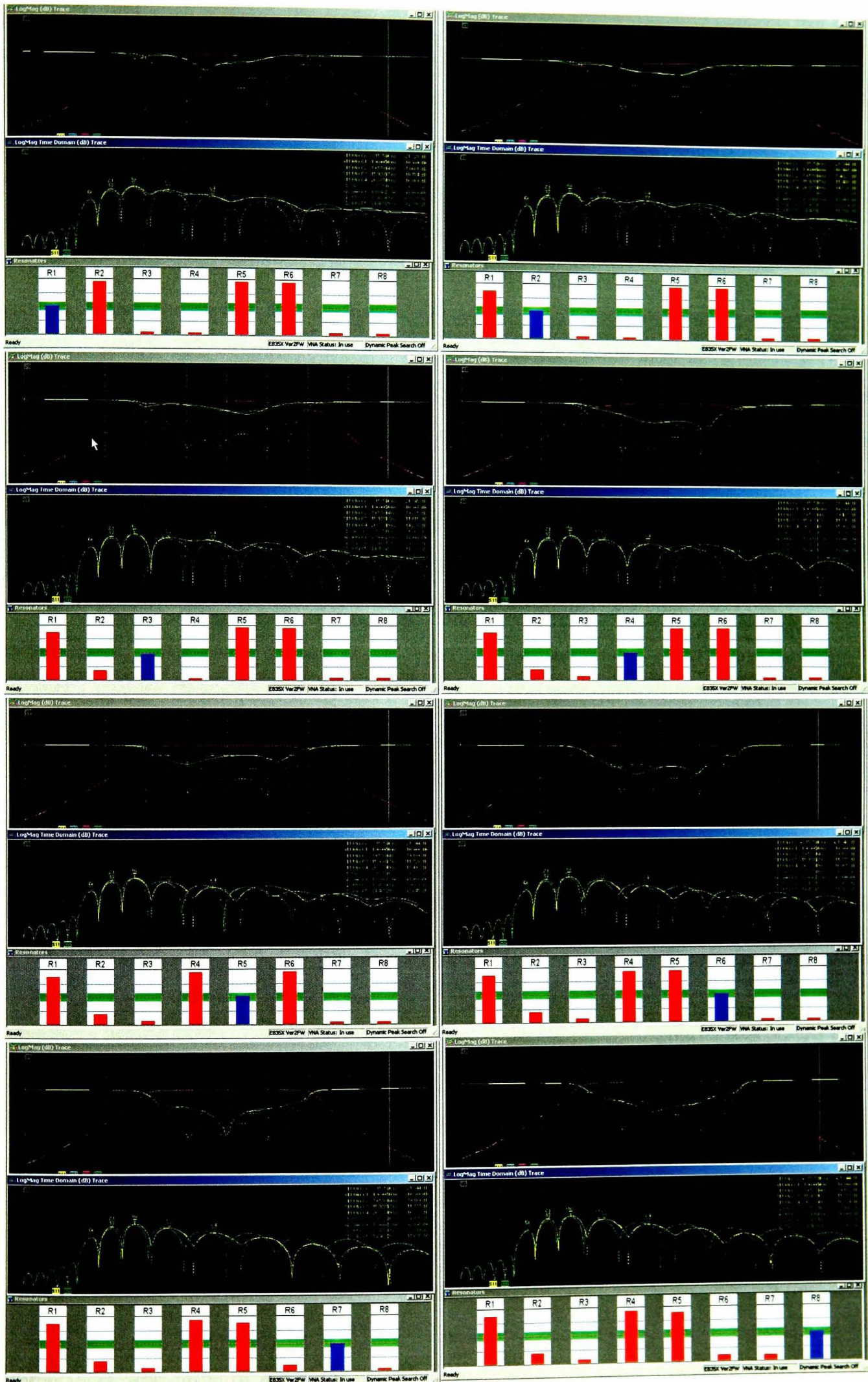


**Figure 7-5: Tuning the filter, one resonator at a time, starting with R1, moving left to right. Note that tuning each resonator changes the apparent tuning of the adjacent resonators**

After the first pass through the filter, the filter shape is approximately correct, but the return loss is not nearly as good as the target filter. From figure 7-5, one can see that during the first pass through tuning the filter, tuning each resonator has a significant effect on the adjacent resonators. Also note the direction of interaction: the adjacent resonator indicators always move in the opposite direction from the resonator being tuned, though it is difficult to see the effect if the adjacent resonator is also tuned far off frequency. For example, when resonator 1 (R1) is tuned (top, left plot), resonator 2 (R2) indicator shows that it is too high in frequency (top, left plot). When R2 is tuned lower (top, right plot), the indicator for R1 goes up, as well as the indicator for resonator 3 (R3). But R3 is so far low in frequency that the indicator barely moves, being in the non-linear region of the tuning indicator. For each plot, the resonator that was tuned is the one that appears as a blue indicator, centered on the target value.

There are some alternative choices in tuning procedures, for example, one might tune R1, then R2, then return to R1 to re-tune it until the tuning indicator shows that it is tuned, then return to R2 to retune it again in turn. Experience has shown that the interactive effects of one resonator on another diminish as the resonators become closer to being tuned. In the next section, the resonator interactions will be discussed extensively. Next R3 might be tuned, and R2 re-tuned until its indicator is centered. But, retuning R2 will cause the indicators for R3 and R1 to show these resonators are not tuned as well. Thus, the method of re-tuning each resonator after the adjacent one is tuned causes many iterations of tuning each resonator. Practically, it takes a great deal more time to change resonator (moving the screwdriver, engaging in the drive in the screw head) than the time it takes to tune resonators. Thus, tuning each resonator in turn, without re-adjusting the preceding resonators has proven to be a good technique to minimize tuning time.

One aspect of the tuning that might be a better choice than that shown in figure 7-5 would be to tune the resonators in a different order, one from outside to inside. Thus, an order that is R1, R8, R2, R7, R3, R6, R4, R5 might be optimum. This is because if resonators 6, 7 and 8 are tuned far off, the tuning of resonator 5 might be more greatly affected than if the resonators 6, 7 and 8 are somewhat tuned first.

A second pass of tuning was performed on the filter, with the results shown in figure 7-6. The tuning proceeded from R1 to R8 in order, with the end result being a nearly tuned filter, and three of the eight resonator indicators showing that the resonators are tuned. It is interesting to note that both R1 and R8 are tuned, as they are least susceptible to interactive effects (they have no masking due to other resonators).

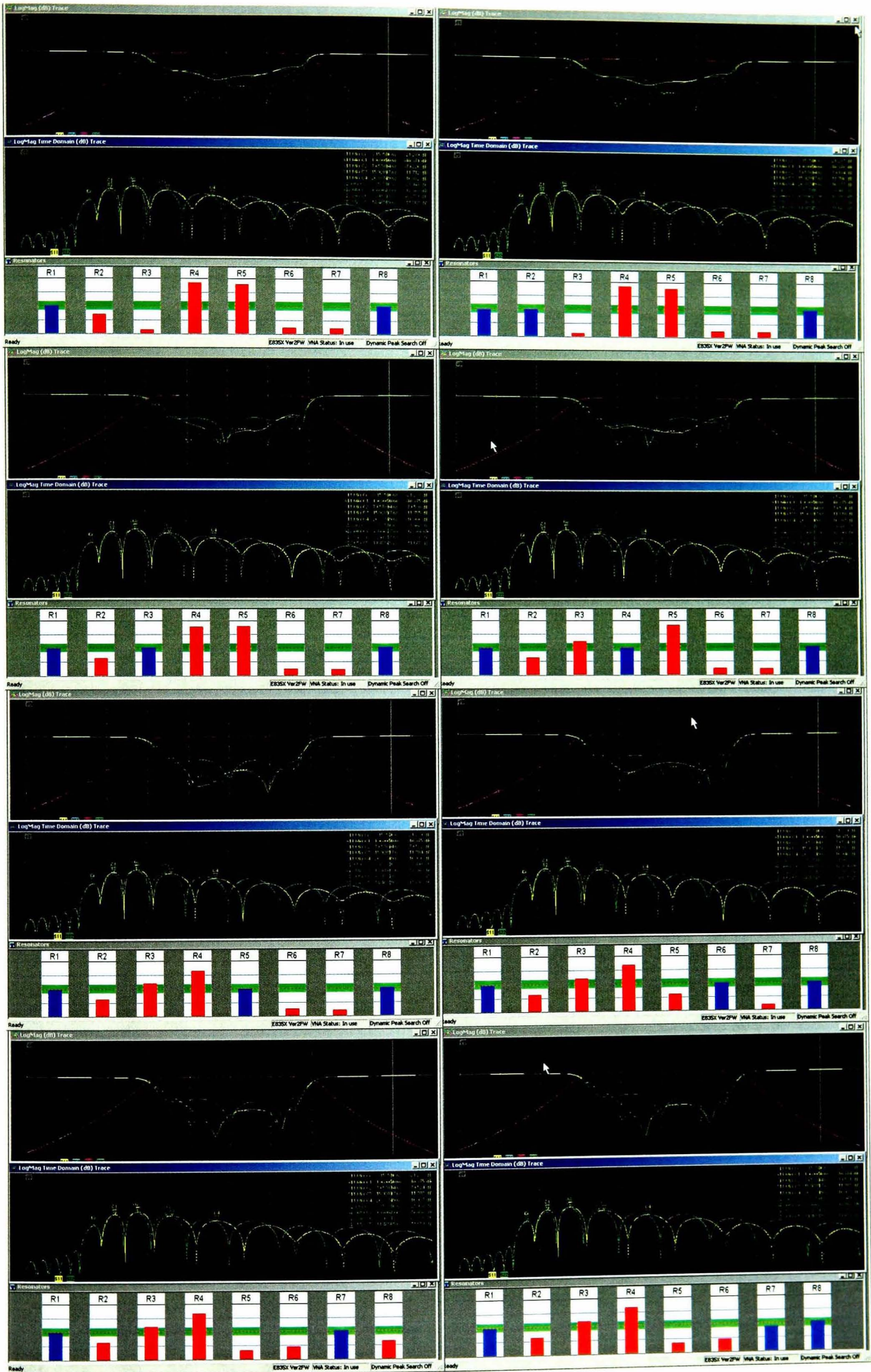


**Figure 7-6: Second pass tuning of 8-pole filter, tuning resonators R1-R8, in order, from left to right, top to bottom. Note that more of the indicators remain acceptably tuned (blue indicators) as the filter resonators are tuned.**

At the end of the second pass of tuning, the pass-band  $S_{21}$  shape is nearly the same as the target filter, but the return loss shape is not quite the same as the target filter. Another pass of tuning is required. In this third round of tuning, figure 7-7, R1 does not need to be tuned (top-left plot, which is the same as bottom-right of figure 7-6), so tuning starts with R2 (figure 7-7, top-right). When R2 is tuned, the indicator for R3 also moves, and shows that it is tuned, so no tuning is done on R3 for this pass. However, when R4 is tuned down, R3 indicator moves back up, showing that R3 is not quite tuned. This continues for R5, and R6. R7 shows indicator shows that it is tuned until R6 is tuned. After R6 is tuned, the indicator for R7 shows red, so R7 is also tuned, and

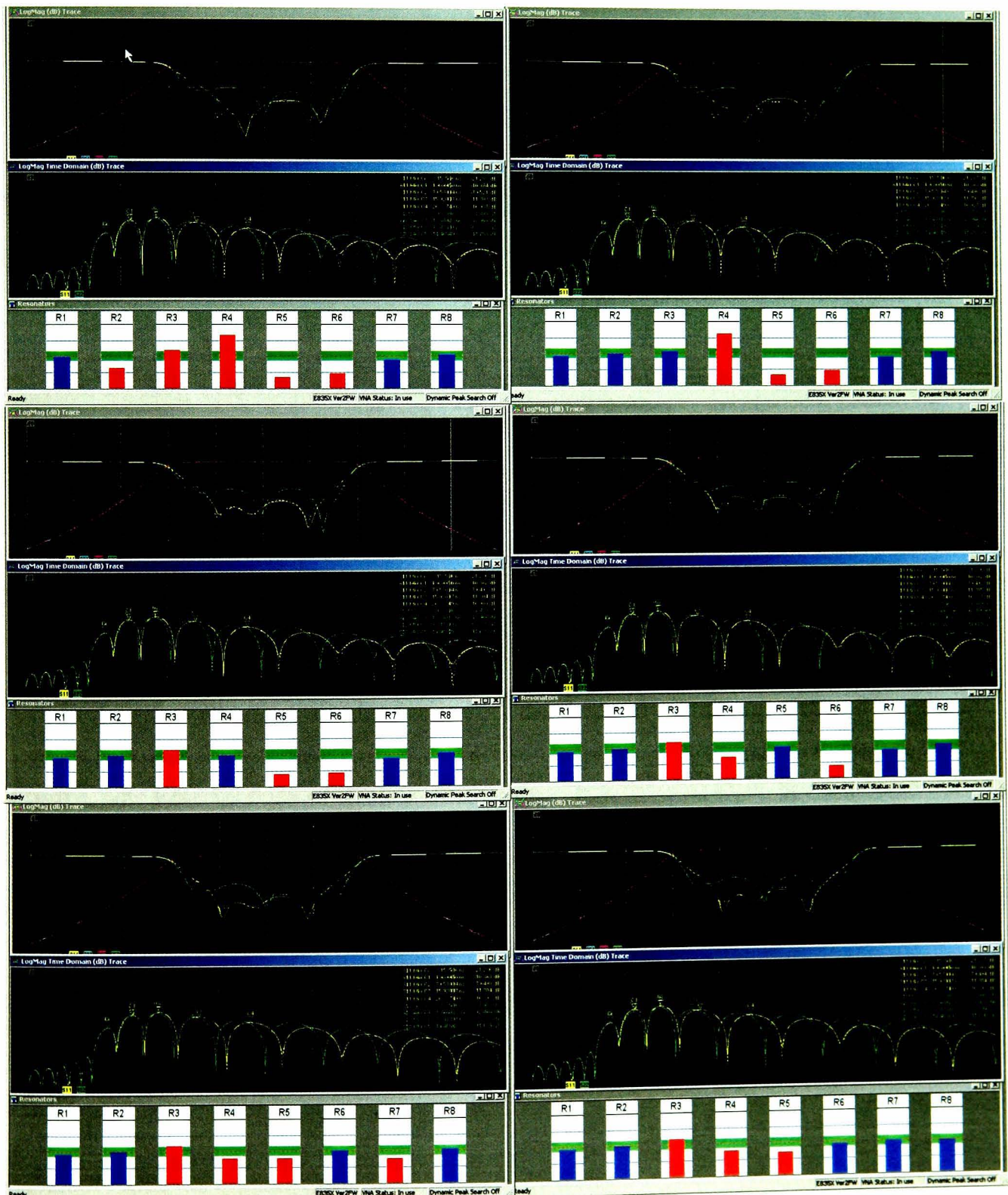


**Figure 7-7: Third pass tuning, only R2 (top right), R4, R5, R6 and R7 are adjusted this time. Top left plot is the same as the bottom right of figure 7-6.**

since R8 indicator shows that it is tuned, the third pass of tuning the filter is completed. At the end of this pass, five of the eight resonators show tuned. The filter return loss is very nearly the same as the target filter, with only a slight discrepancy on the slope of the return loss trace. In a production setting, this tuning would probably be adequate. For this example, a fourth and final tuning pass was performed, as shown in figure 7-8. The upper-left plot is the starting point, and R3 was tuned, which also brought R4 into tune (upper-right). When R5 is tuned up, the R4 indicator shows R4 apparently moving down, out-of-tune (lower-left). A final tuning of R4 brings all resonators into tune.

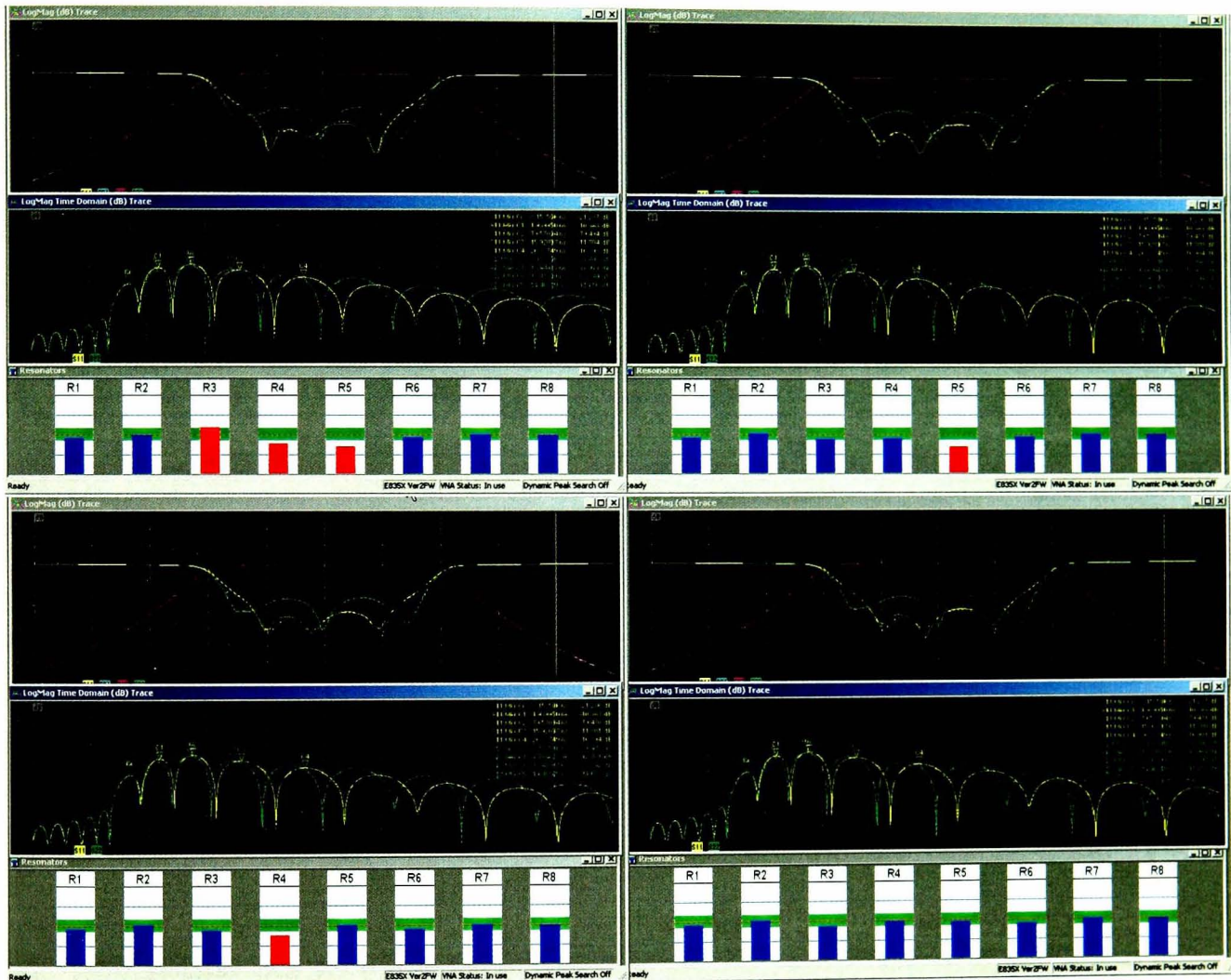


**Figure 7-8: Fourth pass of tuning. Resonators R3, R5 and then R4 are final tuned.**

The preceding tuning process indicates that the tuning of all-poles filters can be deterministically accomplished using the time-gated frequency response as displayed by the tuning indicators. It is also clear that there are substantial interactive effects between resonators, and it would be desirable to account for those effects to reduce the number of iterations when tuning filters. These interactive effects are found to be much more substantial when tuning filters with cross-coupled resonators, to the point of having an adjustment of one resonator affect another resonator more than the one being adjusted. Note that this filter is not quite perfectly tuned, as the final DUT response is not identical to the target response, and some of the resonators are slightly off target.

### 7.3 Compensation for resonator interactions

The interactive effects that adjusting one resonator has on adjacent resonators in a filter have been demonstrated in many of the examples presented thus far. The causes of these interactions have been described, with theoretical explanations for two cases. In the first case, the cause may be due to physical interaction, such as a tuning screw of one resonator interacting with the fields of an adjacent resonator. In another case it may be due to masking or reflection effects, where tuning one resonator up in frequency causes the apparent signal applied to, or reflected from, another resonator to appear to shift in frequency, as demonstrated in section 6.2. A practical method has been developed as described below, which allows compensation of one resonator for the effects of the other resonators, and is effective for whatever mechanism causes the apparent interaction.

#### 7.3.1 The compensation wizard

The first step in compensating for the interactions between resonator tuning elements is to characterize the interactions that occur. The FTS program version 1.3 and greater has a “compensation wizard” which guides a user through a series of measurements that are used to capture these interactive effects. The compensation wizard assumes that one has access to a properly tuned filter, for which each of the resonators can be adjusted. Figure 7-9 shows the dialog box that guides the user.

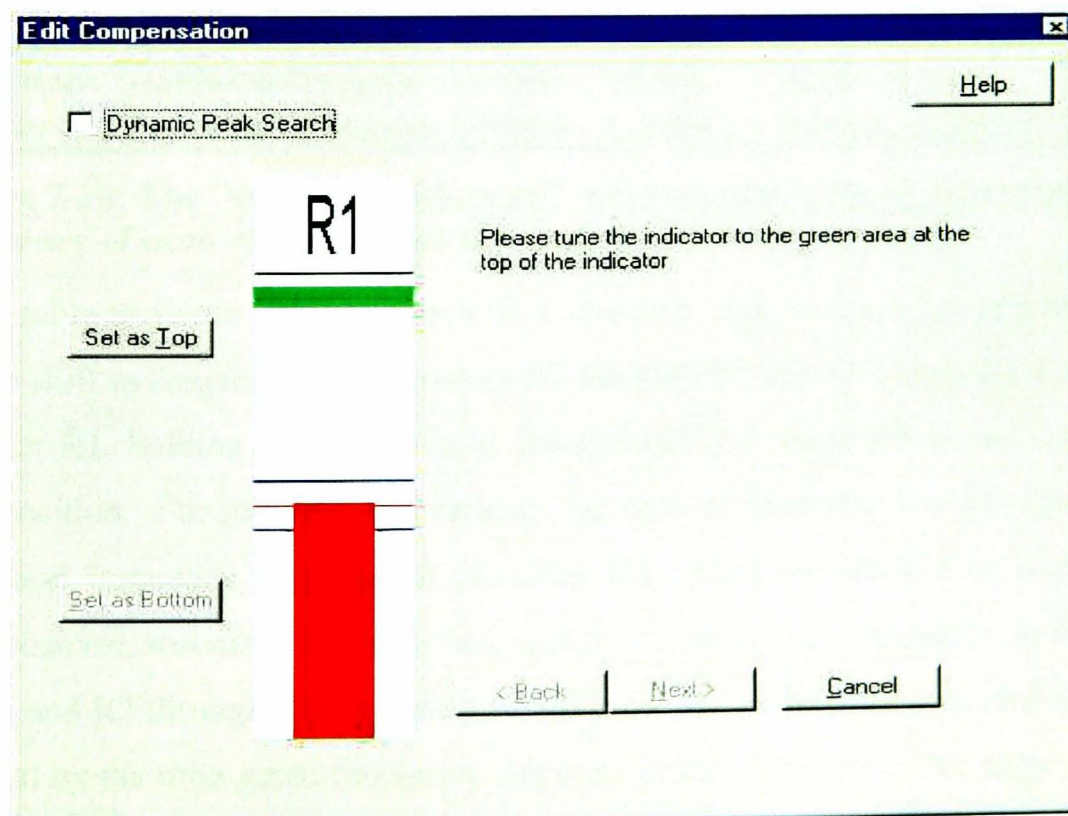


**Figure 7-9: The compensation wizard directs users to tune each resonator up and down in frequency.**

The wizard is used on a reference filter, after the resonator target values have been captured. This wizard guides the user to tune each resonator up and down in frequency, by using one of the tuning indicators with an upper and lower target value. After the user tunes the resonator up in frequency (by approximately half the bandwidth of the filter), the wizard moves the tuning target down in frequency automatically, and indicates to the user to tune the resonator down in frequency. After the resonator reaches the lower target zone, the original target is restored and the user is prompted to return the resonator to the original target value. During the tuning process, the apparent values of all the other resonators are recorded at several frequency intervals, from which the change of the apparent frequency of each other resonator as a function of the apparent frequency of the resonator being tuned is established.

The interactions between resonators are not exactly linear; they diminish as the resonator being tuned varies widely from its target frequency. A linear region of the function is chosen, and the slope of the apparent frequency of each of the resonators to the apparent frequency of the resonator being tuned is determined. This is formed into a resonator interaction matrix, or "compensation table" as shown in figure 7-10.

	R1	R2	R3	R4	R5	R6	R7	R8
R1	1	-0.30703	-0.020558	0.079687	0.0012641	3.0715e-005	-4.5722e-005	0.00018174
R2	-0.15052	1	-0.35957	-0.3786	-0.0096956	0.00013343	1.8933e-005	-0.00032128
R3	0.0035935	-0.12827	1	-0.26045	0.067606	-0.0010192	8.2076e-005	0.00013265
R4	0.0002975	0.0048249	-0.13698	1	-0.29583	0.01345	-0.00018292	0.00037397
R5	0.00014889	-0.00010857	0.013434	-0.36354	1	-0.16161	0.006082	-0.00014759
R6	-4.1827e-005	9.4929e-006	-0.0013698	0.1163	-0.24705	1	-0.1524	0.0066443
R7	-0.00013294	-4.5645e-005	0.00012208	-0.018991	-0.3042	-0.29917	1	-0.19294
R8	-4.757e-005	6.5772e-006	-1.8138e-005	0.0033006	0.046695	-0.020961	-0.36239	1

**Figure 7-10: The "compensation table" which captures the apparent shift in frequency of each resonator due to a shift in any other resonator**

The table in figure 7-10 can be read as follows: the first row records the apparent relative shift in frequency of resonators R2 through R8 which occurs for a unit shift in resonator R1, holding all of the actual resonators R2 through R8 at their tuned (reference) position. For this row, the value of the shift of resonator 1 is determined by the time-gated frequency response of resonator R1. After resonator 1 is returned to its tuned position, resonator 2 is adjusted, and row 2 records the apparent shift of resonators R1 and R3 through R8 for a shift of resonator R2. The frequency shift of R2 is determined by the time-gated frequency response of R2. The rest of the table is filled out in similar manner for all the other resonators. One key aspect of determining the values in this table is to note that since none of the other resonators are mistuned when each

row is created, the apparent shift in the resonator being adjusted is not obscured by offset values in any other resonator.

It is also interesting to note that the off-diagonal elements are not symmetric, but rather the upper diagonal elements are larger for the first half of the filter (resonators R1 through R4) and the lower half of the diagonal is larger for the second half of the filter (R5 through R8). This can be understood by realizing that since the time-gated evaluation of resonators R1 through R4 are evaluated from the  $S_{11}$  response, masking of R2 through R4 will cause their apparent shift to be greater. That is, tuning R1 up in frequency causes a greater apparent shift in R2 when compared to tuning R2 up in frequency, and looking at the effect on R1. Thus, the interaction matrix includes both real interaction effects, such as from interactions of tuning screws, and apparent interaction effects due to masking as described in chapter 3. A similar argument holds for resonators R5 through R8.

The values of this matrix can be utilized to compensate for apparent shifts in frequency of one resonator due to actual frequency shifts in other resonators. Consider the system of linear equations:

$$\begin{aligned}\Delta f_1^* &= 1 \cdot \Delta f_1 + C_{12} \Delta f_2 + C_{13} \Delta f_3 + \cdots C_{1N} \Delta f_N \\ \Delta f_2^* &= C_{21} \Delta f_1 + 1 \cdot \Delta f_2 + C_{23} \Delta f_3 + \cdots C_{2N} \Delta f_N \\ &\vdots \\ \Delta f_N^* &= C_{N1} \Delta f_1 + C_{N2} \Delta f_2 + C_{N3} \Delta f_3 + \cdots 1 \cdot \Delta f_N\end{aligned}\tag{7.1}$$

where  $\Delta f_1, \Delta f_2, \dots, \Delta f_N$  are the difference between the actual frequency of the resonators and their respective target frequencies, and  $\Delta f_1^*, \Delta f_2^*, \dots, \Delta f_N^*$  are the difference between the apparent frequency of the resonators as determined by the time-gated frequency response method and their respective target frequency. This can be written in matrix form as

$$\begin{pmatrix} \Delta f_1^* \\ \Delta f_2^* \\ \vdots \\ \Delta f_N^* \end{pmatrix} = \begin{pmatrix} 1 & C_{12} & \cdots & C_{1N} \\ C_{21} & 1 & \cdots & C_{2N} \\ \vdots & \vdots & \ddots & \vdots \\ C_{N1} & C_{N2} & \cdots & 1 \end{pmatrix} \cdot \begin{pmatrix} \Delta f_1 \\ \Delta f_2 \\ \vdots \\ \Delta f_N \end{pmatrix}\tag{7.2}$$

where the matrix with the  $C_{mn}$  coefficients is called the compensation matrix. One can see that for the case of a properly tuned filter, all the values  $\Delta f_1, \Delta f_2, \dots, \Delta f_N$  are zero, as are all the values of  $\Delta f_1^*, \Delta f_2^*, \dots, \Delta f_N^*$ . When the compensation wizard directs the op-

erator to adjust one of the resonators in frequency, then only the column associated with that resonator is not zero, as in the case of resonator  $R_n$ :

$$\begin{aligned}
 \Delta f_1^* &= 1 \cdot 0 + C_{13} \cdot 0 \cdots + C_{1n} \Delta f_n + \cdots C_{1N} \cdot 0 \\
 &\vdots \\
 \Delta f_n^* &= C_{n1} \cdot 0 + C_{n2} \cdot 0 \cdots + 1 \cdot \Delta f_n + \cdots C_{nN} \cdot 0 \\
 &\vdots \\
 \Delta f_N^* &= C_{N1} \cdot 0 + C_{N2} \cdot 0 \cdots + C_N \Delta f_n + \cdots 1 \cdot 0
 \end{aligned} \tag{7.3}$$

resulting in the simple column matrix

$$\begin{pmatrix} \Delta f_1^* \\ \vdots \\ \Delta f_n^* \\ \vdots \\ \Delta f_N^* \end{pmatrix} = \begin{pmatrix} 1 & \cdots & C_{1n} & \cdots & C_{1N} \\ \vdots & \ddots & \vdots & \ddots & \vdots \\ C_n & \cdots & 1 & \cdots & C_{nN} \\ \vdots & \ddots & \vdots & \ddots & \vdots \\ C_{1N} & \cdots & C_{Nn} & \cdots & 1 \end{pmatrix} \cdot \begin{pmatrix} 0 \\ \vdots \\ \Delta f_n \\ \vdots \\ 0 \end{pmatrix} \tag{7.4}$$

or

$$\begin{pmatrix} \Delta f_1^* \\ \vdots \\ \Delta f_n^* \\ \vdots \\ \Delta f_N^* \end{pmatrix} = \begin{pmatrix} C_{1n} \cdot \Delta f_n \\ \vdots \\ 1 \cdot \Delta f_n \\ \vdots \\ C_{Nn} \cdot \Delta f_n \end{pmatrix} \tag{7.5}$$

Thus,  $C_{mn} = \Delta f_m^* / \Delta f_n$ , for any resonator  $R_m$ , whose apparent frequency shift from the target frequency is  $\Delta f_m^*$ , given a change in resonator  $R_n$  of frequency  $\Delta f_n$ , with all other resonators at their respective target frequency. From this it is easy to see that the compensation matrix coefficients can be determined by taking each row of the compensation table of figure 7-10 and transposing it to become the respective column of the compensation matrix in equation (7.2).

Once the compensation matrix is determined, the actual values of the shift from target frequency of any resonator may be determined, given the inverse of the compensation matrix and the apparent frequencies of all the other resonators,  $\Delta f_m^*$  as

$$\begin{pmatrix} \Delta f_1 \\ \Delta f_2 \\ \vdots \\ \Delta f_N \end{pmatrix} = \begin{pmatrix} 1 & C_{12} & \cdots & C_{1N} \\ C_{21} & 1 & \cdots & C_{2N} \\ \vdots & \vdots & \ddots & \vdots \\ C_{N1} & C_{N2} & \cdots & 1 \end{pmatrix}^{-1} \cdot \begin{pmatrix} \Delta f_1^* \\ \Delta f_2^* \\ \vdots \\ \Delta f_N^* \end{pmatrix} \tag{7.6}$$

The compensation matrix can be inverted one time, as part of the compensation wizard, and values  $\Delta f_1, \Delta f_2, \dots, \Delta f_N$  can be determined during the real-time measurements of the filter through a simple matrix multiplication. This compensation method was added to the FTS application after revision 1.3, and provides a remarkable improvement in usability, as is demonstrated on the 8-pole filter used in the tuning example above [91].

One can see the effect of using the compensation matrix on an actual filter, by studying the effect of mistuning only one resonator. Figure 7-11 shows the filter from figure 7-9, with only resonator R2 mistuned (left). Here it is clear that the apparent frequencies of R1, R3 and R4 are affected. Also shown in figure 7-9 (right) are the tuning indicators with the compensation matrix applied. Here, the compensation is applied to the target for resonators R1, R3 and R4, adjusting the target lower to show that the respective resonators are still properly tuned.

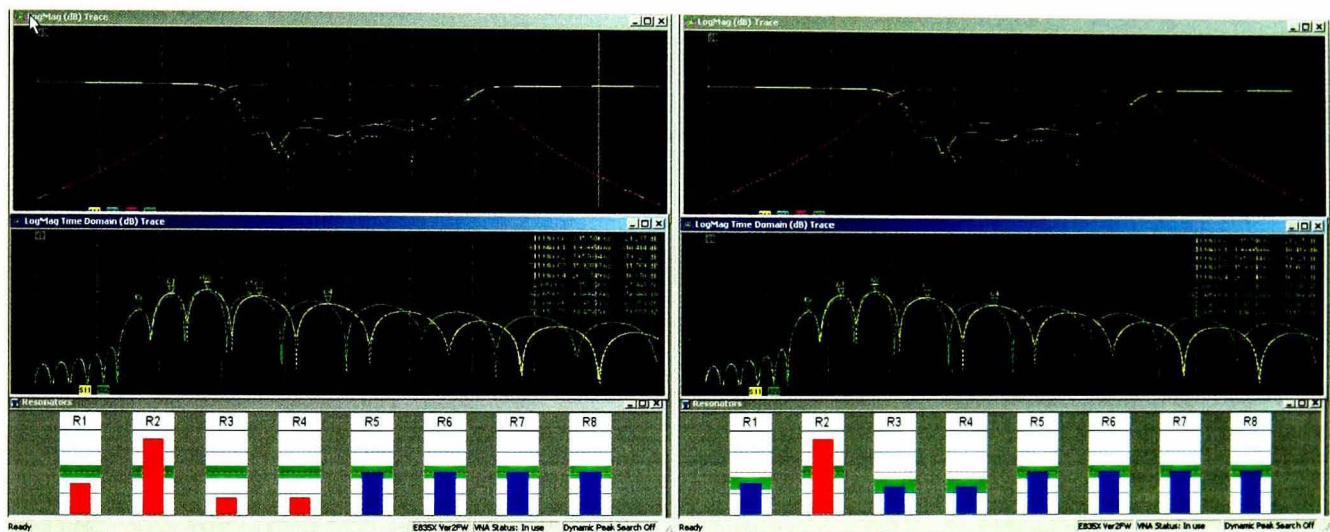


**Figure 7-11: FTS display with only resonator R2 mistuned (left), and same condition but with the compensation matrix applied to the tuning indicators (right)**

There are several formats that might be used to account for the compensation in the apparent frequency. One choice is to display the calculated actual frequency, thus leaving the targets in the center. The choice above is to shift the target by the amount of change between the actual resonator frequency and the apparent resonator frequency. Some people find this display pleasing as it gives a visual indication of when compensation is affecting the target frequency, particularly since the compensation curves are not completely linear, and the compensation may not be correct in instances where the a resonator is very far from its target frequency.

Figure 7-12 shows the FTS dialog box that allows the user to choose the option for displaying the compensation effects. Other choices include setting the target value always in the center, or moving the target value, but limiting the region over which it can move. Keeping the target always in the center is perhaps a good choice for an unskilled

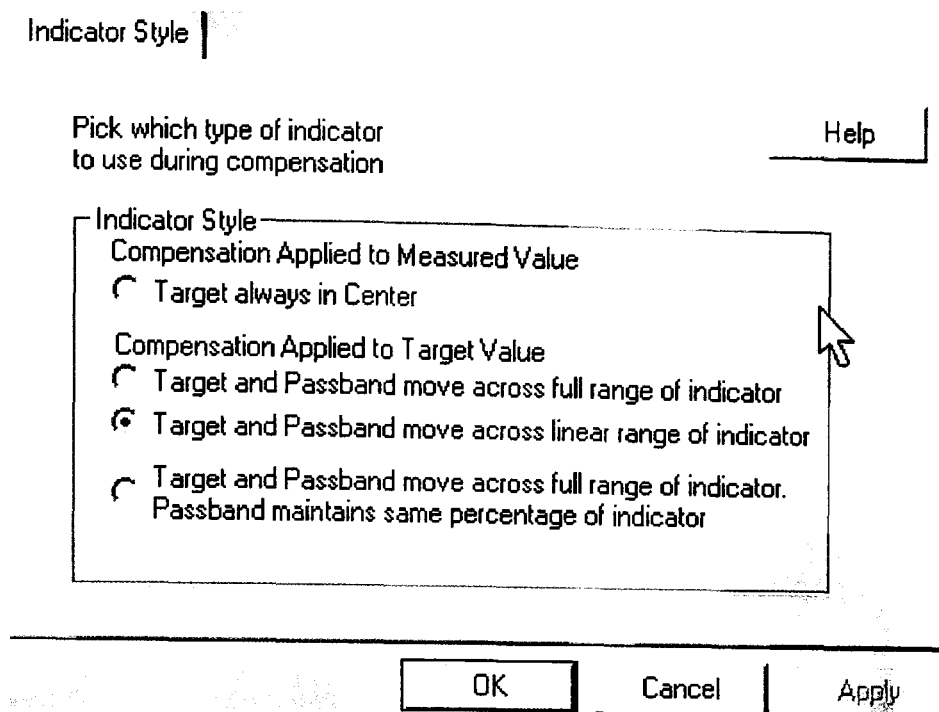


**Figure 7-12: Dialog box for setting the appearance of the compensation effect on the resonator indicators**

operator, but it can sometimes be confusing if the filter is tuned far off. In such a case, the target values may be over compensated, and the tuning indicators will not operate correctly. However, if the target value is moved off the center, then it is clear that substantial compensation is being applied, giving a clue to the operator that the filter may be tuned far enough away from the target to make the tuning method less effective.

The options for moving the target value include moving it over the entire range, in which case the apparent acceptance region shrinks as it moves out of the linear portion of the indicator display. The second, preset option moves the target value in the linear region, but maintains the target always in the linear region, and if the compensation is greater than that, the target is held at the edge of the linear region, and the tuning bar value is compensated. Finally, the target value may move over the entire range of the indicator, with the acceptance band maintaining a constant visual size, so that the acceptance region becomes larger as the target moves farther from the center region.

A second example of the compensation effect is shown in figure 7-13. Here, only resonator 4 is mistuned. In this case, only the two adjacent resonators are affected. Again, the plot on the left is without compensation, and the plot on the right is with compensation. This is a particularly interesting case, as the interactive effect of resonator R4 on R5 cannot be from masking, as the apparent value for frequency of R5 is taken from an  $S_{22}$  measurement, while the R1 through R4 frequencies are taken from an  $S_{11}$  measurement. Clearly, compensation works very well in maintaining the proper targets for other resonators when only one resonator is tuned off frequency, but a real-

world tuning application would see all the resonators off frequency at the start of the tuning process. In the next section, the 8-pole filter used throughout this chapter is completely tuned using the compensation matrix.

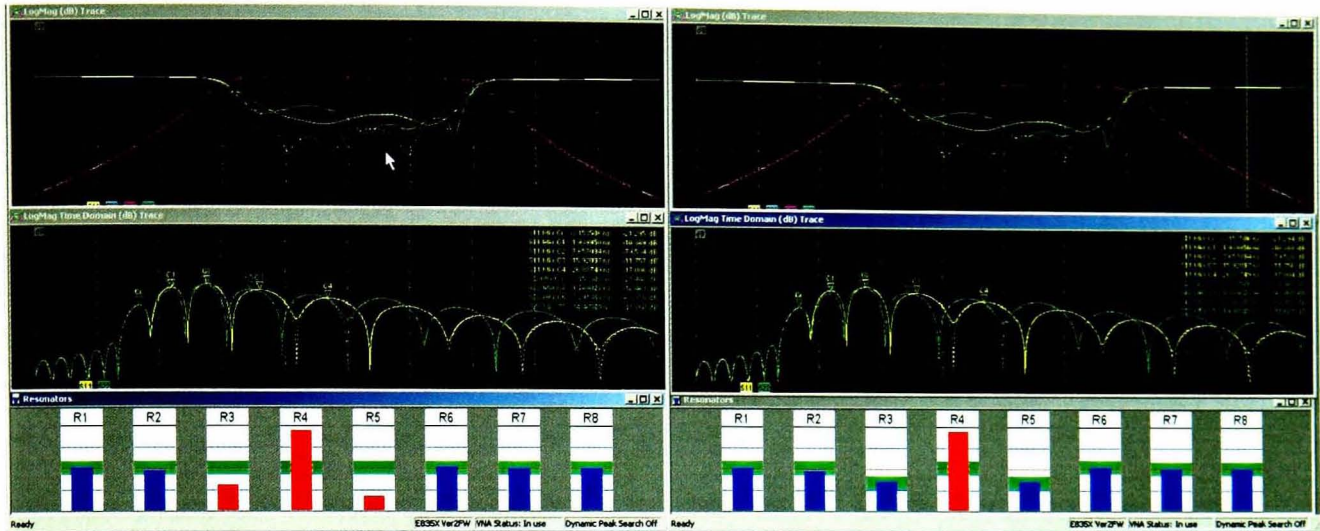


**Figure 7-13: FTS display with only resonator R4 mis-tuned (left), and same condition but with the compensation matrix applied to the tuning indicators (right)**

### 7.3.2 Tuning a filter using compensation

The compensation wizard in FTS was used to characterize the filter from the previous section. Each resonator was adjusted up and down in frequency while monitoring the other resonators' apparent frequencies, resulting in the compensation table of figure 7-10. After the compensation wizard completed, the resonators for the filter were mis-tuned in a manner similar to the filter as found in figure 7-4. Figure 7-14 shows the results of tuning the filter, one resonator at a time, with compensation on. The top-left plot shows the result after R1 tuning, with the target clearly compensated lower, presumably due to the apparent frequency of R2 being too high. The top-right plot shows the result after tuning R2, with its target compensated high, presumably due to R3 resonator being too low in frequency. The other plots proceed through the respective resonators, and one sees that until resonator R6 is reached, the compensation is nearly perfect. When R6 is tuned, R5 comes slightly out of tune, presumably due to incorrect compensation, perhaps due to non-linear effects that are not taken into account. However, when R7 is tuned, R5 returns to being close to its target, though R6's indicator shows it to be slightly out of tune. Finally, when R8 is tuned, the filter is very close to the ideal target value, with only R6 slightly out of tune.

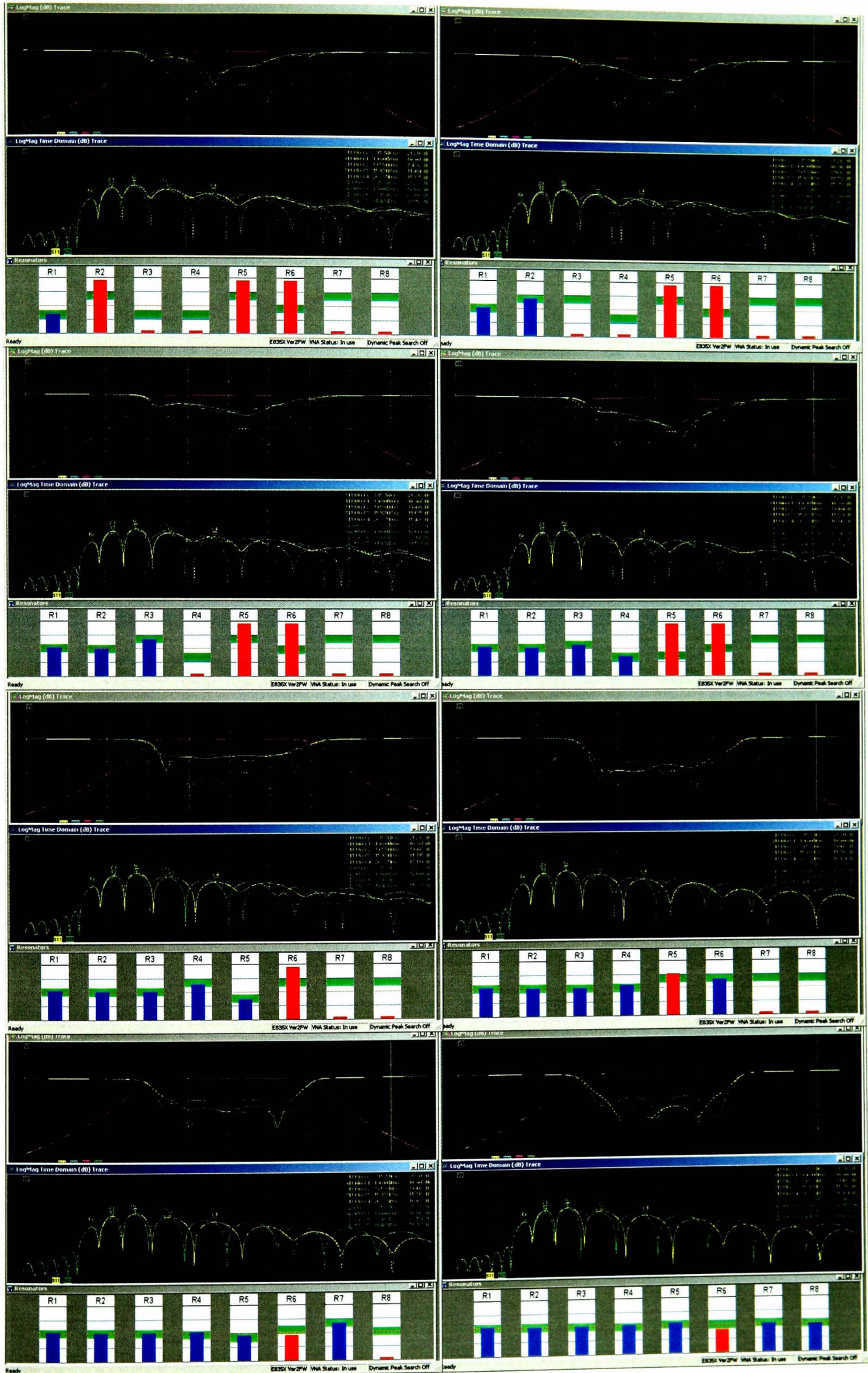


**Figure 7-14: First pass tuning of an 8-pole filter, using FTS with compensation for resonator interactions. Note that the filter is nearly perfectly tuned after 1 pass**

From this example, we see that compensation provides a remarkable improvement in the tuning process, with each resonator tuned only one time for a nearly perfect tuning. Also, the tuning might be better still if the tuning order were changed to tune from the outside resonators first. For this filter, less than 3 minutes was required for the full tuning. Previous experiments with skilled tuners required about 15 minutes for tuning, and un-skilled tuners could take more than 1 hour.

### 7.3.3 Applying compensation to filters with cross coupling

As noted earlier, when filters with cross coupling are tuned using the time-gated frequency response, it is not unusual to have substantially more interaction between resonators, and for substantial interactions to occur between non-adjacent resonators. The compensation methods described above apply equally well to these cases, provided that the value of the cross-coupling element does not appreciably change as part of the tuning process. Many filters have nearly fixed cross-couplings, for which this assumption is true. However, some filter designs employ adjustable cross coupling, where the value of the cross coupling can change dramatically. Such filters do not have a constant compensation matrix, and thus compensation techniques do not work well. Figure 7-15 shows a filter with cross coupling (as evidenced by the transmission zero in the upper part of the pass band), which has been characterized, and for which the third resonator has been mistuned.

In this filter, it is clear that mistuning resonator R3 has a very strong affect on both resonators R4 and R5, with a slightly stronger effect on R5, even though it is not an adjacent resonator. In the right of figure 7-15, the compensation matrix is applied, and resonators R4 and R5 remain near the center of their compensated target values. With-

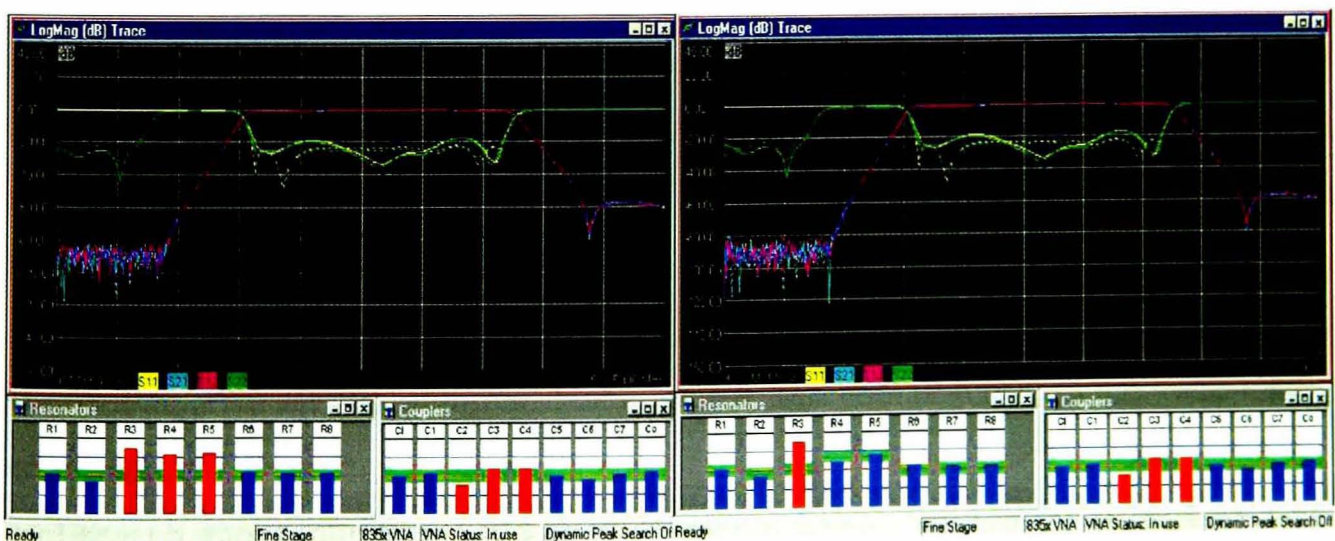


**Figure 7-15: A filter with cross-coupling, with only resonator 3 mistuned (right), and the same case, while applying the compensation matrix (left). This filter also has adjustable coupling elements.**

out compensation, filters such as these have substantial interactions between resonator elements, requiring many iterations to achieve proper tuning.

#### **7.4 Pre-tuning methods in FTS**

The time-gated tuning method described in chapter 6 has many advantages in providing deterministic tuning of filters. Unfortunately, the method works best when all the resonators of a filter are already approximately tuned. For filters where the resonators are not tuned at all, it can be difficult getting the first resonator tuned, as the time-gated tuning response cannot determine even an approximate frequency (too high or too low) if the resonator is so far away in frequency that the time-gated response has no discernable dip from which to determine the resonator frequency.

In many manufacturing environments, the filter production process includes a pre-tuning or pre-setting stage that allows an approximate alignment of the resonators and coupling screws. Often this is done using a mechanical alignment tool, also known as a pre-setting plate, which consists of a metal template to preset the height of the tuning screws. For this type of production process, the filters are already approximately aligned, and the time-gated tuning method used by the FTS works very well. Note that tuning methods based on the short circuit response [6, 7] cannot be used with filters that are pre-tuned.

In other production environments, the filter tuning screws may be constructed in such a way that they cannot be preset, or the tuning screws may not be assembled into the filter until the final tuning process. In these cases, the filters are completely untuned, and the time-gated responses can be difficult to use. At the least, the tuning screws must be applied in order from outside-in, and the response carefully monitored to ensure that the tuning indicator does not swing completely through its range while the tuning screw is assembled. Also, one sometimes finds that the time-gated response indicators show the filter tuned too low (fixed hard against the lower limit) when in fact the tuning screw is too high. This is due to not having a definitive dip in the frequency response. As the tuning screw is adjusted, the response will “flip-over” and start to show the proper indication, but this can be confusing to unskilled operators. For filters of this type, a robust pre-tuning method is desired that will allow an approximate tuning of a filter.

The FTS application uses a modified version of Chen’s method [6] to pre-tune a filter so that the time-gated tuning method can be used for final tuning of the filter. The pre-tuning method makes use of the phase response of the filter, and tracks the absolute

phase as each element of the filter is tuned. However, rather than using the short circuit tuning method, the phase of a reference filter is captured as each resonator is “un-tuned” from a fully tuned filter. For example, the phase at the center frequency of the 8-pole filter is captured as each resonator’s tuning screw, starting with R8, is removed. This is found to be a preferred method as it does not require that the filter elements be fully short circuited, and can be applied to filters for which the tuning elements may not be fully removed. The measurement of the phase of the filter as the elements are fully de-tuned is captured using a “phase-tuning wizard”. Figure 7-16 shows the first dialog box of the phase tuning wizard.

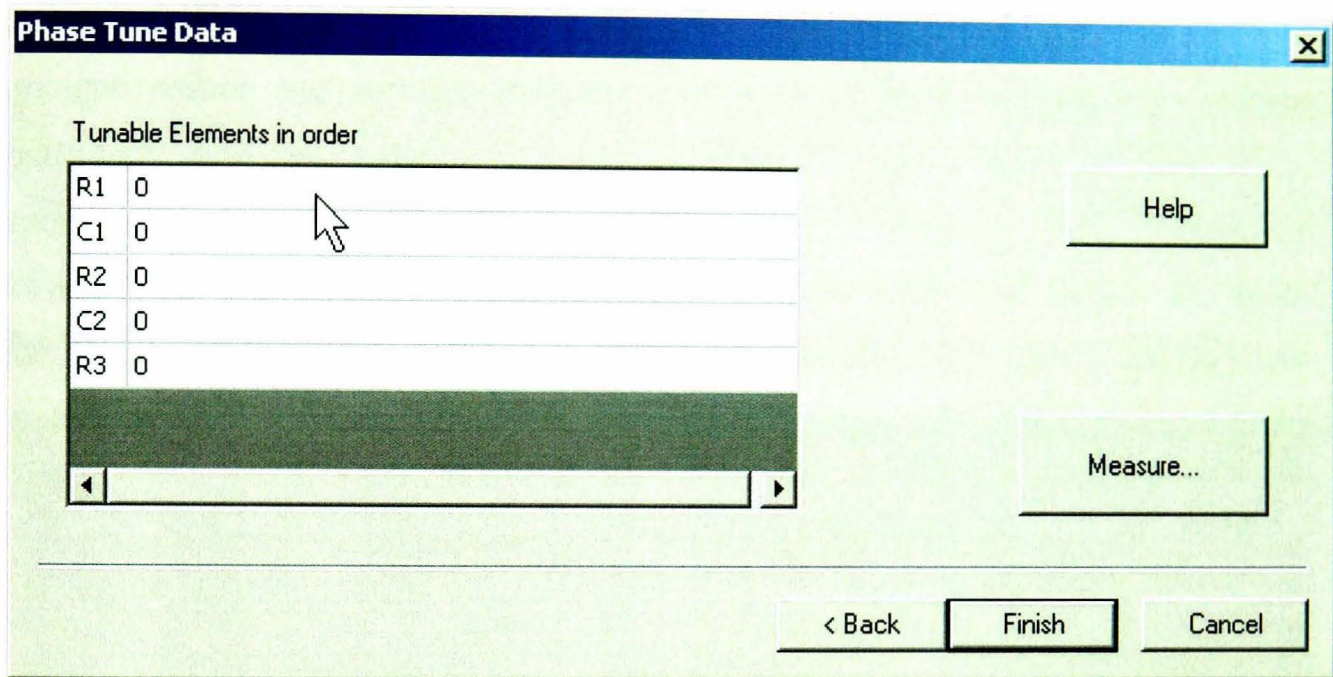


**Figure 7-16: Pre-tuning setup dialog, which captures the phase as individual elements are de-tuned**

During the setup procedure, the operator is prompted to detune each element in its respective order. The phase at the center frequency is recorded for each element. Coupling and even cross-coupling elements can be included as well. However, if coupling elements do not substantially change the phase of the response while being captured, they should not be included as part of pre-tuning. This depends greatly on the design of the filter to be tuned. Some filters have couplings that have a strong effect on resonator tuning, thus have a strong effect on the  $S_{11}$  phase, as they are adjusted. For these cases, it is important to include the coupling element in the pre-tuning process. Other designs are such that the coupling element has little effect. Including these elements in the pre-tuning process can yield poor results, as the coupling element may be mistuned completely, yet still not achieve the same phase as during the reference filter setup. For these cases, the coupling should be preset physically.

After the pre-tuning setup is complete using the reference filter, other filters of the same type may be pre-tuned using their phase response, with guidance from the pre-tuning wizard. For best results, the reference filter is usually first used to capture the time-gated response, before any adjustments are made on its tuning. Next, the resonators are adjusted up and down to capture the compensation table. Finally, the reference filter can be used in the pre-tuning setup to capture the phase of each element, as it is de-tuned. As a last step, the reference filter can be re-tuned using the pre-tuning wizard and the normal time-gated responses.

Figure 7-17 shows the use of the pre-tuning wizard. The upper-left plot shows the initial response before any resonators are tuned. The phase response is shown in the graticule portion, and the tuning indicator (similar to the time-gated frequency response indicators) shows the resonator is tuned too high. The upper-right plot shows the response after resonator R1 is tuned. The pre-tuning wizard can be set to automatically switch to the next resonator when the current resonator reaches its target. The lower-left plot shows the response after five of the resonators have been tuned, and the tuning

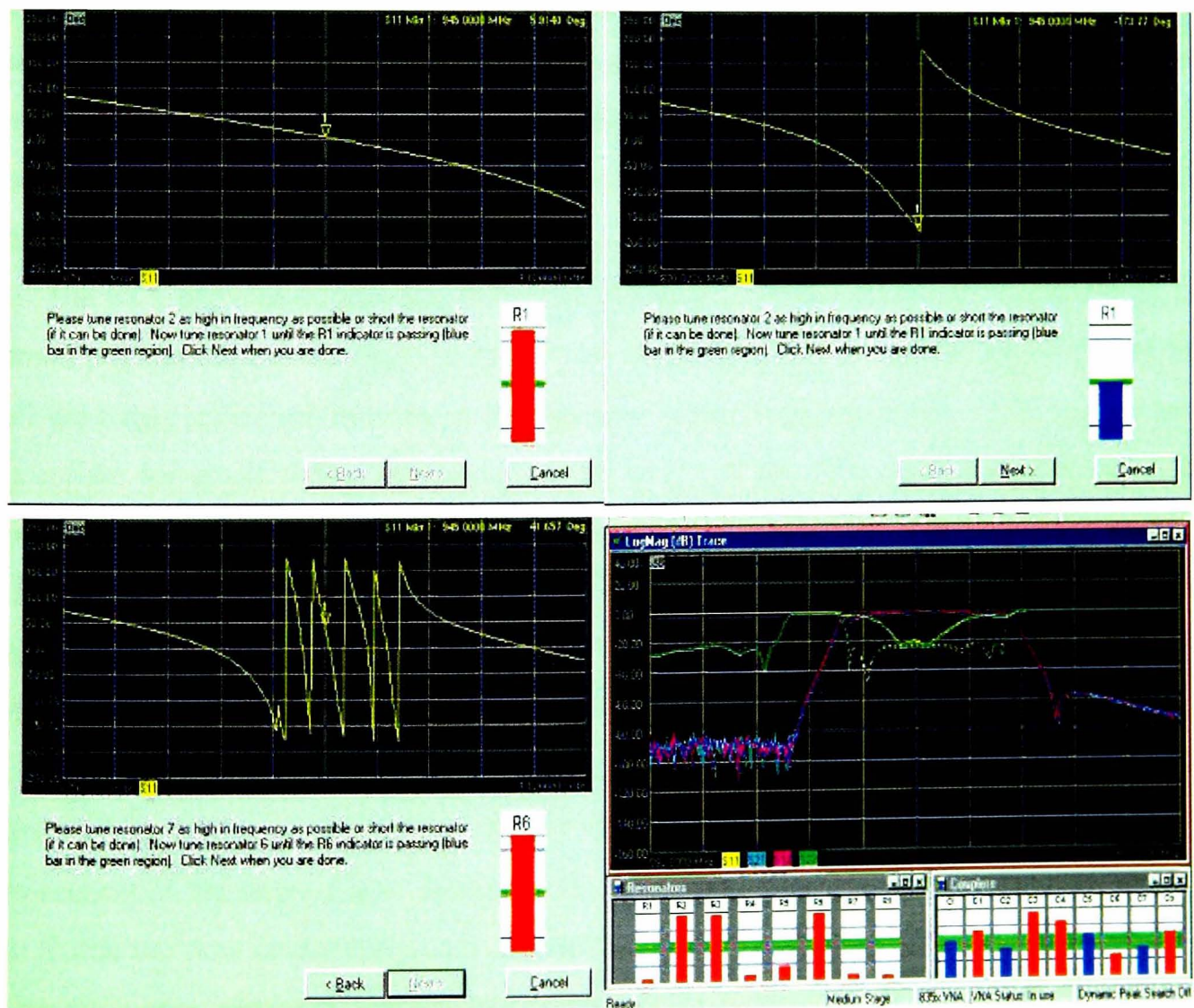


**Figure 7-17: Pre-tuning (phase-tuning) wizard. Before any tuning (upper-left), after tuning R1 (upper-right), before tuning R6 (lower-left), and after pre-tuning all resonators (lower-right).**

indicator for resonator R6 is being displayed. When the last resonator is to be tuned, the display changes to log-magnitude (dB) return loss, as the phase becomes uncertain as the input reflection becomes small. Finally, the lower-right plot shows the frequency domain result of the pre-tuning, where one can see that the  $S_{21}$  frequency response is nearly tuned, but the  $S_{11}$  response needs further adjustment. This is the normal tuning mode of the FTS application, and all 8-resonator indicators, as well as the coupling indicators, are shown.

### **7.5 Changing filter center frequency or bandwidth with FTS**

During a filter tuning process, it is not uncommon for a filter to be tuned until the tuning indicators all pass, but which does not quite meet a specification at one end of its bandwidth. In many cases, if the filter were merely adjusted up (or down) in frequency a slight amount, it would pass its tuning specification. In cases like this, it would be convenient to re-set all the tuning indicators higher by some small frequency shift, without re-characterizing a new reference filter.

Also, filters are often designed to be tuned across a range of frequencies, using the same hardware but with a different tuning adjustment. In these filters, the resonators and coupling elements have a wide adjustment range, and it would be convenient if only one reference filter were needed to support the wide range of frequencies and bandwidths desired.

The FTS application provides solutions for both the above cases. In the first case, a small adjustment can be made to the all the target frequencies values, which results in all the target indicators moving in the direction of the frequency shift. This is only appropriate for small shifts, as the bandwidth target of the filter remains the same as a percentage of center frequency. As such, the coupling indicators will change as well as the bandwidth, and if the target values are changed too far, the filter shape will be affected. This method to shift the frequency is typically used when the change in center frequency is less than one-half of the filter bandwidth.

For large changes in center frequency, or for changes in filter bandwidth while maintaining the same return loss or insertion loss ripple, the FTS application allows a re-scaling of the target filter. In this mode, measured response of the filter is re-scaled to match the new center frequency and span. The time-domain gates are based on the new frequency response, and the tuning targets for resonators and couplings are determined for this new scaling. In this way, it is very easy to create target filters having the same relative return loss or insertion loss ripple, for any bandwidth or center frequency.

## 7.6 Case study: applying FTS techniques to duplexer tuning

The gating technique described in section 6.3 may have application to duplexer tuning. However, modifications must be made to account for the fact that the center frequencies of the antenna port, and either the TX port or the RX port, are not the same. An investigation of using the FTS application for tuning duplex filters in a real-life manufacturing environment was undertaken at a large European filter producer. In this investigation, statistics were collected on the tuning of one specific filter type. This filter was a GSM base station duplexer, with each side comprised of an 8-pole filter with 2 nearly-fixed cross couplings. The TX and RX filters had a bandwidth of approximately 50 MHz, with about 25 MHz separation between the filters. Thus, this filter just meets the criteria established later in section 8.2.3. The data from the manufacturer showed the average filter could be tuned using experienced tuners in approximately 50 minutes, from a completely un-assembled state (all the tuning screws removed from the filter).

For the evaluation of the FTS application, a reference filter response was captured, and the pre-tuning wizard captured the phase tuning of the reference filter. A set of un-tuned filters were prepared, and the tuning process was evaluated in detail for one filter. The filters were set-up with coupling screws set to the same mechanical height as the reference filter, and all the resonator screws backed out fully. The first step in tuning the filter was following the pre-tuning wizard to insert and tune each coupling screw and resonator, which took 4 minutes 36 second. It was noted that this is just about the same time it takes to physically insert the 16 resonator screws. Figure 7-18 shows the frequency response ( $S_{21}$  and  $S_{11}$ ) from the antenna port for the RX (left) and TX (right)

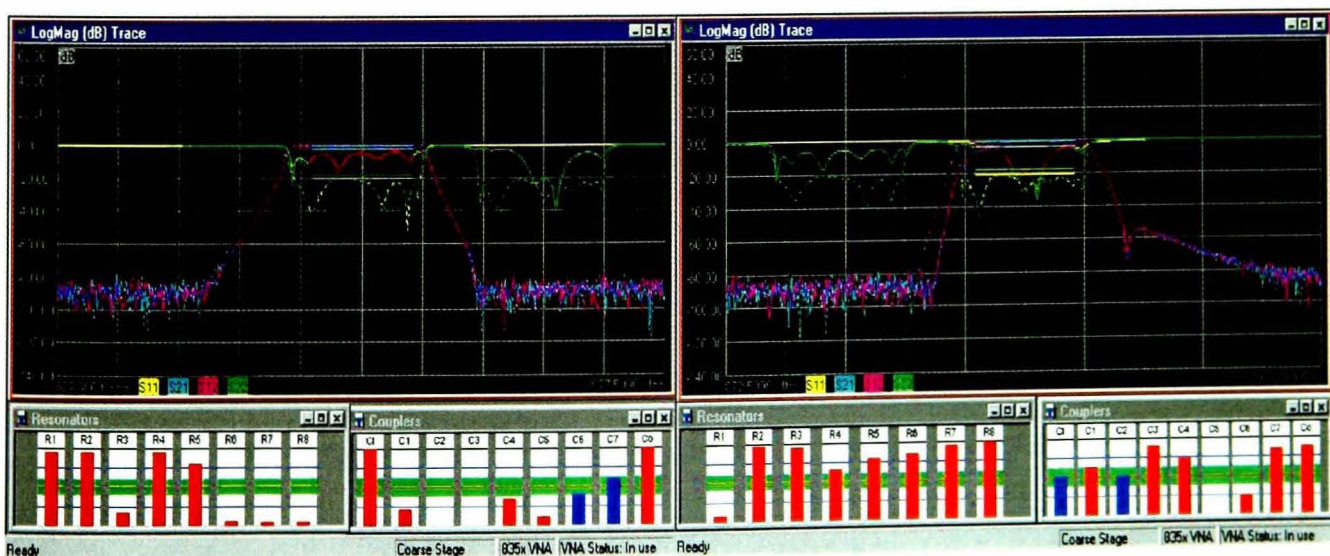


**Figure 7-18: RX (right) and TX (left) paths of the duplexer, after pre-tuning (phase-tuning) each side.**

paths after the pre-tuning process is complete. This is essentially the tuning of each filter for the phase response as each resonator is inserted. From the plots in figure 7-18, it is clear that the filters are approximately tuned (looking at the  $S_{21}$  plots) but the resonator tuning is still far off (looking at the  $S_{11}$  plots). Also, from the  $S_{21}$  bandwidth of the TX side, it is clear that the coupling values are not correct.

Next, the resonators near the antenna (ANT) port for the TX and RX sides (TX8 and RX8, respectively) are tuned, by looking at the antenna port and tuning the last two indicators (R7 and R8) for the case where the frequency is set wide enough to capture both TX and RX side. Experiments indicate [92] that the first TX and RX resonator will show up as nulls in the time-domain as seen from the Antenna port, and the FTS program can use the time gating to have indicators R7 and R8 map to TX8 and RX8.

Using this method, the TX and RX first resonators may be more closely set before the individual sides of the filter are tuned. Figure 7-19 shows the results of this tuning step, with R8 representing the first TX resonator near the antenna port, and R7 representing the first RX resonator. The tuning time for this step was 1 minute 24 seconds (6 minutes total).

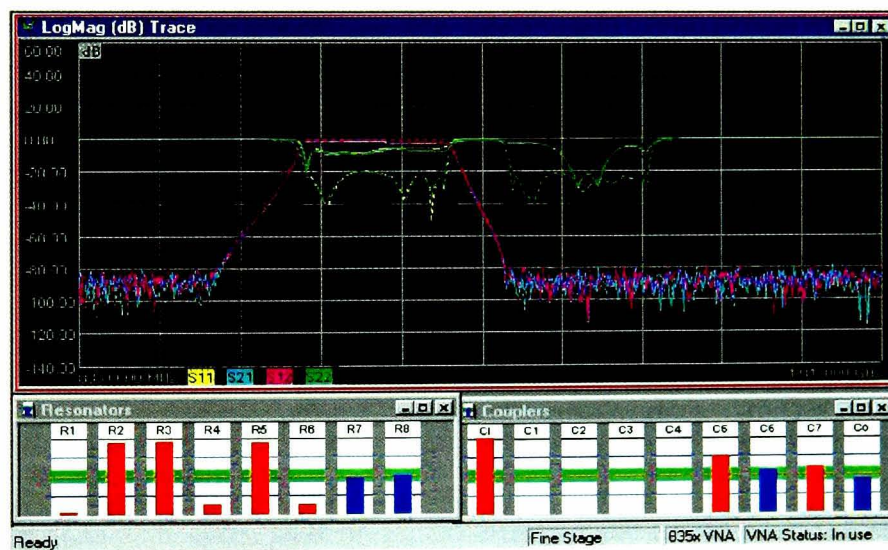


**Figure 7-19: Using FTS and time-gated response to tune the two resonators (TX R1 and RX R1)**

The next step in tuning the duplexer was to change the frequency sweep to center on just the RX side, for RX resonator and coupling tuning, then center just on the TX side for TX resonator and coupling tuning. For each of these steps, the span is reduced to try to eliminate the effects of the opposite side of the duplexer on the side being tuned. For the most part, tuning the resonators from the RX side port is quite easy, as is tuning the TX side resonators from the TX port. It is only the resonators near the Ant port that present difficulties, as the time-domain response for the TX side is distorted by reflections from the RX side, as they appear at the Ant port. Figure 7-20 shows the narrow

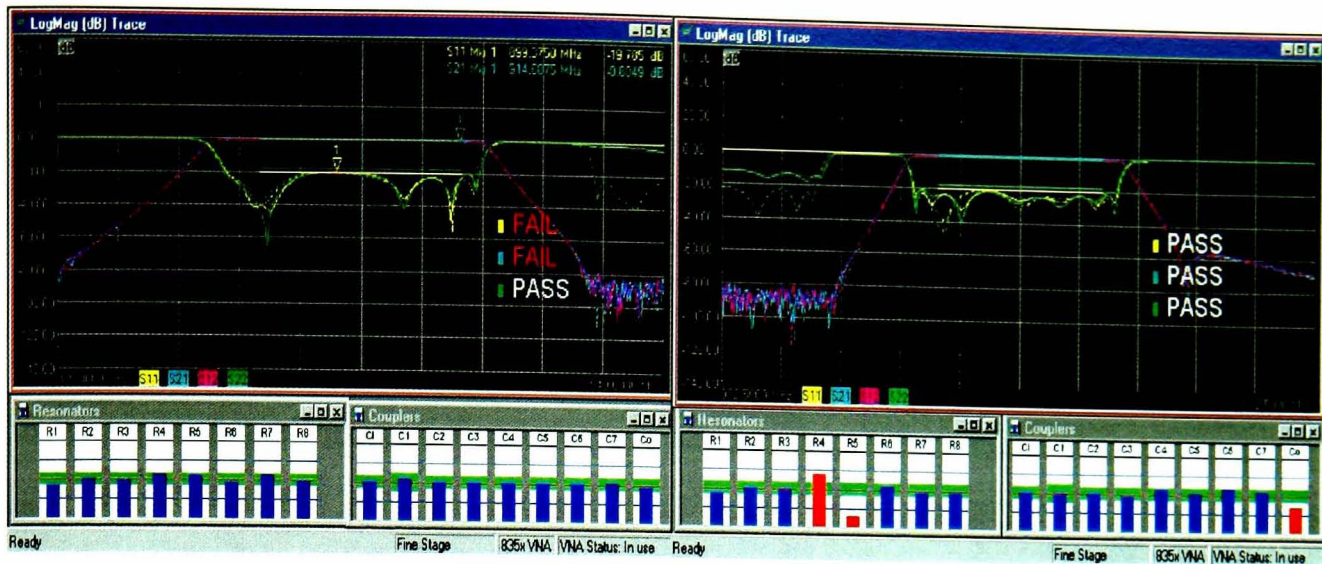


**Figure 7-20: First pass at narrow band tuning for the RX (left) and TX (right) sides of the duplexer.**

band tuning of the RX side (left) and the TX side (right), after adjusting all the resonators. Note that the TX side middle resonators were not adjusted in the FTS application as the TX side passed all its specifications without adjustment of the final two resonators. The RX side fails very slightly in the  $S_{21}$  specification ( $-0.0805$  dB vs.  $-0.08$  dB), and  $S_{11}$  specification ( $-19.78$  dB vs.  $-20$  dB). This tuning takes an additional 14 minutes, for a total time of just under 20 minutes. An additional minute and a half was spent re-tuning the TX8 and RX8 resonator from the antenna port, returning to the reference state used in figure 7-19.

Next, the RX side was fine-tuned to improve its response as much as possible. A little improvement was achieved by adjusting resonator RX2 for best return loss, even if the resonator indicator is out of the target zone. The  $S_{11}$  now meets specification, but  $S_{21}$  is just 0.01 dB out of spec. The TX side was similarly tuned for best improvement, with the final results shown in figure 7-21. The total time after this tuning was 26 minutes. These particular filters have locking nuts, which secure the tuning screws after



**Figure 7-21: Final tuning of the RX (left) and TX (right) filter sections, before locking the screws**

adjustment. Often, when the locking nuts are tightened, the loss of the filter improves. However, just as often, the process of locking the nuts causes a small shift in the resonators, which results in a mistuned filter. The FTS application has a “locking” mode, which is very useful for this process. The locking mode will reset all of the targets to the current resonator values. When the nuts are tightened, any change in the resonator due to tightening the nut is readily apparent, making it easy to maintain the correct resonator tuning while locking down the tuning screws.

In the final tuning step, all the locking nuts were tightened for all the resonators and couplers. The RX and TX sides now pass all specifications, with the RX  $S_{21}$  passing by 0.03 dB. The final performance is shown in figure 7-22. The total tuning time, including locking was 42 minutes. This compares very well with the average tuning time of 50 minutes for the filter without the FTS application. Though the time savings is only about 15 percent, the filter can be tuned by following only the tuning indicators, greatly reducing the skill and training needed for tuning this type of filter.

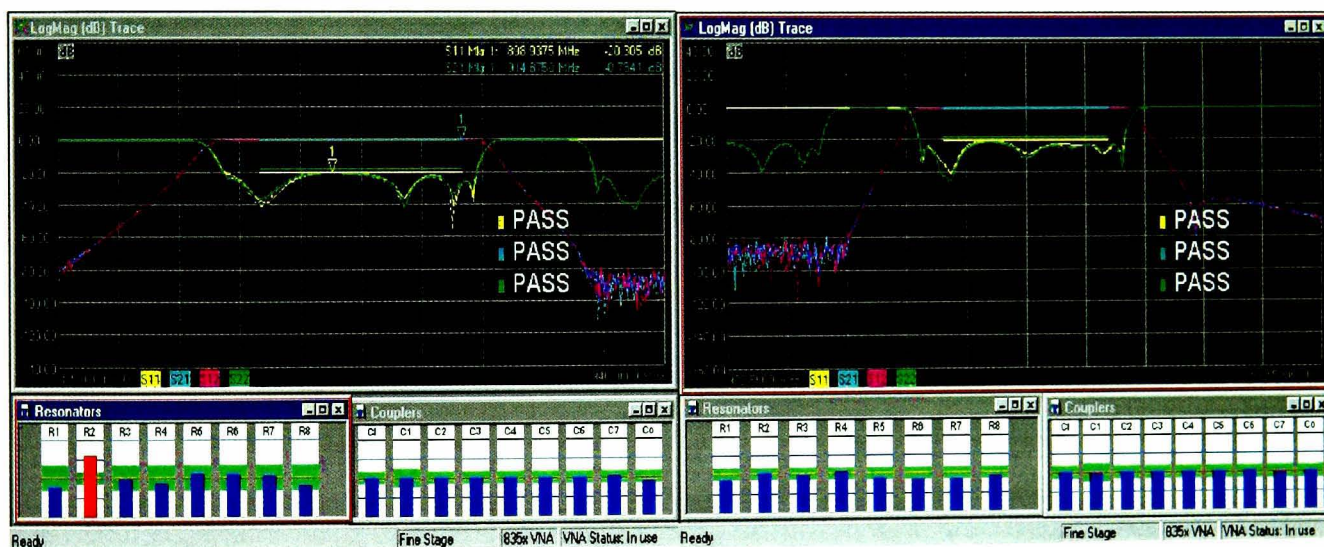


**Figure 7-22: Final tuning after locking RX (left) and TX (right) sides of the duplexer, passing all specifications**

## 7.7 FTS Conclusions

The FTS application works extremely well for all-pole filters, as well as cross-coupled filters where the cross coupling is small or fixed and well controlled. In these cases, FTS has been almost 100% successful in providing a complete tuning solution. Unfortunately, these filters now comprise only a percentage of the commercially developed filters, with most filters having multiple, adjustable cross-couplings or being parts of a duplex filter (in fact, the filter in figures 7-15 and 7-17 is one part of a duplex filter, as is the case study filter).

Some other filter attributes that limit the use of FTS are filters for which the input coupling is fixed, and differs from the target or reference filter. Fixing the input or output couplings is common in many filter manufacturing processes, with some allowing minor changes (through bending wires, etc) and some using fixturing to attempt to get exactly the same input couplings across all filters in a production run. For these filters, the inability to adjust an incorrect input coupling means that the other couplings must be, in essence, re-synthesized to achieve the desired response, such as return loss over a given bandwidth. In some cases, tuning the remaining couplings to the target levels results in a filter that is too narrow or broad, or has an insufficient return loss. This limitation might be overcome if some facility is included to re-synthesize the filter design based on the measured input couplings. Also, if any individual resonators or couplings lack sufficient tuning range to allow them to be tuned to be the same as the target filter, then the FTS method may fail to allow the filter to be tuned, even if other tuning methods might allow the filter to pass a tuning specification. This case is quite similar to the case above where the input or output couplings cannot be tuned.

The FTS application has been tried in cases of duplex filters, with some limited success. Possible extensions of this work to duplex filters and other tuned structures is discussed in the next chapter, as well as limitations, concepts for further extensions of this topic, as well as general conclusions of this thesis.

## Chapter 8 Conclusions and Suggestions for Further Work

### 8.1 Conclusions

This thesis has documented entirely new ideas in the area of filter tuning, based on the VNA time-domain response of the filter, and several new and important results are presented:

The impulse response of the input reflection ( $S_{11}$ ) of a filter has not been previously studied with respect to filter tuning. This thesis for the first time calculates the impulse response of the reflection of a filter, and compares it with the vector network analyzer time-domain response. This comparison results in the conclusion that they are not the same, and that they differ because of the discrete sampling and windowing, which occurs as a part of the time-domain transform. A key contribution in this thesis is the complete mathematical presentation of the VNA time-domain transform as a series of mathematical processes (sampling, truncation, windowing, renormalization) on the inverse Fourier transform. As part of this analysis, the area of time-domain gating is extensively discussed, and a new method of accounting for masking effects of gated responses is presented.

The time-domain transform of the input and output reflections of a filter is shown to be useful in tuning all-pole filters. Using only the time-domain response, a filter can be completely and deterministically tuned by looking at the peaks and nulls in its time-domain response. Experimental results and computer simulations verify that these responses are a characteristic of the filter, and are sufficient to tune the filter. These results have been submitted by the author to peer reviewed conferences, and accepted for publication in the proceedings of these conferences. At a recent MTT workshop on automated filter tuning, the workshop chairman recognized that time-domain tuning was the “only method with clear physical relationship between displayed feature and tuning screw location” [93]. The discovery of the relationship between the time-domain response of a filter and the tuning of its resonators, and the development of the time-domain tuning method has been a significant contribution to the area of microwave filters. The time-domain masking effects are shown to substantially account for the interactions seen when using time-domain responses for tuning filters.

The complete theoretical analysis of the time-domain response of a one-pole filter is presented for the first time in this thesis. This analysis shows that the experimental result, which shows nulls in the time-domain response being associated with resonator

tuning, has a clear theoretical basis. The results for the one-pole filter are shown to be extensible to a multi-pole filter, thus generalizing the theory.

An entirely new tuning-method, utilizing the time-gated frequency response of a filter, is shown here. This method, for which two patents have been granted, provides for a direct readout of the frequency of an individual resonator in a multi-pole filter. With this method, a software application was developed, and this thesis presents the results of applying this technique to various filter tuning experiments. As a result, the only obstacle to single-pass tuning of all-pole filters is the interaction of one resonator with another during the tuning process. Even this obstacle is addressed with an new method, for which there is a patent pending, that determines resonator interaction, and provides a simultaneous correction for every resonator for the interaction with every other resonator.

These methods for all-pole filters are shown here to be extensible to filters with cross-coupled resonators, in cases where the cross coupling is sufficiently less strong than the main coupling. This method is also extensible to duplex filters, where the filter responses are not completely adjacent.

Finally, some ideas for extensions of these techniques to more complex filter types, and to combining these techniques with other filter tuning methods are suggested.

This research topic was instigated from both a personal desired to understand the time-domain response of filters arising from the discovery of the relationship between the VNA time-domain response and a filter's tuned response, and a professional desire to commercialize this invention for benefit of the author's sponsors and the filter community. With the development of ideas for this research, culminated with the conclusion of this thesis, both of these goals have been accomplished.

## **8.2 Suggestions for further work**

An obvious extension of the methods described in the previous chapters for tuning all-pole filters, and filters with small and fixed cross-couplings is to the area of duplex filters, filters with multiple cross-couplings, or other filter configurations. While the time-gated tuning method has been attempted with filters of these types, and has met with some success, the extension of its application to complex filters presents new challenges. Investigation of a means to extend these tuning methods to other filter types is one possible area suitable for research to extend the results beyond those reported in

this thesis. Some of the possible areas for extension to these more complex filter types are discussed below.

### **8.2.1 Duplex Filters**

The TX and RX filters described in section 1.1.3 are often integrated with an antenna combiner to create a duplexer. Duplexers significantly increase the complexity of the filter tuning process, especially if the TX and RX channels are very close. One consequence of close channel separation is the need for transmission zeros (which implies, among other techniques, cross-coupling of resonators) to produce sharp cut-offs between the TX and RX bands.

### **8.2.2 Duplex filter configurations:**

The combiner for the TX and RX side can take on several different configurations. The method of combining can also affect the interaction between the TX and RX sides of the duplexer. Two common configurations include the common resonator configuration, and the common port configuration.

#### **8.2.2.1 Common resonator configuration**

The common resonator configuration utilizes one resonator coupled to the antenna port. This resonator is coupled to the first RX resonator and the first TX resonator. For this configuration, the common resonator must form a filter element with a bandwidth that covers both the TX and the RX bands. This configuration is sometimes used when the RX and TX channels are closely spaced. FTS can be setup to have a one section filter tuned from the common port, with a frequency span that covers both TX and RX frequencies. The effects of the two following resonators have not been extensively studied, but some preliminary experiments indicate that it is possible to align the first common resonator using a properly configured frequency sweep in FTS.

#### **8.2.2.2 Common port configuration**

The common port configuration utilizes coupling structures from the RX and TX sides of the duplexer to couple to the common antenna port, and is more commonly used in practice than the common resonator approach. These coupling structures are designed to isolate one side from another, for example, using quarter wave type structures from the first resonator on of each side to the common antenna port. The phase is adjusted such that the TX resonator presents a short at the RX frequency, and the quar-

ter wave line transforms this to a high impedance at the common port for the RX band. A similar arrangement is used for the TX side.

### **8.2.3 Effects of adjacent channel resonators on time-domain responses**

The adjacent channel, if closely spaced, affects the time-domain response of the other channel. Typically, if the channel spacing is greater than one-half bandwidth at the 3-dB down points of the filter, the TX and RX sides can be tuned independently. If the channels are more closely spaced, the response from one side will substantially affect the other side.

### **8.2.4 Strategies to tune duplex filters in time-domain**

Tuning duplex filters with close spacing in the time-domain requires different strategies than those presented in the case study of section 7.6 above. Some tuning strategies for closely spaced duplexers were first described by the author in [92], also included as published paper 6. It describes an experiment in which the techniques from Chapter 4 were extended to a duplexer with close spacing. Figure 6 from [92] shows a model of a duplexer with a common port configuration. Figure 8 from this paper shows the time-domain response and frequency response of a real duplexer. As described in [92], the resonators are identified with specific nulls, and the methods of the paper are used to determine the effective frequency of each resonator.

### **8.2.5 Isolating the effects of adjacent filter resonators**

The first resonator of the TX side (the low side channel) is set as low as possible to isolate the RX side from the TX side. This affects the response of the RX side, and distorts it from the desired response. However, this new response is the appropriate response with the TX side isolated, and the effective values of the RX resonators are recorded as described. The TX first resonator is returned to its original position, the RX first resonator is set as high as possible, and the TX is similarly recorded. These values are recorded as shown in Table 3 of [92].

To tune a duplexer, the RX resonator is set high, and the TX side tuned according to Table 4 of [92]. Next the TX side first resonator is set low, and the RX side is tuned according to the same table. Finally, the first TX resonator is tuned according to Table 2 of [92].

Just as with the cross-coupled filter of chapter 4, using the time-domain response to tune a duplex filter may be possible, but it is very tedious. These early experiments

with tuning duplexes indicate that more study is required. Some interesting possibilities might be subtracting a calculated response of one path, say the RX path from the other path, say the TX path, where the RX path resonators are set far off. After tuning the TX side, its response might be able to be subtracted in some way from the overall response to leave just the Rx response.

### **8.2.6 Closely spaced duplexers and FTS**

Experiments with duplexers that have the pass-bands closer than one-half a bandwidth have proved very difficult to tune using FTS. The problem appears to be one of overlapping time-domain responses. That is, looking from the antenna port, one can consider the overall time-domain response to be the superposition of two responses, one from the TX side and one from the RX side. As such, the nulls typically associated with each resonator are no longer sufficiently distinct.

One consequence of this overlap is that the nulls appear to move in time as the resonator associated with the null is tuned. This implies that the null is a consequence of more than just one resonator, and moves in time as the value of the sum of the two time-domain responses cancel at different times as one resonator is tuned. Since the time-gated technique pre-supposes that the gate times are fixed, these moving nulls present a significant problem.

Duplexers that are quite closely spaced often achieve the sharp cut-off frequencies by adding cross coupling to sections in each filter. As the cross coupling becomes strong, further difficulties are seen in tuning filters with time-domain techniques.

## **8.3 Areas for investigation for applying FTS methods to other filters**

The success of the case study in the previous section also illustrates the limitations of the FTS method for tuning complex filters. The following sections describe areas for further investigation of the time-domain and time-gated (FTS) tuning methods.

### **8.3.1 Filters with extracted resonators**

Other filters which exhibit similar problems are filters with an additional resonator extracted at the input or output port, which sharpens the stop-band response [94]. In these filters, a single shorted resonator (or more rarely, multiple resonators) is connected to the input and/or output port of the filter, in much the same way as a duplexer. This resonator is shorted, that is, it is not generally connected to other resonators. As a shorted resonator, it presents a short circuit to the input at a frequency determined by

the resonator. Alternatively, it can be designed to present an open circuit at resonance, connected by a quarter wave transmission line, thus presenting a narrow band short. It acts in many ways as a duplexer, where the duplex path is terminated in a short. This short creates a transmission zero for the desired path.

Some experimentation has been done on these filter types, using FTS, with limited success. It seems the duplex aspect is such that one might consider the extracted resonator as a very closely spaced duplex path. Some of the techniques presented in [92] might apply, and in general these filters are tuned by shorting the first resonator in the main path, and tuning the extracted resonator. From this it is hoped that its effect on the time-domain response of other resonators is the same as that of a reference filter, so that the other resonators may be deterministically tuned. If the extracted resonator is very close in frequency, any mistuning in it results in errors in tuning all the other resonators, yielding an unsatisfactory tuning process.

### **8.3.2 Filters with strong cross coupling**

Strong cross coupling causes a similar problem to that of filters that are closely spaced. Strong cross coupling is characterized by the coupling value for the cross coupling approaching that of the main coupling. In this case, the time-domain response of the input to the cross-coupled stage can be thought of as the sum of the response from the main coupling and the response of the cross coupling. In the case where the cross coupling is not strong, the response is only slightly perturbed. Often, the cross-coupling value can be set precisely by looking at the  $S_{21}$  transmission response, and setting the zero value. Once this is fixed, the nulls associated with various resonators are also fixed, and it is simple to characterize the frequency for each resonator.

However, for filters that designed using cascaded triplets [95], the cross coupling may be very strong, and it is quite difficult to establish a reasonable tuning order using FTS. An interesting extension to this technique might be to establish some tuning method for triplets, based on reflection response, then use time-domain techniques along with de-masking to apply the method to cascaded triplets.

### **8.3.3 Filters with embedded amplifiers or isolators**

Many filters used in wireless systems have embedded isolators at the inputs, in the case of TX filters, or low noise amplifiers (LNA) in the outputs, as in the case of RX filters. The addition of these non-bilateral devices causes substantial problems when trying to apply FTS or time-domain techniques to their tuning.

Time-domain based techniques rely on the reflection response of filters, as do many of the other techniques presented in chapter 1, and as such they are not successful if any element in the filter is substantially unilateral. Adding an isolator at the input to a filter means the time-domain response at the input will be that of the isolator load, regardless of the filter resonator tuning. For this type of filter, the input response is difficult to see, so any reflection based tuning must be done based only on the output reflection response, with its associated limitations of tuning a filter from only one end. Adding an LNA at the output of a filter causes a similar unilateral behavior. However, with the advent of higher dynamic range VNAs, it might also be possible to tune these filters using FTS by looking at the leakage back through the isolator or LNA, if some way can be made to account for the larger, but unchanging response of the LNA.

While this thesis has looked primarily at reflection responses from both sides, there may be some way of applying the de-masking techniques to allow better tuning from only one side of the filter. Or perhaps the time gating can be applied to some of the input sections to remove their effects from the transmission response of the remaining elements, thus simplifying the tuning process by reducing the order of the filter that remains to be tuned.

#### **8.3.4 Combining FTS methods with other methods**

Another natural extension of the FTS method is to apply some of the time gating techniques discussed here to other methods presented in chapter 1, in hopes that attributes of each method enhances the other. One area in particular might be in using time-domain responses as part of an optimization criteria, as together they may provide faster convergence or avoid local minima problems. The fuzzy logic and artificial neural networks techniques might also be well served by using both frequency and time-domain data for training data and evaluation data. This is particularly intriguing as the time-domain methods have been shown to be quite intuitive in tuning simple filter structures, and adding fuzzy logic or neural network ideas to time-domain methods may overcome the difficulties observed in tuning more complex structures.

## Appendix 1

### Time domain reflection response of 3 pole Butterworth filter

A 3-pole Butterworth low-pass filter was chosen for the first calculations, due to its relatively simple transfer function. Once the time domain response of the low-pass filter is known, the envelope for a 3-pole Butterworth band-pass filter is determined.

The frequency response of the input reflection of a 3 pole Butterworth filter is

$$S_{11}(j\omega) = \frac{-\omega^6 + 2\omega^4 - j(2\omega^5 - \omega^3)}{1 + \omega^6} \quad (\text{A1.7})$$

The transfer function (in the  $s$  domain) is,

$$S_{11}(s) = \frac{-s^3}{s^3 + 2s^2 + 2s + 1} \quad (\text{A1.8})$$

Which through long division becomes

$$S_{11}(s) = s^3 + 2s^2 + 2s + 1 \overline{) \begin{array}{r} -1 \\ -s^3 \\ \hline -(-s^3 - 2s^2 - 2s - 1) \\ \hline 2s^2 + 2s + 1 \end{array}} \quad (\text{A1.9})$$

or

$$S_{11}(s) = -1 + \frac{2s^2 + 2s + 1}{s^3 + 2s^2 + 2s + 1} \quad (\text{A1.10})$$

from which the denominator may be factored to get

$$S_{11}(s) = -1 + \frac{2s^2 + 2s + 1}{(s+1)(s^2 + s + 1)} = -1 + \frac{s^2 + s^2 + s + s + 1}{(s+1)(s^2 + s + 1)} \quad (\text{A1.11})$$

which can be further factored to obtain

$$S_{11}(s) = -1 + \frac{s^2 + s}{(s+1)(s^2 + s + 1)} + \frac{s^2 + s + 1}{(s+1)(s^2 + s + 1)} = -1 + \frac{s(s+1)}{\cancel{(s+1)}(s^2 + s + 1)} + \frac{\cancel{s^2 + s + 1}}{(s+1)\cancel{(s^2 + s + 1)}} \quad (\text{A1.12})$$

or

$$S_{11}(s) = -1 + \frac{s}{(s^2 + s + 1)} + \frac{1}{(s+1)} \quad (\text{A1.13})$$

From [96] the Laplace transform is given in the form of

$$\mathbf{L}\{e^{-at} \cos(\omega t)\} = \frac{s+a}{(s+a)^2 + \omega^2} \quad (\text{A1.14})$$

and

$$\mathbf{L}\{e^{-at} \sin(\omega t)\} = \frac{\omega}{(s+a)^2 + \omega^2} \quad (\text{A1.15})$$

and factoring the middle portion of equation (A1.13) in a similar form such as

$$\frac{s}{s^2 + s + 1} = \frac{s}{s^2 + 2as + a^2 + \omega^2} = \frac{s}{(s+a)^2 + \omega^2} \quad \text{and} \\ \text{setting } 2a = 1, \text{ and } a^2 + \omega^2 = 1, \text{ and solving for } a \text{ and } \omega \quad (\text{A1.16}) \\ \text{we find } a = \frac{1}{2} \text{ and } \omega = \frac{\sqrt{3}}{2}$$

and finally, taking the middle portion in the form of equation (A1.16) and factoring again one gets

$$\frac{s}{(s+a)^2 + \omega^2} = \frac{s+a}{(s+a)^2 + \omega^2} - \left(\frac{a}{\omega}\right) \cdot \frac{\omega}{(s+a)^2 + \omega^2} \quad (\text{A1.17})$$

which is now in the form of equations (A1.14) and (A1.15). The first portion of equation (A1.13) is recognized as the transform of a delta function, and the last portion is recognizable as the transform of a simple exponential such that the inverse Laplace transform of equation (A1.13) can be found from Laplace transform tables with the result

$$S_{11}(t) = -\delta(t) + \left\{ e^{-t} + e^{-t/2} \left( \cos\left(\frac{\sqrt{3}}{2}t\right) - \frac{\sqrt{3}}{3} \sin\left(\frac{\sqrt{3}}{2}t\right) \right) \right\} \cdot U(t) \quad (\text{A1.18})$$

### Response of a 1 pole network

The  $S_{11}$  frequency response of a 1-pole network (for example, an RC network with source and load impedance of R, and consisting of a shunt C) is

$$S_{11}(\omega) = -1 + \frac{2^2}{2^2 + (\omega RC)^2} - j \frac{2\omega RC}{2^2 + (\omega RC)^2} \quad (\text{A1.19})$$

In the s domain, the input impedance is

$$Z_{11}(s) = \frac{1}{\frac{1}{R} + sC} \quad (\text{A1.20})$$

and the input S-parameter  $S_{11}$  is

$$S_{11}(s) = \frac{Z_{11} - R}{Z_{11} + R} = \frac{-sCR}{sCR + 2} \quad (\text{A1.21})$$

which can be put in the form of a proper fraction by long division to yield

$$S_{11}(s) = -1 + \frac{2}{sCR + 2} \quad (\text{A1.22})$$

which for C=2, and R=1 reduces to

$$S_{11}(s) = -1 + \frac{1}{s+1} \quad (\text{A1.23})$$

for which the inverse Laplace transform may be determined directly from transform tables to find

$$S_{11}(t) = \left[ e^{-t} \cdot U(t) - \delta(t) \right] \quad (\text{A1.24})$$

## References

---

- [1] Zverev, *Handbook of Filter Synthesis*, John-Wiley & Sons, New York, 1967, pg. 2.
- [2] Atia, A.E., "Nonminimum-Phase Optimum-Amplitude Bandpass Waveguide Filters", *IEEE Transactions on Microwave Theory Tech*, MTT-22, No. 4, April 1974, pp. 425-431.
- [3] Blinchikoff and Zverev, *Filtering in the Time and Frequency Domains*, John-Wiley & Sons, New York, 1976, pp 130-133.
- [4] Dishal, M., "Alignment and Adjustment of Synchronously Tuned Multiple-Resonant-Circuit Filters", *Proceedings of the IRE*, Vol. 39, Nov., 1951, pp 1448-1455
- [5] Williams, A.E., Egri, R.G., Johnson, R.R., "Automatic Measurement of Filter Coupling Parameters", *1983 MTT-Symposium Digest*, pp 418-420.
- [6] Chen, M.H., "Short-Circuit Tuning Method for Singly Terminated Filters", *IEEE Transactions on Microwave Theory Tech*, Vol MTT-25, No 12, Dec. 1977, pp 1032-36.
- [7] Atia, A.E., Yao, H.W., "Tuning & Measurements of Couplings and Resonant Frequencies for Cascaded Resonators", *2000 IEEE MTT-S Digest*, pp. 1637-1640.
- [8] Ness, J., "A unified approach to the design, measurement, and tuning of coupled-resonator filters", *IEEE Transactions on Microwave Theory Tech*, Vol 46, No 4, Apr. 1998, pp 343-351.
- [9] Accatino, L., "Computer-Aided Tuning of Microwave Filters", *1986 IEEE MTT-S Digest*, pp 249-252.
- [10] Atia, A.E., and Williams, A.E., "Measurements of Intercavity Couplings", *IEEE Transactions on Microwave Theory Tech.*, June 1975, pp. 519-522
- [11] Thal, H., "Computer-aided Filter Alignment and Diagnosis", *IEEE Transactions on Microwave Theory and Techniques*, Vol. MTT-26, No. 12, Dec. 1978, pp. 958-963.
- [12] Ishizaki, T., *et al*, "A Computer Aided Accurate Adjustment of Cellular Radio Filters", *IEEE MTT-S Int. Microwave Symp. Digest*, 1990, pp. 139-142.
- [13] Kajfez, D., Hwan, E., "Q-factor measurement with Network analyzer", *IEEE Transactions on Microwave Theory and Techniques*, Vol MTT32, No 7, July 1994, pp.
- [14] Kahrizi, M., *et al*, "Computer Diagnosis and Tuning of Microwave Filters using Model-Based Parameter Estimation and Multi-Level Optimization", *IEEE MTT-S Int. Microwave Symp. Digest*, 2000, pp 1641.
- [15] Marshall, P., Tissi, P., "A New Algorithm for the Accurate Alignment of Microwave Networks", *IEEE Transactions on Microwave Theory Tech*, Vol 39, No. 10, Oct. 1991, pp 1754-1758.
- [16] Yu, J., Fidler, P., "An Automatic LC Filter Tuning System by Optimization", *ICECS 1996*, pp. 215-218.
- [17] Harscher, P., Vahldieck, R., "Automated computer controlled tuning of waveguide filters using adaptive network models," *IEEE Transactions on Microwave Theory and Techniques*, Vol. 49, No. 11, Nov 2001, pp. 2125-2130.
- [18] Harscher, P., Vahldieck, R., Amari, S., "Automated Filter Tuning Using Generalized Low-pass Prototype Networks and Gradient-Based Parameter Extraction", *IEEE Transactions on Microwave Theory and Techniques*, Vol. 49, Nov 12, Dec 2001, pp. 2532-2538.
- [19] Mirafteb, V., Mansour, R., "Computer-Aided Tuning of Microwave Filters Using Fuzzy Logic", *IEEE Transactions on Microwave Theory and Techniques*, Vol. 50, No. 12, Dec. 2002, pp. 2781-2788.
- [20] Ibbetson, D., "A Synthesis-Based Approach to Automated Filter Tuning", *IEE Colloquium on Microwave Filters and Multiplexers(Ref. No. 2000/117)*, Nov. 2000, pp. 11/1 – 11/3.

- 
- [21] Ibbetson, D., "Practical Computer-Aided Filter Tuning", *IEEE MTT-S International Microwave Symposium Workshop Notes*, Workshop WFB-06, Philadelphia, Pennsylvania, 8-13 June 2003.
- [22] Tang, W.C., "A Fully Automated Filter Tuning Robot for A Fully Automated Filter Tuning Robot for Wireless Base Station Diplexers Wireless Base Station Diplexers," *IEEE MTT-S International Microwave Symposium Workshop Notes*, Workshop WFB-07, Philadelphia, Pennsylvania, 8-13 June 2003.
- [23] Jervis, B.W., Crofts, M., "Comparison of computer-aided tuning algorithms applied to the amplitude response of passive analogue filters", *IEE Proc.-G*, Vol 138, No. 3, June 1991, pp 363-371.
- [24] Dunsmore, J., "Simplify Filter Tuning in the Time-domain", *Microwaves and RF*, vol. 38, no. 4, pp. 68-84, March 1999.
- [25] Dunsmore, J., "Tuning Band Pass Filters in the Time-domain", *1999 IEEE MTT-S International Microwave Symposium Digest*, June 1999, Anaheim, Ca., Vol. 3. pp. 1351-1354.
- [26] Agilent Technologies, Application Note AN 1287-8, *Simplified Filter Tuning Using Time-domain*, Agilent part no. 5968-5328EN, 1999.
- [27] Blinchikoff and Zverev, *Filtering in the Time and Frequency Domains*, John-Wiley & Sons, New York, 1976, chapter 1.
- [28] Guillemin, *Introductory Circuit Theory*, John-Wiley & Sons, New York, 1953, pg 273.
- [29] Johnson, *Introduction to Filter Theory*, Prentice-Hall, Englewood Cliffs, New Jersey, 1976, pg 3.
- [30] Bracewell, *The Fourier Transform and Its Applications*, 2<sup>nd</sup> Edition, Revised, McGraw-Hill, New York, 1986, pg 219.
- [31] Glass, Carter, *Linear Systems with Applications and Discrete Analysis*, West Publishing Co., St. Paul, 1976 pg 247
- [32] Bracewell, *The Fourier Transform and Its Applications*, 2<sup>nd</sup> Edition, Revised, McGraw-Hill, New York, 1986, pg 227.
- [33] Glass, Carter, *Linear Systems with Applications and Discrete Analysis*, West Publishing Co., St. Paul, 1976 pg 480.
- [34] Blinchikoff and Zverev, *Filtering in the Time and Frequency Domains*, John-Wiley & Sons, New York, 1976, pg. 59.
- [35] Bracewell, *The Fourier Transform and Its Applications*, 2<sup>nd</sup> Edition, Revised, McGraw-Hill, New York, 1986, pg 9.
- [36] Glass, Carter, *Linear Systems with Applications and Discrete Analysis*, West Publishing Co., St. Paul, 1976 pg 195.
- [37] Johnson, *Introduction to Filter Theory*, Prentice-Hall, Englewood Cliffs, New Jersey, 1976, pg 28, 174.
- [38] Matthaei, Young, Jones, *Microwave Filters, Impedance-Matching Networks, and Coupling Structures*, Artech House, Dedham, Mass. 1980, republished from McGraw-Hill, 1964, pg 17.
- [39] Johnson, *Introduction to Filter Theory*, Prentice-Hall, Englewood Cliffs, New Jersey, 1976, pg 22.
- [40] Blinchikoff and Zverev, *Filtering in the Time and Frequency Domains*, John-Wiley & Sons, New York, 1976, pp 60-63.
- [41] Williams and Taylor, *Electronic Filter Design Handbook*, 2<sup>nd</sup> Edition, McGraw Hill Publishers, 1988, pg 1-4.
- [42] Blinchikoff and Zverev, *Filtering in the Time and Frequency Domains*, John-Wiley & Sons, New York, 1976, pg 167.

- 
- [43] Blinchikoff and Zverev, *Filtering in the Time and Frequency Domains*, John-Wiley & Sons, New York, 1976, pg 108.
- [44] *ibid.*, pp 96-99.
- [45] *ibid.*, pp 100-103.
- [46] *ibid.*, pp 124-127.
- [47] R. Levy, "Filters with Single Transmission Zeros at Real or Imaginary Frequencies", *IEEE Transactions on Microwave Theory Tech.*, vol MTT-24, pp. 172-181 No. 4, April 1976.
- [48] Blinchikoff and Zverev, *Filtering in the Time and Frequency Domains*, John-Wiley & Sons, New York, 1976, pp 173-186.
- [49] Williams and Taylor, *Electronic Filter Design Handbook, 2<sup>nd</sup> Edition*, McGraw Hill, 1988, pp 5-19 – 5-24.
- [50] Hewlett-Packard application note 95-1, Reprint of Hewlett-Packard Journal, Feb. 1967.
- [51] Matthaei, Young, Jones, *Microwave Filters, Impedance-Matching Networks, and Coupling Structures*, Artech House, Dedham, Mass. 1980, republished from McGraw-Hill, 1964, pp 44.
- [52] Hayt, W. H., *Engineering Electro-magnetics, 3<sup>rd</sup> Edition*, McGraw-Hill, New York, 1974, pp. 443-453
- [53] Ramo, Whinnery, and Van Duzer, *Fields and Waves in communication Electronics*, John Wiley & Sons, New York, 1965, pp. 558-561
- [54] Cohn, S., "Direct-Coupled-Resonator Filters", *Proceedings of the IRF*, Feb. 1957, pp. 187-196
- [55] Matthaei, Young, Jones, *Microwave Filters, Impedance-Matching Networks, and Coupling Structures*, Artech House, Dedham, Mass. 1980, republished from McGraw-Hill, 1964, pp 427-434.
- [56] *ibid.*, pp. 434-438.
- [57] Kurzrok, R.M., "General three-resonator filters in waveguide," *IEEE Transactions on Microwave Theory Tech*, MTT-14, Jan. 1966, pp 46-47.
- [58] Glass, Carter, *Linear Systems with Applications and Discrete Analysis*, West Publishing Co., St. Paul, 1976 pg 480.
- [59] Bracewell, *The Fourier Transform and Its Applications, 2<sup>nd</sup> Edition, Revised*, McGraw-Hill, New York, 1986, pg 7-16.
- [60] *ibid.*, 359
- [61] Oppenheim & Schaffer, *Discrete-time Signal Processing*, Prentice-Hall, Englewood Cliffs, New Jersey, 1989, pp 622-628.
- [62] Hines, M., Stinehelfer, H., "Time-domain Oscillographic Microwave Network Analysis Using Frequency-Domain Data", *IEEE Transactions on Microwave Theory and Techniques*, Vol. MTT-22, No. 3, March 1974, pg 276-282.
- [63] Sharrit, D., "Vector network analyzer with integral processor", US Patent No. 4,703,433
- [64] Rytting, D., "Let Time-domain Provide Additional Insight into Network Behaviour", Hewlett-Packard RF & Microwave Measurement Symposium and Exhibition, April 1984.
- [65] Dunsmore, J., "Advanced Filter Tuning using Time-domain Transforms", *Proceedings of the 29<sup>th</sup> European Microwave Conference*, 5-7 Oct. 1999, Munich, Vol. 2, pp. 72-75.
- [66] Bracewell, *The Fourier Transform and Its Applications, 2<sup>nd</sup> Edition, Revised*, McGraw-Hill, New York, 1986, pg 78.
- [67] *ibid.*, pg 356 .

- 
- [68] Oppenheim & Schafer, *Discrete-Time Signal Processing*, Prentice Hall, Englewood Cliffs, New Jersey, 1989.
- [69] *ibid.*, pp. 445-455
- [70] *ibid.*, pg. 453.
- [71] Papoulis, A., *The Fourier integral and its applications*, McGraw-Hill, New York, 1962, pg.38.
- [72] Thomson, W., *Laplace Transformation 2<sup>nd</sup> Ed.*, Prentice-Hall, New Jersey, 1960, pg. 21
- [73] Blinchikoff and Zverev, *Filtering in the Time and Frequency Domains*, John-Wiley & Sons, New York, 1976.
- [74] Bracewell, *The Fourier Transform and Its Applications, 2<sup>nd</sup> Edition, Revised*, McGraw-Hill, New York, 1986, pg 108.
- [75] Lu, K., Brazil, T., "A Systematic Error Analysis of HP8510 Time-Domain Gating Techniques with Experimental Verification", 1993 IEEE MTT-S Digest, pg 1259.
- [76] Bilik, V., Bezek, J., "Improved cable correction method in antenna installation measurements", *Electronic Letters*, 20 August 1998, Vol. 34, No. 17 pg 1637.
- [77] Pozar, D., *Microwave Engineering 2<sup>nd</sup> Edition*, John Wiley, 1998, pg 94
- [78] Agilent 8753ES User Guide, Chapters 5 and 6, Agilent Part 08753-90472, available at <http://cp.literature.agilent.com/litweb/pdf/08753-90472.pdf>
- [79] Kurzkrok, R.M., "General Four-Resonator Filters in at Microwave Frequencies," *IEEE Transactions on Microwave Theory Tech*, MTT-14, June 1966, pp 295-296.
- [80] Rhodes, J.D., Cameron, R. J., "General Extracted Pole Synthesis Technique with Applications to Low-Loss TE<sub>011</sub> Mode Filters", *IEEE Transactions on Microwave Theory and Techniques*, Vol. MTT-28, No. 9, Sept. 1980, pp. 1018-1028
- [81] Agilent Technologies, Application Note AN 1287-10, *Advanced Filter Tuning Using Time-domain Transforms*, Agilent part no. 5980-2785EN, 2001.
- [82] Matthaei, Young, Jones, *Microwave Filters, Impedance-Matching Networks, and Coupling Structures*, Artech House, Dedham, Mass. 1980, republished from McGraw-Hill, 1964, pp 9-14.
- [83] Blinchikoff and Zverev, *Filtering in the Time and Frequency Domains*, John-Wiley & Sons, New York, 1976, pg 61.
- [84] Williams and Taylor, *Electronic Filter Design Handbook, 2<sup>nd</sup> Edition*, McGraw Hill Publishers, 1988, pg 1-3.
- [85] Dunsmore, J. P., Fetter, T. B., "Tuning method for filters having multiple coupled resonators", U.S. Patent 6,356,163, Granted March 12, 2002.
- [86] Dunsmore, J. P., Fetter, T. B., "Tuning method for filters having multiple coupled resonators", U.S. Patent 6,380,819, Granted April 30, 2002.
- [87] MTT-S International Microwave Symposium Workshop Notes, Workshop WFB, Philadelphia, Pennsylvania, 8-13 June 2003..
- [88] "Agilent Filter Tuning Software Product Overview", Agilent part no. 5988-2460EN.
- [89] Dunsmore, J., "Novel Tuning Application for Coupled Resonator Filter Tuning", *Proceedings of the 2001 Asia-Pacific Microwave Conference*, 3-6 Dec. 2001, Taipei, Taiwan, Vol.2 894-897.
- [90] Ericsson, J., Sariaslani, D., Bhowmik, J., Dunsmore, J., "Variable scaled graphical indicator to display dynamic data", US Patent Pending, Application Number 20030006987, Filed Jan. 9, 2003.
- [91] Dunsmore, J., Hubert, S., Kerr, J., Sariaslani, D, Patent pending,, not yet published.
- [92] Dunsmore, J., "Duplex Filter Tuning using Time-domain Transforms", *Proceedings of 30th European Microwave Conference*, 3-5 Oct. 2000, Paris, Vol.2 pp. 158-161.

- 
- [93] Swanson, D., "Introduction to Computer Aided Filter Tuning", *IEEE MTT-S International Microwave Symposium Workshop Notes*, Workshop WFB-00, Philadelphia, Pennsylvania, 8-13 June 2003.
- [94] Yeo, K.S.K., Lancaster, M.J., Hong, J.S., "The Design of Microstrip Six-Pole Quasi-Elliptic Filter with Linear Phase Response Using Extracted-Pole Technique", *IEEE Transactions on Microwave Theory Tech*, Vol. 49, No. 2, Feb. 2001, pp. 2350-2356.
- [95] Levy, R., Petre, P., "Design of CT and CQ Filters Using Approximation and Optimization", *IEEE Transactions on Microwave Theory Tech*, Vol. 49, No. 12, Dec. 2001, pp. 321-327.
- [96] Glass, Carter, *Linear Systems with Applications and Discrete Analysis*, West Publishing Co., St. Paul, 1976 pg 615

## Published Papers

### Paper 1

Dunsmore, J., "Tuning Band Pass Filters in the Time-domain", *1999 IEEE MTT-S International Microwave Symposium Digest*, June 1999, Anaheim, Ca., Vol. 3. pp. 1351-1354.

### Paper 2

Agilent Technologies, Application Note AN 1287-8, *Simplified Filter Tuning Using Time-domain Transforms*, Agilent part no. 5968-5328EN, 1999.

### Paper 3

Dunsmore, J., "Advanced Filter Tuning using Time-domain Transforms", *Proceedings of the 29<sup>th</sup> European Microwave Conference*, 5-7 Oct. 1999, Munich, Vol. 2, pp. 72-75.

### Paper 4

Agilent Technologies, Application Note AN 1287-10, *Advanced Filter Tuning Using Time-domain Transforms*, Agilent part no. 5980-2785EN, 2001.

### Paper 5

Dunsmore, J., "Novel Tuning Application for Coupled Resonator Filter Tuning", *Proceedings of the 2001 Asia-Pacific Microwave Conference*, 3-6 Dec. 2001, Taipei, Taiwan, Vol.2 894-897.

### Paper 6

Dunsmore, J., "Duplex Filter Tuning using Time-domain Transforms", *Proceedings of 30th European Microwave Conference*, 3-5 Oct. 2000, Paris, Vol.2 pp. 158-161.

## **Paper 1**

Dunsmore, J., "Tuning Band Pass Filters in the Time-domain", *1999 IEEE MTT-S International Microwave Symposium Digest*, June 1999, Anaheim, Ca., Vol. 3. pp. 1351-1354.

# Tuning Band Pass Filters in the Time Domain

Joel Dunsmore

Hewlett-Packard, Microwave Instruments Division

1400 Fountaingrove Parkway, Santa Rosa, Ca., USA 95403

**Abstract** -This new idea in coupled-resonator filter tuning is based on the time domain response of filter return loss. With this method, individual responses of each resonator and coupling coefficient can be distinguished and can be precisely set to a desired filter response; interactions can be immediately determined and accounted for.

## I. Introduction:

With this entirely new technique, coupled-resonator bandpass filters can be easily and precisely tuned. Coupled-resonator filters are the workhorse filters of the RF and microwave communications industry. The center frequency of each resonator must be precisely tuned, and each coupling between resonators must be precisely set to achieve the proper passband response, and to get low return loss (or reflection) and small passband ripple. Until now, the resonator tuning and setting of the coupling coefficients has been as much art as science. This paper presents a method of tuning filters based on the time domain response of its return loss, where the time domain response is obtained by a special type of discrete inverse Fourier transform of the frequency response. It was previously thought that there could not be sufficient resolution in the time domain to make it useful in looking at bandpass filters, but this paper demonstrates that when properly set up the time domain response can distinguish the individual responses of each resonator and coupling aperture. From this, each resonator may be individually and deterministically tuned. If a filter has adjustable coupling, the coupling coefficients may be precisely set based on the desired filter response, and any interaction caused by adjusting coupling structures and resonators can be immediately determined and accounted for. With this method, rela-

tively inexperienced filter tuners, with only a few minutes instruction can be tuning multiple pole filters with great success.

## II. Details, Coupled Resonators in the Time Domain:

A five-pole coupled-resonator filter with four coupling structures will be used to illustrate the new tuning technique. A schematic of the filter is shown in Figure 1. To set up the measurement for time-domain tuning, the frequency sweep must be centered at the desired center frequency of the bandpass filter. Remarkably, the tuning method will tune the filter to exactly the chosen center frequency. The frequency span must be set to approximately two to five times the expected bandwidth. The appendix explains why this setup guarantees sufficient resolution to distinguish individual resonators. The time domain response is obtained by activating the BANDPASS MODE under the TRANSFORM menu of the Vector Network Analyzer (e.g. HP 8753E). To setup the time domain response display, it is helpful to set the start time somewhat before zero, and the stop time somewhat beyond twice the delay of the filter (remember: reflections must travel through the filter twice). The proper start and stop times may be estimated from the number of filter resonators (N) and the bandwidth (BW) of the filter: start time at  $t=-(2/\pi BW)$ , and the stop time at  $t=(2N+1)/\pi BW$ .

Figure 2 shows the frequency response and the bandpass mode time response of the return loss of a fifth-order Chebyshev filter with 0.25 dB of passband ripple (lighter trace) and the same filter with the second resonator mis-tuned. Notice the distinctive dips in the time response (right) of S11 of the filter. These are characteristic nulls that will occur if the resonators are exactly

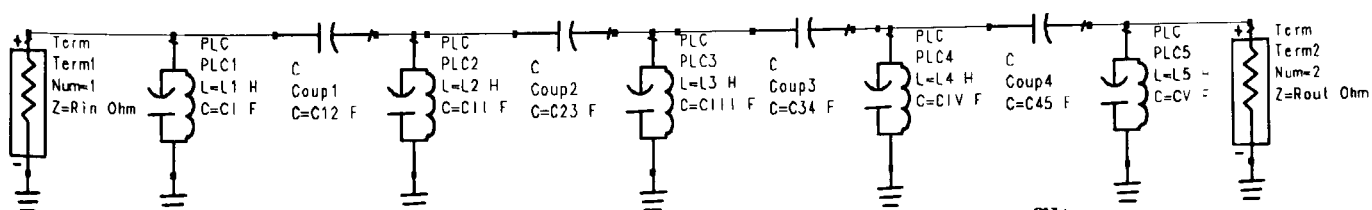
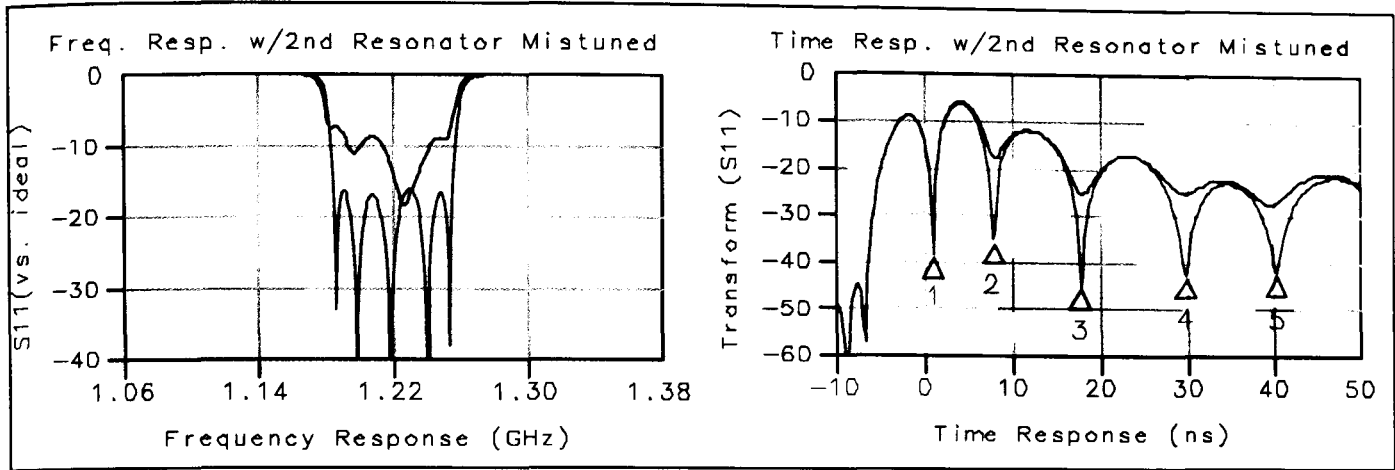


Figure 1: Schematic Diagram of a coupled resonator filter



**Figure 2: Frequency response (left) and Time Domain response (right) of the return loss (S11) of a perfectly tuned filter (lighter trace) and a filter with the second resonator mis-tuned (darker trace).**

tuned. If the center frequency of the measurement were changed even slightly, all the nulls would start to disappear, indicating that the filter is not longer tuned. The peaks between the nulls relate to the coupling factors of the filter. This type of response holds true for any all-pole filter, regardless of filter type.

The essence of the tuning technique is that the dips in the time domain response correspond exactly to each resonator in the filter. When the resonator is tuned properly, the null is deep. If the resonator is not tuned, the null starts to disappear. Though it may seem remarkable that this exact relationship exists, extensive testing with many different kinds of filters, as well as simulations and direct mathematical derivation confirm this relationship. The nulls in the time domain associated with the five resonators are marked in Figure 2. Figure 2 also shows the results of a simulation with only the second resonator mis-tuned from its ideal (derived) value. In this case the capacitor CII was tuned to a few percent above its ideal value. It is clear that the dip has nearly disappeared. The dip will only be maximized when the capacitor is returned to its ideal value. Note that severely mis-tuning one resonator can affect the response from the other "down stream" resonators.

Figure 3 shows a similar response to the adjustment of resonators 3 and 4. In the dark gray trace, resonator 3 is mis-tuned, in the light gray trace resonator 4 is mis-tuned. Note that though the frequency response for the 4<sup>th</sup> resonator mis-tuned will be *identical* to the frequency response trace in Figure 2 where the second resonator is mis-tuned, the time domain responses are quite different. In a symmetric filter, such as this Chebyshev filter, one cannot determine which resonator is mis-tuned from the frequency response. Thus, for a symmetric filter the magnitude response in the frequency domain is identi-

cal for mis-tuning of either the second or fourth resonator. But in the time domain representation, it is easy to see which resonator is mis-tuned.

The benefits of looking at filters in the time domain go beyond tuning the filter during the manufacturing process. Many filters must be qualified over extensive environmental conditions. With this technique, any changes in the filter performance due to changes in the resonators can be easily seen, when compared to a reference time domain trace taken before the environmental stress is applied. For the first time, the contributions of individual elements inside the filter can be determined.

### III. Filters with Adjustable Coupling:

For all-pole filters, the coupling coefficients uniquely determine the filter attributes. To change from a

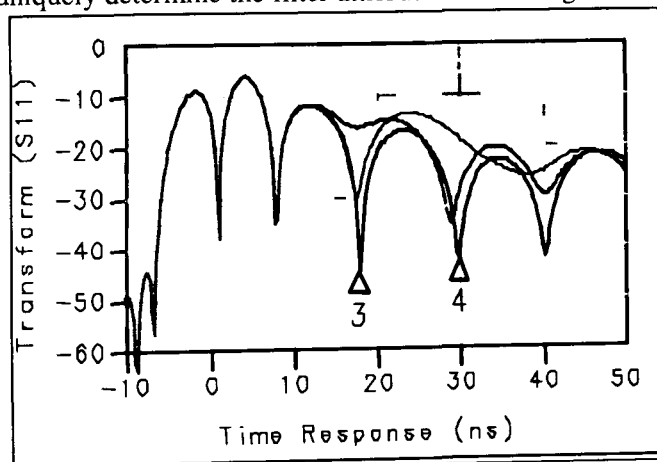


**Figure 3: Time Domain response of a filter with only resonator 3 (dark gray trace) and only resonator 4 (light gray trace) mis-tuned. The perfectly tuned filter case is shown in the black trace**

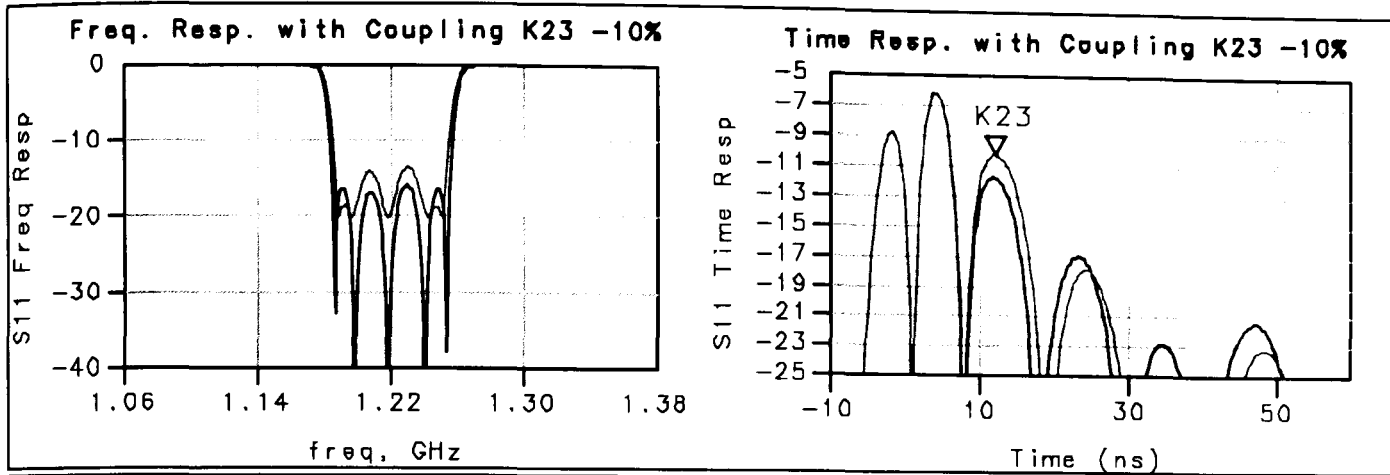


**Figure 4: Freq. and Time Domain responses of a filter with a change to one coupling, K23 (light gray) and the ideal filter (dark gray)**

Butterworth to a Chebyshev, you need only change the coupling. The effect of coupling is also apparent in the time domain, as shown in Figure 4. The peaks of the time response correspond to the coupling between the resonators, with the first peak representing the input coupling. In Figure 4, the coupling between resonators 2 and 3 was reduced 10%, resulting in a higher return loss peak. Note that the peaks from the input coupling and first coupling did not change at all! This leads us to a method for adjusting the coupling of an un-tuned filter. One detail to note is that for the peaks before the peak for which the coupling was adjusted, there is no change in height. But for peaks after the adjusted coupling, the peak values are different. This makes sense if we consider that by reducing the coupling factor K32, we cause a greater reflection of energy at that point in the filter, thereby reducing the energy available to reflect off the other stages of the filter.

In Figure 5, we see the result of increasing K12 by 10%. In this case, the peak corresponding to K12 (darker trace) is lower. This corresponds to larger coupling, and thus, less energy reflected. The peaks from the

following filter couplings will increase, due to the larger energy passing through coupling K12. With this understanding, it is possible to propose a tuning method that would allow adjusting coupling of a filter to realize a desired filter response.

Unlike the resonator tuning, where the adjustment of one resonator only weakly affects the adjustment of another, when tuning the coupling factors one must consider the effects of previous coupling. Therefore, tuning must be done in order from the input (and output) ports to the center of the filter. Also, coupling must be adjusted to some target value, which is most easily established by some sort of template filter. For the first example of coupler tuning, we will consider a real filter example where the target response is established by a "golden" filter standard that was tuned in the frequency domain by an experienced engineer. This "golden" filter is measured and stored in the network analyzer memory. In this case, the desired bandwidth was about 80 MHz, with better than 3dB return loss desired over the center portion of the bandwidth. The filter to be tuned was measured and the measurements are overlaid, as shown in Figure 6. The

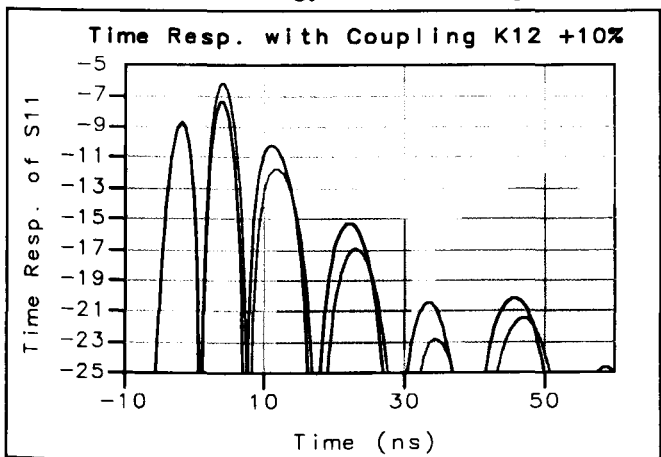


**Figure 5: Effects of increasing coupling K12 (light trace) compared with ideal (dark trace)**

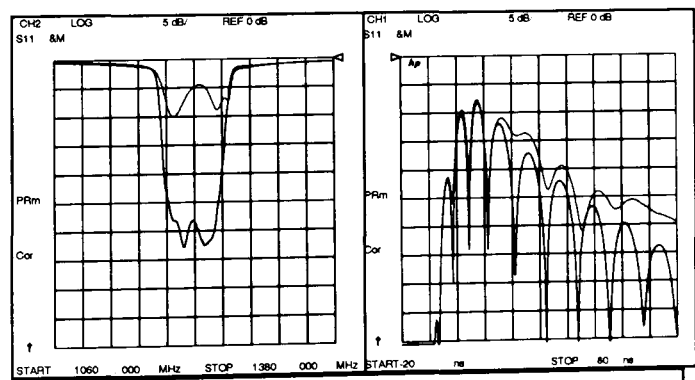


**Figure 6: "Golden Filter and Filter to be tuned in the frequency and time domain.**

M

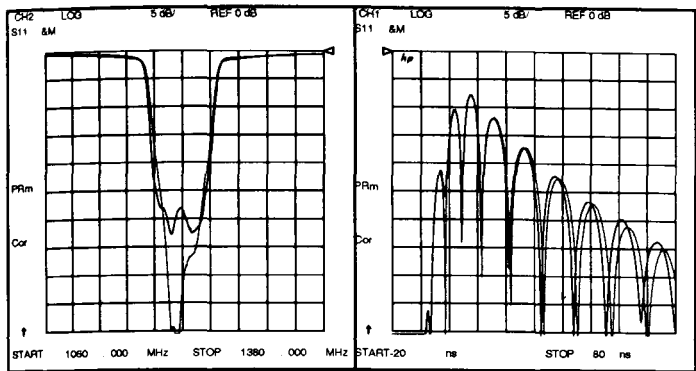


**Figure 7: Freq. And Time response after tuning the filter to match coupling peaks, with the "golden" filter in the dark trace and the filter to be tuned in the light trace**

tuning process entails first pre-adjusting the tuning screws, visually setting the screws to approximately the same position as the "golden" filter. From this we see that the resonators are not properly adjusted, as the nulls associated with them are not as deep as the template filter. Next the resonators are tuned using the nulling process to tune the filter to the center frequency. Finally, the peaks associated with the coupling are adjusted to match the peak values of the "golden" filter template, followed by re-adjusting the resonators to compensate for any interaction from the coupling adjustment. Figure 7 shows the result of this tuning. In fact, the return loss of the "golden" filter (darker trace) is not quite as good as the final return loss of the filter to be tuned. Examining the time domain trace of the "golden" filter reveals that the first resonator is not perfectly tuned, as noted by the lack of a deep null associated with it.

The method above works well if there exists a properly tuned filter, but an often difficult design chal-

lenge is creating the template filter in the first place. Using time domain tuning, it is possible to create a new filter shape without explicit knowledge of the coupling response of the filter. The idea for this design method is to use a circuit simulator to create a filter response from a lumped element model of the desired order. This can be done by optimizing for return loss, pass band ripple, cut-off, bandwidth, among other attributes. The frequency response of the simulation can be downloaded into the network analyzer memory trace, and the time domain transform then applied. From this, a template trace is created that provides a target for tuning the coupling structures. The center frequency of the filter is simply tuned using the nulling method. Figure 8 shows two filter responses. The light trace is a simulation of an 8-pole filter, optimized to give 25 dB return loss and a 130 MHz bandwidth. The coupling coefficients and resonator tuning were variables in the optimization. The other trace is a real 8-pole filter, tuned in the time domain. This is in fact the same filter as in the previous example, but adjusted to have an 80% wider bandwidth. The coupling was tuned to match the peaks, and the resonators were tuned to maximize the nulls. This 8-pole filter with 7 adjustable couplings was tuned in about 6 minutes. The final result is remarkably close to the simulated response, especially considering that the simulated filter was a lumped element, capacitively coupled filter, and the real filter was a distributed coupled-resonator filter with inductive (B-field) coupling.

#### IV. Conclusion:

This filter tuning technique is remarkably flexible, works with a wide variety of filter and resonator structures, and can be used during both the design and manufacturing stages to gain insight into the filter behavior and to speed the final tuning process.

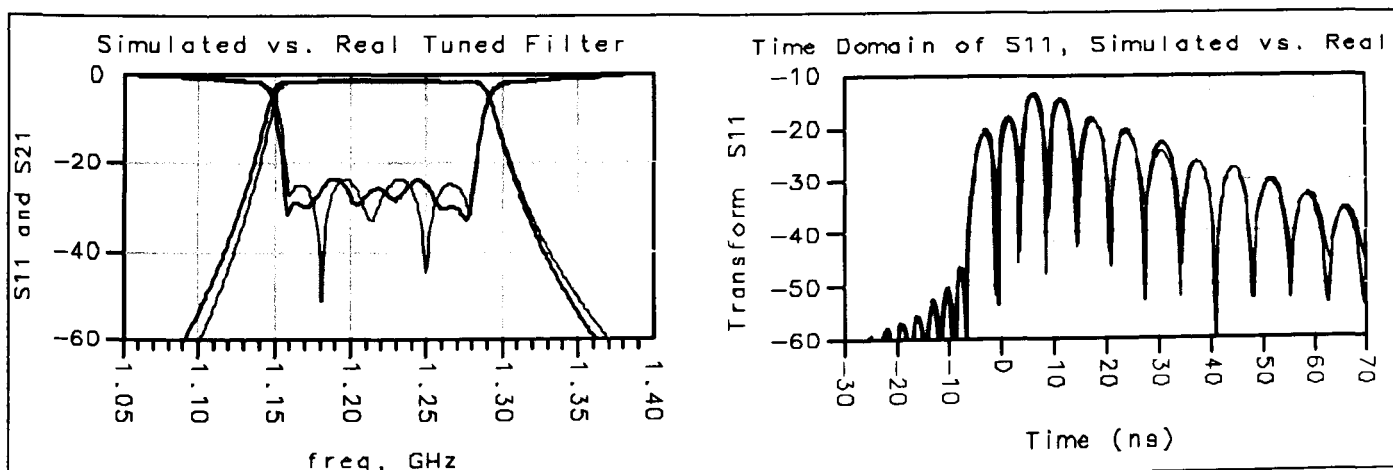


**Figure 8: Simulated filter (light trace) and real filter (dark trace) tuned match to the time domain response of the simulated filter**

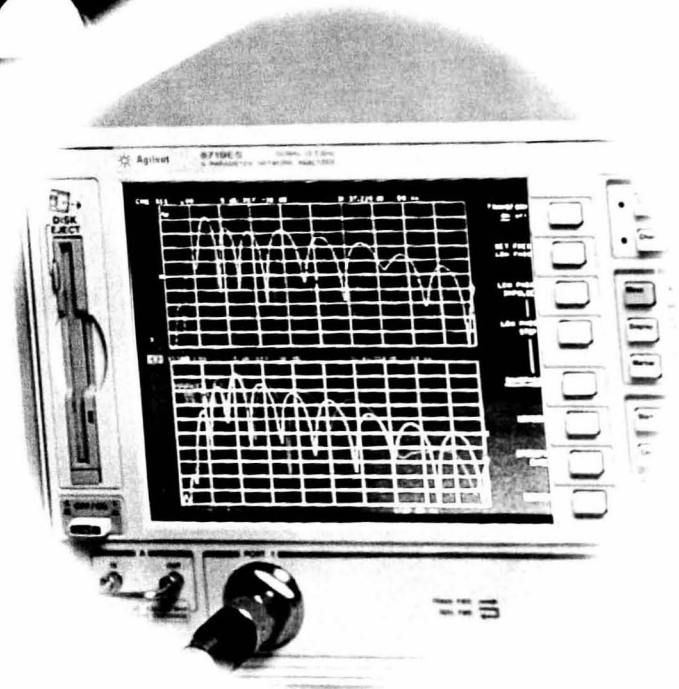
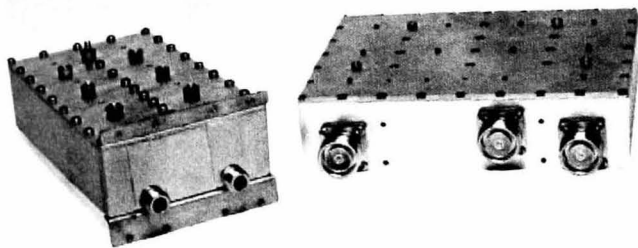
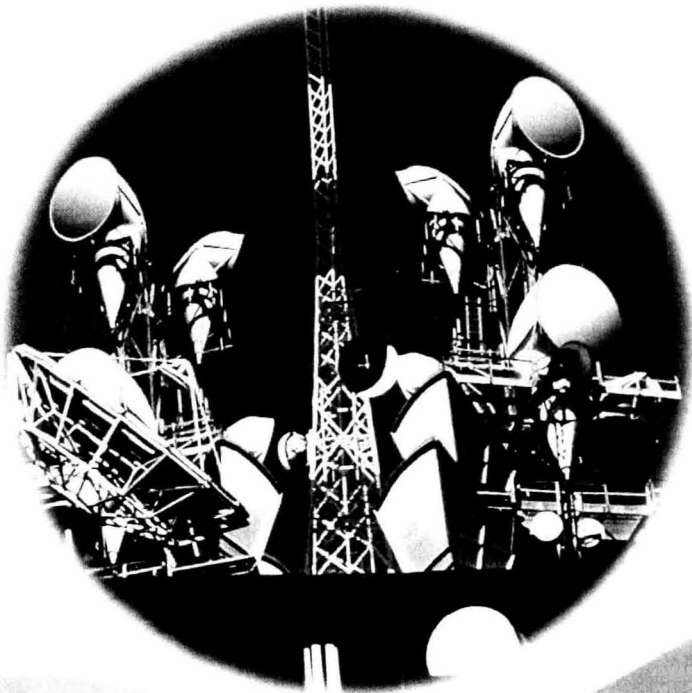
## **Paper 2**

Agilent Technologies, Application Note AN 1287-8, *Simplified Filter Tuning Using Time-domain Transforms*, Agilent part no. 5968-5328EN, 1999.

# Agilent AN 1287-8

## Simplified Filter Tuning Using Time Domain

Application Note



**Agilent Technologies**  
Innovating the HP Way

# Table of Contents

<b>3</b>	<b>Introduction</b>
3	Difficulties of filter tuning
4	Ideal tuning method
<b>5</b>	<b>Basic characteristics of bandpass filters</b>
<b>6</b>	<b>Time-domain response of simulated filters</b>
7	Effect of tuning resonators
8	Effect of tuning coupling apertures
<b>10</b>	<b>Practical examples of tuning filters</b>
10	Setting up the network analyzer
11	Example 1: Tuning resonators only
13	Example 2: Tuning to a “golden filter”
16	Example 3: Using simulated results for a template
<b>17</b>	<b>Effects of loss in filters</b>
<b>18</b>	<b>More complex filters</b>
18	Cross-coupled filters
19	Duplexers
<b>20</b>	<b>Conclusion</b>
<b>21</b>	<b>References</b>
<b>22</b>	<b>Summary: Hints for time-domain filter tuning</b>
<b>23</b>	<b>Appendix A: Understanding basic bandpass filter design</b>
<b>25</b>	<b>Appendix B: Using time-domain in the network analyzer for filter tuning</b>

# Introduction

The increase in wireless communications services is forcing more and more channels into less frequency spectrum. To avoid interference, very stringent filtering requirements are being placed on all systems. These systems usually employ coupled resonator filters to handle the power levels and provide the needed isolation. The difficulty of tuning these filters quickly and accurately often limits manufacturers from increasing their production volumes and reducing manufacturing cost.

In a coupled-resonator cavity-tuned filter, the center frequency of each resonator must be precisely tuned. The couplings between resonators must also be precisely set to achieve the proper passband response, low return loss (reflection), and small passband ripple. Setting coupling coefficients and tuning the resonators are as much art as science; often a trial-and-error adjustment process. Until now, there has been no alternative.

This application note describes a method of tuning a filter using the time-domain response of its return loss, which makes filter tuning vastly easier. It is possible to tune each resonator individually, since time-domain measurements can distinguish the individual responses of each resonator and coupling aperture. Such clear identification of responses is extremely difficult in the frequency domain. Coupling coefficients may be precisely set to provide a desired filter response, and any interaction caused by adjustment of the coupling structures and resonators can be immediately determined and accounted for.

Perhaps the most important advantage of the time-domain tuning method is that it allows inexperienced filter tuners to successfully tune multiple-pole filters after only brief instruction. Such rapid proficiency is impossible with previous tuning methods. This technique also lends itself well to the automated production environment, which has always been a challenge.

## Difficulties of filter tuning

The interactive nature of coupled-resonator filters makes it difficult to determine which resonator or coupling element needs to be tuned. Although some tuning methods can achieve an approximately correct filter response, final tuning often requires the seemingly random adjustment of each element until the final desired filter shape is obtained. Experienced tuners can develop a feel for the proper adjustments, but months are often required before a novice can be proficient at tuning complex filters. The time and associated cost of tuning, and the difficulty and cost in training new personnel can limit a company's growth and responsiveness to changing customer needs.

Some companies have attempted to automate the tuning process, using robotics to engage and turn the tuning screws, and an algorithmic process to accomplish the tuning. The tuning algorithms are a particular problem, especially when a filter is nearly tuned, at which point the interaction between stages can be so great that final tuning cannot be achieved. New filter designs may require entirely new algorithms, making it even more difficult for test designers to keep up with changing requirements. Manufacturing changes that affect the filter components, such as tool wear or changing vendors, may also cause algorithms and processes to become less effective.

In some cases, tuned filters go through temperature cycling or other environmental stress as part of the manufacturing process, and their characteristics may change as a result. It can be very difficult to identify which resonators or coupling apertures need to be retuned using conventional filter tuning methods.

### **Ideal tuning method**

The solution to these difficulties would be a tuning method that is simple, flexible, and deterministic. That is, one in which the individual adjustment goals for each tuning element, resonator, and coupling aperture would not depend upon the other elements in the filter. The response to each tuning screw would be easily identified, and any interactive effect would be immediately seen and accounted for. Ideally, each screw would only need to be adjusted once. Finally, the tuning method would not depend on filter type or shape, or number of filter poles.

This application note presents a technique that clearly identifies the resonator or coupling aperture that needs to be tuned, and enables the operator to see and correct for interactions. Filters can be tuned to match any filter shape within their tuning ranges. Although this technique does not meet the ideal goal of requiring only a single adjustment of each screw, it greatly simplifies and speeds up the filter-tuning process.

# Basic characteristics of bandpass filters

First, let's review some basic information and characteristics about bandpass filters.

Bandpass filters are commonly designed by transforming a low-pass filter response to one that is centered about some new frequency. Coupled resonators, which may be lumped LC resonators, coaxial line resonators, cavity resonators, or microwave waveguide resonators, are used to create the upward shift in frequency. The terms resonator, cavity resonator, and cavity will be used interchangeably in this application note. More details on bandpass filter design can be found in Appendix A.

The center frequency of the filter is determined by setting the resonators. In most designs, all resonators are set exactly to the center frequency, with the effects of adjacent coupling included in the calculation of the resonant frequency.

The filter shape, bandwidth, ripple, and return loss are all set by the coupling factors between the resonators. When properly tuned, the resonators have almost no effect on the filter shape. The only exception is that the input and output resonators set the nominal impedance of the filter. Usually an input or output transformer is used to match to a desired impedance. Of course, when the resonators are not properly tuned, the return loss and insertion loss will not be at the optimal levels.

Because the resonators are coupled to each other, tuning one resonator will have the most effect on the adjacent resonators, but it will also have some smaller effect on the remaining resonators. The extent of the effect depends on the coupling factor.

With this information in mind, we are ready to explore the new time-domain tuning technique.

# Time-domain response of simulated filters

To introduce this tuning method, we will use simulations to examine what happens to the time-domain response of a bandpass filter when it is tuned. We will start with a relatively simple filter: a five-pole coupled resonator filter with four coupling structures, designed for a Chebyshev response with 0.25 dB of passband ripple. In this example, a filter response will be simulated by Agilent Technologies' Advanced Design System (ADS) microwave design software, so that the exact values of constituent components are known. The frequency sweeps will be performed in the simulator, and the results will be downloaded to the vector network analyzer (VNA), where the instrument's time-domain transform application can show the effects of filter tuning. The schematic for the filter is shown in Figure 1.

To set up the measurement for time-domain tuning, the frequency sweep **MUST** be centered at the desired center frequency of the bandpass filter. This is critical, since the tuning method will tune the filter to exactly that center frequency. Next, the span should be set to approximately two to five times the expected bandwidth.

Figure 2 shows the frequency response and time response of the filter. Notice the distinctive dips in the time-domain  $S_{11}$  response of the filter. These are characteristic nulls that occur if the resonators are exactly tuned. The peaks between the nulls relate to the coupling factors of the filter, as we will see later. Markers 1 through 5 have been placed to show the characteristic dips corresponding to resonators 1 through 5 in the filter. Although there are some dips to the left of marker 1, those are not part of the filter response. Generally the peaks corresponding to the filter response will be much higher in magnitude than the ones in the  $t < 0$  region, which are not meaningful, and usually the dip corresponding to the first resonator will occur near  $t = 0$ .

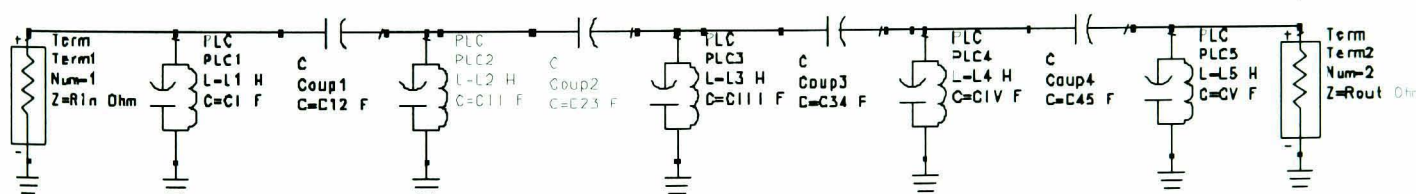


Figure 1. Schematic for five-pole coupled resonator bandpass filter

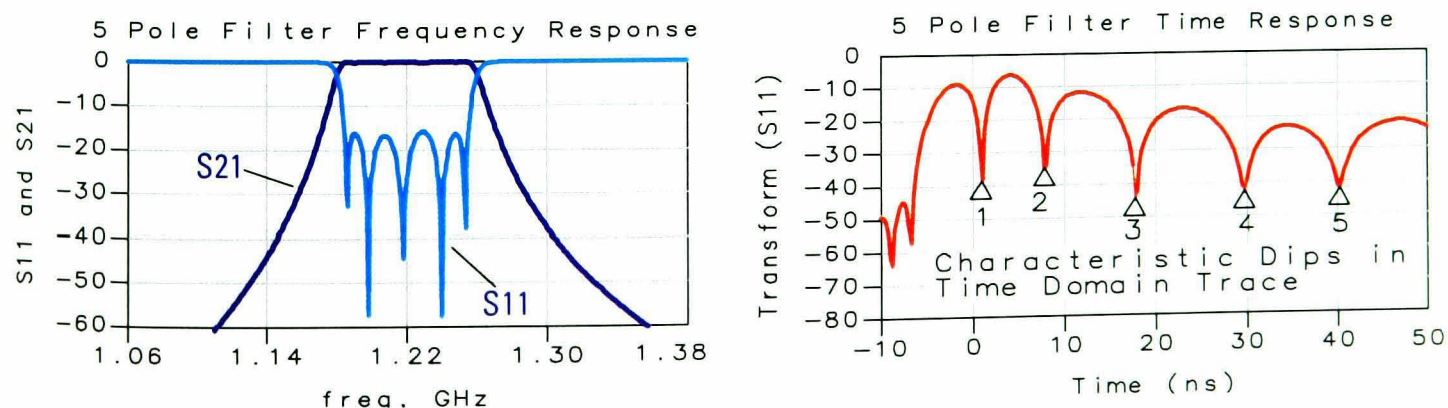


Figure 2. The frequency and time-domain response of a bandpass filter

### Effect of tuning resonators

The example filter starts out with the ideal design values, which yields the desired response since it is properly “tuned” by definition. To understand the time-domain response to tuning the resonators, we will monitor the time-domain response while changing (mistuning) the resonator components in the simulation. Figure 3 shows the time-domain traces for three conditions (with the ideal response in the lighter trace). The upper plots show the filter with the second resonator mistuned 2% low in frequency. Note that the first dip has not changed, but the second dip is no longer minimized, and neither are the following dips. If a resonator is substantially mistuned (more than 1%), it will significantly mask the dips of following resonators. Therefore, to identify the mistuned resonator, look for the first dip that is no longer at a minimum. In this case, we see that mistuning resonator 2 causes the second null to move away from its minimum value.

The lower plots show one response with only the third resonator mistuned 2% high and another one with only the fourth resonator mistuned 2% low. Again, it is easy to identify which resonator is mistuned by looking for the first dip that is no longer minimized. Additional simulations have shown that the characteristic dips are minimized only when the corresponding resonators are set to their correct values. Changing the tuning in **either** direction causes the dips to rise from the minimum values.

The key to this tuning technique is to adjust the resonators until each null is as low as possible. The adjustment will be mostly independent, although if all the resonators are far from the final value the first time through, adjusting a succeeding resonator may cause the null of the previous resonator to rise from its minimum. If this occurs, the null for the previous resonator should be optimized again. Once the succeeding resonator has been tuned and the previous one optimized, additional smaller adjustment to the second resonator will have very little effect on the dip corresponding to the first resonator.

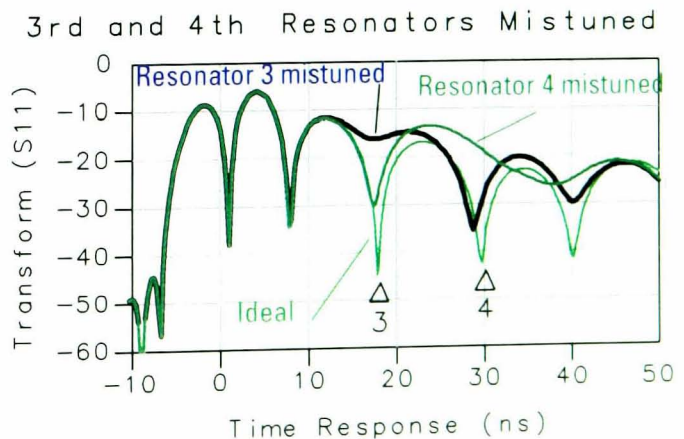
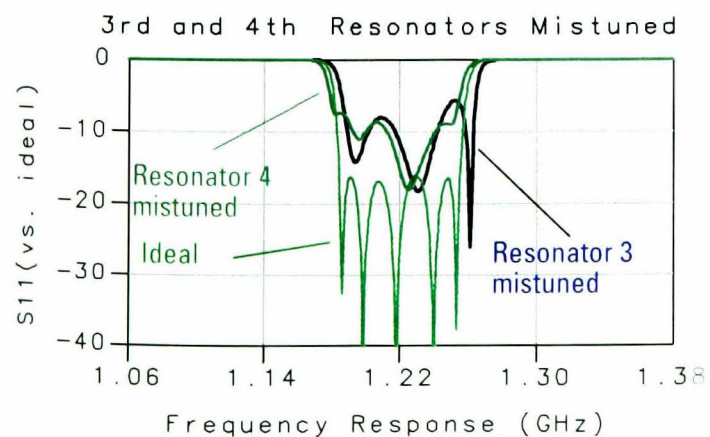
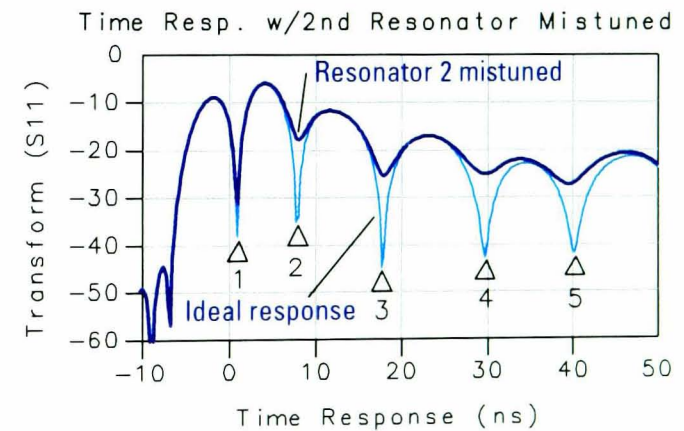
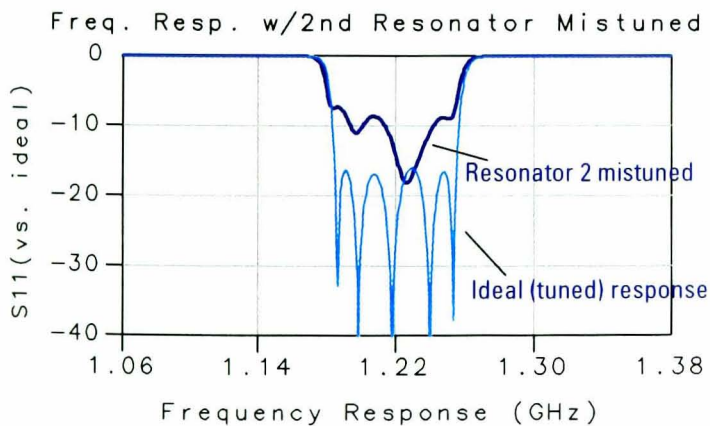


Figure 3. The response of a bandpass filter to tuning the resonators

Those who are familiar with the resolution limits of time-domain measurements will know that time-domain resolution is inversely proportional to the frequency span being measured, and they may wonder how it is possible to resolve individual resonators in a filter when the frequency span is only two to five times the filter's bandwidth. Appendix B explains how the time-domain transform relates to bandpass filter measurements in more detail.

One more thing to note from Figure 3 is that the  $S_{11}$  frequency response when resonator 2 is mistuned looks almost identical to  $S_{11}$  response when resonator 4 is mistuned. This illustrates why it can be difficult to determine which resonator requires tuning when viewing only the frequency-domain measurements.

### Effect of tuning coupling apertures

Although simple filters may only allow adjustments of the resonators, many filters also have adjustable couplings. To understand the effects of adjusting the coupling, we will go back to our original "tuned" simulated filter. First, we will examine what happens when we **increase** the first coupling factor by 10%. Figure 4 shows the  $S_{11}$  response in both frequency and time domains, both before and after changing the coupling factor. In the frequency domain, we see that the filter bandwidth is slightly wider and the return loss has changed. This makes intuitive sense, because increasing the coupling means more energy should pass through the filter, resulting in a wider bandwidth.

In the time-domain, there is no change in the first peak, but the second peak is smaller. While it might seem that the first peak would be associated with the first coupling factor, remember that the first coupling factor comes after the first resonator in the filter, and we have already seen that the first dip after the first peak is related to the first resonator. It turns out that the first peak can be associated with the input coupling, which has not been adjusted in this filter.

The reduction in height of the second peak when coupling is increased makes sense, because increasing the coupling means more energy is coupled to the next resonator. Thus less energy is reflected, so the peak corresponding to reflected energy from that coupling should decrease. Note that the following peaks are higher than before. More energy has been coupled through the first coupling aperture, so there is more energy to reflect off the remaining coupling apertures.

It is important to recognize that changing the first coupling factor will affect the responses of all the following peaks. This suggests that coupling factors should be tuned starting with the coupling closest to the input and moving towards those in the center of the filter. Otherwise, improperly tuned coupling near the input can mask the real response of the inner coupling factors.

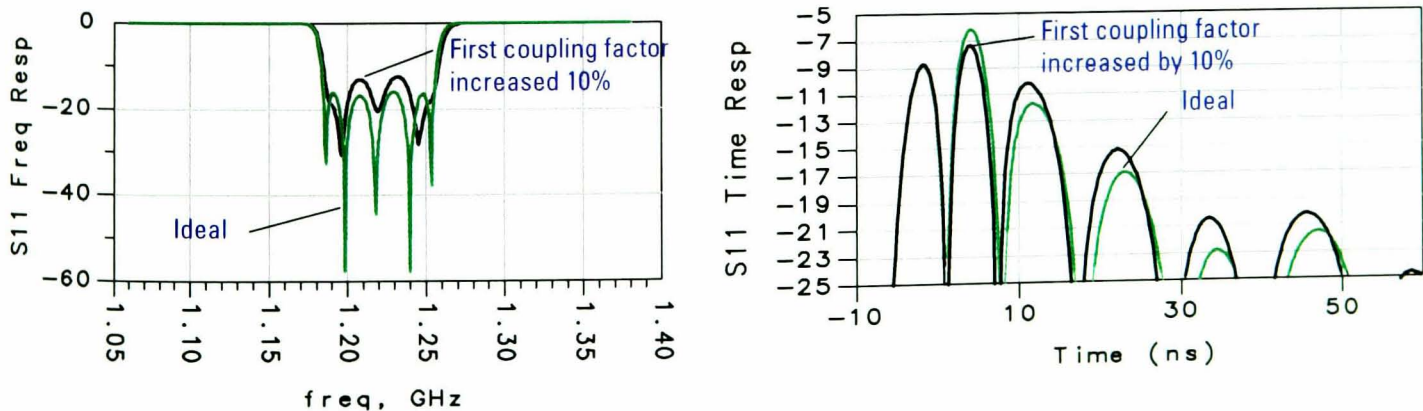


Figure 4. Effect of increasing first coupling factor (darker trace is after adjustment)

Now consider what happens if we take the original filter and **decrease** the second coupling coefficient by 10%. Figure 5 shows that in the frequency domain, the bandwidth of the filter has been reduced slightly and the return loss has changed. Again, this makes sense because decreasing the coupling means less energy will pass through the filter, corresponding to a narrower bandwidth.

Examining the time-domain trace, we see no change in the first 2 peaks, but the third peak is higher, consistent with more energy being reflected as a result of the decreased coupling. Since the amount of energy coupled to the following resonators and apertures is reduced, the following peaks are all lower in value. Note how well the time-domain response separates the effects of changing each coupling, allowing the couplings to be individually adjusted. In contrast, the  $S_{11}$  frequency response trace in Figure 4 is very similar to the one in Figure 5, so it would be very difficult to know which coupling changed from looking at the frequency-domain response.

Thus, we have seen that the coupling factor can be related to the height of the time-domain reflection trace between each of the resonator nulls. The exact relationship also depends on the ratio of the filter bandwidth to the frequency sweep used to compute the time-domain transform. The wider the frequency sweep (relative to the filter's bandwidth), the more total energy is reflected, so the higher the peaks.

The magnitudes of the peaks are difficult to compute because changing the coupling of one stage changes the height of the succeeding peaks. A detailed explanation of relationship between the time-domain response and coupling coefficients is beyond the scope of this application note. Even though it may not be easy to calculate these peaks simply from the coupling coefficients, once the desired values of the peaks are determined, the apertures may be tuned directly in the time domain. One method for determining the desired magnitudes of the peaks is by using a template as described in the next section.

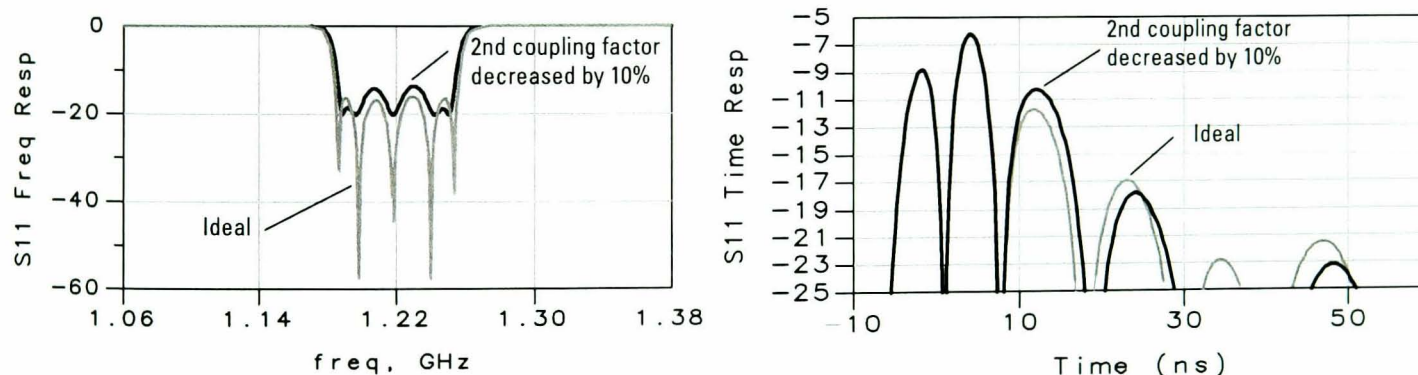


Figure 5. Effect of decreasing second coupling factor (darker trace is after adjustment)

## Practical examples of tuning filters

Now that we have an understanding of the relationship between tuning resonators or coupling apertures and the corresponding results in the time-domain response, we are ready to put the theory into practice.

For multi-pole cavity filters that have fixed apertures, it is only necessary to tune for the characteristic dips in the time domain in order to achieve optimal tuning of the filter. To tune a filter with variable coupling coefficients, it is easiest to tune the coupling to a target time-domain trace or template. This target time-domain response for any filter type may be determined in several ways. One method is to use a “golden” standard filter that has the same structure and is properly tuned for the desired filter shape. This filter can be measured and the data placed in the analyzer’s memory. Each subsequent filter can be tuned to obtain the same response.

An alternative is to create a filter from a simulation tool, such as Agilent’s Advanced Design System. The simulated response can be downloaded into the network analyzer and used as a template. This is a very effective approach, as there is great flexibility in choosing filter types. The only caution is that each real filter has limits on the  $Q$  of the resonators and the tuning range of the coupling structures and resonators. It is important to make the attributes of the simulation consistent with the limitations of the structures used in the real filters.

In this section, we will begin with a discussion of how to set up the network analyzer to tune band-pass filters in the time domain, and then we will show three examples to illustrate how to tune both resonators and coupling apertures in real filters.

### Setting up the network analyzer

It is essential to set the center frequency of the analyzer’s frequency sweep to be equal to the desired center frequency of the filter, since tuning the filter in the time domain will set the filter’s center to this frequency. Choose a frequency span that is 2 to 5 times the bandwidth of the filter. A span that is too narrow will not provide sufficient resolution to discern the individual sections of the filter, while too wide a span will cause too much energy to be reflected, reducing the tuning sensitivity.

The primary parameter to be measured is  $S_{11}$  (input match). However, for time-domain responses more than halfway through the filter, the responses often get more difficult to distinguish. Even in low-loss filters, there can be significant return loss differences between the input and output due to loss in the filter. In addition, there is a masking effect that tends to make reflections from couplings and resonators farther from the input or output appear smaller, since some of the incident energy has been lost due to earlier reflections in the device. For these reasons, the most effective way to tune is to look at both sides of the filter at once, so a network analyzer with an S-parameter test set is recommended. To aid in tuning, the instrument’s dual-channel mode can be used to measure the reverse return loss ( $S_{22}$ ) on a second channel. With this setup, you will tune the first half of the resonators and couplings using the  $S_{11}$  response, and tune the remaining ones using the  $S_{22}$  response. Keep in mind that you need to count resonators and coupling apertures starting from the port where the signal is entering the filter for that measurement. Thus for  $S_{11}$ , the first dip would correspond to the resonator closest to the input port of the filter. For  $S_{22}$ , the first dip would correspond to the resonator closest to the output port of the filter.

For the network analyzer time-domain setup, the bandpass mode must be used. The start and stop times need to be set so that the individual resonators can be seen. For most filters, the start time should be set slightly before zero time, and the stop time should be set somewhat longer than twice the group delay of the filter. If the desired bandwidth is known, the correct settings can be approximated by setting the start time at  $t = -(2/\pi BW)$  and the stop time at  $t = (2N+1)/(\pi BW)$ , where  $BW$  is the filter's expected bandwidth, and  $N$  is the number of filter sections. This should give a little extra time-domain response before the start of the filter and after the end of the filter time response. If you are tuning using both the  $S_{11}$  and  $S_{22}$  responses of the filter, you can set the stop time to a smaller value, since you will use the  $S_{22}$  response to tune the resonators that are farther out in time (and closer to the output port).

The format to use for viewing the time-domain response is log magnitude (dB). It may be helpful to set the top of the screen at 0 dB.

### Example 1: Tuning resonators only

The first example is a simple five-pole cavity filter with fixed apertures, so only the resonators can be tuned to adjust the center frequency. This filter has a center frequency of 2.414 GHz and a 3 dB bandwidth of 12 MHz. The network analyzer is set up for this same center frequency and a span of 50 MHz. Dual channel mode is used to display both  $S_{11}$  and  $S_{22}$ . The time-domain response is set up to sweep from -50 ns to 250 ns.

Experience has shown that it is best to begin tuning from the input/output sides and move toward the middle. Figure 6 shows the time-domain response after the first and fifth resonators have been tuned to obtain the lowest dips. Note that the first resonator closest to the input corresponds to the first dip in  $S_{11}$ , while the fifth resonator, which is the first one when looking in the reverse direction, corresponds to the first dip in  $S_{22}$ . These responses are good illustrations of masking. Even though the fifth resonator is correctly tuned, you cannot see that from looking at the  $S_{11}$  response. Similarly, you cannot see that the first resonator is tuned by looking only at the  $S_{22}$  response.

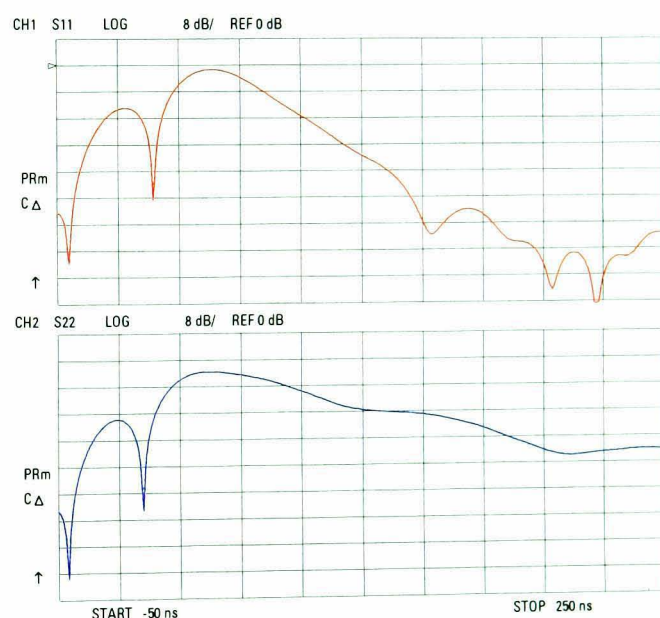
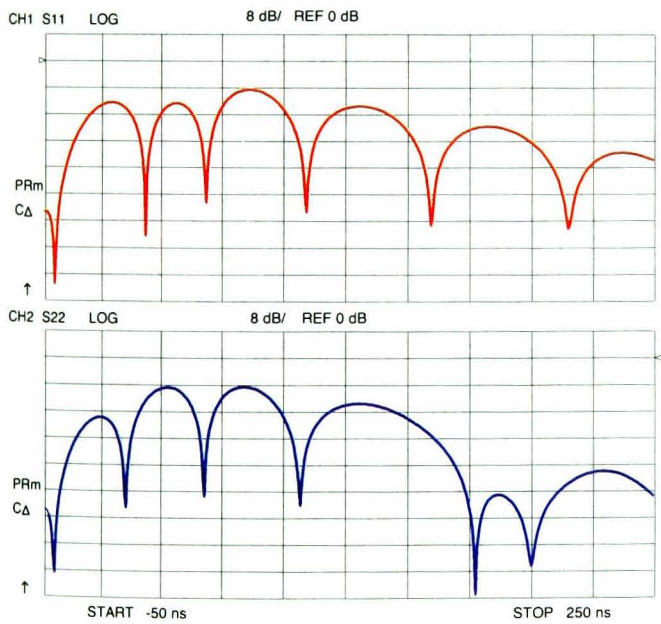
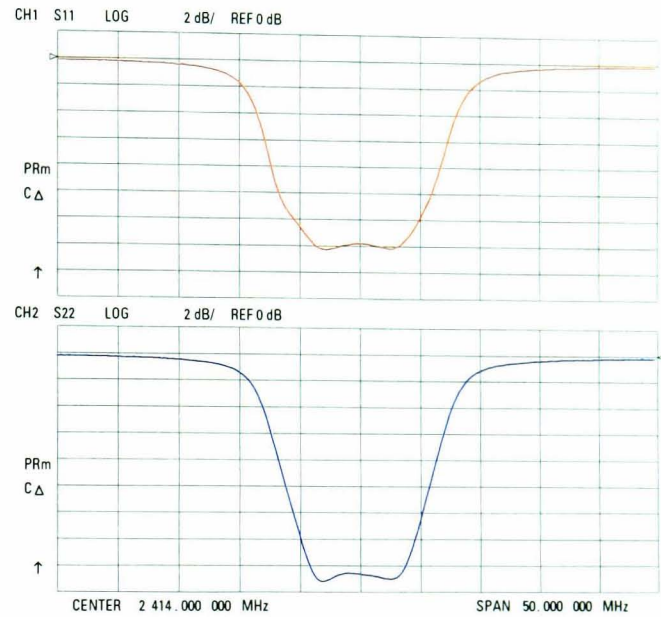


Figure 6. Time-domain response of 5-pole filter after tuning resonators 1 and 5

Next, we tune the second resonator, readjusting the first one as needed to keep its dip minimized. Then we go back to the output side and tune the fourth resonator, readjusting the fifth one as needed. Finally, we tune the third resonator in the middle, readjusting the second and fourth resonators as needed. It may be necessary to go back and readjust each of the resonators again to fine-tune the response. Figure 7 shows the time-domain response after the filter has been tuned. Figures 8 and 9 show the frequency domain reflection and transmission responses. Note that the center frequency has been set precisely to 2.414 GHz without looking at the frequency domain while tuning. With frequency domain tuning methods, it is often possible to tune the filter to have the correct shape while the center frequency is slightly off. The time-domain tuning method centers the filter very accurately.



**Figure 7. Time-domain response of 5-pole filter after tuning all resonators**



**Figure 8. Final reflection frequency response**

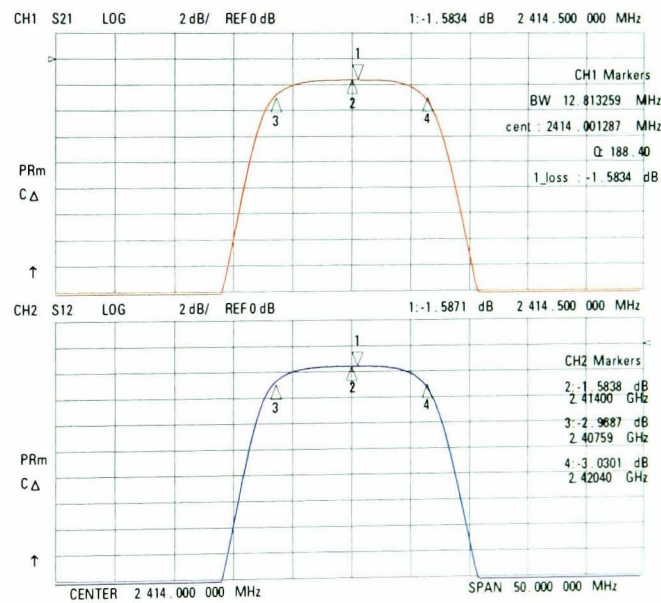


**Figure 9. Final transmission frequency response**

Now, what if we want to change the center frequency of the filter, for example to 2.42 GHz? We simply need to repeat the tuning process with the analyzer's center frequency set to the new frequency. Figure 10 shows the time-domain response (in bold) that results from measuring the 2.414 GHz filter after changing the network analyzer's center frequency to 2.42 GHz. The original time-domain response is shown in the lighter trace. It is clear that the resonator dips are no longer at their minimums, so the resonators need to be retuned. Adjusting the resonators to minimize the dips again will result in a filter tuned to a center frequency of 2.42 GHz.

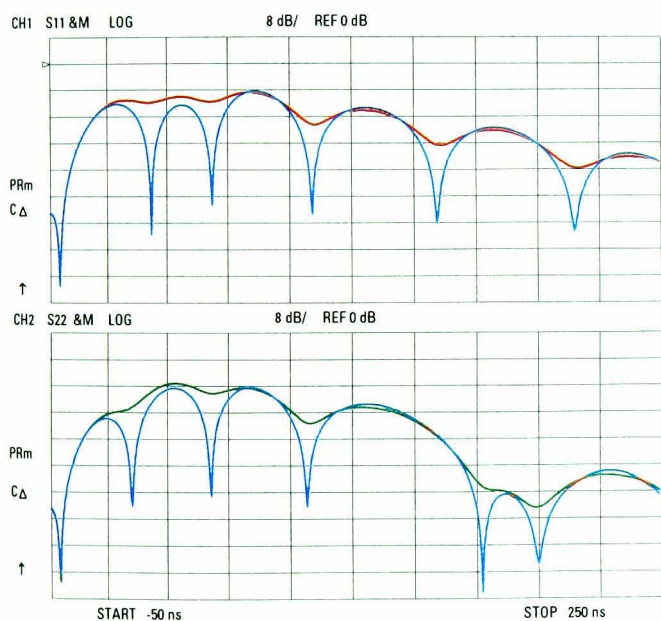


**Figure 10. Time-domain response with center frequency changed**

### Example 2: Tuning to a “golden” filter

The second example uses a filter that has eight poles with seven tunable interstage coupling structures, along with input and output coupling. In the discussion that follows, we use a “golden” filter that was tuned by an experienced engineer to obtain the desired frequency response and return loss. A second, untuned test filter, shown in Figure 11, was used as a test example. Figure 12 shows the time-domain and frequency-domain plots of both filters. A four-parameter display mode is used to show both the  $S_{11}$  and  $S_{22}$  (input and output return loss) in both the time and frequency domains.

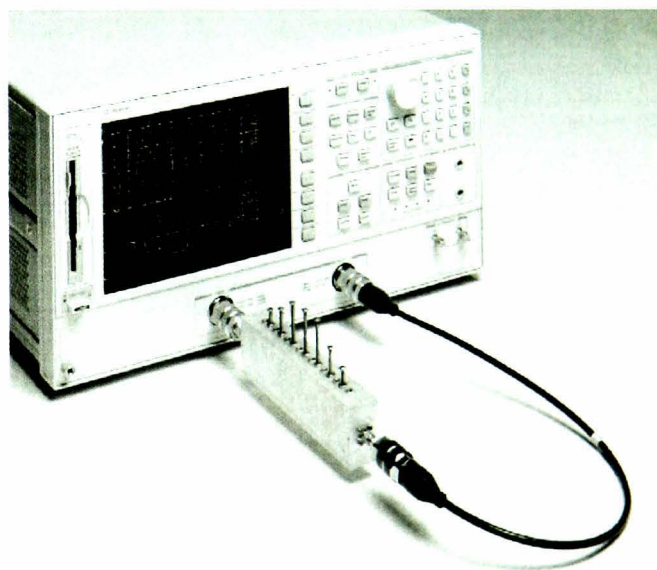


**Figure 11. Eight-pole, seven-aperture filter used for Examples 2 and 3**

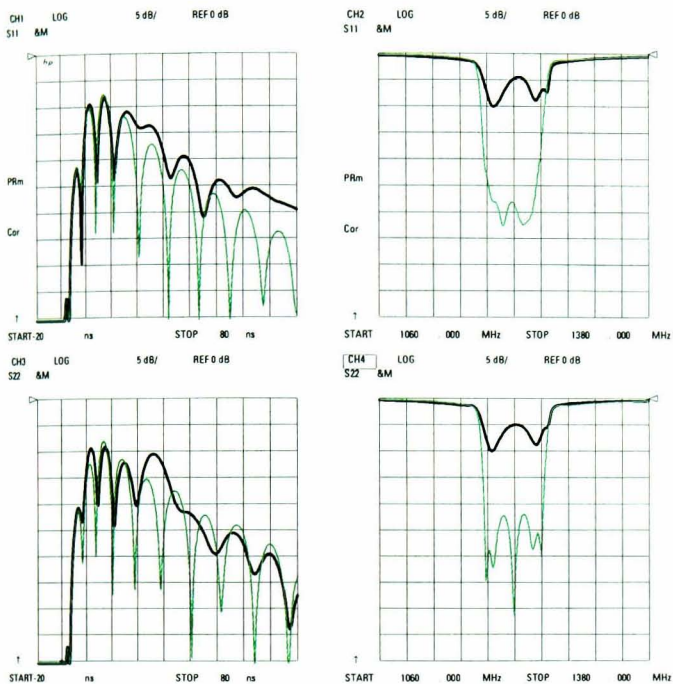


**Figure 12. The response of a "golden" filter (lighter trace) and an untuned filter of the same type (darker trace)**

The test filter was pre-tuned by arranging the coupling screws (the long screws in the picture) to about the same height as the "golden" filter. Such pre-tuning is commonly done to get the coupling apertures closer to the correct value before beginning to tune, but it doesn't work for situations where a previously tuned filter is not available.

The first step in tuning this filter is to assume that the inter-stage coupling is close to correct, and adjust the resonators to optimally tune the filter without adjusting the coupling screws. The setup for this filter is a center frequency of 1220 MHz and a span of about 320 MHz. The filter bandwidth is about 80 MHz, so the time domain is initially set up from about -8 ns ( $-2/\pi BW$ ) to about 70 ns ( $(2N+1)/\pi BW$ ). After the first tuning, -20 ns and 80 ns are determined to be a good choice for time settings.

Following example 1, each of the eight resonators are tuned, starting with the two outside resonators and continuing until the center resonators are tuned. Each is tuned by minimizing the response (making the deepest dip). Again we begin by first tuning the two outside resonators (numbers one and eight), looking at both  $S_{11}$  and  $S_{22}$ , then retuning them after the next inside resonators (two and seven) are tuned. After the third set of resonators are tuned (three and six) the second resonators (two and seven) are re-tuned. This continues one more time for the fourth and fifth resonators. After this initial tuning is complete, the filter exhibits a very nice frequency response (Figure 13), but does not match the desired response. Now it is time to tune the coupling structures.

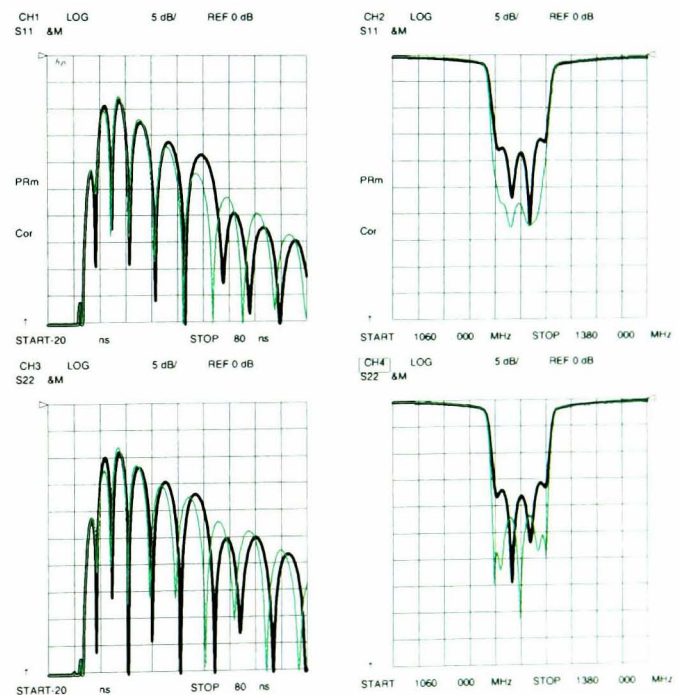


**Figure 13. The response of a "golden" filter (lighter trace) and a filter where only the resonators are tuned (darker trace)**

To tune the coupling structures, the scale can be changed so that it is easy to see the peaks of the time-domain response. For this example, four-parameter display capability is used to show the time domain in full scale with a close-up view of the peaks. With this display it is easier to adjust both the peaks and the dips. To tune the coupling, start by tuning the coupling apertures that are closest to the input and output of the filter and work towards the center, to avoid masking effects from improperly tuned outer couplings. Turn the screw in to increase the coupling (reduce the peak). After each coupling screw is adjusted, readjust the resonators on each side to make the dip as low as possible, starting from the outside and working in. Figure 14 shows the result after the first pass of adjusting the coupling structures and resonators from the outside in.

This filter response is nearly identical to the template filter. The coupling (and hence return loss) is not symmetrical for input and output, but it is also not symmetrical for the “golden” filter used as a template. If the filters had no loss, the input and output match would be the same. The loss in the filter causes the input match to be different from the output match. It is possible to tune this filter to have exactly the same input and output match, but with a lossy filter, one match may be improved only at the expense of the other.

Also, note that the filter tuned in the time domain has better return loss than the “golden” filter, and that from the time-domain trace, we can see that the first resonator is not optimally tuned according to the time-domain tuning process, even though the filter has been tuned by an expert.

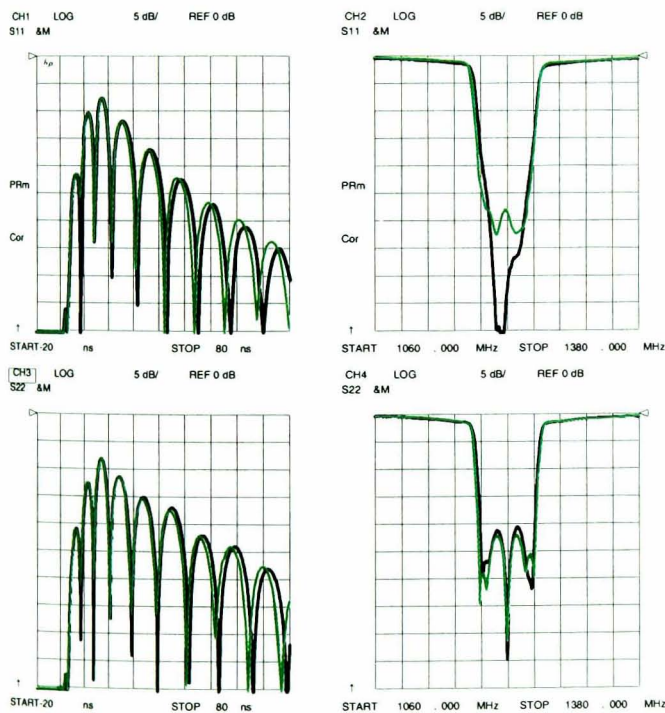


**Figure 14. The response of a “golden” filter (lighter trace) and another filter with both couplings and resonators tuned (darker trace)**

### Example 3: Using simulated results for a template

Using a simulated filter response to create a template for tuning the filter is the basis for the final example of tuning. An ideal eight-pole Chebyshev filter is simulated, and any value can be chosen for bandwidth or ripple. For this filter, a wider bandwidth with larger ripple was chosen. We will attempt to tune the same filter used in example 2 to yield this new filter shape. Since the example filter does not have adjustable input and output coupling, there are limits on the filter shape that can be achieved. In this case, the bandwidth was fixed, and a return loss value that yields the same value for input coupling in the time domain as that of the example filter was chosen.

The frequency response of the simulation was downloaded into the network analyzer and used as a template. In the simulation, loss was added to the resonator structures to approximate the total loss of the real filter. This allows the  $S_{11}$  and  $S_{22}$  from the simulation to better match the actual time-domain response of the filter. The effects of loss are discussed in more detail in the next section.

Each coupling aperture and resonator is tuned to achieve the same time response as the simulated template, following the procedure described in Example 2. The last coupling structure is not tunable, but it is close enough to avoid distorting the overall response.

Figure 15 shows the result with the simulated trace, and the final tuned filter. The results are remarkably close, considering that the filter was tuned only in the time domain, and that the simulation used capacitively-coupled lumped elements, while the real filter had magnetically coupled distributed elements. Using this technique, virtually any filter shape that can be simulated can be used as a template for a real filter that can be easily and deterministically tuned, as long as the filter elements have the tuning flexibility. Even inexperienced tuners can follow this simple tuning technique because each coupling and resonator structure can be distinguished in the time domain.

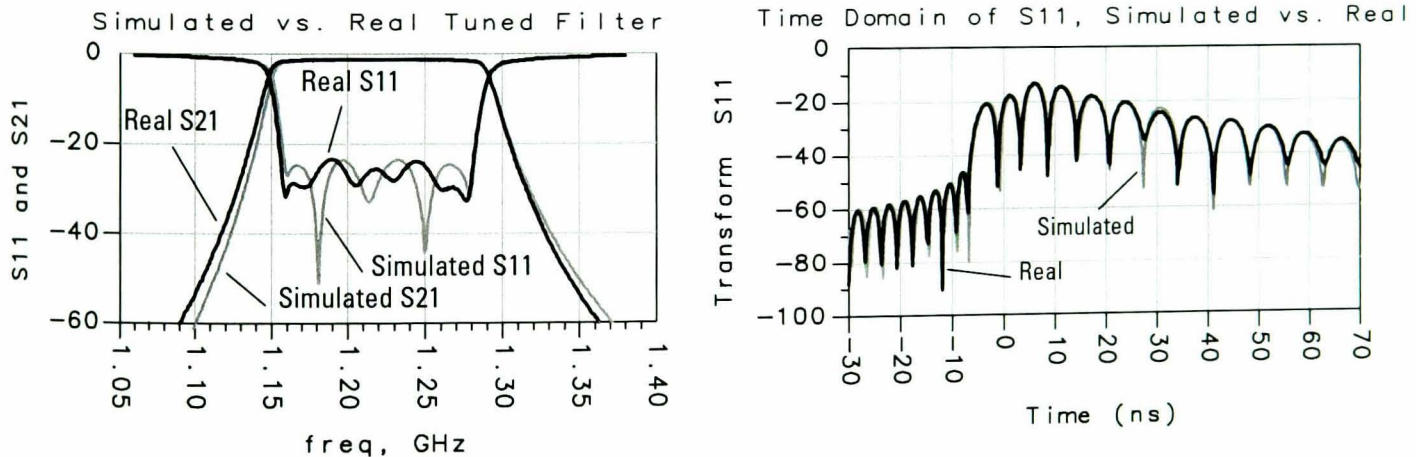


Figure 15. An example of a simulated filter and a real filter tuned to match the time-domain response.

## Effects of loss in filters

Earlier, there was a caution about considering the effects of loss when using simulation to generate the time-domain trace. A lossy filter has peaks in the time-domain trace that are lower than those of a lossless filter, and the differences in the peak levels are greater for the apertures that are farther into the filter. Therefore, tuning a lossy filter to a template based on the simulation of a lossless filter will probably result in incorrect settings of the coupling factors.

Trying to set the coupling apertures in the lossy filter to match the template of a lossless filter requires increasing the peaks in the time-domain trace higher than the proper value, so the coupling must be reduced to get more reflection. Usually it will not be possible to match all of the peaks, especially the ones for the apertures that are farther into the filter, because as we observed earlier in Figure 5, decreasing one coupling factor will cause the corresponding peak to increase, but the following peaks will all decrease.

In the frequency domain, the result is that you may be able to achieve a similar return loss, but the filter will be narrower due to the higher reflection, as shown in Figure 16.

For many cases, filter loss may be ignored, but for higher-order filters, it may be necessary to include the loss of each resonator in the model. Further, while many simulators allow loss to be applied to filter shapes, they do not distribute the loss throughout the filter. Thus, to properly account for loss, it may be necessary to create a filter structure using lossy resonators with discrete coupling in between.

To match a filter's return loss to a lossless filter simulation, it may be necessary to tune a lossy filter primarily from the  $S_{11}$  (input) side. The loss of the filter will cause the  $S_{22}$  time-domain response to differ from the  $S_{22}$  of a lossless simulated filter. Since the forward reflection and transmission ( $S_{11}$  and  $S_{21}$ ) are more important in most cases, tuning from the  $S_{11}$  side will provide better results.

If a template for a lossless filter must be used, you may need to adjust the coupling apertures so they don't completely match the peaks; that is, allow them to be a little lower to account for the loss in the filter.

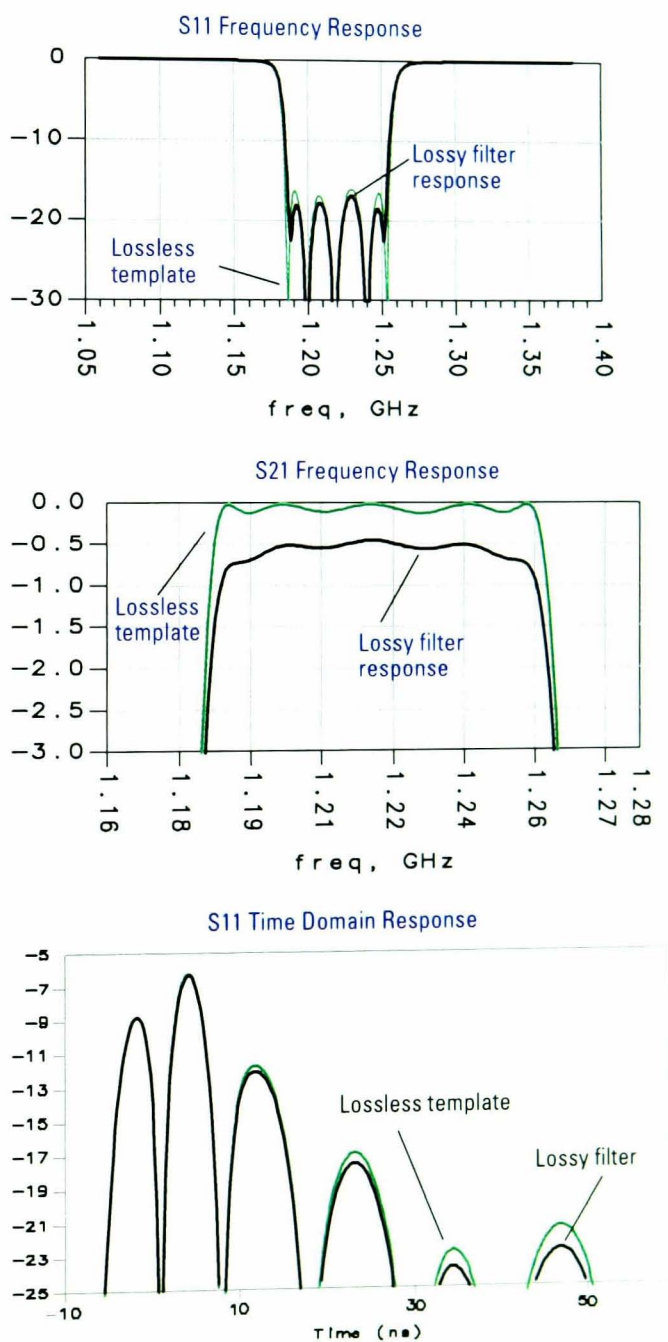


Figure 16. Comparison of lossless and lossy filters

# More complex filters

## Cross-coupled filters

Finally, many filters are more complex than the traditional all-pole filters. Cavity-resonator filters often have “cross-coupling” that effectively adds one or more transmission zeros, similar to an elliptic-filter response. If these zeros, which create very narrow isolation regions in the transmission response, are close to the filter passband edges, they can distort the time-domain filter response so that it no longer shows a deep null associated with the resonator near the structure that creates the zero. In general, the resonators that are not cross-coupled can still be tuned using the nulling technique described earlier. But what about the cross-coupled resonators?

Some filters have transmission zeros that are symmetrical as shown in Figure 17; the response from the zeros can be seen on both sides of the passband. These filters can usually be tuned with the methods previously described. The symmetry of the zeros keeps the cross-coupled resonators at approximately the same frequency as the other resonators, so all of the resonators can be tuned close to their proper values by tuning for deep nulls in the time-domain response.

Some fine-tuning may be necessary, either by tuning in the frequency domain, or by using the techniques described in the next section.

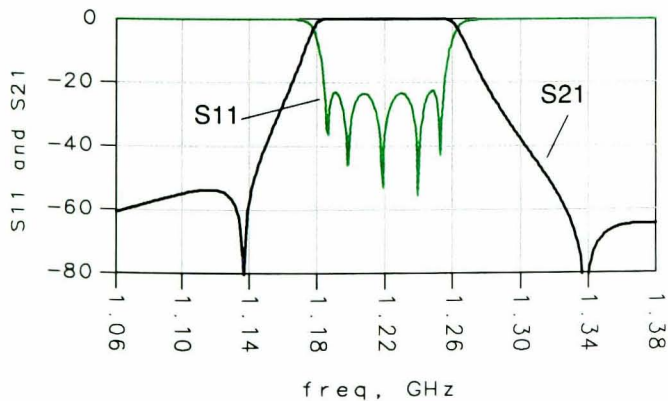


Figure 17. Transmission and reflection responses of a filter with symmetrical transmission zeros

For filters that have asymmetrical zeros as shown in Figure 18, the resonators that are cross-coupled do not have the same frequency as the other resonators, so the dips in the time-domain response that correspond to these resonators will not be minimized when viewed with the network analyzer's center frequency set to the filter's center frequency. Tuning the resonators to a template may not yield the correct response, because there is more than one setting of the tuning screw that can yield the same amplitude response. Recall that when we were discussing the time-domain response of a simulated filter, we found that tuning the resonator either too high or too low will both cause the dip to rise up from the minimum value. The setting is unique only when you are tuning for a null. However, we can modify the time-domain filter tuning technique to account for this.

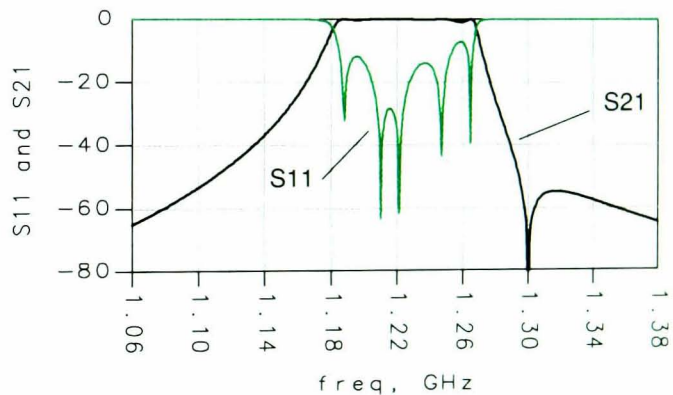


Figure 18. Transmission and reflection responses of a filter with asymmetrical transmission zeros

Recall that the all-pole filters we've been examining have resonators that are all tuned to the same frequency, with the effects of coupling included. We set the network analyzer's center frequency to that frequency, and when we look at the reflection response in the time domain, we get nulls corresponding to each resonator when that resonator is set to the analyzer's center frequency. For filters with asymmetrical responses, if we can determine the correct frequency of the cross-coupled resonators, we should be able to set the analyzer's center frequency to that new value, and tune the dip corresponding to the cross-coupled resonator to its minimum value to properly tune the resonator. Now the challenge is how to determine the correct frequency of the cross-coupled resonators.

One way is to calculate the correct frequency mathematically based on the filter design. Simulation tools can be very useful for doing this.

An alternative method is to derive the information empirically using a “golden” or template filter. You can set up the analyzer for a frequency sweep on one channel and the time-domain response on another channel. Identify the dip in the time-domain trace corresponding to the cross-coupled resonator. Watch the change in this dip as you slowly vary the center frequency of the analyzer’s sweep. You should see the dip reach a minimum when the analyzer’s center frequency is set to the correct frequency for that resonator. Use this information to set up a new instrument state for use in tuning that particular resonator. All of the resonators that are not cross-coupled will probably still need to be tuned with the analyzer’s center frequency set to the filter’s center frequency. However, depending on the coupling, a cross-coupled resonator may also pull the frequency of its adjacent resonators slightly off from the filter’s center frequency, so you may need to find the correct frequencies for some of the neighboring resonators using this method as well.

In general, cross-coupling will not have much impact on tuning the coupling apertures, since the amount of cross-coupling tends to be light and has minimal effect on the peaks in the time-domain response corresponding to the coupling apertures.

For filters with cross-coupled resonators, the recommended order of tuning is:

1. Start out with the coupling screws pre-tuned (to match the physical settings of a “golden” filter), as described in Example 2.
2. Set the analyzer’s center frequency to the filter’s center frequency and tune all of the resonators to minimize the dips to get all of the resonators close to the proper settings, ignoring the error for the cross-coupled resonators for now.

3. Tune the coupling apertures to match the time-domain response to the template values.

4. Go back and fine-tune the cross-coupled resonators and any other resonators that need to be tuned to a frequency other than the filter’s center frequency.

## Duplexers

Tuning duplexers using the time domain can be a problem if the passbands are too close together. If the passbands are separated by at least one bandwidth, and you can set up the analyzer for a span of at least two times the bandwidth without seeing the other filter, you should be able to tune the duplexer using the techniques described in this application note. If the passbands are closer than one bandwidth apart, you will get interference from the response of the other filter, and you may not be able to clearly distinguish the responses due to individual resonators in the time domain. In this case, you may be able to partially tune the filter using time domain, but you will need some other method to complete the tuning.

Many duplexers have common elements (one or more resonators) in the antenna path that will form part of the response for both the Tx-Ant and the Ant-Rx paths. To tune these resonators, it may be necessary to set their frequencies to the center frequency **between** the Rx and Tx bands, instead of tuning them to the center frequency of either passband.

Both cross-coupled resonator filters and duplexers are more advanced topics that require more research. Further refinement of time-domain filter tuning techniques for dealing with such filters is currently under development.

## Conclusion

While various techniques to simplify the process of filter tuning have been tried, until now, none have succeeded fully because coupled-resonator filters are inherently resistant to techniques that cannot account for characteristics such as coupling interaction. The method described in this application note goes a long way toward solving this problem. It allows coupling apertures to be tuned to match any filter shape within their tuning ranges, and resonators to be adjusted to provide a perfectly matched filter, with interaction immediately seen and corrected.

While a better understanding of some types of filters such as cross-coupled filters is needed, this technique already shows enough promise in allowing filters to be tuned easily that the current trend to automate filter tuning on the production line may not be needed. Alternately, this time-domain tuning may allow automation to become practical for the first time. It certainly makes it easier to train inexperienced filter tuners quickly. These attributes alone make the technique worthy of implementation and further study.

## References

*The Fourier Transform and Its Applications*, second edition, Ronald N. Bracewell, McGraw-Hill, 1978.

*Electronic Filter Design Handbook*, (Chapter 5), Williams and Taylor, McGraw-Hill, 1988.

*Filtering in the Time and Frequency Domains*, Blinchikoff and Zverev, John Wiley & Sons, 1976.

"Simplify Filter Tuning in the Time Domain," Joel Dunsmore, *Microwaves and RF*, March 1999, pp. 68-84

## Summary: Hints for time-domain filter tuning

- Set the center frequency of the network analyzer equal to the desired center frequency for the filter.
- Set the frequency span to be 2 to 5 times the bandwidth of the filter.
- Use 201 points in the sweep for a good compromise between sweep speed and resolution.
- Measure  $S_{11}$  on one channel and  $S_{22}$  on the other channel. If desired, 4-parameter display can be used to view both the frequency- and time-domain responses at once. Viewing both domains while tuning may provide better insight for optimizing the filter's response.
- Select the bandpass time-domain transform.
- In the time domain, choose the start limit to be about one resonator's delay on the minus side; approximately  $t = -(2/\pi BW)$ . Choose a stop limit of about 2 to 3 times the full filter's delay; approximately  $t = (2N+1)/(\pi BW)$ , where  $N$  is the number of filter sections (resonators) and  $BW$  is the filter's 3 dB bandwidth in Hz.
- Use log magnitude format (dB), and set the reference position to 10 (top of the graticule) and the reference value to 0 dB.
- If the filter has tunable apertures, set the coupling screws approximately correct; for example, by adjusting them to the same physical height as those on a "golden" filter.
- Tune the resonators first, adjusting for deepest dips in the time-domain trace. Start with the resonators at the input and output sides and work towards the middle.
- Tuning one resonator may cause the previous resonator to become slightly untuned. In this case, go back and retune the previous resonator, then optimize the current resonator again.
- Tune the coupling apertures from the input and output sides first and work towards the middle. After adjusting each coupling screw, readjust the resonators on each side to make the dips as low as possible.
- If the filter has cross-coupled resonators, fine-tune the cross-coupled resonators to their correct frequencies.
- Repeat the tuning process at least once to fine-tune, or as needed to achieve desired response.

# Appendix A: Understanding basic bandpass filter design

Many bandpass filters are designed by starting with a low-pass prototype that has the desired characteristics, such as passband ripple, input return loss, or stop-band rejection. The values for the prototype low-pass filter elements that are necessary to obtain these characteristics may be found in most filter design books (see References). This prototype low-pass filter can be transformed into a bandpass filter by changing the inductors and capacitors into LC circuits, with the center frequency of each LC circuit at the desired bandpass filter center frequency. Figure 19 shows an example of a prototype 3-element low-pass filter with the corresponding bandpass filter structure. The equations for calculating the values of the filter elements are also found in most filter design books.

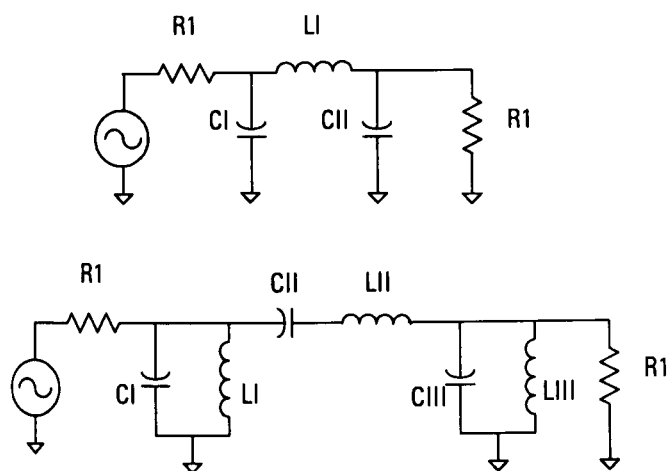


**Figure 19. 3-element prototype low-pass filter and corresponding bandpass filter**

This design technique results in filters that approximately retain the desired filter shape. However, many narrowband (less than 10% bandwidth relative to the center frequency) bandpass filters designed with this method end up with LC elements that cannot be realized. For these narrowband filters, an alternative design technique has been developed that uses coupled resonators as the main elements. With this technique, each resonator is tuned to the filter's center frequency, with the effects of the adjacent coupling elements included. The resonator's center frequency is calculated by treating the adjacent coupling capacitors as though they were shorted to ground, so that the capacitances will be in parallel with the capacitance in the resonator. Figure 20 shows the bandpass filter from Figure 19 transformed into its equivalent coupled-resonator structure.

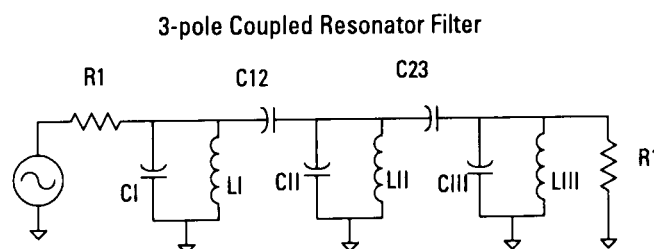


**Figure 20. Equivalent 3-pole coupled resonator filter**

A second aspect of the coupled-resonator design technique is that any changes in filter type and order affect only the coupling factor between the resonator structures. Thus the filter shape, bandwidth, ripple, and return loss depend only on the coupling between resonator sections, when the resonators have been properly tuned. These filters retain the shape factors of the prototype low-pass filter.

A circuit simulation program has been used to model the response for the mathematically simple three-pole Butterworth low-pass filter. Examining this filter's response using the time-domain transform shows that the characteristic nulls in the time-domain transform are indeed a consequence of the filter design. Repeating this simulation with a bandpass filter shows that the bandpass filter has exactly the same time-domain reflection impulse magnitude response as the low-pass prototype. Since the low-pass prototype's impulse response has the characteristic dips, and this filter has optimal circuit element values since it has no tunable components, we can conclude that the dips must also be present in a properly tuned bandpass filter.

The actual values of the elements used in the resonator are of little consequence, except that they affect the input and output impedances, so input and output coupling often include an impedance transformer to ensure a 50-ohm match.

These couplings can be capacitive, which is frequently the case in lumped-element filters, or inductive (sometimes called magnetic or B field coupling) which is often the case in cavity-tuned filters. In the latter, the coupling structure is an opening in the wall between sections that permits the circulating magnetic fields to couple. These openings or apertures can be made adjustable by narrowing the width of the opening, which reduces coupling, or adding a shorted tuning element, such as a machine screw, which increases coupling.

For many filters, the coupling factor changes only slowly with frequency, so that the center frequency of the filter can be changed over a substantial range without changing the basic shape of the filter. This is because the center frequency of the filter is determined only by tuning the center frequency of each resonator.

An intuitive way to think about this is that the coupling of other sections is what slightly pulls the center frequency of different resonators to move the poles about the necessary amount to produce the desired filter response. So, if a tuning technique can assure that each resonator is properly tuned, the total filter response will be correct.

In a simple cavity resonator filter, all resonators have the same center frequency, with the effects of the resonator coupling included in the calculation of resonator frequency. This frequency is also the center frequency of the filter. However, this is not true for filters with transmission zeroes, where cross-coupling between resonators will cause the cross-coupled resonators to be at a different center frequency than the other resonators. These cross-coupled resonators may pull the adjacent resonators slightly off from the center frequency of the filter as well. Thus, in tuning these filters, we need to determine the correct center frequency of the cross-coupled resonators (and possibly some of the adjacent resonators), and tune those resonators for that frequency, while tuning the remaining resonators to the filter's center frequency. A better understanding of using time-domain filter tuning for cross-coupled filters is still needed, and more research is being done on this topic.

## Appendix B: Using time-domain in the network analyzer for filter tuning

To understand how to set up the network analyzer for time-domain filter-tuning measurements, it is helpful to review some basics of the time-domain transforms.

Normal time-domain reflectometers (TDRs) are inherently broadband and low-pass in nature. This means they are only useful for measuring DC-coupled circuits. They cannot be used for measuring bandpass filters, since the filters will appear to be almost totally reflective. However, a special mode of the network analyzer time-domain transform called bandpass mode can be used on band-limited devices.

In this mode, the center frequency of the frequency sweep is effectively translated to DC, and the inverse Fourier transform is applied from minus one-half of the frequency span to plus one-half of the span. This is important when looking at a bandpass filter with a frequency response that is the same as a low-pass filter response translated up in frequency to the center of the bandpass filter.

The time-domain transform represents the return loss as a function of length through the device under test. For time-domain transforms to be useful, they must have enough resolution to resolve the distinguishing characteristics of the network being measured. In general, the resolution of a transform is inversely proportional to the frequency span, although in bandpass mode the resolution is reduced by half because half the span is for negative frequencies and half for positive frequencies.

Looking at measurements of bandpass filters with a broad frequency sweep causes the same problem as in a low-pass TDR measurement: you see a near-total reflection at the input, and almost no other reflections. A normal network analyzer sweep of the bandpass filter, perhaps over two or three times the filter's bandwidth, would be a narrow sweep and was previously thought to have insufficient resolution to determine any characteristics of the filter. However, if the measurement is properly set up, the resolution limitation does not apply in measuring filters.

When a filter is examined in the time domain, each filter section has substantially more delay than its physical size would suggest. This is because the delay of a filter is inversely proportional to its bandwidth. The narrower the bandwidth, the longer the delay. For multiple-section filters, the transmission delay is approximately  $N/\pi BW$ , where  $BW$  is the bandwidth in Hz and  $N$  is the number of sections. Each section can be considered to add about  $1/N$  of the delay. Thus the reflection delay of each section is about  $2/\pi BW$ , and the total delay for reflection is about  $2N/\pi BW$  (twice as much as the transmission delay because the signal must go through the filter and back).

If the frequency bandwidth used to sweep the filters is at least two times the filter bandwidth, there will be sufficient resolution to discern the individual sections of the filter. The frequency span should not be too wide, or too much of the energy will be reflected, and tuning sensitivity will be reduced. Depending upon the filter, a frequency span of two to five times the filter bandwidth can be used.

### **Paper 3**

Dunsmore, J., "Advanced Filter Tuning using Time-domain Transforms", *Proceedings of the 29<sup>th</sup> European Microwave Conference*, 5-7 Oct. 1999, Munich, Vol. 2, pp. 72-75.

# Advanced Filter Tuning using Time Domain Transforms

Joel Dunsmore

Hewlett-Packard Company, Santa Rosa, California, U.S.A.

**Abstract** – The author has continued development on advanced techniques in tuning coupled-resonator filters based on the time domain response of a filter. This paper presents techniques to precisely tune filter coupling and resonators accounting for coupling masking, and effects of transmission zeros from cross coupled resonators.

## I. INTRODUCTION:

In previous presentations, the author has shown that coupled-resonator band-pass filters can be easily and deterministically tuned [1,2]. To achieve the proper pass band response, and to get low return loss and small pass band ripple, the center frequency of each resonator must be precisely tuned, and each coupling between resonators must be precisely set. In these papers, Dunsmore demonstrated a method of tuning filters based on the time domain response of its return loss, where the time domain response is obtained by a special type of discrete inverse Fourier transform of the frequency response. The technique works well for all-pole, low-loss filters, but there were several difficulties in tuning filters with more complex structures. This paper reviews the time domain tuning techniques, and presents a method that resolves the problem of dealing with filters that have cross-coupled resonators which result in transmission zeros near the filter passband. With this method, relatively inexperienced filter tuners, with only a few minutes instruction can be tuning multiple pole filters with great success.

### Basic All-Pole Filters:

A five-pole coupled resonator filter with four coupling structures will be used to illustrate the basic tuning technique. A schematic of the filter is shown in Fig. 1, with the distributed loss of the filter represented as shunt resistance. To apply the tuning method, the network analyzer's frequency sweep must be centered at the desired center frequency of the bandpass filter. The frequency span must be set to at least two to five times the expected filter bandwidth. The BANDPASS mode of time domain transform is applied to the return loss trace. Fig. 2 shows the frequency response and the band-pass mode time re-

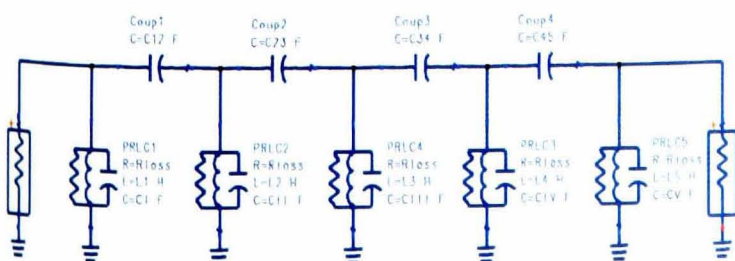


Figure 1: Schematic of a band pass filter

sponse of the filter, a fifth-order Chebyshev with 0.25 dB of passband ripple. Each plot shows two traces, one is the filter return loss response with ideal values for all the components, and the second trace showing the effect of mis-tuning one of the resonator elements (in this case, the second resonator). The upper plot is the frequency response and the lower plot is the time domain response.

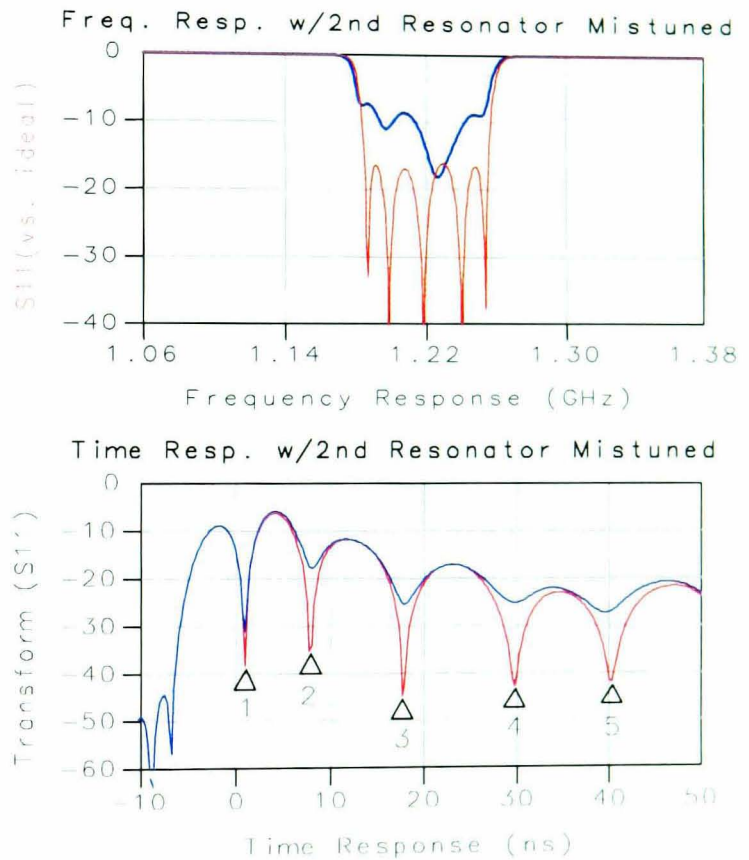


Fig. 2: Freq. and Time Response of a band pass filter.

Notice the distinctive dips in the time response S11 of the filter (indicated by the triangles labeled 1-5). These are characteristic nulls that occur if the resonators are exactly tuned. If the center frequency of the measurement were changed even slightly, the nulls would start to disappear, indicating that the filter is no longer tuned. The peaks between the nulls relate to the coupling factors of the filter. This type of response holds true for any all-pole filter, regardless of filter type.

The essence of the tuning technique is that the dips in the time domain response corresponded exactly to each resonator in the filter. When the resonator is tuned properly, the null is deep. If the resonator is not tuned, the null starts to disappear. Though it may seem remarkable that this exact relationship exists, extensive testing with many different kinds of filters, as well as simulations and direct mathematical derivation confirm this relationship. Figure 2 shows the time domain response with only the

second resonator mis-tuned from its ideal (derived) value. In this case the capacitor CII was tuned to a few percent above its ideal value. It is clear that the dip has nearly disappeared. The dip will only be maximized when the capacitor is returned to its ideal value. Note that mistuning one resonator can affect the response from the other “down stream” resonators.

## II. BASIC TUNING METHOD

The basic time domain tuning method for simple, all-pole filters is to measure the time domain response of S11 and S22 of the filter. The filter resonators are adjusted with the following steps:

- 1) Starting with the first and last resonator, tune to create a deep null in the time response (it will be at approximately  $t=0$ ).
- 2) The next resonator from the input and output are then tuned for deep nulls (which will appear approximately at  $t=1/BW$  where BW is the filter bandwidth). Tuning the second resonator will slightly pull the first, since they are coupled.
- 3) The previous resonators (first and last, in this case) are re-adjusted to restore the null in the time domain trace to make it as deep as possible.
- 4) Continue in this manner, working in toward the center, until all the resonators have been adjusted for a deep null.

This first adjustment will exactly center the filter and provide optimum tuning for the coupling factors given. Many filters have adjustable coupling factors that must be tuned to generate the desired filter response, particularly bandwidth and return loss. The coupling adjustment can be accomplished with the following steps:

- 1) Create a filter template, from measuring an existing filter or from a filter simulation, and load it into the network analyzer’s memory traces for S11 and S22.
- 2) After the initial resonator tuning above, adjust the input (and output) coupling to match the amplitude of the first (and last) peak of the target filter response. Re-adjust the first (and last) resonator to restore the first (and last) nulls to make them as deep as possible.
- 3) Adjust the next coupling from the input and output to match the associated peak in the template response. Re-adjust the resonators adjacent to this coupling to restore the nulls to be as deep as possible.
- 4) Continue in this manner until all couplings have been adjusted to match the peaks of the filter template, and all resonators have their associated nulls as deep as possible.

Note that adjusting one coupling will affect all couplings that follow. More information on this can be found in [2].

## III. FILTERS WITH CROSS-COUPLED RESONATORS

For many communication applications, it is necessary to make a filter skirt response steeper than normally obtained by all-pole type filters. Discrete transmission zeros (where the S21 goes to zero) can be obtained in the filter stop band by adding cross-coupling (coupling between resonators other than nearest neighbors). The number of resonators

which the coupling “skips over” will determine the characteristics of the transmission zeros. Skipping over an odd number of resonators, as seen in Fig. 3, results in an asymmetric frequency response, with a zero on only one side of the pass band. Skipping over two resonators results in transmission zeros on both sides of the pass band. The time domain response of these filters differs from the all-pole filters, in that tuning the characteristic nulls to be as deep as possible does not result in the filter being properly tuned. Fig. 4 shows the frequency and time response of the 4 pole filter with asymmetric cross coupling from Fig. 3. The filter, in this case, had coupling adjustments for only the input, output and cross-coupling. The coupling between resonators was fixed. The filter was optimized for return loss in the pass band and rejection in the upper stop band.

Notice from the time response that the nulls are not deep for many of the resonators. To understand why this is, and how to tune these filters, one must first look back at the design methods for the simple, all-pole filters.

### All-Pole Filter Design:

All-pole filters are designed by starting with a low pass prototype filter, then applying a transform to shift it up in frequency from “DC-centered” to the desired center frequency [3,4]. The essence of the design process is that the coupling values are derived only from the low-pass proto-

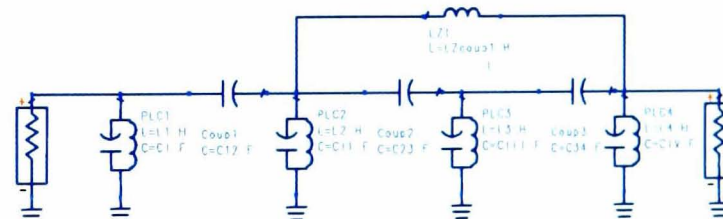


Fig. 3: Schematic of a filter with cross coupling (2-4).

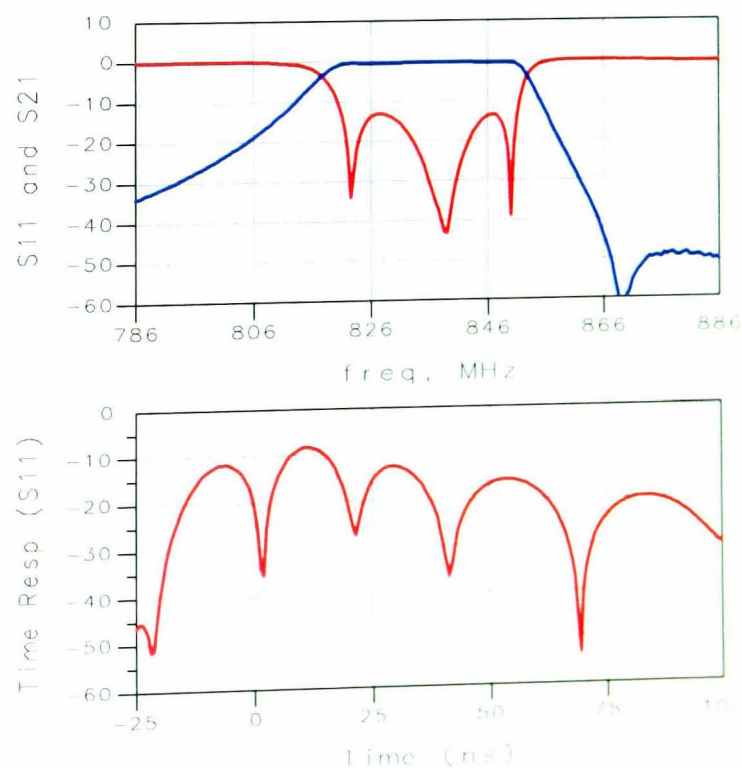


Fig. 4: Freq. and Time response of a cross-coupled filter

type component values. The resonator values are derived by making the resonant frequency of the node (which includes the input and output coupling) equal to center frequency of the filter. For example, in the filter in Fig. 1, the resonant frequency of the second node is defined by the elements L2 in parallel with CII plus C12 and C23 (the coupling elements), and it exactly equals the filter center frequency. This is true for all the nodes, including the first and last, which, however, add in only one coupling.

The time domain response of a filter node is found to have a deep null whenever the frequency sweep of the network analyzer is exactly centered on the resonant frequency for that node. Further, the time domain response shows the response of the filter nodes separated in time. This separation is caused by the delay through each filter section, which Fano showed to be inversely proportional to the filter bandwidth. The time domain response will have sufficient resolution if the frequency sweep is at least twice as wide as the filter bandwidth.

To illustrate this point, consider the response of a filter to an impulse, as shown in Fig. 5. As the impulse proceeds through each node of the filter, part is reflected and most is transmitted. If the filter is uncharged before the pulse arrives, the reflection from the first node will look as though the coupling capacitance, C12, is grounded on the far side. That is the time domain reflection will be the same as a circuit that is tuned to the “node frequency” consisting of C12 + CI in parallel with L1. Since the pulse goes to zero after time zero, the reflection from node 2 will look as though both C12 and C23 are grounded. The delay between these pulses will be due to the coupling, thus less coupling (which results in a narrower filter) will have more delay. From above, note that is exactly the same relationship that is used to design the all-pole filter. Thus, it becomes clear why tuning for deep nulls with the network analyzer tuned to the filter center frequency succeeds: The response from each individual node is centered on the same frequency.

### The Effects of Cross-Coupling:

With cross-coupling added to the filter, the time domain response is no longer has the simple relationship to filter tuning. Further, especially in filters with asymmetric transmission zeros, the tuning of the filter is not optimum

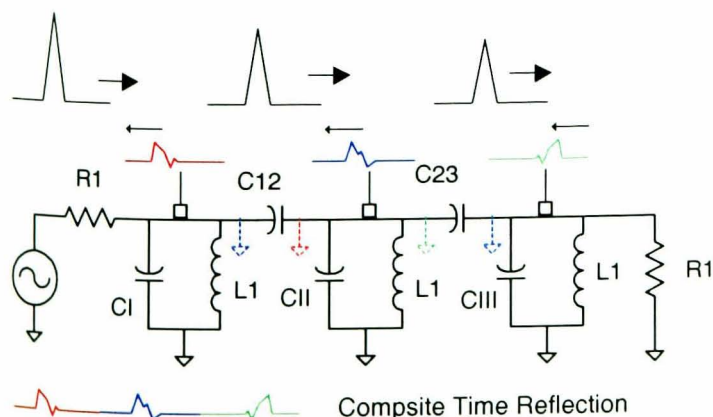


Fig. 5: The time domain response separates the response from each node

when each node frequency is centered at the filter center frequency. (Recall that the node frequency is here defined to be the resonant frequency of the node with all connected couplings -- including cross coupling -- grounded). The resonators are often “pulled” to compensate for the effect on the pass-band of the transmission zeros in the stop-band, thus achieving the desired pass-band return loss specification. This results in an asymmetric shape to the return loss, as demonstrated in Fig. 4. Tuning for deep nulls results in a filter that does not meet the return loss specifications. However, the discussion about Fig. 5 points to a method that will allow tuning filters with cross coupling in the time domain.

The argument for the time response of any particular node of a filter having a deep null when the node frequency is exactly centered on the network analyzer frequency still holds. The difficulty with these complex filters is that the node frequencies are no longer easy to determine. But one can use the network analyzer itself, on a properly tuned or “golden” filter, or on a simulated filter, to discover the individual node frequencies. This is done setting up the vector network analyzer (VNA) in dual channel mode, with one channel on frequency domain and one on time domain. The center frequency of the VNA is adjusted while looking at the null associated with a particular resonator. When the null is maximized, that frequency is recorded as the node frequency for that resonator. Fig. 6 illustrates the time response of the filter tuned at the filter center frequency, and then tuned to a frequency which maximizes the null associated with resonator 2 (one of the resonators with cross coupling).

This process is repeated for each of the filter’s resonators, adjusting the VNA center frequency until each null is maximized. For best sensitivity, the frequency span is reduced to just two times the bandwidth. Table 1 below gives the node frequencies determined for each resonator for the filter from Fig. 4. Armed with this information, and using the measurement from Fig. 4 as the tuning template, a filter tuning process for complex filters can be defined.

Resonator No.	Node Frequency
1	836.25 MHz
2	833.85 MHz
3	834.55 MHz
4	836.45 MHz

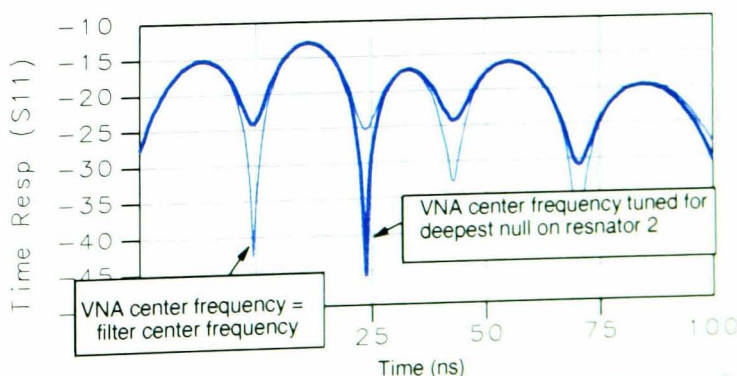


Fig. 6: Change in time response when the VNA center frequency is tuned.

### Time Domain Tuning Process for Complex Filters

The filter from Fig. 4 with all four resonators, the input and output coupling and the cross coupling de-tuned, is used to demonstrate this process.

- 1) Assuming that the input and output coupling is sufficient to produce an approximate filter shape, start by tuning the filter as though it were an all-pass filter. Figure 7 shows the frequency response before any tuning, and after the resonators (but not coupling) have been adjusted for maximum null.
- 2) Adjust the coupling to align the peaks with the target filter, remembering to re-adjust the resonators to get deep nulls. Fig. 8 shows the result of coupling adjustment.
- 3) Adjust the cross coupling to set the zero frequency to match the S21 frequency response target, as shown in Fig. 9.
- 4) Finally, to get the resonators tuned to their correct final value, set the VNA center frequency to that

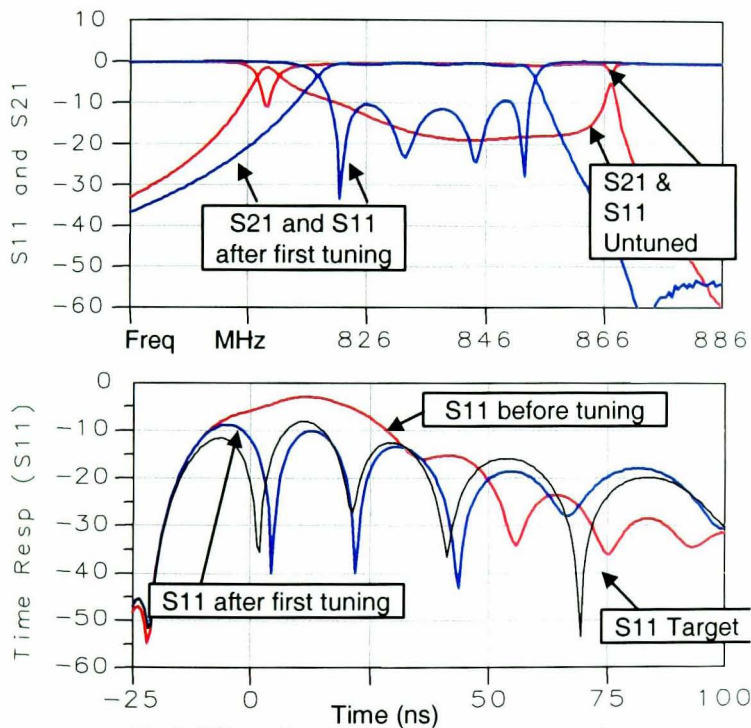


Fig 7: Filter after tuning resonators for nulls

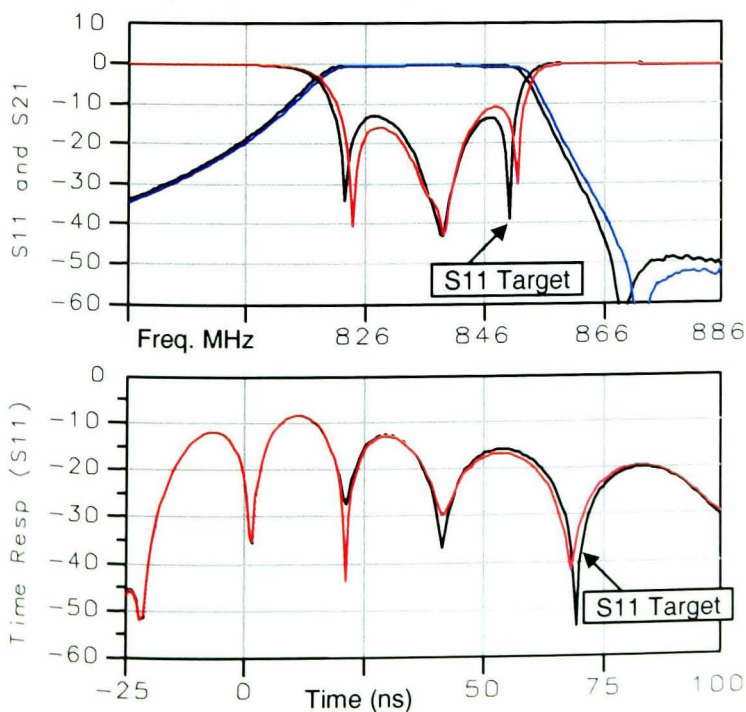


Fig. 8: Response After Adjusting Coupling

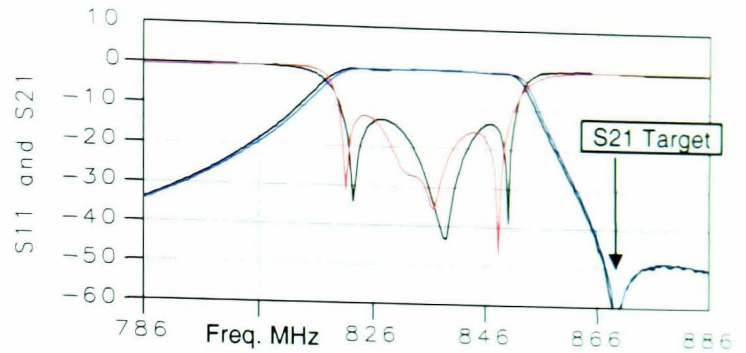


Fig. 9: Freq. Response after Adjusting Cross Coupling

listed in Table 1 for each resonator, and tune that resonator for maximum null. After a first pass, go back again and retune each resonator to account for the pulling affect of tuning the other resonators. Fig. 10 shows the final result of tuning this filter. It is clear that the final response is nearly identical. Remember that the return loss tuning was done entirely in the time domain.

### IV. CONCLUSIONS:

This paper has presented a tuning method for adjusting complex coupled-resonator filters. This method allows deterministic tuning of resonator frequency, coupling factor, and cross-coupling.

### REFERENCES

- [1] Joel Dunsmore, "Simplify Filter Tuning using Time Domain Transforms", *Microwaves & RF*, March 1999.
- [2] Joel Dunsmore, "Tuning Band Pass Filters in the Time Domain, *Digest of 1999 IEEE MTT-S Int. Microwave Sym.*, pp. 1351-1354.
- [3] Zverev, "Handbook of Filter Synthesis", John Wiley and Sons, 1967.
- [4] Williams and Taylor, "Electronic Filter Design Handbook, 2<sup>nd</sup> Edition", McGraw Hill Publishers, Chapter 5, 1988.

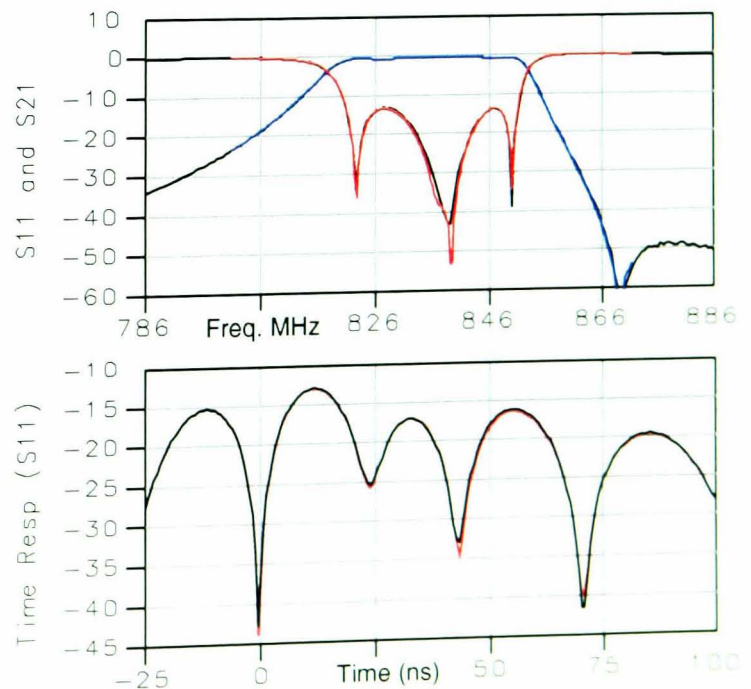


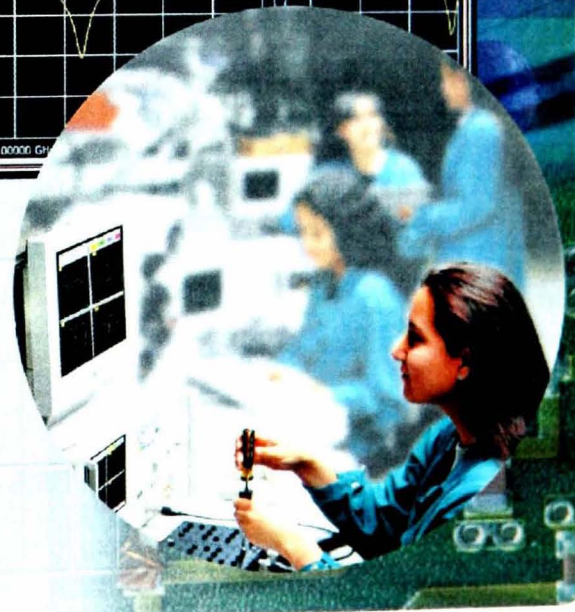
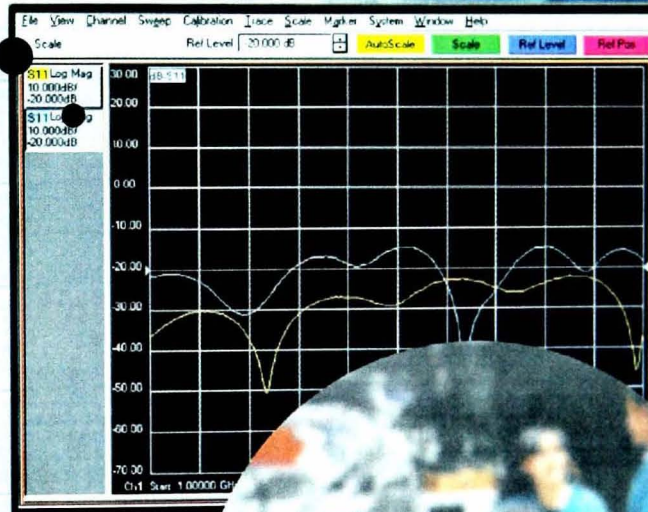
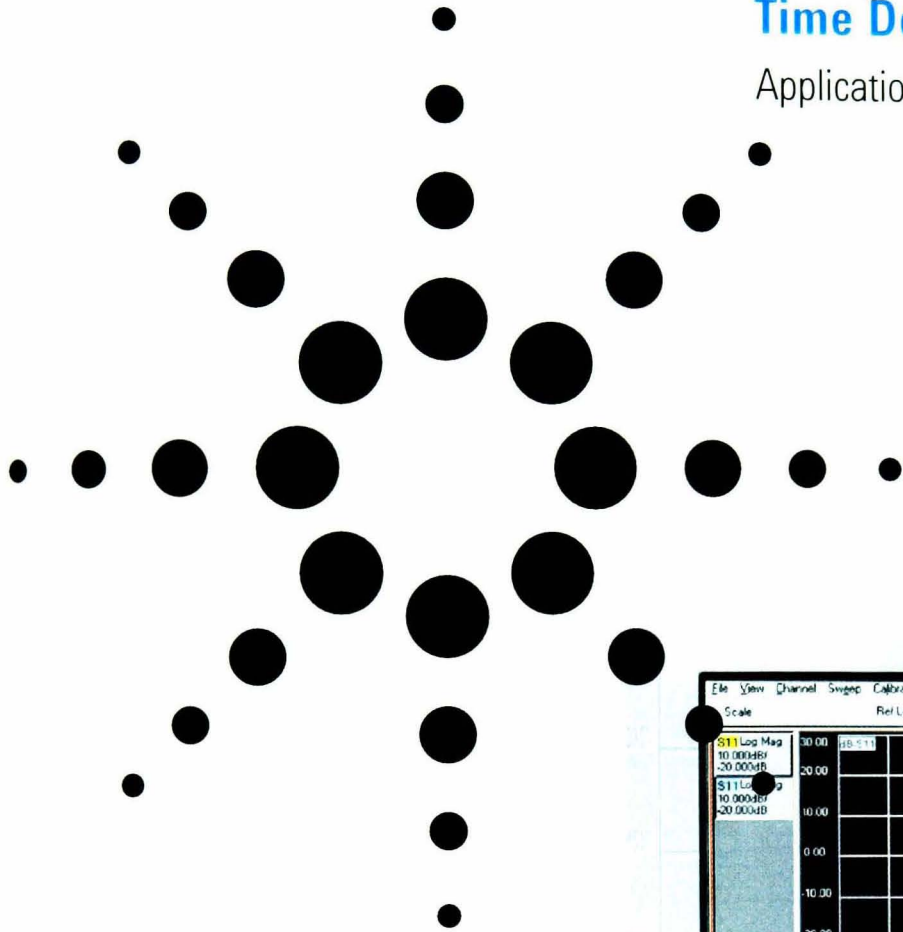
Fig 10: Final Tuning, note that the final filter response is nearly identical to the target response.

## **Paper 4**

Agilent Technologies, Application Note AN 1287-10, *Advanced Filter Tuning Using Time-domain Transforms*, Agilent part no. 5980-2785EN, 2001.

# Agilent Network Analysis Solutions Advanced Filter Tuning Using Time Domain Transforms

Application Note 1287-10



Agilent Technologies

## Introduction

The level of experience and expertise required to accurately tune coupled-resonator cavity filters, cross-coupled filters, and duplexers effectively precludes these devices from mass production at high speed. Ironically, these same filters are increasingly needed in large quantities, as a result of the spectral density resulting from the runaway success of wireless communications services. The time required to tune these filters accurately limits manufacturers from increasing their production volumes and reducing manufacturing cost. Fortunately, it is possible to dramatically reduce both the time required to tune these types of filters, as well as the experience and expertise required. The method removes filter tuning from the realm of art, and makes the process predictable and repeatable. Even relatively inexperienced filter tuners can tune multiple-pole filters with great success with a minimal amount of training.

The basic technique has been comprehensively covered in Agilent application note 1287-8, which also describes how coupled-resonator band-pass filters can be easily and deterministically tuned. To achieve the proper passband response, and to achieve good return loss and passband ripple, the center frequency of each resonator is precisely tuned, and each coupling between resonators is precisely set. The method is based on the time-domain response of a filter's return loss, in which the time-domain response is obtained by a special type of discrete inverse Fourier transform of the frequency response. Readers are encouraged to review the material contained in application note 1287-8 for information about the basic technique and how it is applied to tuning coupled-resonator cavity filters.

This application note reviews these time domain tuning techniques, and extends the technique for use in tuning filters with cross-coupled resonators that produce transmission zeros near the filter passband, as well as duplexer filters that have a common (antenna) port, an upper passband (transmit) port, and a lower passband (receive) port.

Together with application note 1287-8, this application note provides a comprehensive compilation to filter tuning in the time domain, including theory, application, set-up, and tuning procedures.

## The technique defined

A five-pole coupled resonator filter with four coupling structures will be used to illustrate the basic tuning technique. A schematic of the filter is shown in figure 1, with the distributed loss of the filter represented as shunt resistance. To apply the tuning method, the network analyzer's frequency sweep is centered at the desired center frequency of the bandpass filter. The frequency span is set to two to five times the expected filter bandwidth. The bandpass mode of time domain transform is applied to the return loss trace. Figure 2 shows the frequency response and the bandpass mode time response of the filter, a fifth-order Chebyshev with 0.25 dB of passband ripple.

Each plot shows two traces. The lighter (red) one is the filter return loss response with ideal values for all the components, and the darker (blue) trace shows the effect of mistuning one of the resonator elements (in this case, the second resonator). The upper plot is the frequency response and the lower plot is the time domain response. Notice the distinctive dips in the time response S11 of the filter (indicated by the triangles labeled 1-5). These are characteristic nulls that occur if the resonators are exactly tuned. If the center frequency of the measurement is changed even slightly, the nulls start to disappear, indicating that the filter is no longer tuned. The peaks between the nulls relate to the coupling factors of the filter. This type of response holds true for any all-pole filter, regardless of filter type.

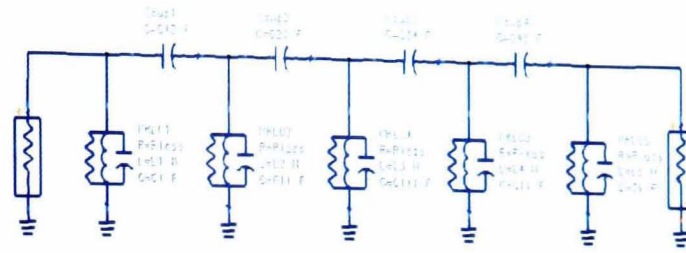


Figure 1.

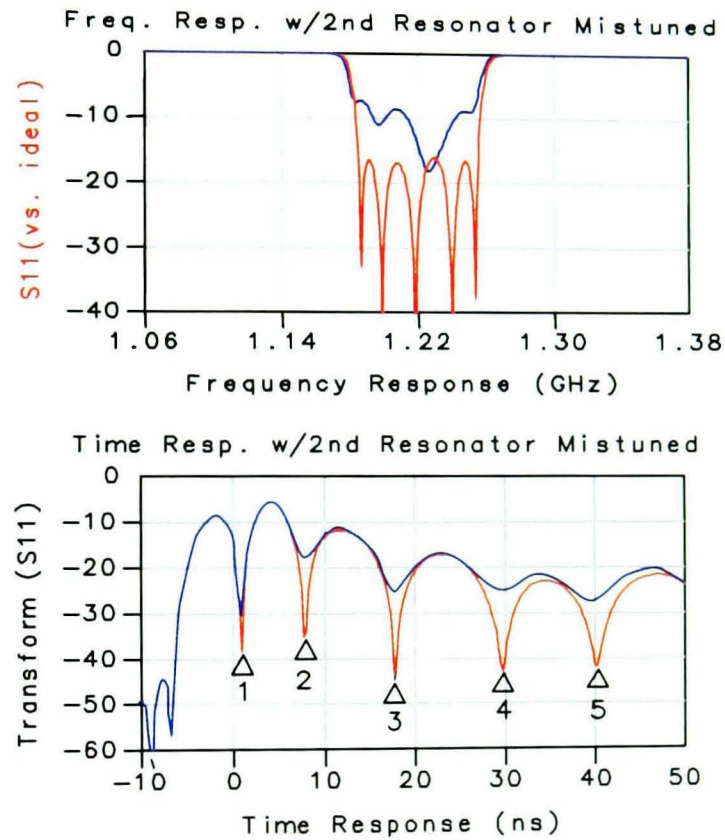


Figure 2.

The essence of the tuning technique is that the dips in the time domain response correspond exactly to each resonator in the filter. When the resonator is tuned properly, the null is deep. If the resonator is not tuned, the null starts to disappear. Though it may seem remarkable that this exact relationship exists, extensive testing with many different kinds of filters, as well as simulations and direct mathematical derivation, confirm this relationship. Figure 2 shows the time

domain response with only the second resonator mistuned from its ideal (derived) value. In this case the capacitor CII was tuned to a few percent above its ideal value. It is clear that the dip has nearly disappeared. The dip will only be maximized when the capacitor is returned to its ideal value. Note that mistuning one resonator can affect the response from the other "downstream" resonators.

## Basic tuning method

The basic time domain tuning method for simple all-pole filters, is to measure the time domain response of S11 and S22 of the filter. The filter resonators are adjusted with the following steps:

1. Starting with the first and last resonators, tune to create a deep null in the time responses of the S11 and S22 measurements respectively (the nulls will be at approximately  $t=0$ ).
2. The next resonator from the input and output are then tuned for deep nulls (which will appear approximately at  $t=1/BW$  where BW is the filter bandwidth). Tuning the second resonator will slightly pull the first, since they are coupled.
3. The previous resonators (first and last, in this case) are readjusted to restore the null in the time domain trace to make it as deep as possible.
4. Continue in this manner, working in toward the center, until all the resonators have been adjusted for a deep null.

This first adjustment will exactly center the filter and provide optimum tuning for the given coupling factors. Many filters have adjustable coupling factors that must be tuned to generate the desired filter response, particularly bandwidth and return loss. The coupling adjustment can be accomplished with the following steps:

1. Create a filter template by measuring an existing tuned filter or from a filter simulation, and load it into the network analyzer's memory traces for S11 and S22.
2. After the initial resonator tuning described above, adjust the input and output coupling to match the amplitude of the first peak of the target S11 and S22 filter response. Readjust the first and last resonator to restore the first S11 and S22 nulls to make them as deep as possible.

3. Adjust the next coupling from the input and output to match the associated peak in the template response. Readjust the resonators adjacent to this coupling to restore the nulls to be as deep as possible.
4. Continue in this manner until all couplings have been adjusted to match the peaks of the filter template, and all resonators have their associated nulls as deep as possible.

Note that adjusting one coupling will affect all couplings that follow, so it is important to start with the couplings at the input and output and work toward the center.

## Tuning filters with cross-coupled resonators

For many communication applications, it is necessary to make a filter skirt response steeper than normally obtained by all-pole type filters. Discrete transmission zeros (where the  $S_{21}$  goes to zero) can be obtained in the filter stopband by adding cross-coupling (coupling between resonators other than nearest neighbors). The number of resonators that the coupling “skips over” will determine the characteristics of the transmission zeros. Skipping over an odd number of resonators, as seen in figure 3, results in an asymmetric frequency response, with a zero on only one side of the passband. Skipping over two resonators results in transmission zeros on both sides of the passband. The time domain response of these filters differs from the all-pole filters, in that tuning the characteristic nulls to be as deep as possible does not result in the filter being properly tuned.

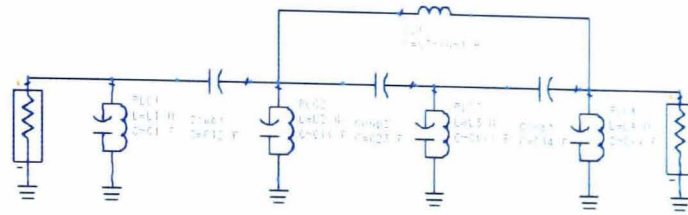


Figure 3.

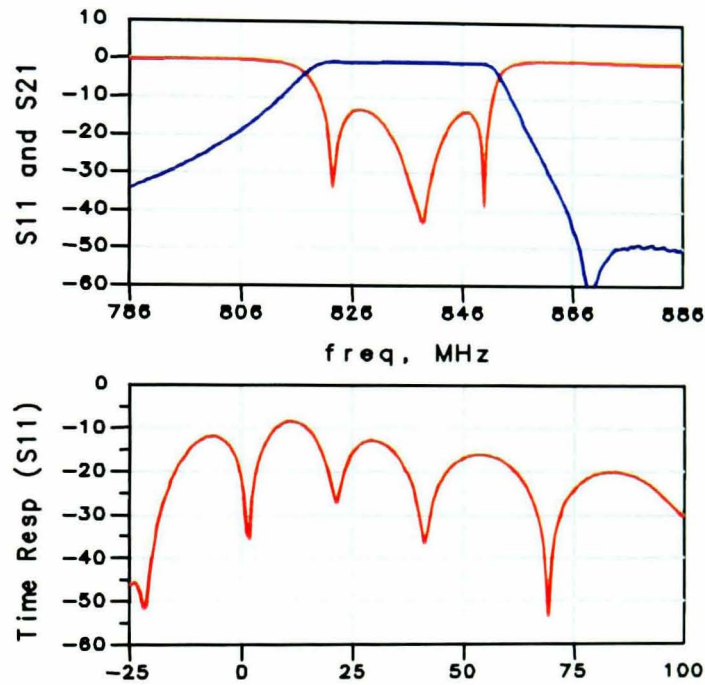


Figure 4.

Figure 4 shows the frequency and time response of the four-pole filter with asymmetric cross coupling from figure 3. The filter, in this case, had coupling adjustments for only the input, output, and cross-coupling. The coupling between resonators was fixed.

The filter was optimized for return loss in the passband and rejection in the upper stop band. Notice from the time response that the nulls are not deep for many of the resonators. The design methods for simple, all-pole filters help illustrate why this is so, and how to tune these filters.

## All-pole filters

All-pole filters are designed by starting with a low-pass prototype filter, then applying a transform to shift it up in frequency from “DC-centered” to the desired center frequency. The essence of the design process is that the coupling values are derived only from the low-pass prototype component values.

The resonator values are derived by making the resonant frequency of the node (which includes the input and output coupling) equal to the center frequency of the filter. For example, in the filter in figure 1, the resonant frequency of the second node is defined by the elements  $L2$  in parallel with  $CII$  plus  $C12$  and  $C23$  (the coupling elements), and it exactly equals the filter center frequency. This is true for all the nodes, including the first and last, which have only one coupling added.

The time domain response of a filter node has a deep null whenever the frequency sweep of the network analyzer is exactly centered on the resonant frequency for that node. Further, the time domain response shows the response of the filter nodes separated in time. This separation is caused by the delay through each filter section, which Fano showed to be inversely proportional to the filter bandwidth. The time domain response will have sufficient resolution if the frequency sweep is at least twice as wide as the filter bandwidth.

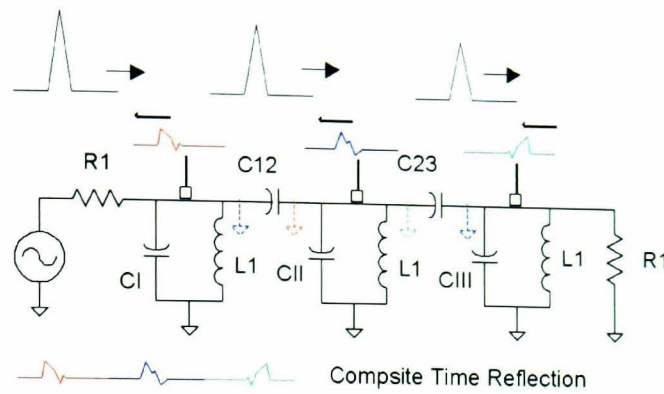


**Figure 5. The time domain response separates the response from each node.**

To illustrate this point, consider the response of a filter to an impulse, as shown in figure 5. As the impulse proceeds through each node of the filter, part is reflected and most is transmitted. If the filter is uncharged before the pulse arrives, the reflection from the first node will look as though the coupling capacitance,  $C12$ , is grounded on the far side. That is, the time domain reflection will be the same as a circuit that is tuned to the “node frequency” consisting of  $C12 + C1$  in parallel with  $L1$ . Since the pulse goes to zero after

time zero, the reflection from node 2 will look as though both  $C12$  and  $C23$  are grounded. The delay between these pulses will be due to the coupling, so less coupling (which results in a narrower filter) will have more delay. This is the same relationship used to design the all-pole filter. It then becomes clear why tuning for deep nulls with the network analyzer tuned to the filter center frequency succeeds: The response from each individual node is centered on the same frequency.

### Effects of cross coupling

With cross-coupling added to the filter, the time domain response no longer has the simple relationship to filter tuning. Further, especially in filters with asymmetric transmission zeros, tuning of the filter is not optimum when each node frequency is tuned to the filter center frequency. Recall that the node frequency is defined to be the resonant frequency of the node with all connected couplings, including cross coupling, grounded. The resonators are often “pulled” to compensate for the effect on the pass-band of the transmission zeros in the stopband, thus achieving the desired passband return loss specification. This results in an asymmetric shape to the return loss, as demonstrated in figure 4. Tuning for deep nulls results in a filter that does not meet the return loss specifications. However, the discussion about figure 5 points to a method that will allow tuning filters with cross coupling in the time domain.

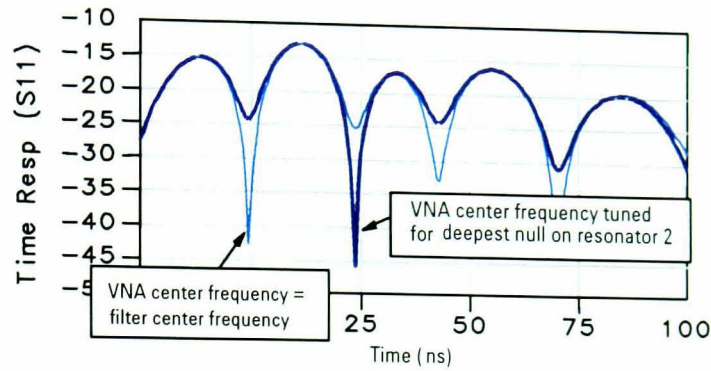


**Figure 6. Change in time response when the VNA center frequency is tuned.**

The argument still holds for the time response of any particular node of a filter having a deep null when the node frequency is exactly centered on the network analyzer frequency. The difficulty with these complex filters is that the node frequencies are no longer easy to determine. But the network analyzer itself can be used, on a properly tuned or “golden” filter, or on a simulated filter, to discover the individual node frequencies. This is done by setting up the vector network analyzer (VNA) in dual-channel mode, with one channel on frequency domain and one on time domain. The center frequency of the VNA is adjusted while looking at the null associated with a particular resonator. When the null is maximized, that frequency is recorded as the node frequency for that resonator.

Figure 6 illustrates the time response of the filter tuned at the filter center frequency, and then tuned to a frequency that maximizes the null associated with resonator 2 (one of the resonators with cross coupling).

This process is repeated for each of the filter’s resonators, adjusting the VNA center frequency until each null is maximized. For best sensitivity, the frequency span is reduced to just two times the bandwidth. Table 1 gives the node frequencies determined for each resonator for the filter from figure 4. Armed with this information, and using the measurement from figure 4 as the tuning template, a filter tuning process for complex filters can be defined.

**Table 1. Node frequency for each resonator**

Resonator no.	Node frequency
1	836.25 MHz
2	833.85 MHz
3	834.55 MHz
4	836.45 MHz

## Tuning of complex filters

The filter from figure 4, with all four resonators, the input and output coupling, and the cross coupling detuned, is used to demonstrate this process.

1. Assuming that the input and output coupling is sufficient to produce an approximate filter shape, start by tuning the filter as though it were an all-pole filter. Figure 7 shows the frequency response before any tuning, and after the resonators (but not coupling) have been adjusted for maximum nulls.
2. Adjust the coupling to align the time domain response peaks with those of the target filter, remembering to readjust the resonators to get deep nulls. Figure 8 shows the result of coupling adjustment.
3. Adjust the cross coupling to set the zero frequency to match the S21 frequency response target, as shown in figure 9.
4. Finally, to get the resonators tuned to their correct final values, set the VNA center frequency to that listed in table 1 for each resonator, and tune that resonator for maximum null. After a first pass, go back again and retune each resonator to account for the pulling effect of tuning the other resonators. Figure 10 shows the final result of tuning this filter. It is clear that the final response is nearly identical. Remember that the return loss tuning was done entirely in the time domain.

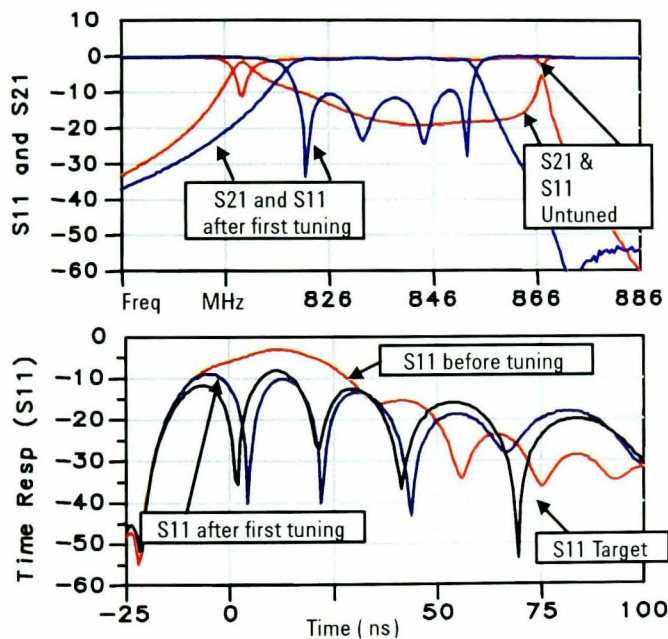


Figure 7.

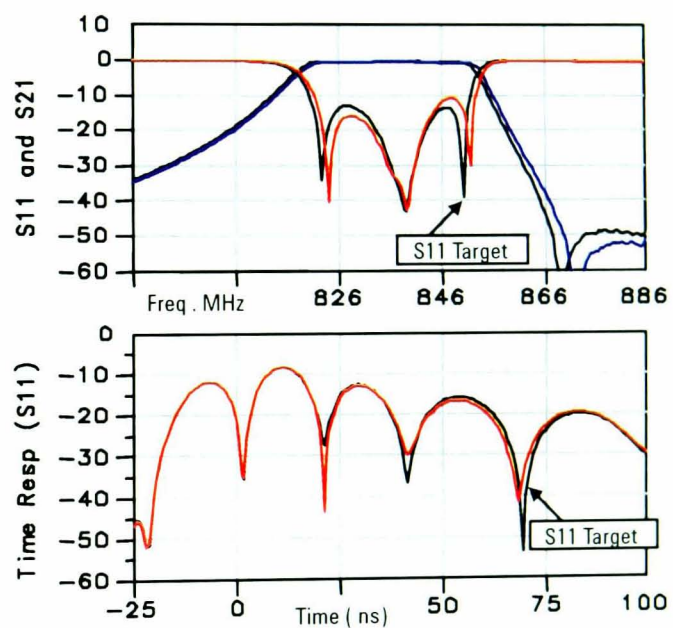


Figure 8.

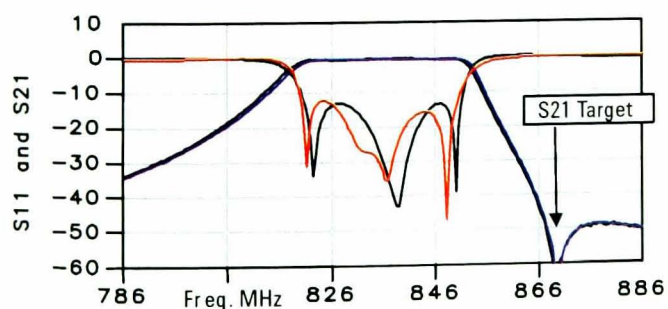


Figure 9.

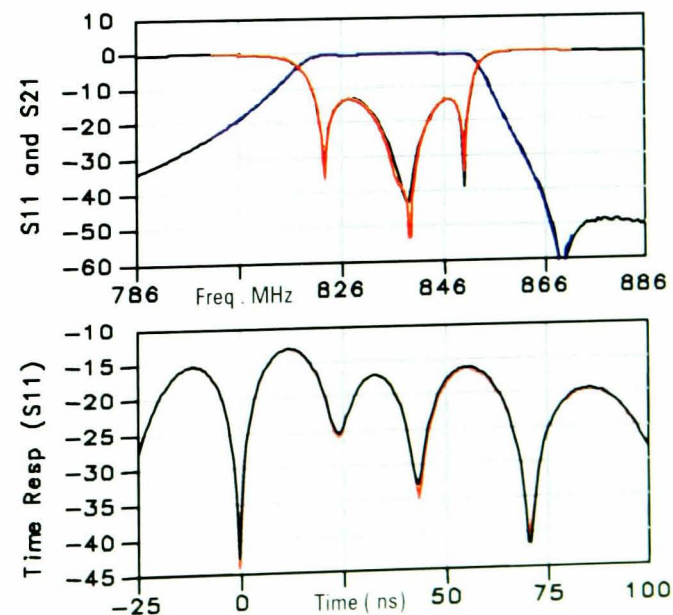


Figure 10.

## Duplex filter tuning

Duplex filters (sometimes called duplexers), as seen from the antenna port, have two paths that contribute to the return loss response, each with its own delays and responses. The task for the filter tuner, and the focus of this section, is to separate these responses so that each side of the filter can be deterministically tuned.

Duplex filters are used primarily to separate the transmission channel (Tx) from the receive channel (Rx) in a wireless communications base station. Because the Tx and Rx are nearly adjacent, the filters tend to be very asymmetric to create sharp cutoffs for each band. Figure 11 shows the schematic of such a duplexer. Note that a single cross-coupling is used in each side, but that the cross-coupling is capacitive in one side and inductive in the other. This gives a lower transmission zero for the Rx band (Rx is upper in this case) and an upper transmission zero in the Tx band as shown in figure 12.

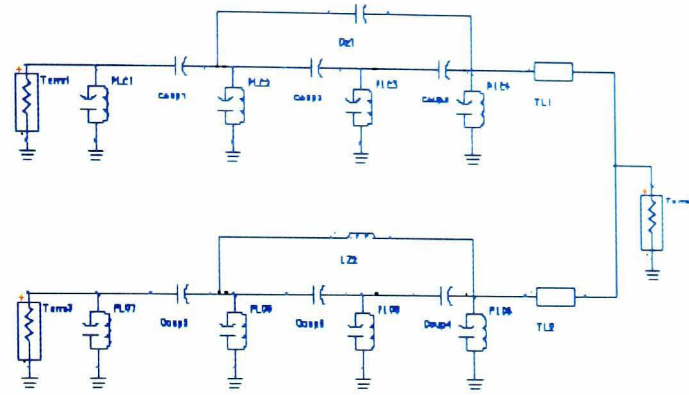


Figure 11.

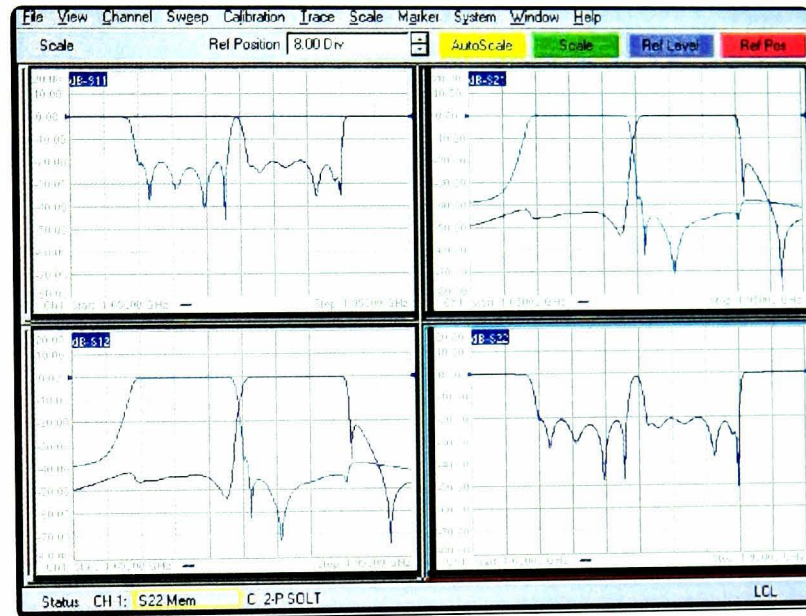


Figure 12.

Duplexers that have more than a bandwidth of separation between the Tx and Rx bands are easily tuned with the method noted above for tuning filters with cross-coupling. That is because the network analyzer can be centered on the Tx band, with the span at greater than two bandwidths, and still not have the Rx band interfere with the input or output reflection response. However, most duplexers have substantially less than one bandwidth between the edges of the Tx and Rx bands (a typical filter might have an 80 MHz bandwidth with 20 MHz of separation). These types of duplexers make time-domain tuning difficult, because

resonator responses at the common port can come from either the Tx side or the Rx side.

In figure 11, the duplexer uses quarter-wave transformers to isolate each side of the duplexer (the input impedance of the Tx side is a short circuit at the Rx frequency). Other topologies couple the common port to a broader-band common resonator, which is in turn coupled to the first resonator on both the Tx and Rx sides. With this configuration, the common resonator clearly cannot be centered on either the Tx or Rx passbands, instead it is centered somewhere in between.

## Time domain response of duplexers

The time domain response of duplexers is complicated by the fact that at the common port, reflections from both the Tx side and Rx side will cause some nulls in the time domain. Figure 13 shows the time domain and frequency response of a real duplexer. To view the time-domain response in a way that makes sense, it is necessary to set the network analyzer center frequency to the frequency between the Rx and Tx pass-bands. The span of the analyzer must be set to at least two times the overall bandwidth of the Tx and Rx bands. The following example of tuning a real duplex filter uses a duplexer which has the common port coupled to a common resonator, which in turn is coupled to both the last (5th) Tx resonator and the last (6th) Rx resonator.

### Setting up the tuning process

Just as with the complex filter of figure 4, the tuning process for a duplexer requires a properly tuned prototype filter to allow the node frequencies and target couplings to be determined. However, the nodes will be more difficult to associate with individual resonators, especially from the common port.



**Figure 13. Top half of display:** Upper trace = antenna common  
Lower trace = Rx  
**Lower half of display:** Upper trace = antenna common  
Lower trace = Rx

## Identifying the resonator

The upper half of figure 13 shows that there are more nulls in the time domain response of the reflection from the common port than there are from the Tx port. The first null is associated with the common resonator (figure 14). The second null association is found by changing the tuning slightly on the last Tx resonator, and in the same manner the last Rx resonator can be associated with the third null from the common port (figure 15). Depending upon the filter, it may also be possible to identify other resonators in the Tx or Rx filter, but soon the nulls become confusing, with the tuning of one resonator affecting two nulls.



**Figure 14.** Tuning the common ANT resonator shows a response change primarily in the first null. In this way the first node resonator is determined and the first node frequency can be found by changing the VNA frequency to find the deepest null



**Figure 15.** Tuning the Rx 6 resonator shows the primary effect at the second null. By looking for the frequency of the VNA, which makes the null deepest, we know this node frequency. Note: the next null also shows some effect from tuning

### Finding node frequencies

Once the association of nulls with resonators has been done from the common port for the last Tx and Rx resonators, the individual node frequency for each resonator is found by tuning the analyzer's center frequency until the associated null is deepest. This frequency is also recorded for each null while measuring reflection from the Tx and Rx ports, and for the first several nulls from the common port. These frequencies (in MHz) are shown in table 2.

### Separating Tx and Rx Responses

These node frequencies will be used for the final tuning of the duplexer, but experimental research shows that it is not practical to try to tune the duplexer directly to these frequencies. This is because there is so much interaction from the Rx side on the Tx response, especially at the common port, that the resonators cannot be sufficiently isolated unless they are already very close to their correct values. The solution for initial tuning is to mistune one side (say the Tx side) and then recharacterize the filter for the Rx side node frequencies. Figure 16 shows the response of the duplexer with Tx5 (the one closest to the common port resonator) mistuned.

In figure 16, the VNA center frequency is changed such that the null associated with the Rx 6 resonator measured at the common port is deep (time domain, upper trace). This frequency is recorded in table 3 as Rx 6 frequency. But with the same filter measured at the Rx port, with an analyzer center frequency of 1850 MHz (time domain, lower trace), each Rx node is nearly a null.

Table 2. Node frequency for tuned duplexer

Common port		Tx port		Rx port	
Node	Freq.	Node	Freq.	Node	Freq.
Com	1800	TX1	1747	RX1	1848
RX6	1800	TX2	1749	RX2	1848
TX5	1796	TX3	1750	RX3	1851
RX5	1805	TX4	1760	RX4	1841
TX4	1788				
RX4	1810				

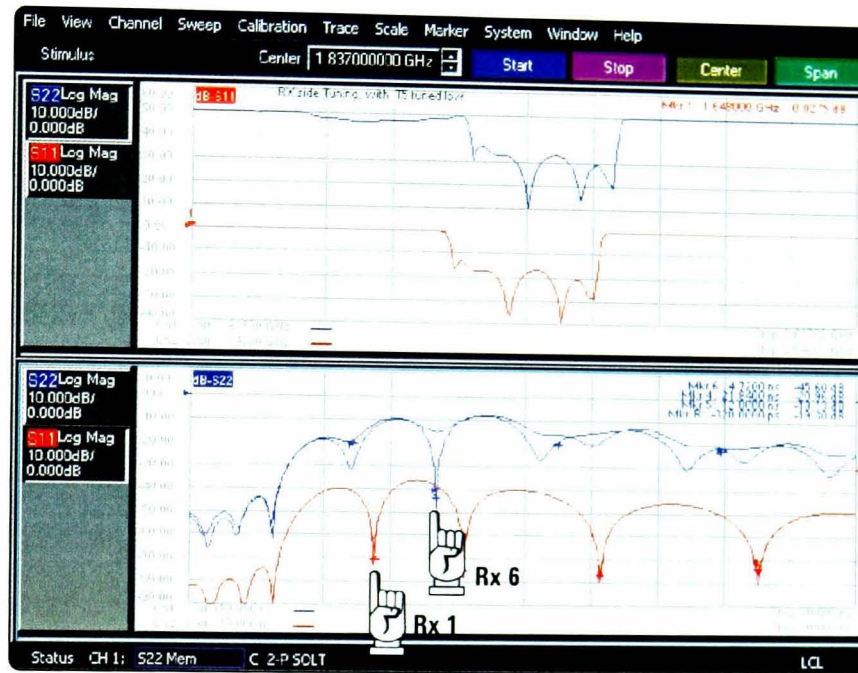


Figure 16. The upper trace shows the Rx path frequency response with a VNA center frequency selected to obtain the deepest null for the respective resonators. These frequencies are recorded for the Rx filter tuned and the Tx first resonator tuned low.

Table 3. Node frequency for duplexer with sides isolated

Common Port		Tx Port *		Rx Port **	
Node	Freq.	Node	Freq.	Node	Freq.
Com	1803** 1793*	TX1	1746	RX1	1848
RX6**	1829	TX2	1749	RX2	1848
TX5*	1762	TX3	1749	RX3	1850
RX5**	1848	TX4	1787	RX4	1850
TX4*	1738				
RX4**	1860				

\*Rx untuned; \*\*Tx untuned

After the Rx frequencies are determined, the Rx 6 resonator is set high, and the Tx resonator frequencies are determined in a similar way. The precise node frequency for each node was recorded in table 3.

Note that from the Tx and Rx ports, the node frequencies are nearly unchanged, indicating that these are very nearly isolated from their respective other sides even in a tuned duplexer.

## Tuning a filter

A duplexer tuning process proceeds as follows:

1. Start with resonator RX6 tuned high in frequency. Tune the Tx side of the filter, and common port according to the starred (\*) frequencies in table 3. Tune coupling and cross-coupling as described in application note 1287-8.
2. Tune resonator TX5 as low as possible. Tune the Rx side of the filter using the double starred (\*\*) frequencies in table 3. Figure 17 shows tuning starting with Rx1 and common. The result of tuning all Rx resonators is shown in figure 18. The VNA is set to the common resonator frequency (about 1800 MHz) so the Rx nulls don't appear deep. Here, Tx 5 resonator is not yet tuned.
3. Final tune TX5 and TX6 to the frequency in table 2. Final tune all resonators to table 2 values. Results shown in figure 19.

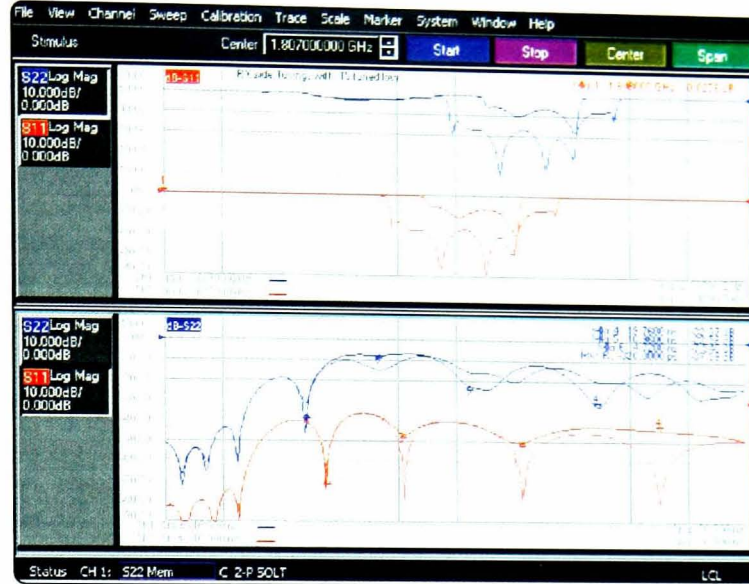


Figure 17. The Rx side of the filter is being tuned here. The upper plot shows the S11 and S22 of the filter; each set to a different center frequency appropriate for the first and last resonator. The lowest plot shows the null from each resonator.

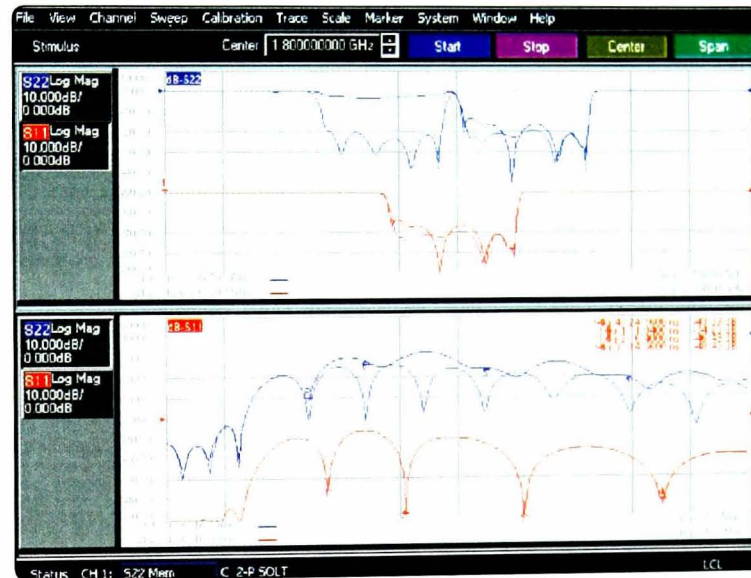


Figure 18.



Figure 19.

## More complex filter tuning

### Dealing with multiple or strong cross couplings

In the example filter shown in figure 3, the coupling value for the cross coupling was much less than the main coupling. For such cases, the cross coupling does not have a strong effect on the time domain response. However, some filters have very strong cross coupling (coupling of the same order as the main coupling), or multiple cross couplings. In these cases, it may be necessary to take a different approach to tuning the filters.

One approach that has been effective is to remove the cross couplings (either by tuning them to a very low value, or shorting out cross couplings if they are not adjustable). This will result in a filter that does not have the desired shape, but does have the correct settings for the resonators and main coupling.

This is similar to the method used to isolate the Tx side of the duplexer from the Rx side. The resulting filter has only one path for coupling, and can be characterized as an all pole filter. A “golden” trace of this filter can be captured without the cross coupling.

When tuning an untuned filter, it can be set to have the same response as the “golden” filter, with the cross coupling removed. All that remains is to set the cross coupling back to verify the final filter response.

Another option for filters with adjustable cross couplings is to set the cross coupling first, before tuning the rest of the filter. This method may be effective for filters where the cross coupling has a strong effect on the

pass band response. To do this, one may short out the resonators beyond the cross coupling, essentially making a new filter with the cross coupling being the main path through the filter. A “golden” trace may be taken with a filter thus modified, and the value of the cross coupling in the time domain may be recorded. When tuning an untuned filter, the process is reversed. The resonators beyond the cross coupling are shorted and the cross coupling is set in the time domain. The shorting of the resonators is removed, and the filter is tuned as described above. This may be effective in dealing with cross coupling that is used for linearizing group delay in filters.

## Conclusions

In this application note, we have shown ways to extend the time domain tuning techniques to more complex filters. These filters may contain complex transmission responses, with cross couplings. These filters may also contain multiple paths, such as in duplexers, or even multiplexers. While good progress has been made on extending these techniques, there remain many opportunities for enhancements to these methods, and many filter types that require further investigation. Agilent Technologies is continuing research into the area of filter tuning, and will continue to provide state-of-the-art tuning techniques and applications to support innovation in the area of coupled resonator filter design.

## Other resources

### Tuning coupled resonator cavity filters

1. Joel Dunsmore, "Simplify Filter Tuning Using Time Domain Transforms", *Microwaves & RF*, March 1999.
2. Joel Dunsmore, "Tuning Band Pass Filters in the Time Domain, *Digest of 1999 IEEE MTTT Int. Microwave Sym.*, pp. 1351-1354.
3. "Simplified Filter Tuning Using Time Domain," Application note 1287-8, literature number 5968-5328E

### Tuning cross-coupled resonator filters

4. Joel Dunsmore, "Advanced Filter Tuning in the Time Domain," *Conference Proceedings of the 29th European Microwave Conference*, Vol. 2, pp. 72-75.

### Tuning duplexer filters

5. Joel Dunsmore, "Duplex Filter Tuning Using Time Domain Transformers," *Conference Proceedings of the 30th European Microwave Conference*, Vol. 2, pp. 158-161.

### Filter design

6. Zverev, "Handbook of Filter Synthesis," John Wiley and Sons, 1967.
7. Williams and Taylor, "Electronic Filter Design Handbook, 2nd Edition," McGraw Hill Publishers, Chapter 5, 1988.

## **Paper 5**

Dunsmore, J., "Novel Tuning Application for Coupled Resonator Filter Tuning". *Proceedings of the 2001 Asia-Pacific Microwave Conference*, 3-6 Dec. 2001, Taipei, Taiwan, Vol.2 894-897.

# NOVEL TUNING APPLICATION FOR COUPLED RESONATOR FILTER TUNING

JOEL DUNSMORE  
Agilent Technologies  
1400 Fountaingrove Parkway  
E-mail: joel\_dunsmore@agilent.com

This paper describes a novel software application that provides a method by which coupled-resonator filters may be tuned with little or no experience. The value of each resonator and coupling is displayed relative to a target value. The filter is properly tuned simply by adjusting each resonator and coupling such that the displayed value equals the target value.

## 1 Introduction

This paper describes the new FTS (Filter Tuning Software) that provides a graphical guided interface for tuning coupled-resonator filters. With coupled-resonator filters, the center frequency of each resonator must be precisely tuned, and each coupling between resonators must be precisely set to achieve the proper pass-band response, and to get low reflection and small pass-band ripple. Recently, there have been several papers describing methods to achieve tuning of these filters. One of these methods requires that the filter is short-circuited [1], rather than terminated in their characteristic impedance, extracting values for filter poles and zeros. Another method proposes using optimization techniques to match a filter's response to a polynomial filter function [2], but was tested against only simulated filters, and does not address the interactive problems faced in real-world tuning situations.

In previous papers [3],[4] Dunsmore reported tuning techniques that make use of the time domain response of filters. These papers demonstrated that the individual resonators and couplings of a filter could be identified with aspects of the time domain reflection response of the filters. In particular, the peaks of the response are identified with the filter coupling factors, and the nulls of the time domain response are associated with the resonator tuning. Unfortunately, while these methods were deterministic, it was difficult for an inexperienced operator to evaluate the time domain response of the filter. Further, for filters with cross coupling, the methods required many different frequency sweeps to allow tuning of the resonators. Finally, the methods presented could not identify easily whether the resonators were tuned too high or too low.

## 2 Description of the Novel Filter Tuning Software

This paper presents the results of new processing algorithms and innovative graphical displays that extend these previous methods to create a software application that provides an intuitive, simple and real-time tuning display for tuning coupled-resonator filters.

### 2.1 Reference Filters

This new tuning method derives values for resonator tuning targets by evaluating the response of a target or "golden" filter. This golden filter can be a physical prototype filter, properly tuned, or can be the response generated from a simulated filter. Fig. 1 shows one step in the process of capturing the golden filter data, where the individual peaks of the target filter (those peaks associated with the coupling values, as described in [3]) are automatically determined. The nulls between the peaks are associated with the individual resonators of the filter. The upper trace is from the input side (S11) of the filter; the lower trace is from the output side (S22) of the filter. This process is repeated for three spans: a coarse tuning span, a medium-tuning span, and a fine-tuning span. By proper processing of

this data using new algorithms that isolate each resonator, each resonator's target frequency and the coupling factors are determined.

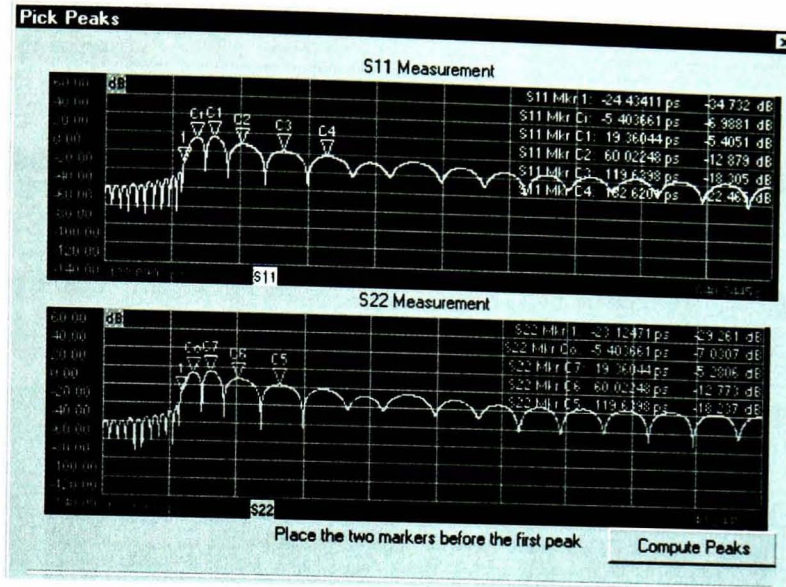


Figure 1: Capturing the "golden" filter data for the medium tuning span: the data shown is in time domain

Figure 2 shows the tuning display after capturing the golden filter data. The upper portion shows the S-parameters of the filter along with limit lines or marker values. The lower portion contains the new tuning indicators, which are identified with each resonator and with each coupling. The input and output couplings are identified with Ci and Co. Since these tuning indicators represent the target filter, which is being re-measured, they are all perfectly aligned.

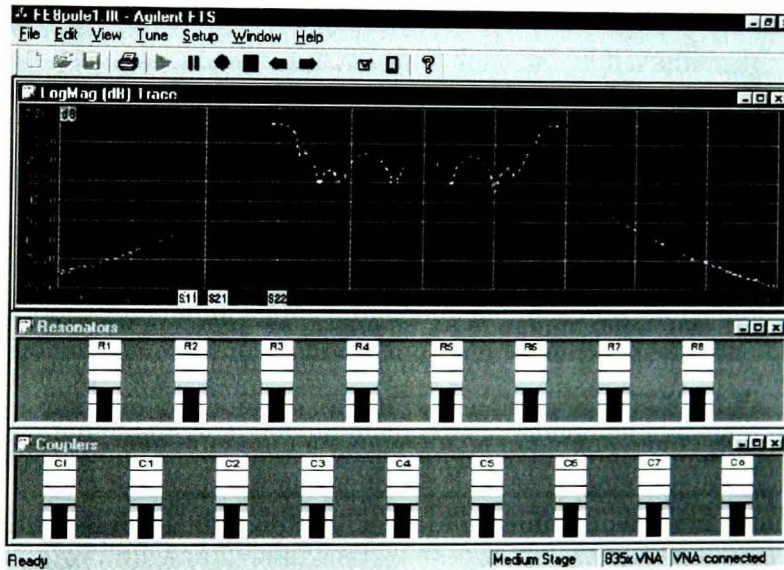


Figure 2: The FTS display of S-parameters (upper), resonator tuning indicators (center), and coupling indicators (lower) of the golden filter

## 2.2 Applying Filter Tuning Software to un-tuned filters

Figure 3 shows the tuning display of an un-tuned filter, in the coarse tuning mode. The S-parameters of the golden filter are shown as dashed lines. Coarse tuning sets the frequency-sweep span, by default, at 10 times the target bandwidth. This wide frequency span is chosen so that even if the filter is badly mistuned, all the resonators will be within the frequency sweep. In the coarse tuning mode, the order of tuning is important. For example, if the input coupling is very far off, it will not be possible to resolve couplings or resonators past the input coupling. For this reason, tuning should proceed from the outside elements to the center elements. For each tuning element, the tuning display indicator has 3 configurable ranges. For example, if the resonator is too low, the indicator will the

below the target line. The middle (green) zone represents an acceptable tuning region. The tuning indicator is linearly proportional to the resonator frequency over the center third of the display. Outside of this range the indicator compresses the tuning response of the resonator. This provides for high sensitivity when the tuning is close to the target zone.

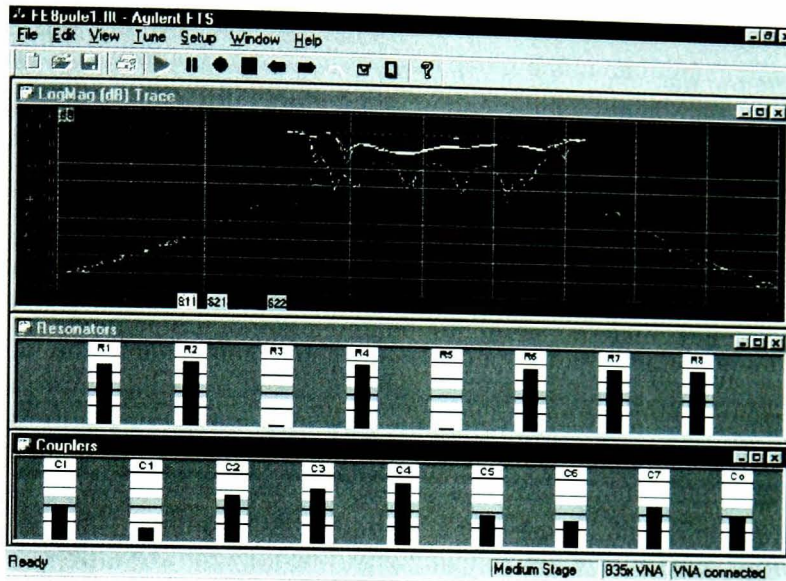


Figure 3: FTS display of an un-tuned filter

Figure 4a shows the response of the filter after tuning each resonator and each coupling to be in the green target zone. The filter is very nearly tuned. However, there is not sufficient resolution in coarse tuning to exactly tune the filter. The same filter is shown in Figure 4b in fine tuning mode (medium tuning mode is skipped, in this case). From this display, it is clear which resonators and couplings must be re-adjusted to perfect the tuning. The result of tuning each resonator to be in the green target region in fine tuning is a response with the S-Parameters from the golden filter being nearly identically matched to the filter being tuned.

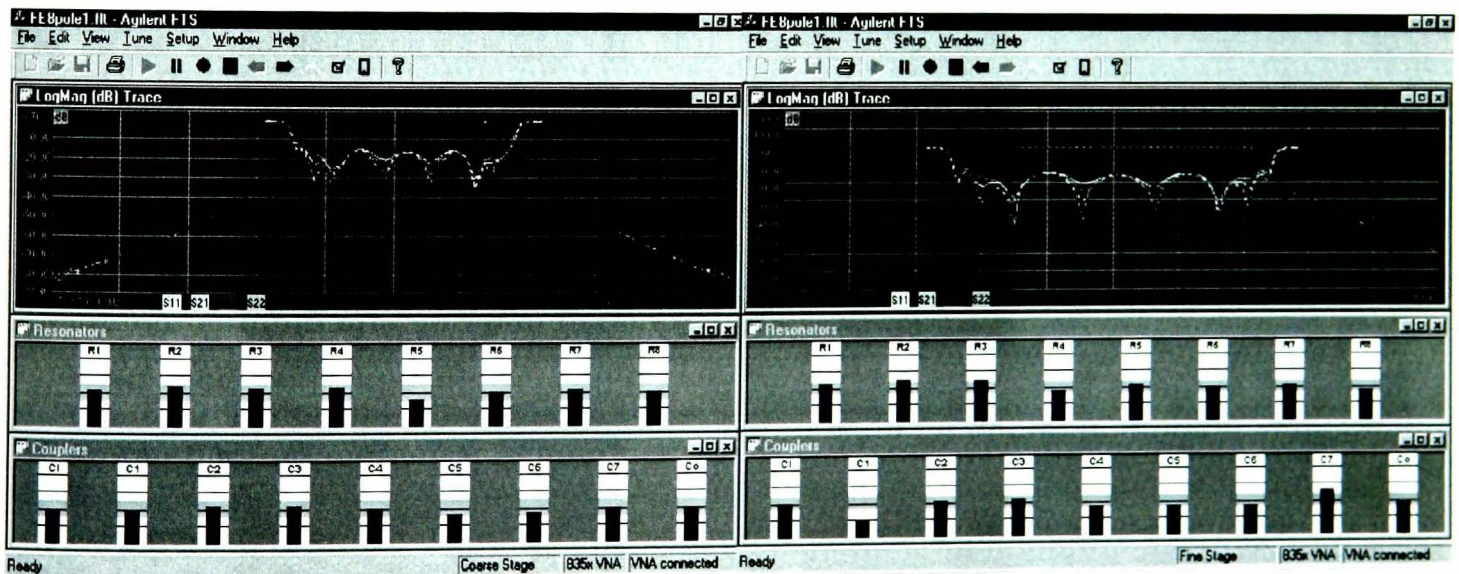


Figure 4a: Filter tuned in coarse tuning range,

Figure 4b: The same filter shown in fine tuning range

There are some limitations on this tuning technique. The tuning of resonators and couplers are interactive, requiring several iterations to achieve perfect tuning. The effects of these interactions and possible methods for compensating will be discussed. The algorithms developed apply to all-pole filters with adjustable couplings and adjustable resonators, and to filters with cross coupling where the cross coupling is either not adjustable, or can be tuned with an independent method. The paper will also describe possible extensions to duplex filters, and filters with multiple, adjustable cross couplings. Finally, experimental results in reduction of tuning time and new operator training will be presented.

### 3 Extensions to more complex filter types

A tuning method for complex filters, such as filters with cross coupling or duplex filters, has been described [5] using time domain techniques. Though deterministic, these methods are limited in that they require many steps to tune filters. The filter tuning software can be applied to these more complex filter types. For duplex filters with channel separations of greater than 1 filter bandwidth, each filter path can be treated individually. For duplexers with closer spacing, special tuning techniques must be used to separate the RX from the TX side. Additionally, a third reference filter file can be used that spans both the TX and RX frequency range. The first two nulls in time domain response of the ANT port connection represent the first TX resonator (if it is the higher frequency) and the first RX resonator.

Filters with cross coupling may also be tuned with this method. For cross-coupled filters, the target frequencies for each resonator will be different, but are easily determined from a reference filter. These frequencies are represented by the center of the tuning indicator. Currently, this method does not provide an explicit tuning indicator for the cross coupling, if it is adjustable. However, filters with adjustable cross coupling can be adjusted by observing other parameters. For example, filters with transmission zeros can be adjusted as described, with the cross coupling adjusted while observing the zero frequency in the S21 log magnitude display. For filters with cross coupling intended to flatten group delay, the group delay of S21 can be observed while adjusting the cross coupling.

### 4 Conclusion

The tuning techniques presented provide the first simple, easy to learn application for tuning complex, coupled resonator filters. The techniques and algorithms used provide for a visual and intuitive understanding of the effect of tuning selected elements in a filter structure, and ensure that proper tuning is accomplished.

### Acknowledgements

The author would like to acknowledge the Filter Tuning Software team: Bobby Bhowmik, Johan Ericsson, Phil Hoard, Sean Hubert and Dara Sariaslani.

### References

- [1] Atia, AE, Yao, HW, "Tuning & Measurements of Couplings and Resonant Frequencies for Cascaded Resonators", *2000 IEEE MTT-S Digest*, pp. 1637-1640.
- [2] Kahrizi, M, et al, "Computer Diagnosis and Tuning of Microwave Filters using Model-Based Parameter Estimation and Multi-Level Optimization", *2000 IEEE MTT-S Digest*, pp 1641.
- [3] Dunsmore, J., "Simplify Filter Tuning in the Time Domain", *Microwaves and RF*, vol. 38, no. 4, pp. 68-84, March 1999.
- [4] Dunsmore, J., "Tuning Band Pass Filters in the Time Domain", *1999 IEEE MTT-S Digest*, pp. 1351-1354.
- [5] Agilent Technologies Network Analysis Solutions: Advanced Filter Tuning Using Time Domain Transforms", Application Note 1287-10, Copyright 2000.

## **Paper 6**

Dunsmore, J., "Duplex Filter Tuning using Time-domain Transforms", *Proceedings of 30th European Microwave Conference*, 3-5 Oct. 2000, Paris, Vol.2 pp. 158-161.

# Duplex Filter Tuning using Time Domain Transforms

Joel Dunsmore

Agilent Technologies, Santa Rosa, California, U.S.A.  
joel\_dunsmore@agilent.com

**Abstract** – The author has continued development on advanced techniques in tuning coupled-resonator filters based on the time domain response of a filter. This paper updates techniques to precisely tune filter coupling and resonators, accounting for effects of transmission zeros from cross-coupled resonators, and presents new methods for tuning duplex filters.

## I. INTRODUCTION:

In previous presentations, the author has shown that coupled-resonator band-pass filters can be easily and deterministically tuned [1,2]. To achieve the proper pass band response, and to get low return loss and small pass band ripple, the center frequency of each resonator must be precisely tuned, and each coupling between resonators must be precisely set. In these papers, Dunsmore demonstrated a method of tuning filters based on the time domain response of its return loss, where the time domain response is obtained by a special type of discrete inverse Fourier transform of the frequency response. The technique works well for all-pole, low-loss filters, but there were several difficulties in tuning filters with more complex structures. In further work, Dunsmore demonstrated methods for tuning more complex filters, such as those with cross-coupled resonators [3]. This paper reviews these time domain tuning techniques, and presents a new method that resolves the problem of dealing even more complex filters: duplex filters. These filters have a common (antenna) port, an upper pass band port (e.g. TX port), and a lower pass band port (e.g. RX port). This new method may be extended to filter types with arbitrary pass band characteristics.

The time domain tuning method presented earlier relied on the filter having a unique time domain response. But with duplex filters, as seen from the antenna port, there are two paths that contribute to the return loss response, each with its own delays and responses. What was needed was a method to separate these responses in such a way that each side of the filter could be deterministically tuned.

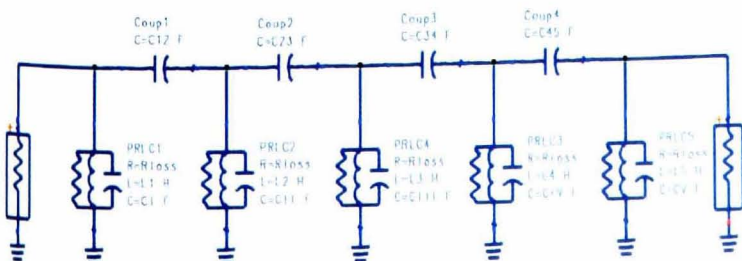


Figure 1: Schematic of a band pass filter

## II. TIME DOMAIN TUNING REVIEW

*Basics: Tuning All-Pole Filters:*

Before presenting the new method, it would be helpful to review time domain tuning on simpler filters. A five-pole coupled resonator filter with four coupling structures will be used to illustrate the basic tuning technique. A schematic of the filter is shown in Fig. 1. To apply the tuning method, the network analyzer's frequency sweep must be centered at the desired center frequency of the bandpass filter. The frequency span must be set to at least two to five times the expected filter bandwidth. The BANDPASS mode of time domain transform is applied to the return loss trace. Fig. 2 shows the frequency response and the band-pass mode time response of the filter, a fifth-order Chebyshev with 0.25 dB of passband ripple. Each plot shows two traces, one is the filter return loss response with ideal values for all the components, and the second trace showing the effect of mis-tuning one of the resonator elements (in this case, the second resonator). The upper plot is the frequency response and the lower plot is the time domain response. Notice the distinctive dips in the time response S11 of the filter (indicated by the triangles labeled 1-5). These are characteristic nulls that occur if the resonators are exactly tuned. If the center frequency of the measurement were changed even slightly, the nulls would start to disappear, indicating that the filter is no

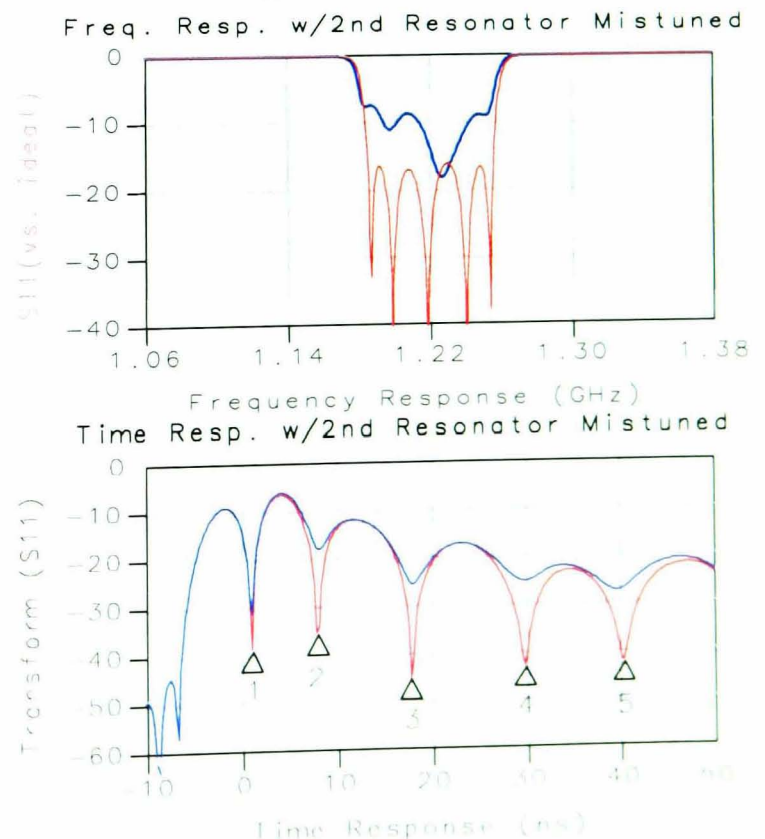


Fig. 2: Freq. and Time Response of a band pass filter.

longer tuned to the analyzer center frequency. The peaks between the nulls relate to the coupling factors of the filter. This type of response holds true for any all-pole filter, regardless of filter type.

The essence of the tuning technique is that the dips in the time domain response corresponded exactly to each resonator in the filter. The nulls in the time domain will be deep if the resonator associated with that null is tuned exactly to the network analyzer center frequency. For simple all-pole filters, their design dictates that the node frequencies are all centered on the filter center frequency. (In [3] the node frequency is defined to be the resonant frequency of the node with all connected couplings -- including cross coupling -- grounded). Figure 2 shows the time domain response with only the second resonator mis-tuned from its ideal (derived) value. In this case the capacitor C11 was tuned to a few percent above its ideal value. It is clear that the dip has nearly disappeared. The dip will only be maximized when the capacitor is returned to its ideal value. Note that mis-tuning one resonator can affect the response from the other "down stream" resonators.

The coupling adjustment can be accomplished by matching the peaks of the time domain response with a target trace. The target can be generated from a simulation or from a previously tuned "golden" filter. Note that adjusting one coupling will affect all couplings that follow. More information on this can be found in [2].

### Filters With Cross-Coupled Resonators

For many communication applications, it is necessary to make a filter skirt response steeper than normally obtained by all-pole type filters. Discrete transmission zeros (where the S21 goes to zero) can be obtained in the filter stop band by adding cross-coupling (coupling between resonators other than nearest neighbors), as shown in Figure 3.

With cross-coupling added to the filter, the time domain response no longer has the simple relationship to filter tuning. That is, especially in filters with asymmetric transmission zeros, the tuning of the filter is not optimum when nulls in the time domain are maximized. This corresponds to the fact that each node frequency is no longer centered at the filter center frequency. One way to look at this is that the resonators are "pulled" to compensate for the effect on the pass-band of the transmission zeros in the stop band, thus achieving the desired pass-band return loss specification. This results in an asymmetric shape to the return loss. Tuning for deep time nulls results in a filter that does not meet the return loss specifications. Figure 4 shows the frequency response of a filter with cross coupling.

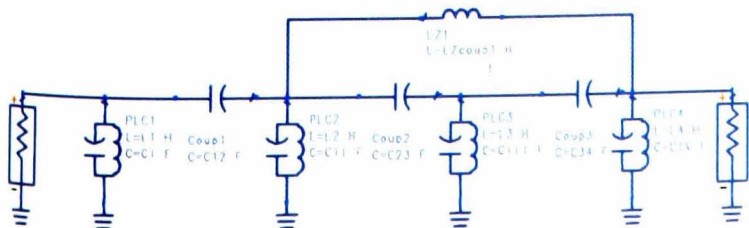


Fig. 3: Schematic of a filter with cross coupling (2-4).

pling in the upper trace. Figure 5 shows the time domain response with two different center frequencies on the vector network analyzer (VNA).

The time response of any *particular* node of a filter will have a deep null when the node frequency is exactly centered on the network analyzer frequency. The difficulty with these complex filters is that the node frequencies are no longer easy to determine. But one can use the network analyzer itself, on a properly tuned or "golden" filter, or on a simulated filter, to discover the individual node frequencies. This is done setting up the VNA in dual channel mode, with one channel on frequency domain and one on time domain. The center frequency of the VNA is adjusted while looking at the null associated with a particular resonator. When the null is maximized, that frequency is recorded as the node frequency for that resonator. Fig. 5 illustrates the time response of the filter tuned at the filter center frequency, and then tuned to a frequency which maximizes the null associated with resonator 2 (one of the resonators with cross coupling).

This process is repeated for each of the filter's resonators, adjusting the VNA center frequency until each null is maximized. For best sensitivity, the frequency span is reduced to just two times the bandwidth. Table 1 gives the node frequencies determined for each resonator for the filter from Fig. 4. Armed with this information, and using the measurement from Fig. 4 as the tuning template, a filter tuning process for complex filters can be defined.

Resonator No.	Node Frequency
1	836.25 MHz
2	833.85 MHz
3	834.55 MHz
4	836.45 MHz

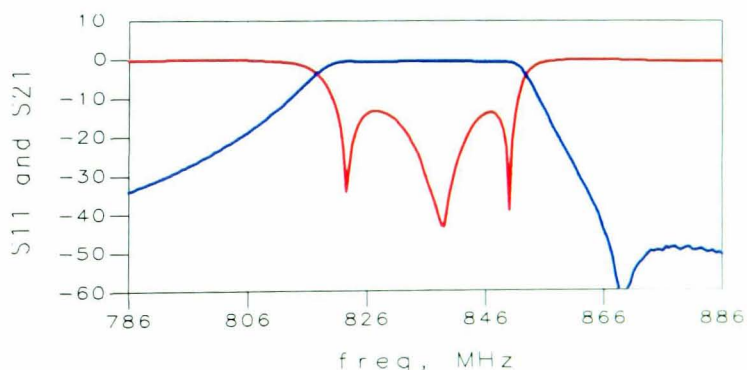


Fig. 4: Frequency response of a filter with cross coupling

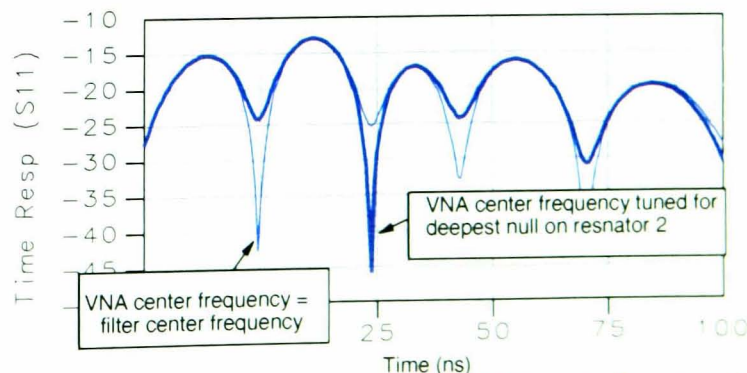


Fig. 5: Change in time response when the VNA center frequency is tuned.

### Time Domain Tuning Process for Complex Filters

The tuning process for complex filters can be summarized in the following steps (these steps are presented with detailed plots of each response in [3]).

- 1) Assuming that the input and output coupling is sufficient to produce an approximate filter shape, start by tuning the filter as though it were an all-pass filter.
- 2) Adjust the coupling to align the peaks with the target filter, remembering to re-adjust the resonators to get deep nulls.
- 3) Adjust the cross coupling to set the zero frequency to match the S21 frequency response target.
- 4) Finally, to get the resonators tuned to their correct final value, set the VNA center frequency to that listed in Table 1 for each resonator, and tune that resonator for maximum null. After a first pass, go back again and retune each resonator to account for the pulling affect of tuning the other resonators.

### III. DUPLEX FILTER TUNING

Duplex Filters (sometimes called duplexers or diplexers) are used in primarily to separate the transmission channel (TX) from the receive channel (RX) in a cellular phone base station. Because the TX and RX are nearly adjacent, the filters tend to be very asymmetric to create sharp cut-offs for each band. Figure 6 shows the schematic of such a duplexer. Note that a single cross-coupling is used in each side, but that the cross-coupling is positive in one side and negative in the other. This gives an upper transmission zero for the RX band (RX is lower in this case) and a lower transmission zero in the TX band as shown in figure 7.

Duplexers which have more than a bandwidth of separation are between TX and RX are easily tuned with the method noted above for tuning filters with cross-coupling. That is because the network analyzer can be centered on the TX band, with the span at greater than 2 bandwidths and still not have the RX band interfere with the input or output reflection response. However, most duplexers these days seem to have substantially less than 1 bandwidth between the edges of the TX and RX bands (a typical filter might have an 80 MHz bandwidth with 20 MHz of separation). These types of duplexers make time do-

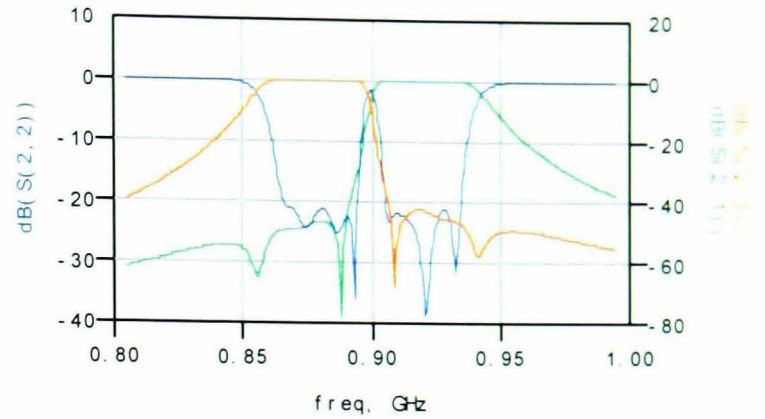


Figure 7: Frequency Response of a Simulated Duplexer

main tuning difficult, because resonator responses at the common port can come from either the TX side or the RX side. In figure 6 the duplexer uses quarter wave transformers to isolate each side of the duplexer (the input impedance of the TX side at the RX frequency is a short circuit). Other topologies couple the common port to a broader-band common resonator which is in turn coupled to the first resonator on each of the TX and RX side. With this configuration, the common resonator clearly cannot be centered on either TX or the RX pass band, but somewhere in between.

### Time Domain Response of Duplexers

The time domain response of duplexers is complicated by the fact that at the common port, reflections from both the TX side and RX side will cause some nulls in the time domain. Figure 8 shows the time domain and frequency response of a real duplexer. To view the time domain response in a way that makes sense, it is necessary to set the network analyzer center frequency to the frequency between the RX and TX pass bands. The span of the analyzer must be set to at least two times the over all bandwidth of the TX and RX bands. The following example of tuning a real duplex filter uses a duplexer which has the common port coupled to a common resonator, which in turn is coupled to both the first TX resonator and the first RX resonator.

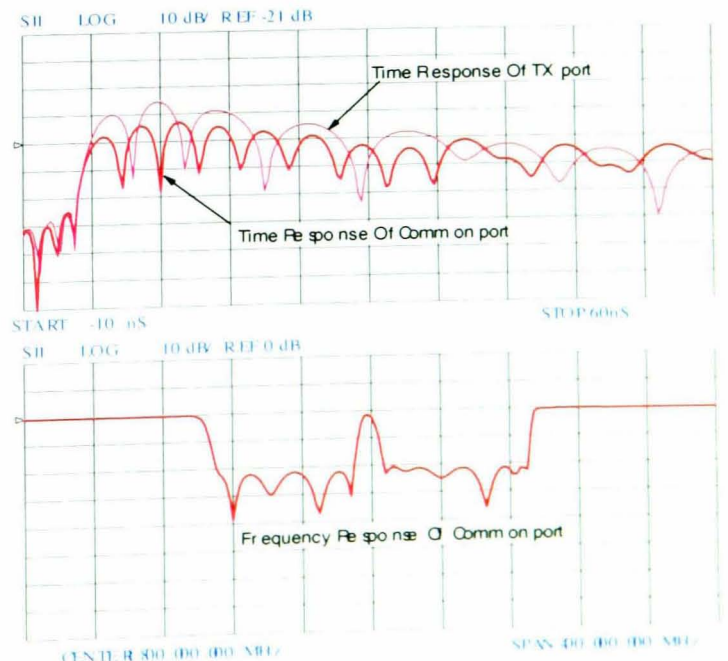


Fig. 8: Time Domain and Frequency Response of a Real Duplexer

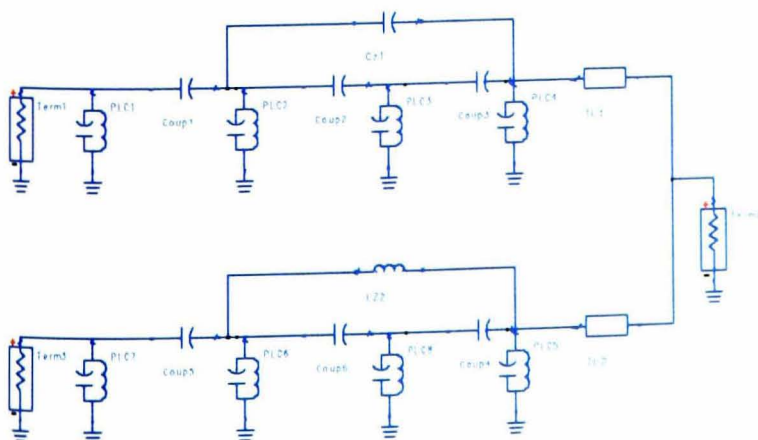


Fig. 6: Schematic Diagram of a Duplexer

### Setting up the tuning process

Just as with the complex filter of figure 4, the tuning process for a duplexer requires a properly tuned prototype filter to allow finding the node frequency and target couplings. However, the nodes will be more difficult to associate with individual resonators, especially from the common port.

The upper trace in figure 8 from the common port shows more nulls in the time domain than from the TX port. The first null is associated with the common resonator. The second null association is found by tuning slightly the TX last resonator, and in the same manner the RX last resonator can be associated with the third null from the common port. Depending upon the filter, it may also be possible to identify other resonators in the TX or RX filter, but soon the nulls become confusing, with tuning of one resonator effecting two nulls. Once the association of nulls with resonators has been done from the common port for the last TX and RX resonator, the individual node frequency for each resonator is found by tuning the analyzer center frequency until the associated null is deepest. This frequency is also recorded for each null from the TX and RX port, and for the first several nulls from Common port. These frequencies (MHz) are shown in table 2.

Common Port		TX Port		RX Port	
Node	Freq.	Node	Freq.	Node	Freq.
Com	1800	TX1	1747	RX1	1848
RX6	1800	TX2	1749	RX2	1848
TX5	1796	TX3	1750	RX3	1851
RX5	1805	TX4	1760	RX4	1841
TX4	1788				
RX4	1810				

These node frequencies will be used for the final tuning of the duplexer, but experimental research shows that it is not practical to try to tune the duplexer directly to these fre-

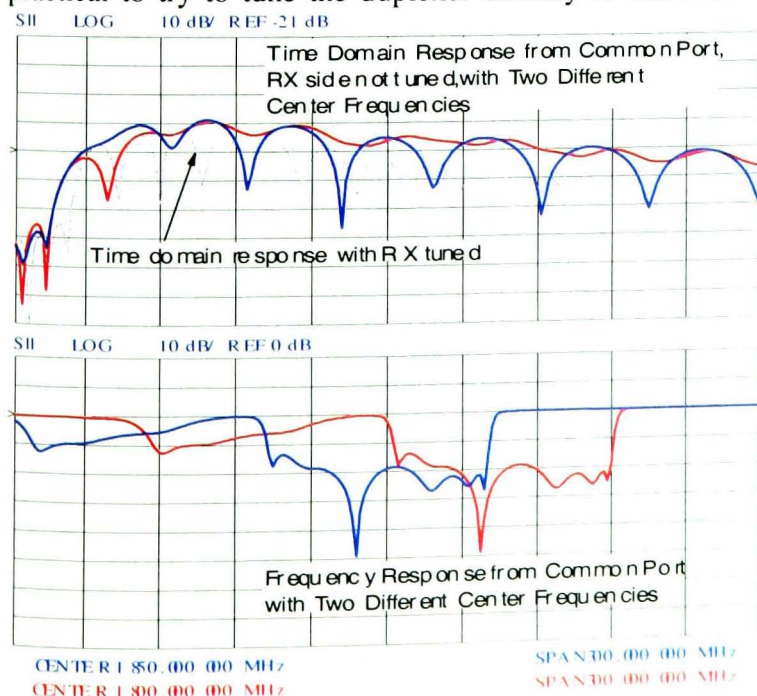


Fig 9: Time and freq. response of filter with RX side not tuned.

quencies. This is because there is so much interaction from the RX side on the TX response, especially at the common port, the resonators cannot be sufficiently isolated unless they are very close to being tuned exactly on. The solution for initial tuning is to mis-tune one side (say the RX side) and re-characterize the filter for TX side node frequencies. Figure 9 shows the response of the duplexer with RX6 and RX5 mis-tuned (the two closest to the common port resonator). With this display it is clear that near the common center frequency of 1800 MHz (lighter trace) the common resonator null is quite deep. But with the same filter measured with an analyzer center frequency of 1850 MHz, each TX node is nearly a null. This was repeated for the RX side, and the precise node frequency for each node was recorded in table 3 below.

Note that from the TX and RX ports, the node frequencies are nearly unchanged, indicating that these are very nearly isolated from their respective other sides even in a tuned duplexer.

Common Port		TX Port *		RX Port **	
Node	Freq.	Node	Freq.	Node	Freq.
Com	1803* 1793**	TX1	1746	RX1	1848
RX6*	1829	TX2	1749	RX2	1848
TX5**	1762	TX3	1749	RX3	1850
RX5*	1848	TX4	1787	RX4	1850
TX4**	1738				
RX4*	1860				

\*TX untuned; \*\*RX untuned

From this a duplexer tuning process proceeds as follows:

- 1) Start with resonators RX6 and RX5 tuned high in frequency. Tune the TX side of the filter, and common port according to starred (\*) frequencies in table 3. Tune coupling and cross-coupling as described in [3].
- 2) Tune resonators TX5 and TX6 as low as possible. Tune the RX side of the filter using the double starred (\*\*) frequencies in table 3.
- 3) Final tune TX5 and TX6 to the frequencies in table 2. Final tune all resonators to table 2 values.

### IV. CONCLUSIONS:

This paper has presented a tuning method for adjusting duplex coupled-resonator filters. The key breakthrough is method for isolating the RX and TX side resonators in time domain to allow independent tuning. More details on the example will be presented in the final paper.

### REFERENCES

- [1] Joel Dunsmore, "Simplify Filter Tuning using Time Domain Transforms", *Microwaves & RF*, March 1999.
- [2] Joel Dunsmore, "Tuning Band Pass Filters in the Time Domain, *Digest of 1999 IEEE MTT-S Int. Microwave Sym.*, pp. 1351-1354.
- [3] Joel Dunsmore, "Advanced filter tuning in the Time Domain", *Conference Proceedings of the 29<sup>th</sup> European Microwave Conference*, Vol. 2, pp. 72-75.
- [4] Zverev, "Handbook of Filter Synthesis", John Wiley and Sons, 1967.
- [5] Williams and Taylor, "Electronic Filter Design Handbook, 2<sup>nd</sup> Edition", McGraw Hill Publishers, Chapter 5, 1988.